Receiver Algorithms that Enable Multi-Mode Baseband Terminals

Yushan Li

A thesis submitted for the degree of Doctor of Philosophy.
The University of Edinburgh.
October 2005

Abstract

Wireless communications is rapidly moving towards so called 4G wireless systems. This has led to an increasing demand to develop integrated mobile terminals which have multi-mode capabilities, i.e. multiple communication systems can coexist. The central goal of this thesis is to determine appropriate structures and algorithms for multi-mode receivers that maximize flexibility without excessive compromise in performance. Attention is focused on the coexistence of multiple communication systems via a simple structure. All algorithms and architectures are developed within the framework of multi-mode receivers. This is in contrast to software-defined radios, the term multi-mode in this thesis being limited to a set of standards and a receiver is expected to handle different systems with low hardware complexity. Dedicated hardware is shared and reused by different systems. DAB, DVB-T, UMTS, HIPERLAN-2 and other potential systems are considered in this thesis. They can be classified into three categories: OFDM based systems, WCDMA and single carrier systems with cyclic prefix.

The work develops multi-mode terminals from the algorithm viewpoint, reducing receiver complexity by taking advantage of the commonalities among different specifications and receiver requirements. For example, the commonalities among DAB, DVB-T and HIPERLAN-2 physical layers are investigated and a common system clock is adopted for these communication systems. In addition, a receiver architecture combining sampling rate conversion and OFDM symbol synchronisation is also presented. The coexistence of WCDMA and OFDM systems from the perspective of using the same equalisation structure is elaborated; chip-level frequency domain equalisation for WCDMA forms a major part of this thesis. Simulation results verify the effectiveness of the proposed equalisation algorithms. Moreover, SC-FDE with more flexible structures, i.e. with a varying length feedback filter or without cyclic prefix, is examined. Then the importance of accurate channel estimation for practical spread spectrum systems is emphasized. A code-multiplexed pilot sequence is used for the purpose of channel estimation in both WCDMA and CP-CDMA systems and to maintain bandwidth efficiency. System performance is improved significantly by a proposed joint iterative channel estimation and parallel interference cancellation algorithm. Finally conclusions are drawn and suggestions for further work presented.

Acknowledgements

This thesis could not have been accomplished without the help and support of numerous people. Foremost, I would like to thank my supervisors Dr. David G. M. Cruickshank and Prof. Steve McLaughlin for their invaluable guidance, encouragement and support during my study in Edinburgh. I feel more confident now than I was three years ago. Thanks for always believing in me! I am also grateful to them for their patience in proof-reading and revising this manuscript and all my deliverables and papers. I would also like to express my appreciation to Dr. Emad A. Al-Susa who was my "third" supervisor and Dr. Chris Williams from the Bristol University for their constructive advice, useful comments and suggestions.

I would like to thank the following members of the Signal and System Group for their assistance and valuable discussions: Prof. Bernard Mulgrew, Dr. David I. Laurenson, Dr. John Thompson and Dr. Norbert Goertz. Special thanks also go to Mobile VCE for the studentship it offered without which I would not be able to finish my PhD study, in particular to Dr. Dean Kitchener from Nortel Networks UK Ltd. and Prof. Mark Beach from the University of Bristol for their prompt responses and useful suggestions.

Also, I would like to express my gratitude to Yiming Wang, Selina Xiaodan Feng, Xiao Wang, Yuefeng Zhou and Edwin Tan, etc. with whom I spent a good time in Edinburgh. I am fortune enough to meet them and enjoy our life together. I am especially grateful to Xusheng Wei, the first person I met in Edinburgh, for the very informative and fruitful discussions between us.

My family are always there with me and always have faith in me. Their unconditional love and unconditional support has been a source of strength for me to overcome every difficulty I encountered. No more words can express my deepest appreciation to my family especially to my parents and brother. This thesis is particularly dedicated to my dear father who passed away in 2003. His love will be with me, for ever.

Thanks for all the people who helped me to turn my dreams into reality.

Contents

List of figures

List of tables

Acronyms and abbreviations

ADSL	Asymmetric Digital Subscriber Lines
AWGN	Additive White Gaussian Noise
ASE	Accumulated Squared Error
BER	Bit Error Rate
BPSK	Binary Phase Shift Keying
CCPCH	Common Control Physical Channel
CDMA	Code Division Multiple Access
CM	Correlation Method
CP	Cyclic Prefix
CP-CDMA	Cyclic Prefix CDMA
CPICH	Common Pilot Channel
DAB	Digital Audio Broadcasting
DCH	Dedicated Channel
DFE	Decision Feedback Equaliser
DFT	Discrete Fourier Transform
DPCCH	Dedicated Physical Control Channel
DPCH	Dedicated Physical Channel
DPDCH	Dedicated Physical Data Channel
DQPSK	Differential Quadrature Phase Shift Keying
DS-CDMA	Direct Sequence CDMA
DSP	Digital Signal Processor
DVB-T	Digital Video Broadcasting - Terrestrial
ETSI	European Telecommunications Standards Institute
FBF	Feed Back filter
FDD	Frequency Division Duplex
FDE	Frequency Domain Equaliser/Equalisation
FDMA	Frequency Division Multiple Access
FEC	Forward Error Correction
FFF	Feed Forward Filter

FFT	Fast Fourier Transform
FH-CDMA	Frequency Hopping CDMA
FPGA	Field Programmable Gate Array
FSE	Fractional Spaced Equalisation
FT	Fractional Tap-length
GD	Gradient Descent
GSM	Global System for Mobile Communications
HDSL	High-Bit-Rate Digital Subscriber Lines
HIPERLAN-2	High Performance Radio Local Area Network - type 2
HSDPA	High Speed Downlink Packet Access
IBI	Inter Block Interference
ICI	Inter Carrier Interference
IDFT	Inverse Discrete Fourier Transform
IFFT	Inverse Fast Fourier Transform
IM	Iterative Method
IMIE	Iterative Method with Initial Estimates
LE	Linear Equaliser
ISI	Inter Symbol Interference
LLR	Log-Likelihood Ratio
LMS	Least Mean Square
LPF	Low Pass Filter
MAI	Multiple Access Interference
MAN	Metropolitan Area Network
MAP	Maximum *a Posteriori*
MC-CDMA	Multi-Carrier CDMA
MC-DS-CDMA	Multi-Carrier DS-CDMA
MIMO	Multiple-Input Multiple-Output
MLSE	Maximum Likelihood Sequence Estimator
MMSE	Minimum Mean Squared Error
MSE	Mean Squared Error
NCO	Numerically Controlled Oscillator
OFDM	Orthogonal Frequency Division Multiplexed
OVSF	Orthogonal Codes with Variable Spreading Factor
PAPR	Peak to Average Power Ratio

P-CPICH	Primary Common Pilot Channel
PER	Packet Error Rate
PIC	Parallel Interference Cancellation
PN	Pseudo Noise
PTS	Partial Transmit Sequence
QAM	Quadrature Amplitude Modulation
QoS	Quality of Service
QPSK	Quadrature Phase Shift Keying
RISIC	Residual Inter Symbol Interference Cancellation
RLS	Recursive Least Square
SC-FDE	Single Carrier Systems with Frequency Domain Equalisation
SCH	Synchronisation Channel
S-CPICH	Secondary Common Pilot Channel
SDR	Software-Defined Radio
SF	Segmented Filter
SFN	Single Frequency Networks
SISO	Soft-Input Soft-Output
SNR	Signal to Noise Ratio
SOVA	Soft-output Viterbi Algorithm
SRC	Sampling Rate Conversion
SS	Spread Spectrum
TDD	Time Division Duplex
TDE	Time Domain Equaliser
TDMA	Time Division Multiple Access
TFCI	Transmit Format Combination Indicator
TPC	Transmit Power Control
UE	User Equipment
UMTS	Universal Mobile Telecommunications System
UW	Unique Word
VCO	Voltage Controlled Oscillator
WCDMA	Wideband CDMA
WLAN	Wireless LAN
WSSUS	Wide Sense Stationary Uncorrelated Scattering
ZF	Zero Forcing

Nomenclature

$ASE_k(n)$	Accumulated squared error of an equaliser with k segments at time n
$b_k^{(m)}$	m-th symbol of the k-th user
$\tilde{b}_k^{(m)}$	Estimated m-th symbol of the k-th user
$\hat{b}_k^{(m)}$	Hard detected m-th symbol of the k-th user
$\hat{b}_{i,k}^{I,(m)}$	Hard detected m-th symbol of the k-th user at the I-th PIC stage
B	Channel bandwidth
B_c	Channel coherence bandwidth
B_s	Transmitted signal bandwidth
$c(t)$	scrambling code signal
$\mathbf{c}_i$	Time domain equaliser
C	Channel capacity
$d(n)$	Desired signal
$d_k(t)$	Transmitted signal of the k-th user
$\hat{d}_m^{(n)}$	Detected symbol and inputs to the FBF, $m = 1, \cdots, N_f$
$\mathbf{D}_i$	Diagonal matrix with elements taken from the N_c points FFT of channel impulse response
$e(n)$	Error signal
$e_k(n)$	Error signal generated by an equaliser with k segments
$e_m^{(n)}$	Error signal between equalised and detected symbol, $\mathbf{e}^{(n)} = [e_0^{(n)}, \cdots, e_{N_f-1}^{(n)}]^T$
$e_r(n)$	Relative distance of the equaliser output to the true chip value
E_d	Total average data channel power
E_k	Average power of the k-th user
E_p	Average power of the pilot channel
$\mathbf{E}^{(n)}$	Frequency domain counterpart of the time domain error signal $\mathbf{e}^{(n)}$
f_c	Carrier frequency
f_d	Doppler spread
$\mathbf{F}$	Fourier transform matrix
$\mathbf{F}^{-1}$	Inverse Fourier transform matrix
$\mathbf{F}^{(n)}$	N_b taps in the FBF vector, $\mathbf{F}^{(n)} = [f_0^{(n)}, \cdots, f_{N_b-1}^{(n)}]^T$

g	Power ratio of CPICH to the whole signal power
$G_i(w)$	Frequency response of the feedback CPICH cancellation filter
$h_I(t)$	Interpolation filter
$h(\tau;t)$	Complex time-varying FIR channel filter
$h_i(l)$	Channel impulse response of the l-th path in the i-th block
$h_l(n)$	Channel impulse response of the l-th path
$\hat{h}_l$	Channel estimate of the l-th path
$\hat{h}_l^{Iter}$	Iterative channel estimate of the l-th path (WCDMA)
$\tilde{\mathbf{h}}_i$	Iterative estimated channel vector for the i-th block (CP-CDMA)
$\hat{\mathbf{h}}_i^{CORR}$	Estimated channel vector using correlation method
$\mathbf{H}(n)$	Channel matrix
$\mathbf{H}_{c,i}$	Circular channel matrix of the i-th block
$H_i(w)$	Fourier transform of $h_i(l)$
$H_I(f)$	Frequency response of $h_I(t)$
I	Iteration number
$\mathbf{I}$	Unitary diagonal matrix
$Im[.]$	Imaginary part
J	MMSE cost function
K	Active users number
L	Channel spread in chips/samples
L_s	Number of tap segments in an equaliser
L_t	Number of taps in one segment
$L(n)$	Equaliser length at time n
$L_f(n)$	Fractional equaliser length at time n
$L_D(\bar{b}_i(n))$	Output from the SISO decoder
$L_D^e(\bar{b}_i(n))$	Extrinsic information from the SISO decoder
$L_D^e(\bar{x}_i(n))$	Interleaved $L_D^e(\bar{b}_i(n))$
$L_E^e(\bar{b}_i(n))$	De-interleaved $L_E^e(\bar{b}_i(n))$
$L_E^e(\bar{x}_i(n))$	Extrinsic information from the SISO MMSE equaliser
m_k	Largest integer less than or equal to kT/T_s
M	Block numbers, one slot is segmented into M blocks
$\mathbf{M}_i$	$N_c \times N_c$ matrix
$\mathbf{M}_{0,i}$	$(L-1) \times (L-1)$ matrix

$\mathbf{M}_{1,i}$	$(L-1) \times N_c$ matrix
$\mathbf{I}$	Unitary diagonal matrix
N	Processing gain/Spreading factor
N_b	Length of the Feedback filter
N_c	Number of chips/samples in one block
N_{CP}	Number of CP samples
N_f	Length of the Feedforward filter
N_s	Number of sub-carriers in an OFDM system
N_w	Channel estimation window
P	$P = N_c/M$, Number of non-zero samples in one slot
P_0	Power of the last two taps in the FBF
P_1	Power of all L_{total} taps in the FBF
$p_i(n)$	Scrambled CPICH signal within the i-th block
$P_i(w)$	Fourier transform of $p_i(n)$
P_tail	Total tail part power
P_{total}	Total power of the interference in the cyclic reconstruction process
$r(n)$	Sampled received signal
$r_l(n)$	Sampled received signal to the l-th RAKE receiver
$r(n)$	Baseband received signal
$r_i(n)$	Received signal in the i-th block
$\bar{r}_i(n)$	Received signal in the i-th block after tail cancellation
$\hat{r}_k(n)$	Regenerated channel distorted waveforms of the k-th user
$\hat{r}(n)$	Estimated pilot sequence for iterative channel estimation
$\check{r}(n)$	Generated interference for PIC
$\dot{r}(n)$	Output from the PIC
$\tilde{r}_i(n)$	Received signal in the i-th block after cyclic reconstruction
$r_{i,tail}(n)$	Tail part of a linear convolution process for the i-th block
$\tilde{\mathbf{r}}_i$	Received signal vector after cyclic reconstruction
$\mathbf{r}(n)$	Received signal vector, $\mathbf{r}(n) = [r(n), r(n-1), \cdots, r(n-N_c+1)]^T$
$\mathbf{r}_i$	Received signal vector in the i-th block
$\mathbf{r}_i^I$	Output from the I-th stage PIC
$\bar{\mathbf{r}}_i$	Received signal vector in the i-th block/slot after tail cancellation

$\bar{\mathbf{r}}_{i,k}$	One slot signal $\bar{\mathbf{r}}_i$ is segmented into M zero padded blocks
$\mathbf{r}_{i,t}$	$= [r_{i,tail}(0), r_{i,tail}(1), \cdots, r_{i,tail}(L-2)]^T$, tail part of a linear convolution process
$\mathbf{r}_{i,tail}$	N_c vector consists of $\mathbf{r}_{i,t}$ and padded zeros
R	$R = P_0/P_1$ Ratio of P_0 to P_1
$\mathbf{R}_i$	Fourier transform of $\mathbf{r}_i$
$\mathbf{R}_i^I$	Fourier transform of $\mathbf{r}_i^I$
$\bar{\mathbf{R}}_{i,k}$	Fourier transform of $\bar{\mathbf{r}}_{i,k}$
$\mathbf{R}^{(n)}$	Fourier transform of the received signal, $\mathbf{R}^{(n)} = [R_0^{(n)}, \cdots, R_{N_f-1}^{(n)}]^T$
$\tilde{R}_i(w)$	Fourier transform of $\tilde{r}_i(n)$
$Re[.]$	Real part
$s_k(n)$	Spreading chip waveform of the k-th user
$s_p(n)$	Spreading sequence assigned to the pilot channel
$\mathbf{s}_k$	Spreading code vector for the k-th user
S_{pilot}	Pilot symbol in a code-multiplexed pilot channel
$\hat{S}_{pilot,l}^{\ m}$	The m-th pilot symbol at the l-th RAKE receiver finger
$S(f)$	Doppler power spectral density
$\mathbf{t}_{i,k}$	Zero padded one slot length tail vector
T	Time duration of a symbol
T_c	Time duration of a chip
T_{ct}	Channel coherence time
T_{CP}	Time duration of CP
T_s	$1/T_s$ is defined as the sampling rate
T_u	Useful symbol duration of an OFDM signal
$\mathbf{T}_{i,k}$	Fourier transform of $\mathbf{t}_{i,k}$
$u(n)$	Unit step function
$\mathbf{u}$	$= [1, 0, 0, \cdots, 0]^T$
v	Constraint length of the convolutional code
$v(n)$	Complex-valued lowpass equivalent AWGN
$v_i(n)$	Complex-valued lowpass equivalent AWGN in the i-th block
$\mathbf{v}(n)$	Noise signal vector, $\mathbf{v}(n) = [v(n), v(n-1), \cdots, v(n-N_c+1)]^T$
$\mathbf{v}_i$	Noise signal vector in the i-th block
$\mathbf{V}_i$	Fourier transform of $\mathbf{v}_i$
$V_i(w)$	Fourier transform of $v_i(n)$

$\mathbf{w}(n)$	Adaptive filter tap coefficients
$W_i(w)$	Frequency domain equaliser
$\mathbf{W}(n)$	Time domain chip level equaliser tap coefficients
$\hat{\mathbf{W}}_{i,k}$	k-th slot-length FDE in the i-th slot
$\mathbf{W}^{(n)}$	N_f taps in the FFF vector, $\mathbf{W}^{(n)} = [W_0^{(n)}, \cdots, W_{N_f-1}^{(n)}]^T$
$\mathbf{W}_{c,i}$	Equivalent time domain circular equaliser matrix
$x(n)$	Baseband transmitted signal
$x_i(n)$	Transmitted signal in the i-th block
$x_{i,residual}(n)$	Time domain data channel signal excluding CPICH
$\hat{x}_i(n)$	Equalised signal in the i-th block
$\mathbf{x}(n)$	Transmitted signal vector, $\mathbf{x}(n) = [x(n), x(n-1), \cdots, x(n-N_c-L-2)]^T$
$\mathbf{x}_i$	Transmitted signal vector of the i-th block
$\mathbf{x}_{i,k}$	One slot transmitted signal $\mathbf{x}_i$ is segmented into M zero padded blocks
$\hat{\mathbf{x}}(n)$	Estimated transmitted signal vector
$\hat{\mathbf{x}}_i$	Estimated signal vector of the i-th slot
$\hat{\mathbf{x}}_{i,k}$	k-th slot-length estimated signal vector in the i-th slot
$\tilde{\mathbf{x}}_i^I$	The I-th stage regenerated transmitted i-th block signal
$\dot{\hat{\mathbf{x}}}_i^I$	Estimated composite signal excluding the u-th user's information
$\mathbf{X}_i$	Fourier transform of $\mathbf{x}_i$
$\dot{\hat{\mathbf{X}}}_i^I$	Fourier transform of $\dot{\hat{\mathbf{x}}}_i^I$
$X_i(w)$	Fourier transform of $x_i(n)$
$X_{i,residual}(w)$	Fourier transform of $x_{i,residual}(n)$
$y(n)$	Output from the RAKE receiver/equaliser
$y_k(n)$	Output from the equaliser with k segments
α	Real factor accounting for unpredictable cyclic reconstruction errors
α_f	Leaky factor used in the FT algorithm
$\alpha_l(t)$	Attenuation factor of the l-th path
α_{down}	Threshold parameter of the dynamic length algorithm
α_{up}	Threshold parameter of the dynamic length algorithm
α_{up}^1	Threshold parameter of the dynamic length algorithm
α_{up}^2	Threshold parameter of the dynamic length algorithm
β	Forgetting factor
δ	Integer constant increment

Δ	Integer constant
Δ_f	Sampling clock frequency error
ϵ	Small predefined threshold in the FT algorithm
$\eta_l(n)$	A mixture of AWGN, multipath interference and MAI on the l-th path
γ_1	Threshold parameter of the dynamic length algorithm
γ_2	Threshold parameter of the dynamic length algorithm
$\lambda_i(n)$	Soft bit of $x_i(n)$
$\vec{\Lambda}_i$	$= [\Lambda_i(0), \cdots, \Lambda_i(N_c - 1)]^T = \mathbf{F}\vec{\lambda}_i$, DFT of $\vec{\lambda}_i$
$\vec{\lambda}_i$	$= [\lambda_i(0), \cdots, \lambda_i(N_c - 1)]^T$
μ	Step-size in adaptive filters
μ_k	$= kT/T_s - m_k$, a fractional difference
$\odot$	Circular convolution
$\otimes$	Element by element multiplication
ϕ	Equivalent fading factor
$\phi_l(t)$	Phase of the l-th path
ρ	Small positive constant in RLS algorithm
σ_d^2	Variance of the transmitted signal
$\sigma_{interference}^2$	Average interference power per chip due to approximate cyclic reconstruction
σ_n^2	Variance of the noise signal
$\sigma_{residual}^2$	Variance of the time domain signal excluding CPICH
σ_{tail}^2	Variance of the tail part signal
τ_l	Propagation delay of the l-th path
τ_m	Channel maximum delay spread
ε	timing offset in the SRC
ε_i	Integer timing offset in the SRC
ε_f	Fractional timing offset in the SRC
$(.)^H$	Hermitian transposition

Chapter 1
Introduction

The first cellular mobile networks emerged in the early 1980s, these used analogue radio transmission technologies and Frequency Division Multiple Access (FDMA) techniques. All the available spectrum was divided into multiple adjacent channels with a certain bandwidth. Individual calls were allocated to different frequency bands. This system had several drawbacks such as small traffic capacity, bad voice quality, etc.

The second generation of cellular mobile networks (For example, Global System for Mobile Communications (GSM) [1]) was introduced in the early 1990s. It uses a set of digital wireless technologies called Time Division Multiple Access (TDMA) which can provide three to four times more capacity than that of the analogue systems. In a TDMA system, several calls share the same frequency resource. The GSM system has achieved great commercial success and is used in many countries in the world, however, it still suffers from a relatively low transmission data rate which can not meet the requirement of high data rate multimedia communication.

The third generation of cellular mobile networks (3G) can offer customers several broadband information services, for example, high data rate, low speed image and video communication, etc. which were unavailable in the first two generation systems. Code Division Multiple Access (CDMA) was selected as the key multiple access technology for the third generation mobile communication system. In a CDMA network, several users share the same channel in both time and frequency. The user's data are distinguished by their specific signature waveforms. CDMA offers great capacity and variable rate services. It is likely to dominate the market in the medium term.

Research in mobile communication is now moving towards the fourth generation (4G). This concept can be considered as both a broadband access and a distribution network with asymmetric and high data rate traffic. As one of the high rate transmission techniques that can reduce inter symbol interference (ISI) effectively, Orthogonal Frequency Division Multiplexed (OFDM) technique has emerged as a potential air-interface technology for both broadcasting and wireless LAN (WLAN) applications. OFDM is supposed to be a promising candidate for the kernel part of 4G, future mobile communications.

In principle, OFDM technology is a form of multi-carrier communication. It modulates several low data rate streams over a number of orthogonal sub-carriers for parallel transmission. The maintenance of orthogonality enables signals to be superimposed to generate OFDM signals without causing interference among sub-carriers. OFDM is a spectrally efficient transmission technique; it can also suppress the effects of the ISI in mobile communications.

CDMA and OFDM are currently the two dominant air interfaces in the consumer market. Significant research efforts has been carried out on the integration of these two techniques. The combination of direct sequence CDMA (DS-CDMA) and multi-carrier modulation is proposed; multi-carrier CDMA (MC-CDMA) and multi-carrier DS-CDMA (MC-DS-CDMA) are two different realizations [2] [3] [4] [5] [6]. In this thesis, the main focus is on current standards, i.e. DS-CDMA based Universal Mobile Telecommunications System (UMTS) [7] and those OFDM based broadcasting systems (Digital Audio Broadcasting and Digital Video Broadcasting) and WLAN.

1.1 Motivation

The most significant drives in all of the wireless personal communications activities are the desire for mobility and flexibility in communications and the demand for real time high data rate transmission. Future wireless multimedia communication systems will be designed mainly focusing on the aspect of satisfying user's requirements. In mobile communications, there is a great demand to develop more sophisticated integrated mobile terminals with multi-mode capabilities. The 4G mobile communication system should be able to provide more services than 3G does. It may support wireless communication services with either fixed or mobile platforms or span over different frequency bands and make wireless access to the Internet possible at anytime and from everywhere. It should facilitate multimedia information services other than merely voice plus text communications. Nowadays, mobile voice and text communications, audio and video communications, wireless networks and Internet are being related to each other more and more closely. Thus 4G is considered to be a multi-functional integrated broadband mobile communication system. A graph of such an integrated network is shown in Figure 1.1.

The central goal of this thesis is to determine appropriate structures for multi-mode receivers that maximize flexibility without excessive compromise in performance. Digital Video Broadcasting - Terrestrial (DVB-T) [8], Digital Audio Broadcasting (DAB) [9] and High Performance

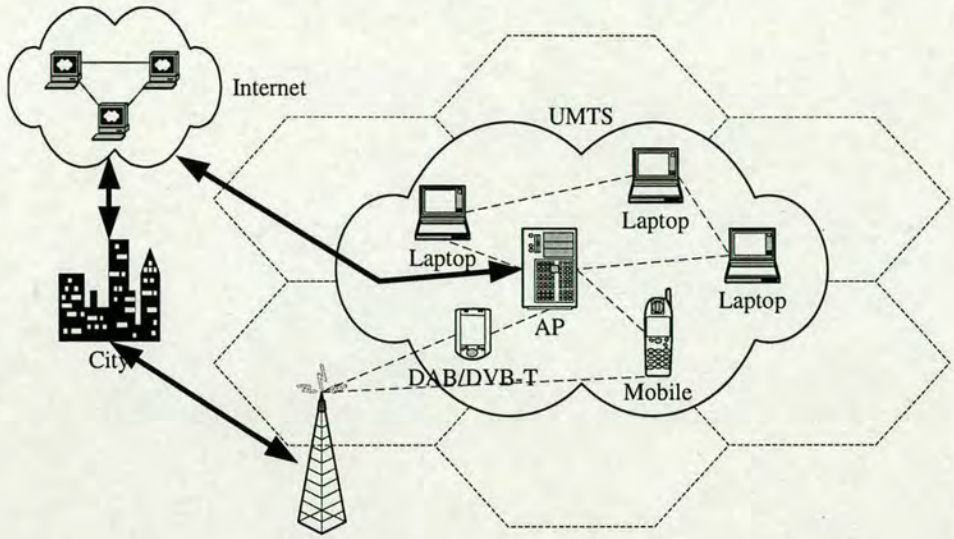

Figure 1.1: *Integrated network, UMTS, DAB, DVB-T, WLAN*

Radio Local Area Network-type 2 (HIPERLAN-2) [10] are the three European Telecommunications Standards Institute (ETSI) standards to be investigated as well as their combination with the UMTS which is considered as a successor to GSM. They are prominent solutions for broadband transmission of multimedia signals and future wireless network connections that can meet the requirements of consumers. These standards are currently receiving a great deal of attention with an increasing requirement for one receiver to cope with these multiple services. By discovering commonalities among the physical layer implementations, based on the design of some new receiver architectures, a multi-mode receiver can then be achieved.

Recently, work has been done toward that goal from a software-defined radio (SDR) point of view [11] [12]. In order to realise such coexistence of several services, they rely on powerful digital processing units, such as programmable digital signal processors (DSPs) and field programmable gate arrays (FPGAs). Obviously, these processors provide more flexibility than dedicated DSPs, however, the terminal needs to be reprogrammed each time it is anticipated to access to a specific service. Moreover, dedicated DSPs are usually faster and consume less power than general-purpose processors. Hereby, the term multi-mode is distinct from SDR, in that it is only limited to a limited set of standards and is expected to handle different systems with low hardware complexity. This can be done by discovering the commonalities in standards definition and processing requirements and thus sharing dedicated hardware among

different systems. For instance, by implementing a chip-level equaliser for wideband CDMA (WCDMA) in the frequency domain, the equaliser of both WCDMA and OFDM based systems can coexist.

In addition to WCDMA and OFDM systems, single carrier systems with a cyclic prefix are of interest in this thesis. They deliver similar performance to OFDM for essentially the same complexity. Nonetheless, the required cyclic prefix inevitably reduces bandwidth efficiency. In this thesis, the problem of removal of the cyclic prefix is investigated. Since reconfigurable terminals for mobile communication systems is the key objective of this thesis, variable length equalisers which allow a reduction in computational complexity are also considered.

The importance of accurate channel estimation for a practical mobile communication system is self evident. To maintain bandwidth and power efficiency, a code-multiplexed pilot channel is transmitted in a spread spectrum system. Generally speaking, good estimates can be obtained with a high power pilot channel. Unfortunately, this leads to high interference in the dedicated data channels. Such systems face a dilemma as to whether to adopt a high power pilot channel for better channel estimates or not. Moreover, practical implementation of the channel estimator should be considered. Consequently, it is of great interest to study an efficient channel estimator for CDMA systems that can work with a low power pilot channel.

1.2 Contributions

The key focus of this thesis is on developing algorithmic techniques that enable multi-mode operation rather than development of a specific architecture. A summary of the contributions is as follows.

- A new receiver architecture combining sampling rate conversion (SRC) and symbol synchronization is suggested. Since the physical layer of IEEE802.11a is similar to that of Hiperlan-2, and particularly the sampling rate of them is the same (20 MHz), only the physical layer of Hiperlan-2 is considered in this thesis. The three OFDM systems (DAB/DVB-T/Hiperlan-2) can use a single system clock effectively [13] [14].
- A chip level minimum mean squared error (MMSE) frequency domain equaliser (FDE) that utilises the common pilot channel for approximate cyclic reconstruction is presented. A high power pilot channel can be deployed in a system for better channel estimation and

the interference caused is removed by an interference canceller in the frequency domain. By adopting the proposed frequency domain equalisation structure for receiving UMTS signal, the coexistence of OFDM systems and UMTS via a simple structure is feasible. A multi-mode receiver can be programmed to switch to a particular transmission more conveniently. The interference cancellation algorithm has been applied to a cyclic prefix CDMA system in [15].

- Further development on the chip level FDE for UMTS is presented. Two other chip level MMSE FDEs based on self cyclic reconstruction [16] and slot segmentation [17] are proposed which require no overlapping processing. A pilot channel with high power is no longer necessary.

- Single carrier systems with frequency domain equalisation (SC-FDE) offer competitive advantages over OFDM and provide another focus in this thesis. A hybrid decision feedback equaliser (DFE) with a variable length feedback filter is derived. This reconfigurable structure achieves desired system performance with a reduced computational complexity [18].

- MMSE turbo equalisation and cyclic reconstruction are combined together to eliminate the normally required cyclic prefix in a SC-FDE system while improving system performance [19].

- Novel iterative channel estimation methods are studied for both WCDMA and cylic prefix CDMA (CP-CDMA) systems [20] [21]. Moreover, parallel interference cancellation (PIC) is introduced into the feedback structure. The proposed joint scheme shows good channel estimation accuracy and significant improvements on system performance.

1.3 Thesis Organization

This thesis is organised as demonstrated in the flow diagram in Figure 1.2 with contributions highlighted. This chapter introduces the motivation context and highlights the contributions of this thesis. In Chapter 2, basic principles and fundamental knowledge that are required for this thesis are given. A generic OFDM receiver architecture for a multi-mode terminal is discussed. Chip level frequency domain equalisers for WCDMA are considered in Chapter 3 and part of Chapter 4. A study of a hybrid DFE with variable length feedback filter forms another part

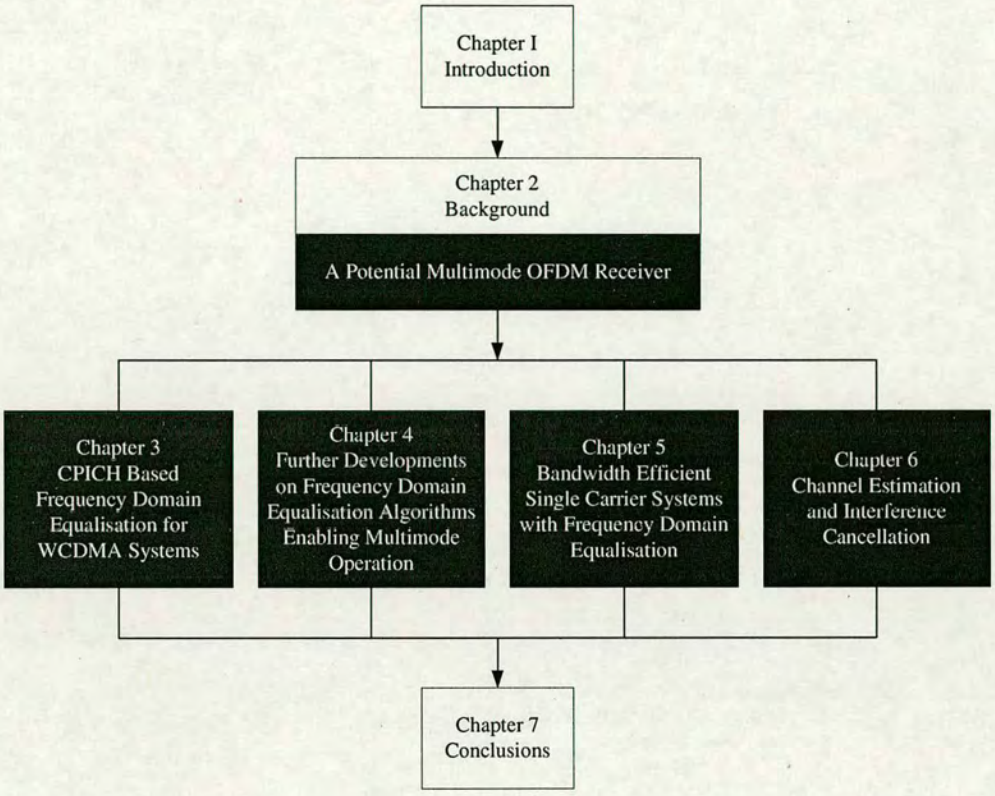

Figure 1.2: *Thesis organization*

of Chapter 4 as further developments on FDE algorithms enabling multi-mode operation. The problem of removing the normally inserted cyclic prefix in a SC-FDE is outlined in Chapter 5. The investigation on channel estimation, as a crucial consideration in a receiver, is presented in Chapter 6. Finally, in Chapter 7 overall conclusions are drawn and future work is discussed.

Chapter 2
Multi-Mode Receiver

In this chapter, a brief review of the necessary background for this thesis are discussed. First, basic principles of multi-carrier transmissions are outlined in Section 2.1 followed by a review of current OFDM based standards in Section 2.2. A generic OFDM receiver is presented in Section 2.3 showing the commonalities among those OFDM based systems. It is the purpose of this thesis to enable a multi-mode terminal to support a number of standards and systems, therefore, besides the OFDM based systems, mobile cellular systems are also considered in the thesis. In Section 2.4, transmitter and receiver structures as well as a fundamental description of spread spectrum systems are described. SC-FDE were proposed recently in [22] [23] [24] and is another kind of system that is of interest to this thesis and is introduced in Section 2.5. As is well known, the equalisation at the receiver can be viewed as a filtering process aiming at compensating the distortion caused by the channel. Section 2.6 describes the idea of dynamically adjusting the equaliser's length by which computational complexity can be reduced. Generally, different sampling rates are specified in different standards. A simple solution to integrate multiple standards within one terminal is to employ multiple clocks, however, this is inefficient and costly. In Section 2.7, a physical architecture of a multi-mode terminal with only one common clock is proposed. Finally, the main ideas discussed in this chapter are summarised.

2.1 Basic Principles of Multi-carrier Transmissions

OFDM is not a new technique; it was first proposed in the 1960s [25] but was mainly employed in wireless high frequency military communication systems. At that time, banks of sinusoidal generators were used for multi-carrier modulation and N_s sub-carriers were then multiplexed in the frequency domain. In 1971, a new modulation scheme using discrete Fourier transform (DFT) and inverse discrete Fourier transform (IDFT) was suggested in [26] to reduce the high complexity in the structure of OFDM systems and after that the OFDM technique became more practical. In the 1990s, OFDM was deployed for high data rate broadband communications and has proven a significant success, over mobile radio FM channels, asymmetric digital subscriber lines (ADSL), DAB, DVB-T, HIPERLAN-2 and IEEE 802.11a [27].

OFDM is one type of high data rate transmission technique used over wireless channels. The frequency response of most wireless channels is non-flat, thus, the key point of OFDM technique is to divide the given channel into several orthogonal sub-channels in the frequency domain. Data streams are modulated on multi-carriers and then several sub-carriers are transmitted in parallel simultaneously. Thus, although the practical overall channel is non-flat with frequency selective characteristic, every sub-channel can be considered flat fading. In theory, sub-carriers are orthogonal to each other and mutually overlapped which leads to a reduction of adjacent carrier interference as well as full use of the available spectrum.

Obviously, the data rate of each sub-carrier in an OFDM system is reduced by spreading the transmitted data over a large number of sub-carriers. The symbol duration is thus extended so that it can weaken the ISI effect caused by multipath propagation. N_s separated modulations can be implemented by the IDFT operation on data streams. At the receiver, the DFT operation is adopted for demodulation. Fast Fourier transform (FFT) and inverse fast Fourier transform (IFFT) are rapid implementations of DFT and IDFT, allowing OFDM modulation/demodulation with a low complexity. Figure 2.1 illustrates an IFFT/FFT-based OFDM baseband system.

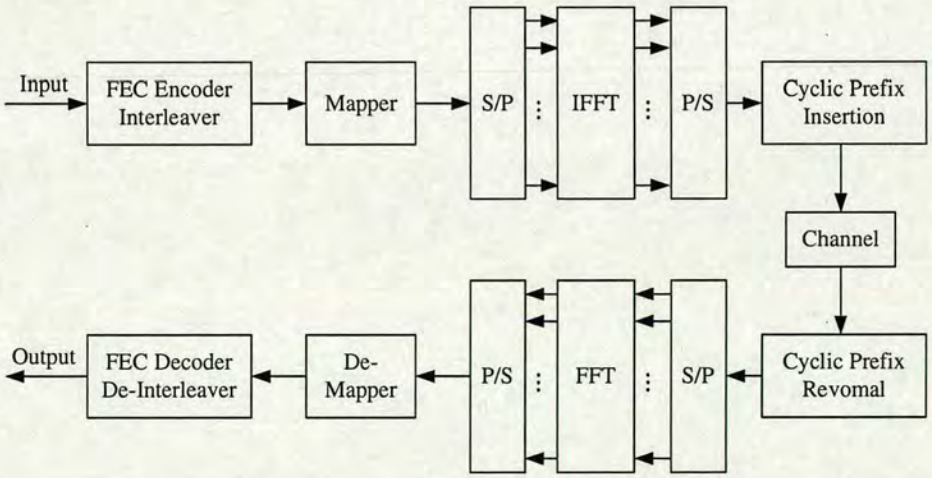

Figure 2.1: *A typical OFDM transceiver baseband configuration*

Before the IFFT-modulation the original binary input data is encoded by a forward error correction (FEC) code and thereafter interleaved and mapped onto BPSK/QPSK/QAM-values. At the receiver, signal samples are demodulated by an IFFT and output sequences are then demapped, deinterleaved and finally decoded to recover the binary output data. At the transmitter, the FEC block inserts redundancy in forms of parity bits for the receiver to correct errors caused

by channel impairments during the transmission process. However, this is at the expense of a reduction in data rates. In order to avoid burst errors, an interleaver is necessary. Consider a sequence of mapped complex data $d_0, d_1, d_2 \cdots d_{N_s-1}$ ($d_n = a_n + jb_n$, where a_n and b_n are real), after the IFFT operation and converting the output $D_0, D_1, D_2 \cdots D_{N_s-1}$ into serial data, we generate OFDM signals in the time domain for transmission. Outputs of the IFFT are given by:

$$D_w = \sum_{n=0}^{N_s-1} d_n e^{j2\pi nw/N_s} = \sum_{n=0}^{N_s-1} d_n e^{j2\pi f_n t_w} \ , \ w = 0, 1, 2, \cdots, N_s - 1 \qquad (2.1)$$

where $f_n = n/T_u$, $t_w = wT_u/N_s$ and T_u is the useful symbol duration of the OFDM signal.

In a frequency division multiplexing (FDM) system, sub-carriers are spaced apart with guard bands inserted which reduce the spectrum efficiency. This had been overcome in OFDM systems by overlapping individual sub-carriers to efficiently use the available bandwidth. Carriers are orthogonal to each others, i.e. linear independent, by selecting the the carrier spacing to be a multiple of $\frac{1}{T_u}$.

A cyclic prefix is appended to combat ISI; each OFDM symbol is preceded by a periodic extension of the signal itself. When the cyclic prefix is longer than the channel impulse response or the multi-path delay, the ISI effect is eliminated. The insertion of a CP reduces the spectral efficiency, however, it simplifies a receiver. The CP enables the multipath channel to circularly convolve with the transmitted symbol. In the frequency domain, the frequency-selective channel distortion on each sub-carrier can be considered as flat fading with a complex fading factor. Therefore, a simple frequency domain one-tap per sub-carrier equaliser can be used to compensate the amplitude and phase distortions.

Although the advantages of OFDM techniques are obvious, it should be pointed out that, there are two major inherent difficulties while regarding OFDM [28] [26] [29]. First, OFDM is highly sensitive to the frequency offset and the phase noise. Thus, accurate time and frequency synchronisation are required; however, it is difficult to implement that. Besides, OFDM exhibits a high instantaneous peak-to-average power ratio (PAPR) which will decrease the power efficiency of the RF amplifier.

2.2 Review of OFDM Based Standards

The history of DAB can be dated back to 1992 with the starting of the EUREKA-147 project. It then became an agreed standard of ESTI. The motivation of DAB is to provide audiences with reliable high quality audio programs with better performance [9] [30] [31] [32]. With DAB, OFDM was used for the first time for wireless transmission.

In 1993, an OFDM based DVB organization was established. Over 200 members from more than 25 different countries are involved in the development of DVB. A number of worldwide accepted DVB standards (DVB-C, DVB-S, DVB-T, DVB-H) have been released; all of those have been agreed by ETSI and the ITU [8] [33] [34].

HIPERLAN-2 is intended for wireless connectivity among networking equipments for the connection of data networks within a local area. HIPERLAN-2 has being developed by ETSI to provide a more flexible and economic approach to wireless network access [10] [35] [36] [37].

2.2.1 Key Features of DVB-T/DAB/HIPERLAN-2

The followings are some key features of DVB-T, DAB and HIPERLAN-2.

1. Carrier Frequency

- DVB-T

  Digital terrestrial television broadcasting is in the UHF/VHF band (VHF 174 to 238 MHz, UHF 470 to 682 MHz) which is assigned by the local spectrum management authority. The nominal central frequency of the RF signal is given by: $470 + 4 + i \times 8$ MHz, $i = 0, 1, 2, 3 \cdots$ (Desired 8 MHz channel spacing) or $174 + 4 + i \times 8$ MHz, $i = 0, 1, 2, 3 \cdots$ (Desired 8 MHz channel spacing) This central frequency may be offset to improve spectrum sharing.

- DAB

  DAB can be transmitted in some countries on frequencies using Band III (around 221 MHz). In the UK a spectrum allocation between 217.5 and 230 MHz has been reserved for digital radio transmissions. Others like Germany and Canada are using L-Band (1452-1492 MHz). DAB receivers currently on the market can receive both Band III and L-Band transmissions.

- HIPERLAN-2

  ETSI introduced HIPERLAN-2 with the center carrier frequency in two frequency bands. Currently, they are called the lower frequency band (5150 MHz to 5350 MHz, assigned for Indoor use only) and the upper frequency band (5470 MHz to 5725 MHz, assigned for both Indoor and outdoor use).

2. Channel bandwidth and data rates

- DVB-T

  Channel bandwidth can be 6, 7, 8 MHz in DVB-T, to be specified by the local spectrum management authority. By adjusting sampling frequency in the receiver, an 8 MHz bandwidth DVB-T system can be easily adapted for 6 or 7 MHz bandwidth system. The data rate of DVB-T ranged from 5 to 32 Mbps for fixed transmission and 5 to 15 Mbps for mobile transmission, depending on the modulation scheme used.

- DAB

  The overall bandwidth of DAB is 1.536 MHz, providing a useful bit-rate capacity of approximately 1.5 Mbps in a complete "ensemble". The DAB system in the UK has spectrum allocated between 217.5 and 230 MHz giving a total of seven blocks of 1.536 MHz, each able to carry a multiplex of services. It offers a flexible audio bit-rate, from 8 Kbps to 384 Kbps, which is adaptable for 5 to 6 high-quality stereo audio programs or about 20 restricted-quality mono programs within each 1.536 MHz.

- HIPERLAN-2

  The central carrier frequencies are spaced 20 MHz apart. The data rate ranges from 6 Mbps to 54 Mbps and can be varied by using various signal alphabets for modulating the OFDM sub-carriers and by applying different puncturing patterns to a single specific convolutional code. The mode dependent parameters are listed in Table 2.1.

3. Modulation, carriers and carrier spacing

- DVB-T

  QPSK, 16QAM and 64QAM are the standardized modulation schemes for DVB-T. QPSK will give the highest reliability but lowest data rate while 64QAM will provide the highest data rate but lowest reliability. Two modes of operation are defined in DVB standard:

Modulation Scheme	Coding Rate R	Bit Rate (Mbps)
BPSK	1/2	6
BPSK	3/4	9
QPSK	1/2	12
QPSK	3/4	18
16QAM	9/16	27
16QAM	3/4	36
64QAM	3/4	54 (Optional)

Table 2.1: *Mode dependent parameters for HIPERLAN-2*

a '2k' mode for single transmitter operation and for small Single Frequency Networks (SFN) and an '8k' mode for both single transmitter operation and for small and large SFN networks. A different number of carriers per OFDM symbol are specified for the two different modulation modes (2k mode: 1705 carriers, 8k mode: 6817 carriers). For 8 MHz channels, in the 2k mode, the useful symbol duration of one OFDM symbol is $T_u = 224\,\mu s$. In order to ensure that the sub-carriers are orthogonal, the minimum carrier spacing should be set to be $1/T_u = 4464$ Hz, thus, spacing between carriers $K_{min}(0)$ and $K_{max}(1704)$ is equal to 7.61 MHz. For the 8k mode with 8 MHz channels, these parameters are $T_u = 896\mu s$, $1/T_u = 1116$ Hz and 7.61 MHz, respectively. A cyclic prefix is introduced to preserve the orthogonality of the sub-carriers. It is inserted in front of the useful data as a copy of the last part of the useful symbol itself while the prefix duration is made larger than the maximum excess delay of the channel. In the DVB-T system, the duration of the allowed guard interval can be 1/4 (1/8, 1/16, 1/32) of the duration of T_u.

- DAB

  In contrast to the DVB-T and the HIPERLAN-2 systems, differential modulation is used in DAB. Differentially encoded Quadrature Phase Shift Keying (D-QPSK) is the only specified modulation scheme in the DAB standard. Different number of carriers and carrier spacing are specified for different transmission mode. The features of different transmission modes in DAB are given in Table 2.2.

- HIPERLAN-2

  BPSK, QPSK, 16QAM and 64QAM are the modulation candidates for HIPERLAN-2 and the physical layer of it is also based on the modulation scheme OFDM. The nominal

	Mode I	Mode II	Mode III	Mode IV
Number of Carriers	1536	384	192	768
Useful Symbol duration T_u	1 ms	250 μs	125 μs	500 μs
Carrier Spacing $1/T_u$	1 kHz	4 kHz	8 kHz	2 kHz
Guard Interval (CP Length)	246 μs	62 μs	31 μs	123 μs
Symbol Duration	1246 μs	312 μs	156 μs	623 μs

Table 2.2: *Features of different transmission modes for DAB*

carrier frequency f_c corresponds to its carrier number $n_{carriers}$, which is defined as:

$$n_{carriers} = (f_c - 5000)/5$$

The nominal carrier frequencies are spaced 20 MHz apart. All transmissions shall be centered on one of the nominal carrier frequencies. For instance, with $T_u = 3.2\ \mu s$ being given as the duration of one OFDM symbol, the sub-carrier spacing is then selected to be the reciprocal of the duration $1/T_u = 0.3125$ MHz. The cyclic prefix duration is $T_u/4 = 0.8\ \mu s$.

2.2.2 Summary

For the sake of convenience, main features of the three systems are listed in Table 2.3.

2.3 Multi-mode Receiver Implementations

The traditional solution to the design of multi-mode receivers encompasses the design of several different receivers: One design, for example, could be a DAB/DVB-T receiver which offers both DAB/DVB-T program receptions. On the other hand, another receiver which is capable of accessing HIPERLAN-2, exchanging or receiving information from the LAN may be required in the same equipment. A straightforward system-on-a-chip solution for the multi-mode receiver then consists of a chip of which its size is the sum of two individual chip-sets, one for the DAB/DVB-T receiver and one for the HIPERLAN-2 receiver. Therefore, it will inevitably lead to high-cost, high-power and large sizes which are not wanted by the user. One possible way to avoid these huge chip-areas is to employ reconfigurable hardware [38]. The hardware configures itself to function either as a DAB/DVB-T receiver or as a HIPERLAN-2 receiver.

	DVB-T	DAB	HIPERLAN-2
Air Interface	OFDM	OFDM	OFDM
Frequency Range	VHF 174-238 MHz UHF 470-682 MHz	Band III (UK) 217.5-230 MHz L-Band 1452-1492 MHz	Indoor 5150-5350 MHz Both In/Outdoor 5470-5725 MHz
Channel Bandwidth	6,7,8 MHz	1.536 MHz	20 MHz
Data Rates	Fixed Transmission 5 to 32 Mbps Mobile Transmission 5 to 15 Mbps	8 to 384 Kbps for audio broadcasting. 1.5 Mbps in a complete "ensemble"	6 to 54 Mbps varied due to different modulation scheme
Modulation	QPSK, 16QAM 64QAM	DQPSK	BPSK, QPSK 16QAM, 64QAM
Carriers	2k mode 1705 carriers 8k mode 6817 carriers	Mode I 1536 carriers Mode II 384 carriers Mode III 192 carriers Mode IV 768 carriers	36, 40, ..., 64 carriers (Lower) 100, 104, ..., 140 carriers (Upper)

Table 2.3: *Comparison of DVB-T, DAB and HIPERLAN-2*

Reconfigurable chipsets are emerging as a new solution for the requirement of both performance and flexibility. Based on the commonalities among different standards, reconfigurable chipsets are deployed to make multi-functional blocks feasible. Software reconfigurable mobile systems are regarded as a necessary part of future 4G wireless systems and more and more work has been conducted in this field.

To design a multi-mode terminal that is able to cover different standards, some cost efficient solution needs to be reconfigurable. The concept of SDR is fully exploited to enhance the flexibility of handsets that allows the handset to operate as a multi-mode receiver; common hardware blocks for different standards are reused under the control of a programmable software core [39].

Comparing the architectures of three standards, it is quite obvious that a strong resemblance among their receiver architectures exists. Making good use of those commonalities, a multi-mode receiver could be implemented with reduced hardware expenses. However, it is not simply mixing them together since each mode has its own working frequency, bandwidth, data rate, and spectrum specifications, etc.

Commonalities among physical layers have been discovered. Figure 2.2 shows a simulation

platform for a generic OFDM transceiver which can be a possible multi-mode transceiver as well. Since we are not interested in the characteristics of the transmitted data, the structures of

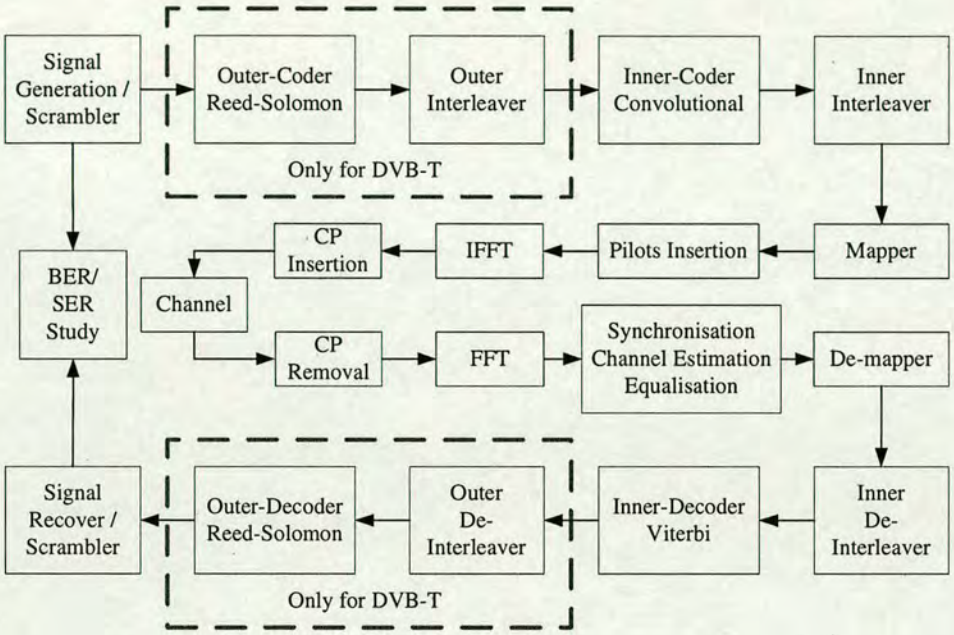

Figure 2.2: *A generic OFDM transceiver block diagram*

the data stream frame are ignored. Investigation in this project only focused on the transmission of the data after it has been generated.

First, data for transmission are generated and scrambled. After, the data stream is pushed into the Outer-Coder that gives Reed-Solomon encoded data output. The Outer-Coder, Outer Interleaver, Outer-Decoder and Outer De-Interleaver are only specified in the DVB-T standard. As in the DVB-T standard, a shortened Reed-Solomon (204,188) code is used as a outer FEC. Due to the redundant parity bits, the bit rate is reduced by about 8%.

In principle, some sub-carriers will be boosted and some will be attenuated while transmitted in a mobile radio channel. Since uncoded OFDM is not satisfactory for use in a real environment, convolutional coding with Viterbi decoding is adopted as a good bit error protection solution. Typical convolutional codes having code rates of 1/2, 1/3, 1/4 are punctured in order to meet the high data rate requirements; some predefined code bits are not transmitted. Punctured rates of 2/3, 3/4, 5/6, 7/8 are allowed in DVB-T and 3/4, 9/16 in HIPERLAN-2. In DAB, variable code rate between 8/9 and 8/32 (equal to 8 / (8+PI), PI=1,...,24) is applied.

Interleaver blocks in both the outer part and the inner part partition the input data stream into blocks and then split them in order to suppress long sequence distortion during data transmission. The interleaver rearranges elements of its input according to the permutation scheme specified in different standards.

DVB-T can share the same mapper block with HIPERLAN-2 while in DAB, only DQPSK modulation is adopted. Differential detection avoids the estimation of the carrier phase, but on the other hand, it is more sensitive to Doppler shift than coherent detection.

In the subsequent discussion, OFDM is the kernel part in the transceiver. N_s separated modulation outputs can be realized with an arbitrary length IDFT operation on the data stream to generate OFDM symbols in the time domain for transmission. Different length IDFTs are used in accordance with the different number of sub-carriers due to different modes in the standards.

Pilots are inserted for the sake of estimating a slowly changing frequency selective fading channel. It can also provide reliability information for the Viterbi soft-decision decoder at the receiver terminal. However, the insertion of pilots will lead to a drop in efficiency.

Obviously, the following blocks in the receiver after channel equalisation can be viewed as a counterpart of the corresponding blocks in the transmitter end.

Currently, more and more broadband mobile multimedia services are emerging. Meanwhile, the next generation mobile communication based on the OFDM air interface, supporting broadband access and distribution network with asymmetric high bit rates, becomes a hot topic for research. In the future, user demands will be the major concern of service providers and industrial organizations. DAB, DVB-T and HIPERLAN-2 are three major broadband wireless access specifications employing the OFDM modulation technique, introduced by ETSI in Europe. In this chapter, a comparison of DAB, DVB-T and HIPERLAN-2 standards, including key features and architectures are analyzed. These specifications show a high degree of commonalities with baseline systems. Based on the commonalities discovered, the architecture of a multi-mode baseband terminal that is capable of coping with multiple standards is presented.

2.4 Spread Spectrum Systems

Spread spectrum (SS) methods are the foundation of 3G communication system. The SS system employs signature codes to distinguish multiple users rather than using time slots or frequency

bands. It modulates user signals at a high speed pseudo-noise (PN) binary-valued sequence so that the spectrum is spread and the bandwidth is much greater than the information rate. Consequently, the modulated signal appears similar to random noise and more difficult to be detected by unintended listeners. This type of digital communication system allocates all resources, both time and frequency, to every simultaneous users [40] and hence supports multiple access via code division and is so called CDMA [41]. CDMA techniques were selected as the key multiple access technology for the third generation mobile communication system because of lots of valuable properties. First, from the Shannon capacity equation:

$$C = Blog_2(1 + SNR) \tag{2.2}$$

where C is the capacity of the channel, B is the bandwidth of the channel and SNR denotes the signal to noise ratio, it can be seen that for any given fixed channel capacity, the SNR can be reduced with increasing the bandwidth B, i.e. the power of transmitting data samples decreases. Compared with FDMA and TDMA, the SS system suffers from lower interference from adjoining channels. From an interference resistance point of view, the SS system is robust to impulsive interference by spreading the data information along the time axis.

2.4.1 Transmitter

There are two primary spread spectrum concepts for multiple access: DS-CDMA and frequency hopping code division multiple access (FH-CDMA). The research area of this thesis is limited to only DS-CDMA systems .

A DS-CDMA downlink scenario is considered in this section: all signals are transmitted symbol and chip synchronously through the same mobile radio channel. The general principle behind DS-CDMA is its spectrum spreading [40] [41] [42]. The information signal with bandwidth B_s is spread over a wideband PN sequence with bandwidth B and $B \gg B_s$. The processing gain is expressed as the bandwidth expansion factor:

$$N = \frac{B}{B_s} \tag{2.3}$$

The envelope of the transmitted signal due to the k-th user can be written as:

$$d_k(t) = \sqrt{E_k} \sum b_k^{(m)} s_k(t - mT), \tag{2.4}$$

where T denotes the symbol interval; E_k, $b_k^{(m)}$ and $s_k(t)$ denote the average power of the k-th user, the m-th symbol of the k-th user and the spreading chip waveform of the k-th user given by the convolution of spreading sequence and the chip waveform, respectively. The total average data channel power can be represented as $E_d = \sum_{k=1}^{K} E_k$. Let T_c be the period of one chip, hence $N = \frac{T}{T_c}$.

After spreading, user data is summed together for transmission. The baseband transmitted signal can be written as:

$$x(t) = \sum_{k=1}^{K} d_k(t), \tag{2.5}$$

The transmitter block diagram is shown in Figure 2.3.

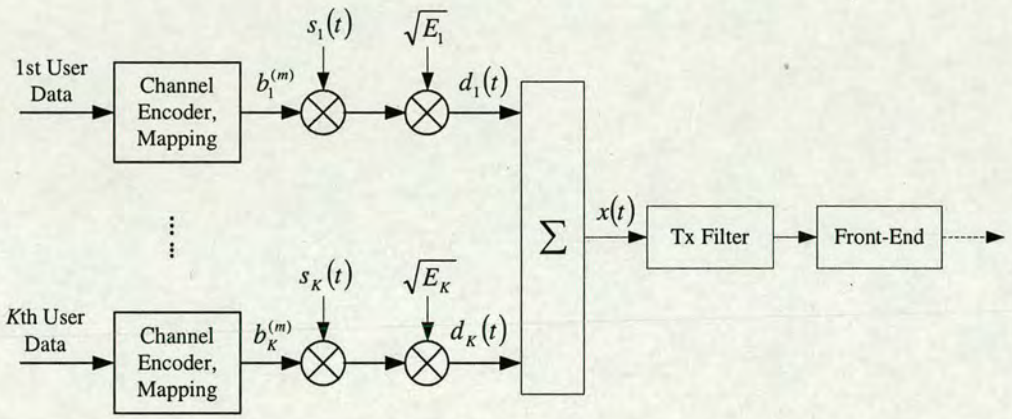

Figure 2.3: *DS-CDMA transmitter block diagram*

2.4.2 Communication Channel

In a mobile wireless communication system, large-scale and small-scale are two types of fading effects. Large scale fading is a deterministic process caused by slow signal power variation or the path loss related to motion over large areas while small-scale fading is a stochastic process representing dramatic changes in signal amplitude and phase due to small changes in small areas.

The small-scale fading can be described via its two manifestations: time variance of the channel and time spreading of the signal [43].

1. Slow and Fast Fading

A channel is said to be slow/fast fading if the channel coherence time T_{ct} is longer/shorter than the time duration of a transmitted symbol. The coherence time measures the time duration where the channel impulse response is considered invariant. The time-varying nature of the channel can be studied in the frequency domain by introducing the Doppler spread f_d and the Doppler power spectral density $S(f)$. The value of f_d is determined by:

$$f_d = \frac{v}{\lambda} \tag{2.6}$$

where v is the relative mobile velocity and λ is the wavelength of the signal. The coherence time T_{ct} is inversely proportional to the Doppler spread as:

$$T_{ct} \approx \frac{1}{f_d} \tag{2.7}$$

From (2.7), it is clear that a slow/fast fading channel has a large/small coherence time or equivalently a small/large Doppler spread [41]. The Doppler power spectral density $S(f)$ is defined as:

$$S(f) = \frac{1}{\pi f_d \sqrt{1 - (\frac{f}{f_d})^2}} \tag{2.8}$$

The well-known U-shape Doppler power spectrum [44] is depicted in Figure 2.4. where f_c is

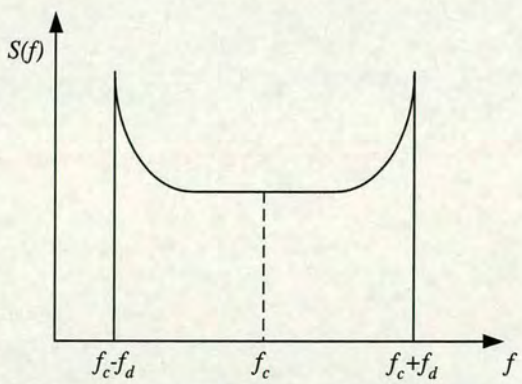

Figure 2.4: *U-shape Doppler power spectrum*

the carrier frequency.

2. Frequency Selective Fading and Flat Fading

The frequency-selective fading and flat fading can be distinguished via two comparisons.

- A channel is said to exhibit frequency-selective/flat fading if the channel coherence bandwidth B_c is smaller/larger than the transmitted signal bandwidth B_s. The coherence bandwidth measures the frequency range over which the channel distorts transmitted signal with equal gain and linear phase.
- If the channel maximum delay spread τ_m is longer than the symbol duration, the fading is viewed as frequency-selective, otherwise, frequency-non-selective (flat).

In the case of frequency selective fading, the channel introduces ISI to the time domain transmitted symbol. An explanation in the frequency domain is that the transmitted signal's spectral components are affected by the channel in a different manner. Similar to (2.7), there is a reciprocal relation between the coherence bandwidth B_c and the maximum delay spread τ_m:

$$B_c \approx \frac{1}{\tau_m} \tag{2.9}$$

In a DS-CDMA system, all user signals that arrive at the receiver from the same basestation have passed through an identical complex channel with frequency selective fading. The complex time-varying FIR filter $h(\tau;t)$ with order L is a composite successive convolution of the transmitter filter, the mobile radio channel and the receiver filter; $h(\tau;t)$ is normally modeled as a wide-sense stationary uncorrelated scattering (WSSUS) zero-mean white Gaussian process as in [41]:

$$h(\tau;t) = \sum_{l=0}^{L-1} \alpha_l(t) e^{-j\phi_l(t)} \delta(\tau - \tau_l T_c) \tag{2.10}$$

where $\alpha_l(t)$, $\phi_l(t)$ and $\tau_l T_c$ are the attenuation factor, phase and the propagation delay of the l-th path, respectively. The envelope of each path $|h(\tau;t)|$ is faded independently according to a Rayleigh distribution and the phase is uniformly distributed over the interval $[0, 2\pi]$.

Instead of estimating the exact channel parameters like the attenuation factors and phases, we estimate only the in-phase and quadrature-phase components $Re[h_l(t)]$ and $Im[h_l(t)]$ as in [45]. These are two conceptually equal viewpoints on channel estimation. The definition of $h(\tau;t)$ can be rewritten as:

$$h(\tau;t) = \sum_{l=0}^{L-1} h_l(t) \delta(\tau - \tau_l T_c) \tag{2.11}$$

we further assume that $\sum_{l=0}^{L-1} E\left\{|h_l(t)|^2\right\} = 1$.

The UMTS Vehicular A channel model [46] is frequently used for BER evaluation in our simulation. The corresponding channel power delay profile is shown in Table 2.4.

Path Delay (nsec)	Avg. Power (dB)
0	0
310	-1.0
710	-9.0
1090	-10.0
1730	-15.0
2510	-20.0

Table 2.4: *Channel power delay profile of the UMTS Vehicular Channel A*

2.4.3 Receiver

In this subsection, we introduce the widely adopted Rake receiver for DS-CDMA. At the receiver, the received signal can be represented in an equivalent lowpass form as:

$$r(t) = \sum_{l=0}^{L-1} h_l(t) \sum_{k=1}^{K} \sqrt{E_k} \sum b_k^{(m)} s_k(t - mT - \tau_l T_c) + v(t) \tag{2.12}$$

where $v(t)$ is the complex-valued lowpass equivalent AWGN.

Since the symbol duration T is N times the chip period or the sample interval T_c, the received signal in (2.12) can be represented in an discrete form:

$$r(mN+n) = \sum_{l=0}^{L-1} h_l(mN+n) \sum_{k=1}^{K} \sqrt{E_k} b_k^{(m)} s_k(n - \tau_l) + v(mN+n) \tag{2.13}$$

where $0 \leq n \leq N-1$. The sampled input signal to the l-th Rake receiver finger is represented as:

$$r_l(mN+n) = h_l(mN+n) \sum_{k=1}^{K} \sqrt{E_k} b_k^{(m)} s_k(n) + \eta_l(mN+n) \tag{2.14}$$

In (2.14), $\eta_l(mN+n)$ accounts for a mixture of additive Gaussian noise, multipath interference

and multiple access interference (MAI).

We use $\hat{h}_l(mN+n)$ to denote the channel estimates, then the L resolved signals are multiplied by the complex conjugates of $\hat{h}_l(mN+n)$ and maximum ratio combined in the Rake receiver. Consequently, the output at the $mN+n$ sample interval can be represented as:

$$y(mN+n) = \sum_{l=0}^{L-1} r_l(mN+n)\hat{h}_l^*(mN+n) \tag{2.15}$$

Finally, despreading and demapping are performed on $y(mN+n)$ to recover the user data symbol. The block diagram of a Rake receiver is shown in Figure 2.5.

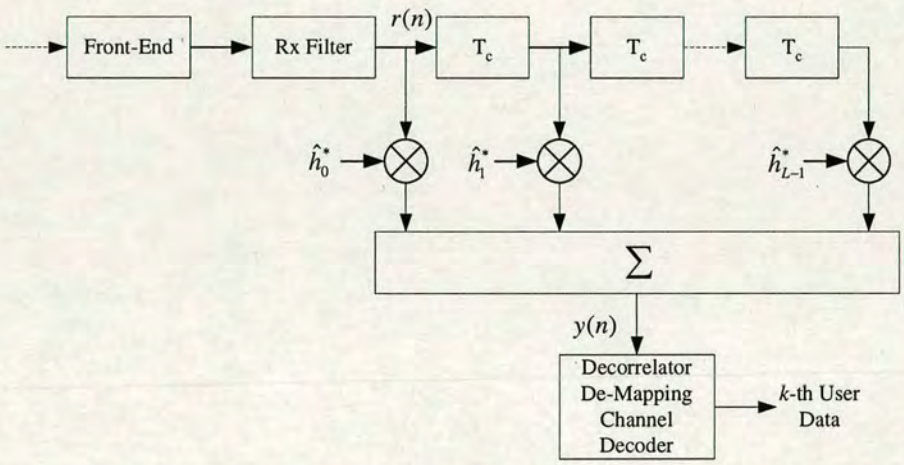

Figure 2.5: *DS-CDMA Rake receiver block diagram*

It has been shown that the Rake receiver performs very well for the single user scenario. However, it can be considered as a single user detection strategy since it ignores other users existence by treating the MAI caused by those users as Gaussian noise. It should be mentioned that the performance of a Rake receiver is dominated by the MAI.

2.4.4 Chip-Level Equalisation

Recently, receivers based on TDMA style channel equalisation at the chip level have been proposed for a WCDMA downlink to ensure adequate performance even with a high number of active users [47]. Chip-level equalisation is employed to reduce the interference and partially restore the orthogonality of the spreading codes at chip level. The spreading codes do not

explicitly appear in the equaliser; the chip-level equaliser require only knowledge of the desired user's spreading code and long code. The reasons for using chip-level equalisers are:

- In the downlink, all signals from the desired base station reach the mobile receiver through the same mobile channel. Therefore, the same equaliser applies to all mobile users from the same basestation.
- The computational complexity of the chip level equalisers is lower compared with other methods such as symbol-level equaliser [48] and multi-user detection [49] while offering acceptable system performance.

Although the symbol-level equalisation outperforms the chip-level equalisation [48], performing equalisation at symbol-level requires the spreading sequences to be short to ensure cyclostationarity of the MAI. This limits its application on the WCDMA downlink since WCDMA uses a long code with one frame (10 *ms*) period [50].

At the receiver, suppose using an equaliser that processing N_c chips at a time, we can describe the received signal vector as:

$$\mathbf{r}(n) = \mathbf{H}(n)\mathbf{x}(n) + \mathbf{v} \tag{2.16}$$

where $\mathbf{r}(n) = [r(n), r(n-1), \cdots, r(n-N_c+1)]^T$, $\mathbf{x}(n) = [x(n), x(n-1), \cdots, x(n-N_c-L-2)]^T$, $\mathbf{v}(n) = [v(n), v(n-1), \cdots, v(n-N_c+1)]^T$ and $\mathbf{H}(n)$ is an $N_c \times (N_c + L - 1)$ matrix defined by:

$$\mathbf{H}(n) = \begin{pmatrix} h_0(n) & \cdots & h_{L-1}(n) & 0 & \cdots & 0 \\ 0 & \ddots & \ddots & \ddots & \ddots & \vdots \\ \vdots & \ddots & \ddots & \ddots & \ddots & 0 \\ 0 & \cdots & 0 & h_0(n) & \cdots & h_{L-1}(n) \end{pmatrix}. \tag{2.17}$$

The linear MMSE chip level equaliser in the time domain is obtained by minimizing the mean squared error between the desired composite chip vector $\mathbf{x}(n)$ and the estimated composite chip vector obtained from the received signal $\mathbf{r}(n)$ and the equaliser tap coefficients $\mathbf{W}(n)$:

$$\mathbf{W}(n) = arg \min_{\mathbf{W}(n)} E\left[|\mathbf{x}(n) - \mathbf{W}(n)\mathbf{r}(n)|^2\right] \tag{2.18}$$

The solution to the estimation problem in (3.6) is given in (2.19) by:

$$\mathbf{W}(n) = \left[\sigma_d^2 \mathbf{H}^H(n)\mathbf{H}(n) + \sigma_n^2 \mathbf{I}\right]^{-1} \mathbf{H}^H(n) \tag{2.19}$$

where σ_d^2 is the variance of $\mathbf{x}(n)$, σ_n^2 is the noise variance and $(.)^H$ denotes *Hermitian transposition*. Subsequently, the estimate of the vector of the sum of all user's chips is given by:

$$\hat{\mathbf{x}}(n) = \mathbf{W}(n)\mathbf{r}(n) = \left[\sigma_d^2 \mathbf{H}^H(n)\mathbf{H}(n) + \sigma_n^2 \mathbf{I}\right]^{-1} \mathbf{H}^H(n)\mathbf{r}(n) \tag{2.20}$$

The Rake receiver can be considered as one kind of chip-level equaliser as well, using the above received signal model, it may be written as:

$$\hat{\mathbf{x}}(n) = \mathbf{H}^H(n)\mathbf{r}(n) \tag{2.21}$$

Note that in this formulation of the Rake receiver the combining of the different resolvable path is done before the despreading process.

Both the MMSE equaliser and the Rake receiver require explicit channel estimation. It is also possible to implement a MMSE equaliser using an adaptive filter that learns the coefficients via an adaptive process. One adaptive approach is to use the least mean square (LMS) algorithm with chips of a pilot channel as the reference signal [47]. However, it should be mentioned that the pilot chips are only an approximate reference signal for the adaptive equaliser in that the information of other users is not available at the receiver. The pilot channel trained equaliser will treat received data other than the pilot channel as noise so that the SNR in the adaptation is low and small step sizes are required. The LMS algorithms are relatively simple in terms of complexity but are relatively slow adapting to changes in the channel. Recursive least square (RLS) type algorithms have fast convergence and better tracking properties but are more complex. There are also other adaptation methods at chip-level such as Griffiths' algorithm, CR-MOE algorithm and Prefilter-Rake equaliser, etc which rely on channel estimation [47]. Linear MMSE equalisers were applied to multi-input multi-output (MIMO) systems in [51] [52]. Other than the linear equalisers, receivers with chip-level DFE for CDMA Downlink had been investigated in [53].

2.4.5 UMTS-FDD System Model

In 1998, WCDMA was selected as the UMTS terrestrial air interface scheme in ETSI. UMTS is capable of providing variable bit rates (144 kbps for vehicle speed, rural environment; 384 kbps for walking speed, urban outdoor; 2048 kbps for fixed, indoor environment) and different quality of service (QoS) for different connections. Variable transmission rates can be achieved by either changing the spreading factor or via multicode transmission. The multicode transmission is realized by orthogonal codes with variable spreading factors (OVSF). The frequency-division duplex (FDD) mode is based on pure DS-CDMA techniques while the time-division duplex (TDD) mode employs an additional TDMA transmission scheme [54] [55]. The FDD mode and TDD mode both operate in the 2 GHz band, with a basic chip rate of 3.84 Mcps and a flexible carrier spacing of 4.4-5.0 MHz. QPSK modulation is adopted and the same channelization code is used for both "I" and "Q" channels. This thesis will only focus on the UMTS FDD downlink transmission.

In the FDD downlink, the dedicated physical data channel (DPDCH) is combined by time multiplexing with the the dedicated physical control channel (DPCCH) to form the dedicated physical channel (DPCH) and transmitted by the dedicated channel (DCH, a transport channel). The general frame structure is shown in Figure 2.6. It can be seen that one frame with duration of 10 *ms* can be divided into 15 slots and each slot contains the time-multiplexed DPDCH and DPCCH.

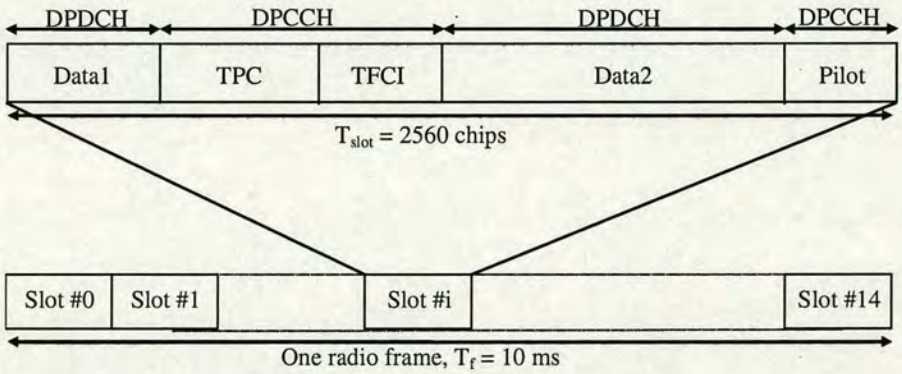

Figure 2.6: *Frame structure for downlink DPCH*

It should be mentioned that although the FDD mode adopts a similar slot time-wise mechanism as the TDD mode, it is not designed to separate different users but to allow the transmission of periodic functions such as transmit power control (TPC) signal and pilots, etc. The transport

format combination indicator (TFCI) is optional within one slot. A simplified block diagram summarised the basestation transmission model is shown in Figure 2.7.

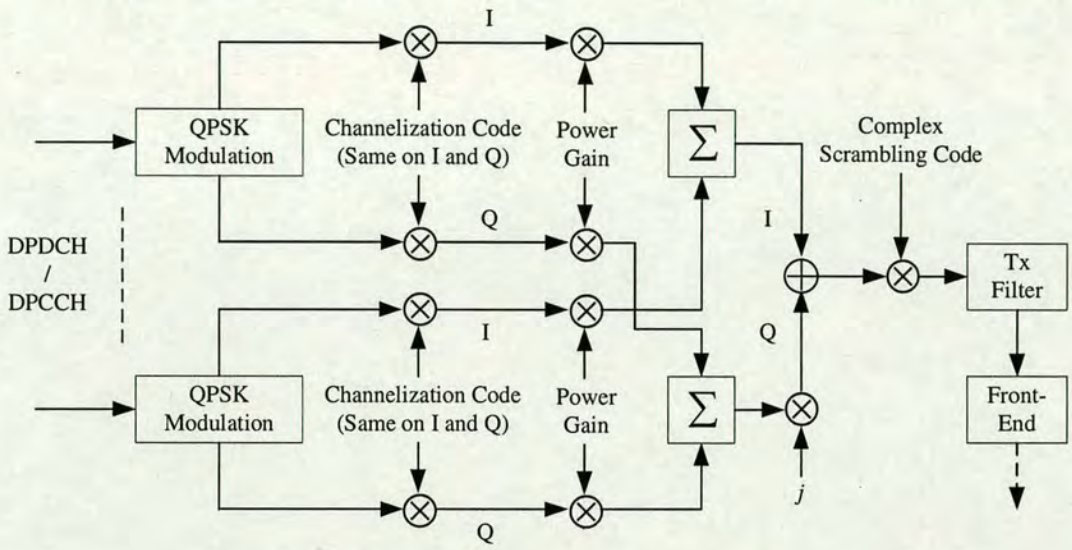

Figure 2.7: *Simplified downlink FDD transmission*

As shown in Figure 2.7, two types of chip rate code are used, scrambling code and channelization code. The scrambling code is a 38400 chip segment of a Gold code of length $2^{18} - 1$ according to the UMTS specifications and used for basestation separation. Root-raised cosine filters with a roll-off factor of 0.22 are used for pulse shaping.

In addition to the dedicated physical channels, other common physical channels are defined, e.g. Common pilot channel (CPICH), Common control physical channel (CCPCH) and Synchronisation channel (SCH), etc. In this thesis, only the CPICH will be discussed in detail since other common channels are not of concern to the receiver structures considered in this thesis. There are two types of CPICH, primary (P-CPICH) and secondary (S-CPICH). The P-CPICH has a fixed channelization code (all ones) and is scrambled by the primary scrambling code. It is broadcast over the entire cell and used as the phase reference for downlink channels. There is one and only one P-CPICH within one cell. The S-CPICH has an arbitrary channelization code and can be transmitted over whole cell or only part of it.

2.5 Single Carrier System with Frequency Domain Equalisation

For single carrier systems subject to frequency selective fading, normally a multiple tap complex time domain equaliser is required to combat ISI. A frequency domain equaliser is a low-complexity solution to this problem. For severe channel time dispersion, the complexity of the frequency domain equalisation processing grows slower compared with time domain processing. Numerous approaches for single-carrier systems with frequency domain equalisation have been proposed recently [23] [56] [57] [58] and these can be employed in MIMO systems [59] [60] [61]. The conventional SC-FDE adopts the same ISI absorbing mechanism as in OFDM; the repetition of the last data symbols in a block is inserted at the beginning of the block as a CP. Frequency domain equalisation is performed on a block of data, involving an efficient FFT operation and a simple channel inversion operation [23].

The SC-FDE provides comparable performance and computational complexity as an OFDM system [56] but avoids the inherent PAPR problem in OFDM and is less sensitive to carrier frequency offsets and phase noise. A block diagram of a conventional CP-based SC-FDE is shown in Figure 2.8. The length of the CP needs to be equal to or larger than the length of the channel impulse response so that interference from the previous block will be eliminated perfectly.

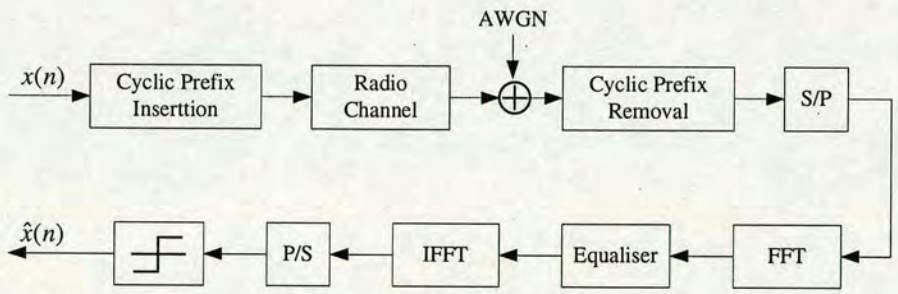

Figure 2.8: *System model of SC-FDE*

Employing a similar architecture as deployed in OFDM, the SC-FDE and OFDM can easily be configured to coexist, thus, this makes a multi-mode receiver architecture simpler.

Due to the advantages that SC-FDE offers, the communications industry has shown interest and as a consequence it has appeared in several different proposals for future standards, especially as an OFDM compatible solution in the IEEE 802.16 Wireless MAN (Metropolitan Area Network)

standardization process [62]. The comparison between SC-FDE and OFDM has been further investigated in MIMO scenarios [59]. The author concluded that MIMO-SC-FDE generally performs better than MIMO-OFDM in terms of the packet error rate (PER).

Recently, the cyclic prefix concept from OFDM was introduced into the conventional DS-CDMA system to enhance current single carrier 3G-system performance [63] [64] [65]. A CP-CDMA system has the advantage of a simple equalisation structure due to the inserted CP, hence, chip-level equalisation is even more attractive for such a system. In addition, recent research work reveals that a CP-CDMA system can achieve comparable system performance to MC-CDMA and it is more suitable for the uplink access [66] [67]. The CP-CDMA system will be dealt with in Chapter 6.

2.6 Varying Length Equaliser Structures

In this section, a short introduction to adaptive filters is given and then a review of the current approaches that are able to adjust filter length dynamically.

2.6.1 Adaptive Filters

Adaptive filter structure with its various applications have been investigated over the past few decades [68] [69] [70] [71]. Two types of filter structures, i.e. linear adaptive filters and non-linear adaptive filters, are generally considered depending on whether the input and output obey the principle of superposition. Compared with non-linear equalisers, the linear equaliser has a simpler structure and its computational complexity is much lower. However, on channels with deep nulls, the non-linear equalisers can perform much better than the linear ones since they can effectively solve the noise enhancement problem.

1. Linear Adaptive Filters

Two adaptive algorithms and their variants, i.e. the LMS algorithm and the RLS algorithm, have been widely adopted. Using a transversal filter structure, the output of the filter $y(n)$ is formed by the summation of all weighted input samples $\mathbf{x}(n) = [x(n), x(n-1), \cdots, x(n-N_c+1)]^T$ with filter tap coefficients $\mathbf{w}(n) = [w_0(n), w_1(n), \cdots, w_{N_c-1}(n)]^T$:

$$y(n) = \mathbf{w}^H(n)\mathbf{x}(n) = \sum_{k=0}^{N_c-1} w_k^*(n)x(n-k) \tag{2.22}$$

The LMS algorithm is an approximation of the steepest decent method by using the instantaneous estimate of the autocorrelation matrix and the crosscorrelation matrix. It is based on the MSE criterion and can be summarised as follows:

- Filtering:

$$y(n) = \mathbf{w}^H(n)\mathbf{x}(n)$$

- Calculating error signal:

$$e(n) = d(n) - y(n)$$

  where $d(n)$ is the desired output at time instant n.

- Updating tap coefficients:

$$\mathbf{w}(n+1) = \mathbf{w}(n) + \mu\mathbf{x}(n)e^*(n)$$

  where μ is the step-size that will affect the convergence rate of the filter and ensure the stability of the algorithm.

The RLS algorithm is based on the least square criterion. In contrast to the LMS approach, it tries to find the solution $\mathbf{w}(n)$ that minimizes the sum of error squares for a particular duration rather than using only the current tap-input samples. The procedure for the RLS is summarised as follows:

- Initialising: (ρ is a small positive constant)

$$\mathbf{w}(0) = \mathbf{0}, \mathbf{R}^{-1}(0) = \rho^{-1}\mathbf{I}$$

- Computing error:

$$e(n) = d(n) - \mathbf{w}^H(n)\mathbf{x}(n)$$

- Computing Kalman gain vector:(β is the forgetting factor)

$$\mathbf{k}(n) = \frac{\mathbf{R}^{-1}(n-1)\mathbf{r}(n)}{\beta + \mathbf{r}^H(n)\mathbf{R}^{-1}(n-1)\mathbf{r}(n)}$$

- Updating inverse of the correlation matrix:

$$\mathbf{R}^{-1}(n) = \frac{1}{\beta}\left(\mathbf{R}^{-1}(n-1) - \mathbf{k}(n)\mathbf{r}^H(n)\mathbf{R}^{-1}(n-1)\right)$$

- Updating tap coefficients:

$$\mathbf{w}(n+1) = \mathbf{w}(n) + \mathbf{k}(n)e^*(n)$$

The computational complexity of the RLS algorithm is much higher than the LMS algorithm, however, it shows a faster convergence property compared to the LMS algorithm.

2. Non-Linear Adaptive Filters

The most commonly used non-linear equalisers are the maximum likelihood sequence estimator (MLSE) and the DFE. The MLSE is optimum from the viewpoint of error probability. Since it tests all the possible transmitted sequences and chooses the symbol sequence with the maximum likelihood as the output, the computational complexity is relatively high and it depends on the length of the channel delay spread. The high computational complexity of the MLSE makes it impractical for systems where the ISI spans a large number of symbols. The DFE is alternatively a reasonable compromise with suboptimal performance.

A DFE consists of two transversal filters, the feedforward filter (FFF) and the feedback filter (FBF). The input to the FFF is the received signal samples and the input to the FBF is a sequence of the previously detected symbols. In practical systems, the equalisers are required to have finite length which will introduce some residual ISI that can not be eliminated. This is due to the MSE criterion, eliminating the ISI without excessively enhancing the noise. The feedback section executes to further eliminate the residual ISI caused by the past transmitted symbols.

The output of the DFE can be expressed as:

$$y(n) = \sum_{k=-(N_1-1)}^{0} w_k^*(n)x(n+k) + \sum_{k=1}^{N_2} w_k^*(n)\tilde{y}(n-k) \tag{2.23}$$

where $\tilde{y}(n-1), \cdots, \tilde{y}(n-N_2)$ are the previously detected symbols. The coefficients of both filters can be combined into one vector $\mathbf{w}(n) = [w_{-(N_1-1)}(n), \cdots, w_0(n), w_1(n), \cdots, w_{N_2}(n)]^T$ and be jointly adapted. The LMS algorithm for the DFE takes the form:

$$\mathbf{w}(n+1) = \mathbf{w}(n) + \mu \mathbf{q}(n) e^*(n) \tag{2.24}$$

where $\mathbf{q}(n) = [x(n-N_1+1), \cdots, x(n), \tilde{y}(n-1), \cdots, \tilde{y}(n-N_2)]^T$, including both the input to the FFF and the FBF. The main drawback of the DFE is error propagation due to incorrect detection on previous symbols. Failure to feed back correct detected symbols will have negative impacts on the system performance, especially when the SNR is low.

2.6.2 Varying Length Equalisers

Basic principles of the adaptive filters have been presented in the above subsection. The step-size and the filter length are two important parameters in an adaptive filter. In this thesis, we only concentrate on adjusting the equaliser length.

In practical mobile communications, the optimum length is unknown to the receiver since it is dependent on the channel. The importance of equaliser length had been examined in [72] [73] [74]. Often, increasing the equaliser length, a lower minimum MSE level is achievable. Choosing a short equaliser length can not fully realise the potential of its ISI elimination ability. However, the advantages of using an equaliser length beyond a certain length is marginal for most mobile communication systems, especially when the SNR is low. On the other hand, due to misadjustment [71] for LMS filters may cause, longer length may introduce more adaptation noise which then increase the MSE level [75]. Additionally, adopting longer length, the convergence rate of the equaliser may be reduced and the computational complexity is also increased. Therefore there is a demand of searching for an 'optimal' length that can achieve a good compromise between system performance and computational complexity.

The varying length filter was first studied in [76], here the author aimed to improve the convergence rate of the adaptive filter by adjusting filter length. In recent years, the topic of equaliser length adjustment was revisited and investigated in [77] [78] [79] [75] [80].

1. Segmented Filter (SF) algorithm

The segmented filter algorithm was proposed in [77]. In this approach, an equaliser was divided

into L_s segments with L_t taps per segment. The structure of the equaliser is shown in Figure 2.9: As can be seen in Figure 2.9, each segment in the transversal filter produces one equalised

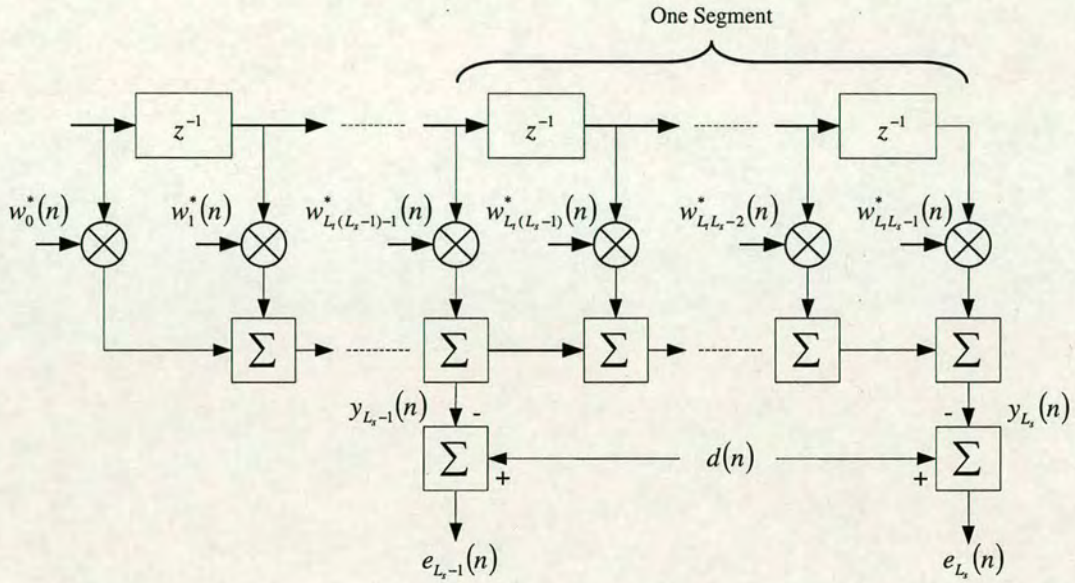

Figure 2.9: *Segmented equaliser structure, L_s segments with L_t taps per segment*

symbol $y_k(n)$, $k \geq 1$, and hence one error signal $e_k(n)$ is defined by:

$$e_k(n) = d(n) - y_k(n) \tag{2.25}$$

where $d(n)$ is the desired symbol at time instant n. Further define the accumulated squared error (ASE) of each segment as:

$$ASE_k(n) = \sum_{i=1}^{n} \beta^{n-i} |d(n) - y_k(n)|^2 \tag{2.26}$$

where $0 < \beta \leq 1$ is a forgetting factor. The basic idea of the SF algorithm is to detect the segment at which the difference between neighboring ASE is trivial. Assuming there are initially L_s segments in the equaliser, the SF algorithm can be summarised as follows:

- Calculate $ASE_{L_s-1}(n)$ and $ASE_{L_s}(n)$
- If $ASE_{L_s}(n) \leq \alpha_{up} ASE_{L_s-1}(n) \Longrightarrow$ Add one segment, i.e. add L_t taps, to the equaliser

- If $ASE_{L_s}(n) \geq \alpha_{down} ASE_{L_s-1}(n) \Longrightarrow$ Remove one segment, i.e. remove L_t taps, from the equaliser

This algorithm continuously calculates $ASE_{L_s-1}(n)$ and $ASE_{L_s}(n)$ for each iteration. The two parameters α_{up} and α_{down} are chosen in the following range:

$$0 < \alpha_{up} \leq \alpha_{down} \leq 1 \tag{2.27}$$

The closer they are to 1, the more frequently the length will change. When one extra segment is added to the equaliser, the taps in this new segment are initialized to zero and when one segment is removed, all the remaining taps maintain their value and the last but one segment becomes the last segment.

2. Gradient Descent (GD) algorithm

In [79], the author presented a length adjustment algorithm that can change the equaliser length along the negative gradient direction of the squared error. Denoting the equaliser tap coefficients and the input at time instant n as $\mathbf{w}_{L(n)+\triangle}(n) = [w_0(n), w_1(n), \cdots, w_{L(n)+\triangle-1}(n)]^T$ and $\mathbf{x}_{L(n)+\triangle}(n) = [x(n), x(n-1), \cdots, x(n-L(n)-\triangle+1)]^T$ where $L(n)$ is the equaliser length and $\triangle$ is an integer constant. An error signal $e_{L(n)}(n)$ is generated by the equaliser with $L(n)$ tap coefficients:

$$e_{L(n)}(n) = d(n) - \mathbf{w}^H_{L(n)}(n)\mathbf{x}_{L(n)}(n) \tag{2.28}$$

The transient gradient of the squared error at time instant n is given by:

$$\nabla J_{L(n)}(n) = \frac{\partial \left(e_{L(n)}(n)\right)^2}{\partial L(n)} = -\frac{1}{\triangle} e_{L(n)}(n)\mathbf{w}'^H_{2\triangle}(n)\mathbf{x}'_{2\triangle}(n) \tag{2.29}$$

where $\mathbf{w}'_{2\triangle}(n)$ and $\mathbf{x}'_{2\triangle}(n)$ consists of the last $2\triangle$ elements of $\mathbf{w}_{L(n)+\triangle}(n)$ and $\mathbf{x}_{L(n)+\triangle}(n)$, respectively.

The length of the equaliser is updated every T_t samples along the negative direction of the smoothed gradient $\bar{\nabla} J_{L(n)}(n) = \frac{1}{T_t}\sum_{i=n-T_t+1}^{n} \nabla J_{L(i)}(i)$ as:

$$L(n+1) = L(n) - \delta sign\left(\bar{\nabla} J_{L(n)}(n)\right) \tag{2.30}$$

where $\delta < \triangle$ is an integer constant increment.

3. Fractional Tap-length (FT) algorithm

The optimum tap-length in terms of achieving good trade-off between MSE and complexity is clearly defined in [75]. In [80], the author compared the advantages/disadvantages of the above two schemes and proposed an improved algorithm. The new approach gives the length adjustment more freedom by relaxing the constraint that the tap-length must be an integer. The tap-length of the equaliser can be treated as an integer plus a fractional value, however, will only be updated when the "fractional" part accumulates to larger enough.

Define $L_f(n)$ as the tap-length with a fractional part, as in [80] we control the length as:

$$L_f(n+1) = (L_f(n) - \alpha_f) - \delta\left(\left(e_{L(n)}(n)\right)^2 - \left(e_{L(n)-\triangle}(n)\right)^2\right) \tag{2.31}$$

where α_f is the leaky factor used to prevent $L_f(n)$ from increasing to an undesirably large value [75]. Unlike (2.30), the step size δ in (2.31) can take fractional values. The actual tap-length $L(n)$ is updated to $L(n+1) = round\left(L_f(n)\right)$ if and only if $|L(n) - L_f(n)| \geq \epsilon$ where ϵ is a small predefined threshold, otherwise, $L(n+1) = L(n)$.

2.7 A Potential Multi-mode OFDM Receiver

In this section, a study of the convergence of several complementary wireless access networks, namely DAB, DVB-T and HIPERLAN-2 and suggests a possible physical layer architecture for a suitable multi-mode terminal. Sampling rate adaptation is the major concern in this section. By using a fixed system clock, a SRC scheme based on Sigma-Delta modulation and linear interpolation is proposed for the multi-mode receiver. Moreover, a new receiver architecture combining SRC and symbol synchronisation is suggested. Simulation result shows that the three OFDM systems can use a single system clock effectively.

2.7.1 Sampling Rate of DVB-T/DAB/HIPERLAN-2

In a multi-mode digital communication receiver, it is required that the terminal must be able to handle various communications standards. When comparing the architectures of the aforementioned three standards, it is quite obvious that a strong resemblance among their receiver architectures exists. This implies that a multi-mode receiver could be implemented with less hardware expense if those commonalities are fully exploited. Generally, different chip/sample/symbol

rates are specified in different standards. An obvious simple solution is to adopt a different dedicated clocks for different standards. However, it seems to be costly and cumbersome, and the receiver size will be greatly enlarged with the increasing of standard numbers. The three systems deploy three different sampling rates, 64/7 = 9.1428571 MHz for DVB-T, 2.048 MHz for DAB and 20 MHz for HIPERLAN-2, respectively. Sampling rate adaptation is the first key issue to be considered for a multi-mode receiver even before synchronisation. Since the sampling rate of HIPERLAN-2 is the highest among the sampling rates of the three investigated standards, a possible solution for this sampling rate conversion problem might be based on the over-sampling of HIPERLAN-2 and then approximating sample data or sampling instants for DAB and DVB-T. The reason for doing so is twofold,

1. 20 MHz is the highest signalling rate among the targeted systems; the multi-mode receiver should be able to handle the highest signalling rate system;

2. No fractional SRC is required for the HIPERLAN-2 system except a simple decimation process.

In this section, the sampling rate relationship of the three standards is illustrated. First, the DVB-T 2k mode is considered. There are 2048 sub-carriers in the DVB-T 2k mode, with T_u (useful symbol duration) = 224 μs and CP interval $T_{CP} = 1/4\,T_u = 56\,\mu s$. The OFDM symbol duration is equal to 224 + 56 =280 μs which exactly consists of $280/0.05 = 5600$ samples while sampled at the frequency of 20 MHz (Sampling rate of the HIPERLAN-2). To make it more meaningful, consider this example. When the starting position of an OFDM symbol is given, assuming that it is the 0-th sample, and then by sampling at 20 MHz, the 5599-th sample will be the last sample of one DVB-T symbol. Not caring about the exact alignment of every sample at this first stage, these 5600 samples contain the full information of a DVB-T symbol. In addition, the starting/ending position of the CP and the useful OFDM symbol can also be determined. Using the new sampling rate, although not every sample within the OFDM symbol is exactly aligned, due to the special relationship between the CP and the useful OFDM symbol, the coarse timing synchronisation can still be realized. The ratio of the sampling rate of HIPERLAN-2 and the sampling rate of DVB-T is 20/(64/7)=2.1875. While sampling the received DVB-T signal at 20 MHz we notice that 0.1875 multiplied by 16 results in an integer; the 16-th DVB-T sample will coincide with the 35-th new sample (sampled at 20 MHz). The boundary of one useful DVB-T OFDM symbol can now be expressed by means of the new samples (sampled at 20 MHz). When sampled at $16 \times 20 = 320$ MHz, which

is 35 times (320/(64/7) = 35) the sampling rate of the DVB-T system, exact samples of the DVB-T system can be collected from the new samples after 35 times decimation. Now let us consider the DAB system case. Mode I in DAB uses 2048 sub-carriers with a sampling rate of 2.048 MHz. When 320 MHz is deployed as the sampling rate of the new system, a DVB-T system will be sampled at a sufficient rate. Consequently, for a DAB system, since 320 MHz is 156.25 times the sampling rate of the DAB system, every 4th DAB sample will happen to coincide with the 625th new sample. The boundary of the useful DAB OFDM symbol can also be expressed by means of the new samples (sampled at 320 MHz). Coming to this, a simple SRC via interpolation and decimation can produce the required DAB symbols from the new samples.

2.7.2 Timing Adjustment by Interpolation

From the previous discussion, it can be concluded that using 320 MHz as a new sampling rate for this particular multi-mode OFDM receiver is a pretty good decision. However, 320 MHz is a very high frequency for a mobile terminal when power consumption is considered.

Interpolation technique, a timing-adjustment operation on the received signal, has already been deployed in digital modems successfully [81] [82]. The fixed free running sampling clock remains independent of the symbol timing. The sample times never coincide perfectly on desired instants. Assume that the received signal $x(t)$ is band limited and being sampled at a rate $1/T_s$. After 'virtually' (*virtually* because actually no analogue signal has been produced) reconstructing the received signal, resample the continuous time output of the interpolating filter $y(t)$ at time instants $t = T$ where $1/T$ is the sampling rate specified in the standard. There is no attempt to recover the continuous analogue signal; what is of interest is the sample value at the very time instants $t = kT$. The new time instant $t = kT$ can be represented by T_s in the form:

$$t = kT = (m_k + \mu_k)T_s \tag{2.32}$$

where $m_k = int[kT/T_s]$, the integer part of kT/T_s means the largest integer less than or equal to kT/T_s and $\mu_k = kT/T_s - m_k$ is a fractional difference. Only the samples at time instants $t = kT$ are required for further processing. The interpolants (new samples) can be calculated

as in [81] by:

$$y(kT) = y\left[(m_k + \mu_k)T_s\right] = \sum_{i=I_1}^{I_2} x\left[(m_k - i)T_s\right] h_I\left[(i + \mu_k)T_s\right] \tag{2.33}$$

where $x(t)$ is a sequence of signal samples taken at intervals T_s, and $h_I(t)$ is the finite-duration impulse response of a fictitious, time-continuous, analogue interpolating filter. $\{I_1T_s, \cdots, I_2T_s\}$ is the area that the interpolating filter operates on. An ideal interpolation filter is a *sinc* function $h_I(t) = \frac{Sin\pi t/T_s}{\pi t/T_s}$ with a transfer function:

$$H_I(f) = \begin{cases} T_s & , \ |f| \leq 1/2T_s \\ 0 & , \ |f| > 1/2T_s \end{cases} \tag{2.34}$$

Practically, a linear interpolator is adequate and efficient if the samples are closely spaced. Hence, in a discrete form,

$$y(k) = (1 - \mu_k)x(m_k) + \mu_k x(m_k + 1) = x(m_k) + \mu_k\left[x(m_k + 1) - x(m_k)\right] \tag{2.35}$$

2.7.3 Proposed Multi-mode Receiver Architecture with Sigma-Delta Modulation

Sigma-Delta modulation is the most popular form of the noise-shaping quantization that uses oversampling and 1-bit quantization. A mathematical explanation of the Sigma-Delta data converters can be found in [83]. In principle, a Sigma-Delta A/D converter consists of two functional blocks: a Sigma-Delta modulator and a decimator. The Sigma-Delta data converter has the advantage of requiring less restrictive anti-aliasing filters by benefiting from the high sampling rate in the modulation process; the anti-alias filter requirements are relaxed.

For a multi-mode DVB-T/DAB/HIPERLAN-2 receiver, when sampled at the integer multiple of 20 MHz (sampling rate of HIPERLAN-2), the new sampling rate (40 MHz, 60 MHz, 80 MHz...), the fractional interval μ_k will cyclically repeat a finite set of values. These fractional intervals μ_k and the integer value m_k in (2.35) can be computed in advance, stored in ROMs and loaded when necessary. We assume perfect synchronisation here; otherwise, fractional intervals need to be corrected on-line due to the synchronisation offsets.

Generally, an OFDM system achieves symbol synchronisation by adjusting the FFT position, including coarse synchronisation and fine synchronisation. The coarse synchronisation can be

done by some CP based approaches [84]. After coarse symbol synchronisation, the residual timing offset will be estimated though pilots and then be compensated.

The fractional timing offset is required to be quantized into L_i uniform intervals where L_i is the integer part of the oversampling ratio. Consequently, it is now easy to adjust the starting instant of an OFDM symbol by fractional offset for the fine symbol synchronisation purpose, which is not a simple task for conventional OFDM receivers. A new multi-mode OFDM receiver architecture is proposed in Figure 2.10. In an ideal case there is no sampling frequency offset. Based on our knowledge of the sampling rate of the three different systems, the known coefficients μ_k and m_k in (2.35) can be stored in memory and loaded into the SRC process when needed (shown by ① in Figure 2.10). Unfortunately, using a free running clock, the

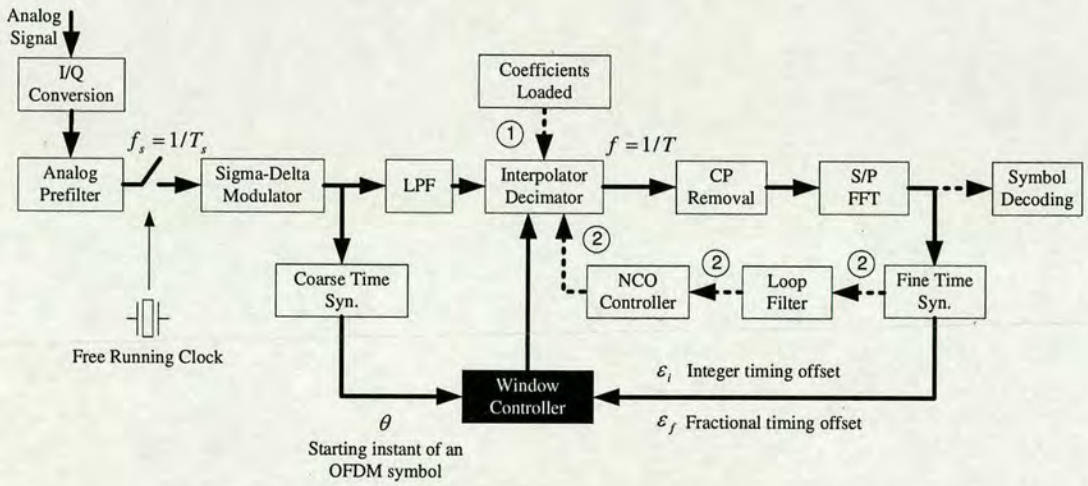

Figure 2.10: *Proposed multi-mode OFDM receiver architecture*

sampling frequency error (the clock used in the transmitter may not be exactly identical to that used in the receiver) is inevitable. Conventional OFDM receivers adopt feedback using a voltage-controlled oscillator (VCO) to adjust the sampling frequency. In the case of the sampling frequency error impairment, all computations need to be performed on line and no extra memory for storing coefficients is required. Alternatively, a numerically controlled oscillator (NCO) controlled interpolator was investigated in [81]. In practice, after the fine time synchronisation process, the output ε ($\varepsilon = \varepsilon_i + \varepsilon_f$, ε_i: integer offset and ε_f: fractional offset) is fed back to the NCO controller, which is responsible for determining μ_k and m_k, and making that information available to the interpolator. Since the fine symbol synchronisation can be done

symbol by symbol only, thus, the coefficients μ_k and m_k will be only updated once per OFDM symbol. The above discussion are based on the assumption that the sampling frequency offset is small; otherwise, the drift between ideal and true sample points will be significant for the 8k mode. In that case, the clock rate needs to be adjusted for sampling rate offset, or timing offset, μ_k and m_k, will need to be changed linearly.

For the sake of convenience, attention is paid to the timing recovery process, which is closely related to the SRC while the frequency synchronisation blocks are left out in the architecture. In the first stage, the received signal is down converted to baseband and the complex baseband signals are generated. By passing the analogue pre-filter, the useful signals are band limited. The analogue input signals are then sampled at the sampling frequency, which is much higher than its signalling rate. According to the receiver structure, signals sampled at high frequency are pushed to a Sigma-Delta modulator and then, a low pass filter (LPF) preceding the interpolation and decimation block is used for anti-aliasing purpose and quantization noise attenuation. Before the interpolation and decimation block is working, the receiver works under the coarse symbol-acquiring mode. As has been stated, the symbol starting instant θ can be coarsely determined by the CP based pre-FFT approaches, thus the starting position of an OFDM symbol and the FFT window position can be determined and set. In this stage, the feedback loop from the post-FFT fine symbol synchronisation is switched off. The window controller uses the information provided by the coarse symbol synchronisation to adjust the starting position for the interpolation and decimation block, which strictly speaking is an interpolation based decimation process.

The sampling clock frequency error Δ_f will cause inter-carrier interference (ICI) and furthermore, a drift in the symbol timing [85]. Nevertheless, in most cases, the sampling frequency offset is very small compared with the high sampling frequency, the ICI caused can be considered as additional noise and the feedback loop in the receiver may be used to periodically compensate for the drift, either integer or fractional. Via ① in Figure 2.10, the pre-stored μ_k and m_k will be loaded into the interpolation based decimator for linear interpolation or polynomial interpolation processing, etc. The sampling rate of the output is approximate to the targeted system signalling rate $1/T$ and post-FFT fine symbol synchronisation is now carried out. Since each different system has its own offset estimation mechanism, we will not focus on every detail (the DVB-T system, for example, examines the phase rotation on pilots to estimate the averaged timing offset). The averaged residual timing offset ε consists of the integer part

ε_i and the fractional part ε_f, both of them will be fed back to the window controller to adjust the symbol position. Since the fractional timing offset can also be compensated via the interpolation based decimation block by shifting quantized fractional samples, which are integer samples with respect to the high sampling rate, the residual timing error will remain comparatively small. In addition, the accumulating timing error due to sampling frequency error can be compensated by the feedback from the error estimation every OFDM symbol.

Alternatively, the NCO control method could be an efficient approach in providing the information of $\{\mu_k, m_k\}$ figured out from the output of the fine symbol synchronisation process (see ② in Figure 2.11). Figure 2.11 shows the performance of a multi-mode receiver with different sampling rates deployed in the Sigma-Delta modulation block. The MSE of the uncoded data in the frequency domain against E_b/N_0 is plotted, a DVB-T receiver is considered in the simulation. Only the impact of linear interpolation based on the Sigma-Delta modulation output

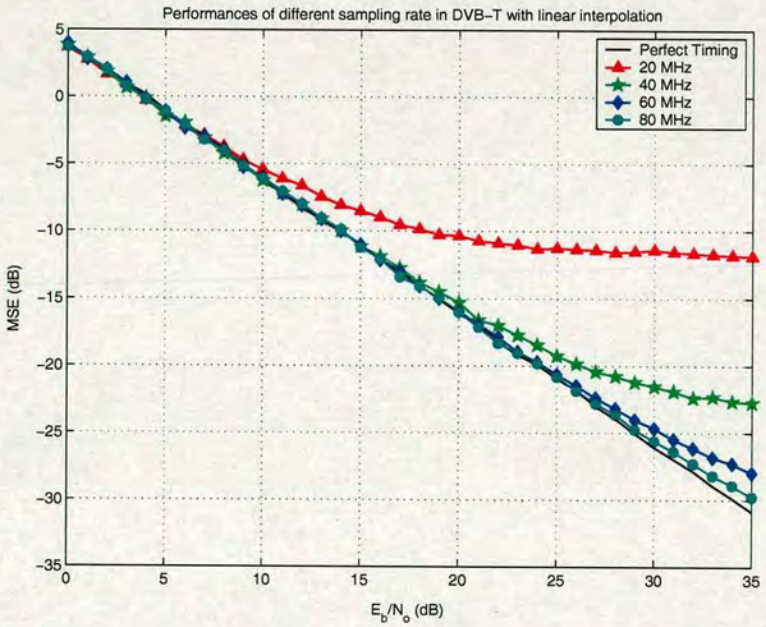

Figure 2.11: *Performances of different sampling rate in DVB-T with interpolation*

at different sampling rates (20 MHz, 40 MHz, 60 MHz and 80 MHz) and the perfect timing case in a DVB-T system is studied while the DAB system is not considered. The reason for this is that the sampling rate of DVB-T is up to 4 times higher than the sampling rate of DAB, so that if a sampling rate is selected that is suitable for DVB-T, then it should with no doubt also be suitable for DAB in terms of using linear interpolation. As can be seen in Figure 2.11, for a DVB-T system, 40 MHz can be chosen as the best compromise between the system perfor-

mance and hardware expense. If it is possible to have higher sampling frequency with not too much power consumption, this will definitely improve the system performance and also enable a fractional spaced equalisation (FSE) which is not sensitive to sample timing.

2.8 Summary

In this chapter, a brief background introduction necessary for the following chapters has been provided. This includes the basic principles of OFDM, spread spectrum systems, adaptive filter theory and single carrier systems with frequency domain equalisation. The basic idea of chip-level equalisation and various varying length filter structures was reviewed. It is indicated that the conventional Rake receiver treats MAI from other users as additive Gaussian noise, therefore, suffers great performance degradation in a highly loaded scenario. Chip-level equalisers can process the 'summed' received signal and achieve better performance than Rake without knowing the spreading sequences of other users. Compared with the multiuser detector and the Rake, chip-level equaliser offers a good balance between computational complexity and system performance; it becomes a promising solution for the DS-CDMA downlink. With the requirement of frequency domain processing for OFDM systems, implementing chip-level equalisation in the frequency domain fits the multi-mode receiver context, this will be the main content of Chapter 3 and part of Chapter 4.

This chapter also presents a study on the issues concerning the convergence of DAB, DVB-T and HIPERLAN-2 and suggests a possible architecture for a suitable multi-mode terminal. Sigma-Delta modulation and linear interpolation are deployed in the receiver for sampling rate adaptation purposes. A new sampling rate is adopted in the multi-mode receiver, which is a integer multiple of 20 MHz (the sampling rate of HIPERLAN-2). A new proposed structure can integrate the three OFDM based systems by a single system clock effectively and in addition, bring advantages to symbol synchronisation of the OFDM systems. Since the other standards (DAB & UMTS) have lower sample rate requirements than DVB-T, 40 MHz would appear a good initial choice.

Chapter 3
CPICH Based Frequency Domain Equalisation for WCDMA Systems

In this chapter, a chip-level MMSE frequency domain equaliser is investigated for the downlink FDD mode in UMTS. The MAI and inter-chip interference is reduced at the chip level before despreading. The P-CPICH in FDD mode carries a higher power than dedicated channels and is utilized for approximate cyclic reconstruction. Since the secondary CPICH does not appear in this study, the word 'CPICH' is used to refer to the primary CPICH. Comparison of the proposed algorithm and other current approaches is presented. Furthermore, it also describes a CPICH interference cancellation structure. Performance of the proposed MMSE-FDE is shown by computer simulations.

This chapter is organized as follows: In Section 3.2, the proposed algorithm is described, followed by a description of the receiver structure. Section 3.3 will deal with the high-power CPICH interference cancellation problem. Simulation results are given in Section 3.4. Finally, conclusions are presented.

3.1 Introduction

OFDM is an air-interface technology used for both current broadcasting and WLAN applications and is a strong candidate for future 4G mobile wireless systems [28]. In many of the discussions regarding 4G communication systems the assumption is that multi-mode terminals will be required, i.e. receiver architectures that are capable of operating in multiple modes and multiple frequency bands [86]. There is a demand for the design of a multi-mode receiver which is capable of handling the OFDM based standards and UMTS. There are already discussions on the coverage and throughput analysis for the integrated system [87]. The OFDM based WLAN standard also specifies a flexible radio access network that can be used with a variety of core networks, including UMTS. It is likely that WLAN will become an important complementary technology to 3G cellular systems, therefore, a multi-mode WLAN & UMTS

receiver is of great interest. To employ a frequency domain equaliser for UMTS in the receiver, making use of the powerful FFT/IFFT for both DS-CDMA and WLAN system in the handset is very attractive. For the reception of the UMTS-FDD downlink signal in a multi-mode receiver, the capability to perform multi-user detection in mobile handsets can require high complexity. The performance of conventional Rake receivers is dominated by the MAI and this can result in a high error rate in a heavily loaded system. Performing equalisation at the symbol-level requires the spreading sequences to be short to ensure cyclostationarity of the MAI. Receivers based on TDMA style channel equalisation at the chip level have been proposed for WCDMA downlink to ensure adequate performance even with a high number of active users [47]. This is shown to be a reasonable approach that achieves a good compromise between receiver complexity and system performance. The received chip waveform, distorted by the multi-path channel, is equalised prior to de-spreading. Orthogonality of the signals from the basestation is restored at chip-level. The restoration can be quantified by an orthogonality factor as described in [88] [89].

Recently, the SC-FDE has been attracting increasing interest [23] [56] [57]. Most of them use the same mechanism as in OFDM, i.e. a cyclic prefix is inserted to mitigate the ISI and make the channel matrix a circular one in order to simplify the receiver. The importance of the CP insertion is twofold; Firstly, the CP with enough length can effectively mitigate interference from the preceding block. Secondly, it is because of the preceding CP that the channel distortion on the transmitted signal becomes a circular convolution process. It is worth mentioning that only in this case (or with zero-padding) can the distortion of the channel be considered as a multiplication in the frequency domain. Unfortunately, the CP-based FDE is not compatible with the current WCDMA system because the CP insertion will inevitably destroy the frame structure and it is incompatible with the standard.

It is desirable to design a receiver without changing the transmitted signal. One possible solution has been proposed for an OFDM system without CP in [90], namely the residual inter symbol interference cancellation (RISIC) algorithm. In the RISIC algorithm, the missing CP is regarded as bursty distortion in a time domain block and the amount of distortion is diminished in an iterative process with hard decision being made in the frequency domain. In [91], the RISIC algorithm is extended with a soft decoder for the FEC incorporated. However, no hard/soft decisions can be made in the frequency domain at the chip-level in a multi-user system and additionally the RISIC is an iterative process which may result in severe delay in the

system.

In this chapter, a new FDE is proposed and investigated which will not change the format of the UMTS transmitted signal. The proposed algorithm utilizes the primary common pilot channel which in the UMTS FDD mode is transmitted for channel estimation and training purposes. The CPICH carries the highest power and dominates the interference experienced at the user equipment (UE). User data could be treated as an independent signal and the aggregation will be considered to be an additive noise on the high power CPICH [92]. Therefore, the CPICH can be used for cyclic reconstruction in the FDE. Although this may lead to degradation in system performance due to approximate reconstruction, simulation results show that it is still bearable because of the spreading gain and the use of overlap-cut technique to further reduce errors.

3.2 Overlap-Cut Algorithm

Originally, the "overlap-save" method [93] was used to calculate linear convolution via circular convolution and it was adopted to implement the block LMS algorithm in the frequency domain [94] [95]. The overlap-save method is one way of using FFTs to produce the linear convolution of two data sequences.

In [96] [97] [98], the authors proposed new approaches to apply the FDE in the downlink of broadband CDMA system without redundancy which they call the overlap-cut method. The overlap-cut method is displayed in Figure 3.1. FFT and IFFT operations are applied on a signal

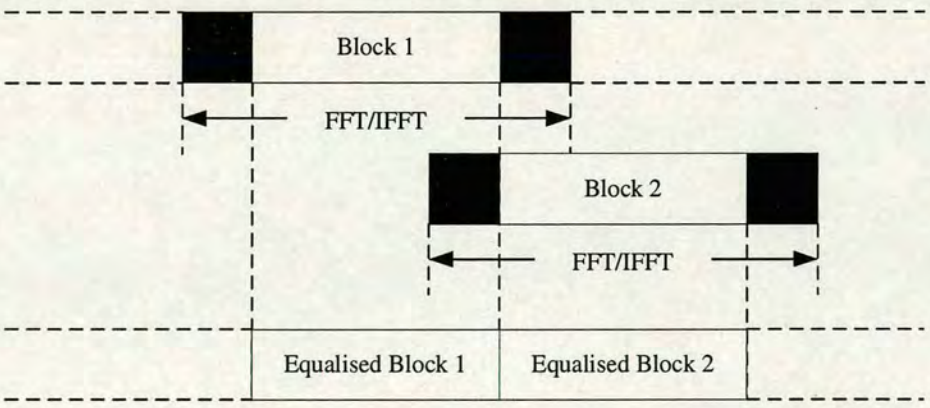

Figure 3.1: *Overlap-Cut method*

block which overlaps with the previous block and the successive block by the shadow area. As has been stated in [96] [97] [98], applying a conventional FDE on a single carrier system without CP gives errors that are significantly larger at the edges of the block. Therefore samples at the beginning and the end of each equalised blocks can be discarded.

This algorithm works well with a long length FFT, but for WLAN only a 64 point FFT/IFFT is used, hence the performance degradation will be significant in some cases. Comparisons between the new method and the overlap-cut algorithm (i.e. without cyclic reconstruction) are given in this thesis. It is noteworthy that better channel estimates can be obtained with higher power CPICH. Simulation results show that the system performance can be improved by the reconstruction of the CP. Furthermore, a CPICH interference cancellation scheme is proposed, thus, after being used for effective channel estimation and equalisation, the interference due to the high power CPICH can be canceled.

3.3 CPICH Based Cyclic Reconstruction

In the UMTS FDD mode, the CPICH signal is continuously transmitted from each base station. This channel is spread by the scrambling code and plays a vital role in the cell searching of mobile station and channel estimation. The CPICH is likely to carry the highest power for effective communication to be established and will result in the most interference experienced at the UE. Thus the CPICH signal can be utilized for approximate cyclic reconstruction. As stated before, a better channel estimate can be achieved with a higher power CPICH, thus, our method will outperform the overlap-cut algorithm in terms of bit error ratio performance with imperfect channel estimation. User data is treated as an independent signal and is considered as an additive noise on the high power CPICH.

In the new FDE, the received discrete-time chips are segmented into multiple blocks according to the given equaliser length N_c. Assuming that the composite channel response $h_i(l)$ is stationary within the *i-th* block and spans over L chips, we may write the received signal in one block as $r_i(n)$, $0 \leq i \leq M-1$, $0 \leq n \leq N_c - 1$, where M is the number of blocks and N_c is the number of chips within one block. $x_i(n)$ denotes the corresponding transmitted signal.

$$r_i(n) = \sum_{l=0}^{L-1} h_i(l)x_i(n-l)u(n-l) + \left(\sum_{l=0}^{L-1} h_{i-1}(l)x_{i-1}(n+N_c-l)(1-u(n-l)) \right) + v_i(n) \tag{3.1}$$

where $u(n)$ represents the unit step function. The second term in (3.1) represents the inter block interference (IBI) term caused by the *(i-1)*-th block. The IBI is removed from the received signal by subtracting it based on the decision made in the previous block and the estimation of the channel impulse response. This process is called tail cancellation [99].

$$\bar{r}_i(n) = r_i(n) - \sum_{l=0}^{L-1} h_{i-1}(l)x_{i-1}(n + N_c - l)(1 - u(n - l)) \tag{3.2}$$

As has been stated previously, time-domain circular convolution is equivalent to frequency-domain multiplication, and vice versa. By the insertion of the CP in OFDM systems, linear channel distortion of the signal results in circular convolution of the transmitted signal and the channel impulse response. With this in mind, it is necessary to reconstruct the resultant effect caused by a virtual CP so that the time and frequency-domain descriptions of the convolution are essentially equivalent. Unfortunately, unlike the data-driven echo cancellation problem in [99], no information on what signal is transmitted within the current block is available, and so the tail part of the block can't be used to reconstruct the circularity.

As noted previously the CPICH carries the highest power and is likely to dominate the interference. Therefore, CPICH signals in the *i*-th block are used to reconstruct the required circularity as shown in (3.3).

$$\tilde{r}_i(n) = \bar{r}_i(n) + \sum_{l=0}^{L-1} h_i(l)p_i(n + N_c - l)(1 - u(n - l)) \tag{3.3}$$

where $p_i(n)$ is used to represent the scrambled CPICH signal within the *i*-th block. The process of adding the second term in (3.3) is called cyclic reconstruction. Thus $\tilde{r}_i(n)$ is an approximate cyclic sequence and the linear convolution becomes a circular convolution in the time domain. Thus, in the frequency domain,

$$\tilde{R}_i(w) \approx H_i(w)X_i(w) + V_i(w) \tag{3.4}$$

where $0 \leq w \leq N_c - 1$, $\tilde{R}_i(w)$, $H_i(w)$, $X_i(w)$ and $V_i(w)$ are the DFT of $\tilde{r}_i(n)$, $h_i(l)$, $x_i(n)$ and $v_i(n)$, respectively.

Defining $W_i(w)$, $0 \leq w \leq N_c - 1$ as the equaliser coefficients in the frequency domain and a MMSE cost function that needs to be minimized (For simplicity, it is defined in the frequency

domain):

$$\begin{aligned} J &= E\left\{\frac{1}{N_c}\sum_{w=0}^{N_c-1}|W_i(w)H_i(w)X_i(w)+W_i(w)V_i(w)-X_i(w)|^2\right\} \\ &= \frac{1}{N_c}\sum_{w=0}^{N_c-1}\left\{E[|X_i(w)|^2\cdot|1-H_i(w)W_i(w)|^2]+E[|V_i(w)|^2\cdot|W_i(w)|^2]\right\} \end{aligned} \quad (3.5)$$

Since $E(|X_i(w)|^2)=\sigma_d^2$, $E(|V_i(w)|^2)=\sigma_n^2$, therefore,

$$J=\frac{1}{N_c}\sum_{w=0}^{N_c-1}\left[\sigma_d^2\cdot|1-H_i(w)W_i(w)|^2+\sigma_n^2\cdot|W_i(w)|^2\right] \quad (3.6)$$

In the right hand side of (3.6), the first term represents the inter chip interference and the second term the noise contribution. We then minimize "J" by setting its gradient with respect to the equaliser coefficients $W_i(w)$ to zero. First,

$$J=\frac{1}{N_c}\sum_{w=0}^{N_c-1}\left\{\sigma_d^2\cdot[1-W_i^*(w)H_i^*(w)-H_i(w)W_i(w)]+(\sigma_n^2+\sigma_d^2\cdot|H_i(w)|^2)W_i(w)W_i^*(w)\right\} \quad (3.7)$$

We then have,

$$\nabla_{W_i(w)}J=\frac{\partial J}{\partial W_i(w)}=\frac{1}{N_c}\left[-\sigma_d^2\cdot H_i(w)+(\sigma_n^2+\sigma_d^2\cdot|H_i(w)|^2)W_i^*(w)\right] \quad (3.8)$$

Let $\nabla_{W_i(w)}J=0$, thus

$$\sigma_d^2\cdot H_i(w)=(\sigma_n^2+\sigma_d^2\cdot|H_i(w)|^2)W_i^*(w) \quad (3.9)$$

The MMSE equaliser in the frequency domain is then given by the following expression:

$$W_i(w)=\frac{H_i^*(w)}{|H_i(w)|^2+\sigma_n^2/\sigma_d^2} \quad (3.10)$$

where σ_n^2, σ_d^2 and $H_i^*(w)$ are the variance of the additive Gaussian noise, the variance of the received signal and the conjugate of $H_i(w)$, respectively.

The equalised signal can then be written as:

$$\hat{x}_i(n)=IFFT\{\tilde{R}_i(w)\cdot W_i(w)\},0\le n\le N_c-1,0\le w\le N_c-1 \quad (3.11)$$

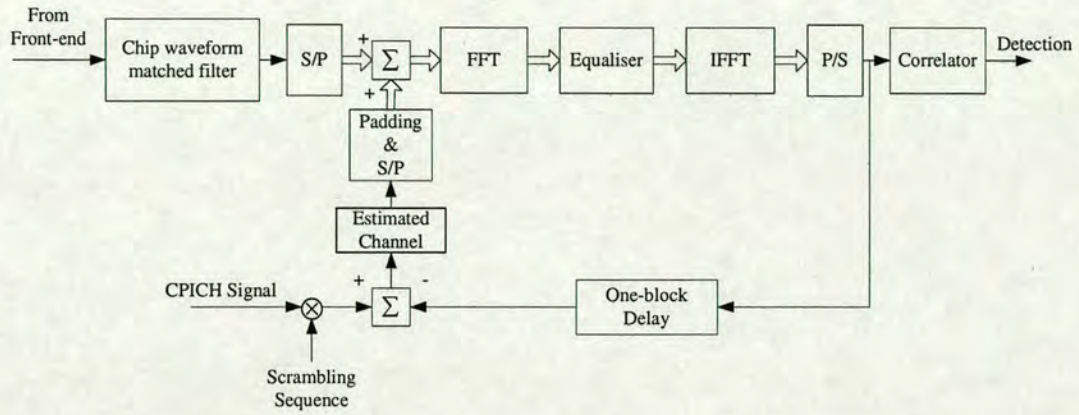

Figure 3.2: *Block Diagram of the Proposed Approach*

Figure 3.2 shows the proposed receiver architecture. The imperfect cyclic reconstructed part will be added at the initial portion of a block of data received from a channel. The contamination due to the imperfect reconstruction can be considered as a noise sequence added to the first $L-1$ data symbol intervals of the block, where L is the channel spread. In the frequency domain, this is considered to be an additive noise spread in the whole signal spectral.

It is worth noting here that although the CPICH based algorithm works reasonably well since the most significant part of the cyclic reconstruction is done, the residual which is treated as additive noise cannot be neglected due to the risk of possible noise enhancement when the transmission channel suffers from deep nulls. Therefore, it is necessary to modify the σ_n^2 term in (3.10) in order to take this interference into account. In other words, σ_n^2 does not represent noise power alone but should also include interference caused by the approximation. It is not easy to decide what σ_n^2 should be since a good estimate of the interference power is not available. Factors such as user numbers, channel duration and equaliser length, etc. will affect the interference power. In the simulations, it was supposed that the variance of the time domain signal excluding CPICH is $\sigma_{residual}^2$, channel is normalized to 1 and with length equal to L, equaliser length is N_c. Since the channel is normalized, we assume that each cursor appears with equal power $1/L$. The variance of the data is $\sigma_{residual}^2$, which can be considered as the average power of each chip. Therefore, the total power of the interference can be calculated by:

$$P_{total} = \sigma_{residual}^2 \sum_{l=1}^{L-1} \frac{l}{L} = \sigma_{residual}^2 \times \frac{L-1}{2} \tag{3.12}$$

Hence, the average interference power per chip is:

$$\sigma^2_{interference} = \frac{P_{total}}{N_c} = \sigma^2_{residual} \times \frac{L-1}{2N_c} \tag{3.13}$$

Then the exact σ_n^2 term should be changed to $\sigma_n^2 + \sigma^2_{interference}$. Consider the difference between the zero forcing (ZF) equaliser and the MMSE equaliser, when a channel has deep spectral nulls, the noise enhancement introduced by the ZF equaliser is very high while the MMSE equaliser can achieve a good tradeoff between the noise amplification and the ISI reduction. The reason for modifying the σ_n^2 term in (3.10) is simply a consideration of the interference caused by the approximation. In this chapter, from now on, the term "σ_n^2" is used instead of "$\sigma_n^2 + \sigma^2_{interference}$" in all formulas. Inevitably, the above approximation will lead to errors in the outputs of the equaliser. It is extremely problematic to quantify the precise impact of these errors on the BER since a nonlinear decision device operates at the output of the equaliser. It is clear that if the approximation is poor then the equaliser BER performance will also be poor, particularly in channels with deep nulls. In order to show the effect explicitly, the output of the equaliser is considered and compared with the true chip value. Only the first block is considered where there is no IBI from the previous block. The simulation scenario includes 12 users traffic, equaliser length is fixed to 64, compatible with the FFT length in WLAN standards. The spreading factor is 16. The relative distance of the equaliser output to the true chip value is defined as:

$$e_r(n) = E\{\frac{|\hat{x}_i(n) - x_i(n)|}{|x_i(n)|}\}, \; 0 \leq n \leq N_c - 1 \tag{3.14}$$

Performance of the proposed cyclic reconstruction algorithm and the algorithm without cyclic reconstruction [96] are both investigated with $g = 20\%$ and $g = 40\%$ (g denotes the power ratio of CPICH to the whole signal power; $g = 10\%$ is currently used in HSDPA systems [100]). The UMTS Vehicular A channel is considered in the simulation, assuming a noise free environment and perfect channel knowledge. The horizontal axis represents the index of chips within one equaliser block and the vertical axis gives the relative distance of the equaliser output to the true chip value defined in (3.14).

As can be seen in Figure 3.3 and Figure 3.4, there is a period at the beginning and the end of each block where the error is significantly larger than the time average. This fact is consistent with that in [96] [97] [98], the effects of the circularity are worst at the edges; the overlap-cut algorithm can effectively improve the system performance. We thus adopt the overlap-cut method to reduce the output errors by overlapping the current block with the preceding one and

the following one. Only the middle parts of the outputs from the equaliser are retained. The solid curve shows the result using CPICH for cyclic reconstruction while no reconstruction is carried out for the dashed curve (algorithm in [98]). From Figure 3.3 and Figure 3.4, we may draw the following three conclusions:

- The higher the CPICH power is, the better the performance of the proposed method compared with the algorithm in [98]. Simulation results show that there is a 2 dB improvement at the BER of 10^{-2}.
- Since large errors will always appear at the beginning and the end of blocks, it is desirable to reduce the errors at these areas by using overlapping blocks. In this thesis, for each block, 25% of the signal overlaps with the previous block and 25% with the following block.
- Both the new algorithm and the algorithm in [98] are based on the overlap-cut idea. To meet a certain error level, the new algorithm can have less overlap area than the one in [98]. From Figure 3.3 and Figure 3.4, it is observed that when $g = 20\%$, $e_r(n) = 0.35$, the overlap can be reduced by 11%. When $g = 40\%$, $e_r(n) = 0.3$, the overlap can be reduced by 17%.

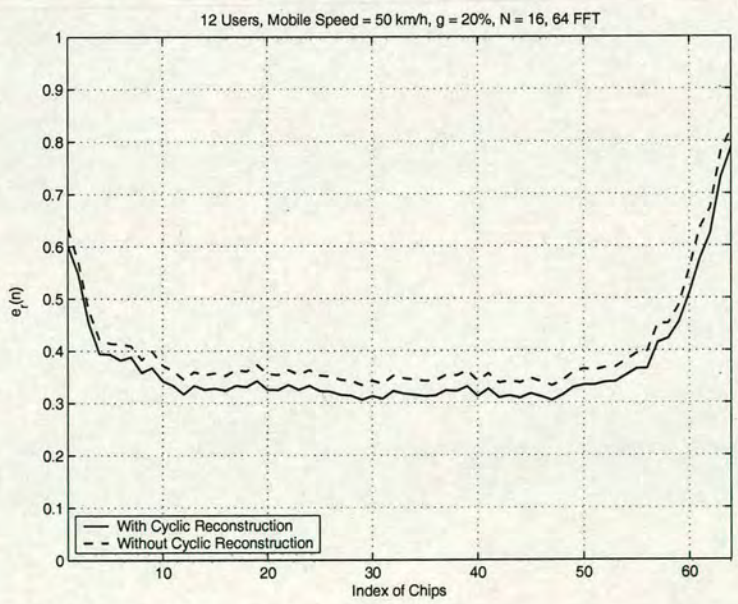

Figure 3.3: *The relative distance to true chip value; $g = 20\%$*

The new approach proceeds as follows:

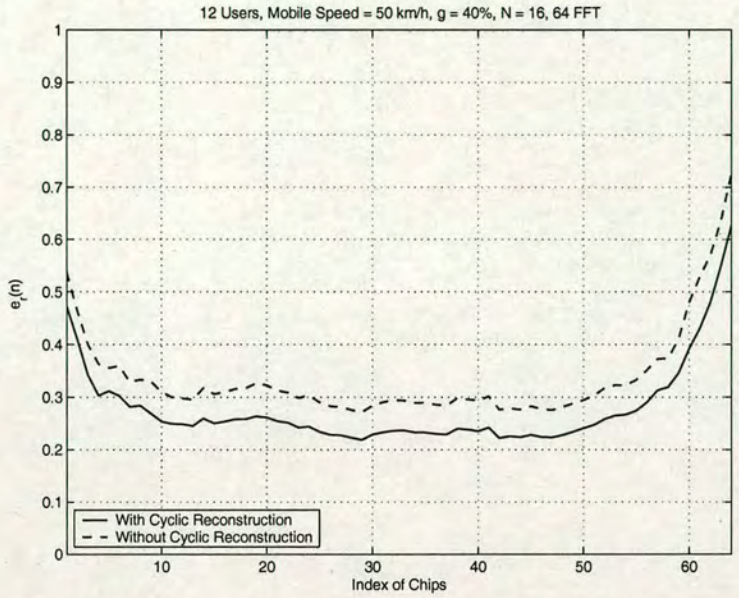

Figure 3.4: *The relative distance to true chip value;* $g = 40\%$

Step 1: Channel Estimation using CPICH;

Step 2: Block segmentation; Remove interferences from the previous block;

Step 3: Use the tail part of the CPICH signal in the current block to reconstruct the circularity;

Step 4: Output from step 3 will be pushed into FFT bins for FFT operation;

Step 5: Frequency equalisation, output transformed back to the time domain by IFFT;

Step 6: Reduce errors by the overlap-cut method and process the successive block.

When a code is transmitted as a training sequence for estimating the channel impulse response, the output of a matched filter to the code is the convolution of the autocorrelation function of the code with the channel impulse response. The autocorrelation function of the long scrambling code, the CPICH after scrambling as well, is nearly an impulse and thus the deconvolution is not required. This is a widely adopted channel estimation scheme [40], details of which will be described in Chapter 6. It is likely that a higher power CPICH will result in a better channel estimation.

3.4 CPICH Interference Cancellation

CPICH dominates the interference in MAI due to its high power. As can be seen from the previous sections, the above mentioned algorithm copes with a high power CPICH. But, unfortunately, this will lead to two drawbacks, one is the high MAI within the current cell and the other is the resultant high interference for neighboring cells. It is desirable to remove this part of interference caused by the high power CPICH as we have enough information at the receiver. Since the CPICH is known at the receiver, no decision is required and the problem then becomes a data aided cancellation problem.

Similar to (3.5), we define the cost function in the frequency domain as:

$$J = E\left\{\frac{1}{N_c}\sum_{w=0}^{N_c-1}(|W_i(w)H_i(w)X_i(w) + W_i(w)V_i(w) - G_i(w)P_i(w) - X_{i,residual}(w)|^2)\right\} \tag{3.15}$$

where $W_i(w)$, $G_i(w)$, $P_i(w)$, $X_{i,residual}(w)$ denote the frequency response of the feedforward equaliser, frequency response of the feedback CPICH cancellation filter, the DFT of $p_i(n)$ and the time domain signal excluding CPICH signal $x_{i,residual}(n)$, respectively. The first term in the bracket is the output of the feedforward equaliser and the third one represents the feedback for CPICH interference cancellation.

Since $x_{i,residual}(n)$ and $p_i(n)$ are mutually uncorrelated, the cost function in (3.15) can be simplified to:

$$\begin{aligned} J &= E\{\frac{1}{N_c}\sum_{w=0}^{N_c-1}(|[W_i(w)H_i(w) - 1]X_{i,residual}(w) + W_i(w)V_i(w) \\ &\quad + [W_i(w)H_i(w) - G_i(w)]P_i(w)|^2)\} \\ &= \frac{1}{N_c}\sum_{w=0}^{N_c-1}\{E[|X_{i,residual}(w)|^2 \cdot |1 - H_i(w)W_i(w)|^2] \\ &\quad + E[|P_i(w)|^2 \cdot |H_i(w)W_i(w) - G_i(w)|^2] + E[|V_i(w)|^2 \cdot |W_i(w)|^2]\} \end{aligned} \tag{3.16}$$

Given $E(|X_{i,residual}(w)|^2) = \sigma^2_{residual}$, $E(|P_i(w)|^2) = \sigma^2_p$, (3.16) can be written as

$$J = \frac{1}{N_c}\sum_{w=0}^{N_c-1}\{\sigma^2_{residual} \cdot |1 - H_i(w)W_i(w)|^2 + \sigma^2_n|W_i(w)|^2 + \sigma^2_p \cdot |G_i(w) - H_i(w)W_i(w)|^2\} \tag{3.17}$$

The gradient of "J" with respect to the equaliser coefficients $W_i(w)$ is given by:

$$\nabla_{W_i(w)}J = \frac{1}{N_c}\left\{-(\sigma^2_{residual} + \sigma^2_p \cdot G^*_i(w)) \cdot H_i(w) + [\sigma^2_n + (\sigma^2_{residual} + \sigma^2_p) \cdot |H_i(w)|^2] \cdot W^*_i(w)\right\} \tag{3.18}$$

Let $\nabla_{W_i(w)}J = 0$, hence

$$(\sigma^2_n + (\sigma^2_{residual} + \sigma^2_p) \cdot |H_i(w)|^2) \cdot W_i(w) = (\sigma^2_{residual} + \sigma^2_p \cdot G_i(w)) \cdot H^*_i(w) \tag{3.19}$$

Therefore, the forward frequency domain equaliser is determined by its coefficients:

$$W_i(w) = \frac{(\sigma^2_{residual} + \sigma^2_p \cdot G_i(w)) \cdot H^*_i(w)}{\sigma^2_n + (\sigma^2_{residual} + \sigma^2_p) \cdot |H_i(w)|^2} \tag{3.20}$$

where $w = 0, \cdots, N_c - 1$. Now inserting (3.20) back into (3.17), by applying the gradient method to it with respect to the feedback filter $G_i(w)$ this time and let $\nabla_{G_i(w)}J = 0$, we are able to determine the coefficients of $G_i(w)$.

The feedback filter coefficients $G_i(w)$ take the form (See Appendix A):

$$G_i(w) = \frac{\sigma^2_{residual} \cdot |H_i(w)|^2}{\sigma^2_{residual} \cdot |H_i(w)|^2 + \sigma^2_n} = \frac{|H_i(w)|^2}{|H_i(w)|^2 + \sigma^2_n/\sigma^2_{residual}} \tag{3.21}$$

Once $G_i(w)$ is determined, $W_i(w)$ is then given by (3.20).

It is easily verified that when $g = 0$, i.e. no CPICH signal is transmitted, then $\sigma^2_p = 0$ and $\sigma^2_{residual} = \sigma^2_d$. Consequently, (3.20) turns into the form which is identical to (3.10), a conventional frequency domain equaliser.

First, the received signal will be equalised by the forward filter with coefficients $W_i(w)$, then, in the frequency domain, the feedback interference cancellation filter with coefficients $G_i(w)$ is operated on the scrambled CPICH signal known at the receiver. The output in the frequency domain given by $W_i(w)\tilde{R}_i(w) - G_i(w)P_i(w)$, subtraction of the feedforward filter output and the feedback filter output, is transformed back to the time domain by IFFT. The whole procedure is summarised in Figure 3.5. With the proposed algorithm in this section, the contribution of the high power CPICH is removed from the compound signal to a degree. The technique of canceling CPICH shows much merit. Before the signals are decoded, the interference is made less significant. The reduction of interference from neighboring cells is not considered.

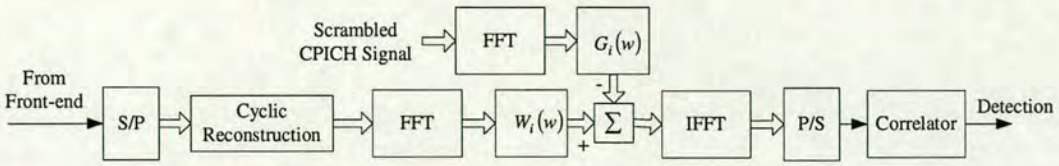

Figure 3.5: *Interference cancellation system model*

3.5 Simulation Results

Computer simulations are carried out at base band for the investigation of the proposed algorithm. QPSK modulation is considered. The system BER performance under the UMTS Vehicular A channel is studied. The length of channel is fixed at 11 chip periods ($2.86\mu s$) when the chip rate is 3.84 Mchips/s. Walsh codes with length 16 are used as channelization codes and a Gold code segment is used as the long scrambling code. In the simulation, the terminal speed is assumed to be 50 km/h and the carrier frequency is 2 GHz. 12 users are included in the simulations. The FDE has a fixed length equal to 64 (FFT/IFFT size in WLAN standards). For each block, 25% of the signal overlaps with the previous block and 25% with the following block.

In order to show the effectiveness of the new proposed algorithm, simulation results with varying CPICH power are presented. Performance of the CPICH based cyclic reconstruction equaliser and the overlap-cut equaliser (without cyclic reconstruction) are compared in terms of the BER performance for one desired user. The bit errors are summed and an average BER is then calculated. The power of the CPICH is taken to be 20% of the total signal power and 40% of the total signal power. The performance under perfect channel estimation and imperfect channel estimation is studied. The system performance is significantly degraded by the error in channel estimation. We present the BER performance under imperfect channel estimation with the channel estimation window $N_w = 256$, $N_w = 512$ and $N_w = 1024$ respectively. The performance of the time domain equaliser with equal length, i.e. 64 taps, under perfect channel estimation is also plotted in Figure 3.6 and Figure 3.7.

It can be observed that the FDE with cyclic reconstruction consistently outperforms that without reconstruction in both cases. Under the perfect channel estimation assumption, the FDE performance is close to that of the time domain equaliser. In Figure 3.8 and Figure 3.9, we repeat

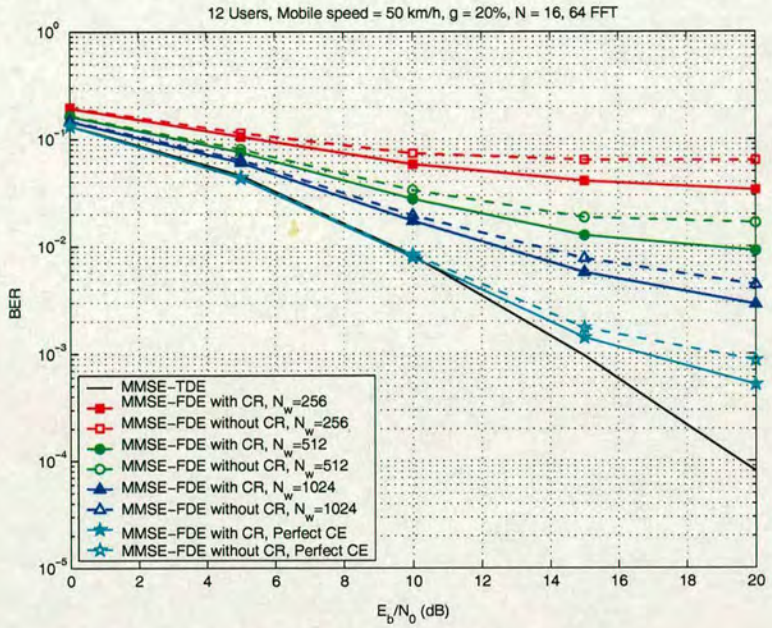

Figure 3.6: *Simulated BER performances; 12 Users; Mobile speed = 50 km/h; $g = 20\%$; $N = 16$; 64 FFT; CR: Cyclic Reconstruction*

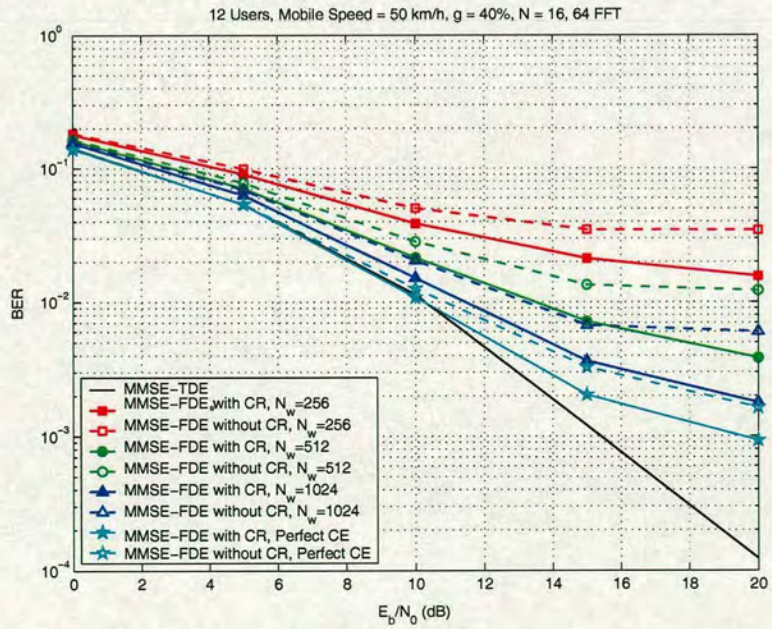

Figure 3.7: *Simulated BER performances; 12 Users; Mobile speed = 50 km/h; $g = 40\%$; $N = 16$; 64 FFT; CR: Cyclic Reconstruction*

the simulation results for performance comparison with different CPICH power and perfect or imperfect channel estimation.

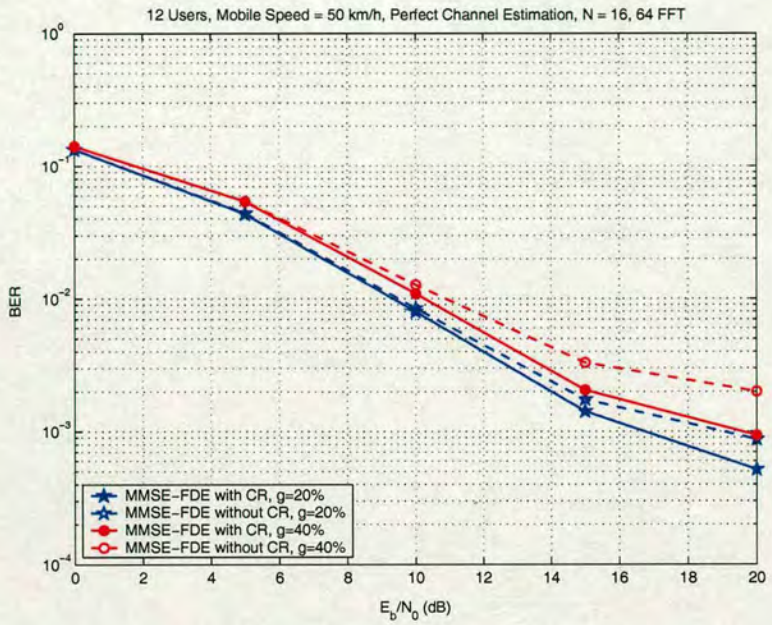

Figure 3.8: *Simulated BER performances; Perfect channel estimation; 12 Users; Mobile speed = 50 km/h; N = 16; 64 FFT; CR: Cyclic Reconstruction*

From Figure 3.8 we see that with perfect channel estimation, in both cases (with cyclic reconstruction or without cyclic reconstruction) system with $g = 20\%$ outperforms system with $g = 40\%$. This is straightforward since high power CPICH introduces high MAI in the system. However, on the other hand, with higher CPICH, we can achieve better channel estimates. As can be seen in Figure 3.9, under imperfect channel estimation, system with $g = 40\%$ will outperform the system with $g = 20\%$. There is a 2 dB improvement for the FDE with cyclic reconstruction ($g = 40\%$) over the FDE without cyclic reconstruction ($g = 20\%$) at the BER of 10^{-2}. From the simulation results presented above, it follows that: The higher the CPICH power is, the better the channel estimates. In other words, if the power ratio of CPICH over the whole signal power is large, the channel estimation quality is good. However, this will lead to a large MAI with large error probability.

Figure 3.10 and Figure 3.11 show the simulated BER performance of the CPICH cancellation algorithm, with CPICH power 20% of the whole signal power in Figure 3.10 and 40% whole signal power in Figure 3.11. With the proposed CPICH cancellation algorithm in this chapter, the contribution of the high power CPICH is removed from the compound signal to some extent.

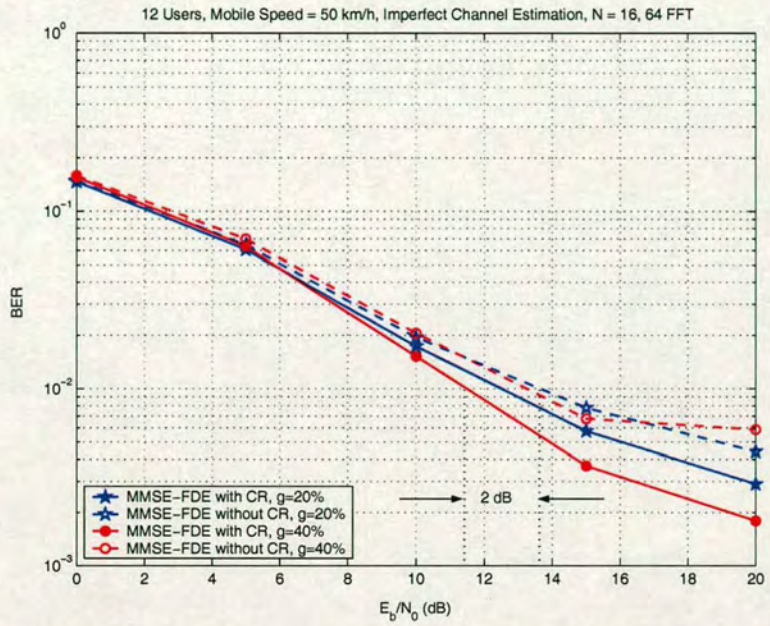

Figure 3.9: *Simulated BER performances; Imperfect channel estimation; 12 Users; Mobile speed = 50 km/h; $N_w = 1024$; N = 16; 64 FFT; CR: Cyclic Reconstruction*

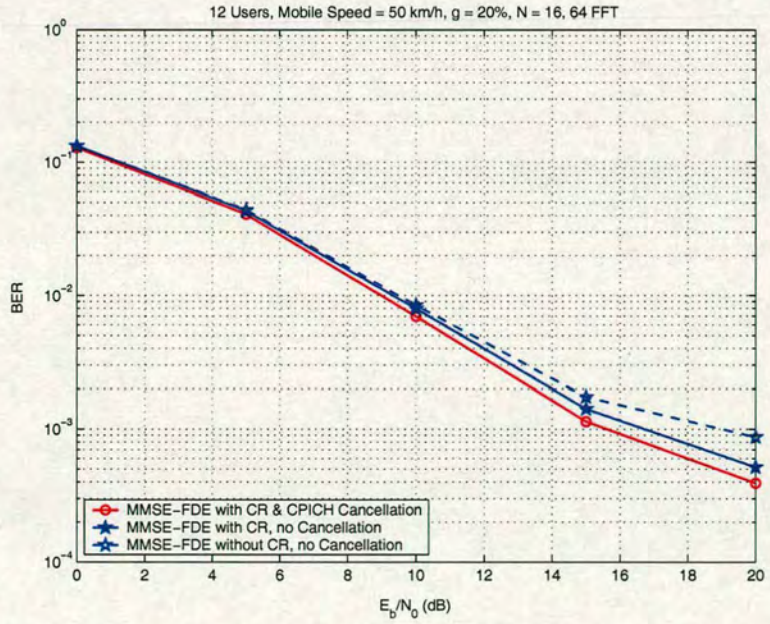

Figure 3.10: *Simulated BER performances with CPICH cancellation; 12 Users; Mobile speed = 50 km/h; $g = 20\%$; Perfect channel estimation; N = 16; 64 FFT; CR: Cyclic Reconstruction*

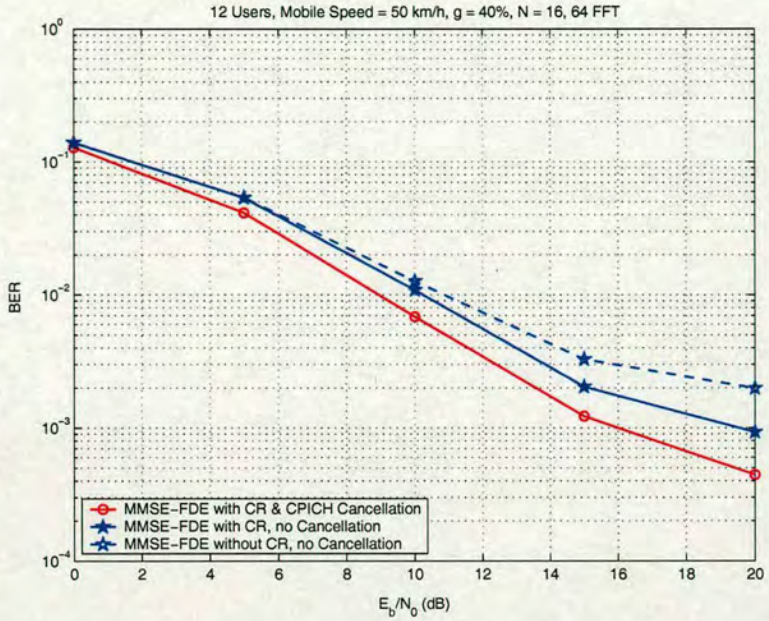

Figure 3.11: *Simulated BER performances with CPICH cancellation; 12 Users; Mobile speed = 50 km/h; $g = 40\%$; Perfect channel estimation; N = 16; 64 FFT; CR: Cyclic Reconstruction*

The MMSE solution achieves a good trade-off between ISI reduction and noise enhancement. The technique of cancelling CPICH shows much merit. We allocate higher power to the CPICH for better channel estimation while at the receiver; the induced high MAI can be effectively reduced. Before the signals are decoded, the interference is made less significant.

3.6 Conclusions

This chapter has described a MMSE frequency domain equaliser for UMTS in downlink transmission and a number of results were presented that demonstrate its effectiveness. A DS-CDMA receiver adopting a chip level frequency domain equaliser would be compatible with the current OFDM based systems. In addition, the complexity of a FDE is independent of the channel frequency selectivity. Unlike the Rake receiver, the number of paths in a frequency selective channel does not affect the complexity of a FDE.

The high power primary common pilot channel transmitted for training and channel estimation purposes has been used for cyclic reconstruction at the receiver. Obviously, the high power common pilot channel is the most significant interferer for the local cell and its neighbouring cell. Large power will improve the channel estimation, however, it will also introduce more

MAI. An interference cancellation algorithm was also presented is this chapter. Both the feed-forward filter and the feedback filter are designed in the frequency domain, and no decision has to be made since we have the information of pilots at the receiver *a-prior*. The MAI is made less significant after the high power CPICH cancellation.

Chapter 4
Further Developments on Frequency Domain Equalisation Algorithms Enabling Multimode Operation

In this chapter, first, two frequency domain chip level equalisers for UMTS FDD are presented. Unlike the equaliser proposed in Chapter 3, these two algorithms do not require a high power pilot channel and can be applied to the current High Speed Downlink Packet Access (HSDPA) system [100]. Second, a hybrid decision feedback equaliser with a feedback filter whose length can be dynamically adjusted is proposed.

The FDE based on self cyclic reconstruction is presented in Section 4.1 and the FDE based on segmentation is proposed in Section 4.2. Finally, the hybrid DFE with varying length FBF is studied in Section 4.3.

4.1 FDE Based on Self Cyclic Reconstruction

For frequency domain equalisation, the circularity of the received block signal needs to be reconstructed if neither cyclic prefix nor zero-padding are used at the transmitter. In this section, we exploit the relationship between the reconstructed part and the equalised signal itself and derive a self cyclic reconstruction scheme.

4.1.1 Self Cyclic Reconstruction

The frequency domain equaliser will process data on a block by block basis. Applying different sizes of FFT, we can separate each slot into multiple blocks. Suppose that we extract one block of discrete received signals of length N_c, $\bar{\mathbf{r}}_i = [\bar{r}_i(0), \bar{r}_i(1), \cdots, \bar{r}_i(N_c - 1)]^T$ (assuming the IBI from the previous block is cancelled out, which can be done by tail cancellation). A linear convolution output is $L - 1$ chips longer than that of a circular convolution. The tail part of a

linear convolution process is defined as $\mathbf{r}_{i,t} = [r_{i,tail}(0), r_{i,tail}(1), \cdots, r_{i,tail}(L-2)]^T$ which is unknown to the receiver and L is the length of channel (channel is assumed to be perfectly estimated at the receiver).

By adding elements of $\mathbf{r}_{i,t}$ to the first $L-1$ elements of $\bar{\mathbf{r}}_i$, we call this process cyclic reconstruction. In a DS-CDMA system such as UMTS, this process is of great importance for frequency domain equalisation since there is no cyclic prefix inserted in the transmitted signal. The block signal after cyclic reconstruction can be written as:

$$\begin{aligned} \tilde{\mathbf{r}}_i = [\tilde{r}_i(0), \cdots, \tilde{r}_i(L-2), \tilde{r}_i(L-1), \cdots, \tilde{r}_i(N_c-1)]^T, \\ \tilde{r}_i(l) = \bar{r}_i(l) + r_{i,tail}(l)\,,\ l = 0, \cdots, L-2 \\ \tilde{r}_i(l) = \bar{r}_i(l)\,,\ otherwise \end{aligned} \tag{4.1}$$

It is worth noting that only the first $L-1$ terms have been modified where L is the channel length and the first $L-1$ elements of $\tilde{\mathbf{r}}_i$ remains unknown. From the above definition, we further define $\mathbf{r}_{i,tail} = [\underbrace{r_{i,tail}(0), \cdots, r_{i,tail}(L-2), 0, \cdots, 0}_{N_c}]^T$, thus,

$$\tilde{\mathbf{r}}_i = \mathbf{r}_{i,tail} + \bar{\mathbf{r}}_i. \tag{4.2}$$

Firstly, we consider a noise-free environment. We then have the input and output relations:

$$\tilde{\mathbf{r}}_i = \mathbf{H}_{c,i} \cdot \mathbf{x}_i, \tag{4.3}$$

where $\mathbf{H}_{c,i}$ is a circular channel matrix and $\mathbf{x}_i$ is a column vector composed of one block of the transmitted signal with N_c samples. The channel impulse response is denoted by $h_i(l), l = 0, \cdots, L-1$ (The channel is assumed quasi-static within one block) which has an N_c point

Fourier transform $H_i(w), w = 0, \cdots, N_c - 1$. The channel matrix $\mathbf{H}_{c,i}$ is thus defined as:

$$\mathbf{H}_{c,i} = \begin{pmatrix} h_i(0) & & & & h_i(L-1) & \cdots & h_i(1) \\ \vdots & h_i(0) & & & & \ddots & \vdots \\ \vdots & \vdots & \ddots & & & & h_i(L-1) \\ h_i(L-1) & \vdots & \vdots & h_i(0) & & & \\ & h_i(L-1) & \vdots & \vdots & h_i(0) & & \\ & & \ddots & \vdots & \vdots & \ddots & \\ 0 & & & h_i(L-1) & h_i(L-2) & \cdots & h_i(0) \end{pmatrix} \tag{4.4}$$

According to its special structures, circular matrix $\mathbf{H}_{c,i}$ can be efficiently diagonalized by Fourier transform and inverse Fourier transform. Let $\mathbf{F}$ and $\mathbf{F}^{-1}$ denotes the Fourier transform matrix and the inverse Fourier transform matrix, respectively. Hence,

$$\mathbf{F} \cdot \tilde{\mathbf{r}}_i = \mathbf{F} \cdot \mathbf{H}_{c,i} \cdot \mathbf{x}_i = \mathbf{F} \cdot \mathbf{H}_{c,i} \cdot \mathbf{F}^{-1} \cdot \mathbf{F} \cdot \mathbf{x}_i = \mathbf{D}_i \cdot \mathbf{F} \cdot \mathbf{x}_i, \tag{4.5}$$

where $\mathbf{D}_i$ is a diagonal matrix with its elements taken from the N_c points Fourier transform of channel impulse response, i.e. $\mathbf{D}_i = diag\{H_i(0), \cdots, H_i(N_c - 1)\}$.

Substituting (4.2) into (4.5),we have:

$$\mathbf{F} \cdot (\mathbf{r}_{i,tail} + \bar{\mathbf{r}}_i) = \mathbf{D}_i \cdot \mathbf{F} \cdot \mathbf{x}_i. \tag{4.6}$$

Equation (4.6) can be further modified to:

$$\mathbf{F}^{-1} \cdot \mathbf{D}_i^{-1} \cdot \mathbf{F} \cdot (\mathbf{r}_{i,tail} + \bar{\mathbf{r}}_i) = \mathbf{x}_i. \tag{4.7}$$

Theoretically, the reconstructed part $\mathbf{r}_{i,t}$ is obtained by the multiplication of the upper triangular block matrix in $\mathbf{H}_{c,i}$ and a vector composed of the last $L-1$ elements of $\mathbf{x}_i$. Therefore, given $\mathbf{H}_{0,i} = \begin{pmatrix} 0 & \cdots & 0 & h_i(L-1) & \cdots & h_i(1) \\ \vdots & \ddots & \vdots & \ddots & \ddots & \vdots \\ 0 & \cdots & \cdots & \cdots & 0 & h_i(L-1) \end{pmatrix}$ and $\mathbf{H}_{1,i} = \mathbf{0}_{N_c-L+2\_by\_N_c}$, we can yield:

$$\mathbf{r}_{i,tail} = [\ \mathbf{H}_{0,i} \quad \mathbf{H}_{1,i}\ ]^T \cdot \mathbf{x}_i. \tag{4.8}$$

Substituting (4.7) into (4.8), as a result, we have:

$$\mathbf{r}_{i,tail} = [\ \mathbf{H}_{0,i} \quad \mathbf{H}_{1,i}\ ]^T \cdot \mathbf{F}^{-1} \cdot \mathbf{D}_i^{-1} \cdot \mathbf{F} \cdot (\mathbf{r}_{i,tail} + \bar{\mathbf{r}}_i). \tag{4.9}$$

In order to simplify the notation, a new $N_c \times N_c$ matrix $\mathbf{M}_i$ is introduced:

$$\mathbf{M}_i = [\ \mathbf{H}_{0,i} \quad \mathbf{H}_{1,i}\ ]^T \cdot \mathbf{F}^{-1} \cdot \mathbf{D}_i^{-1} \cdot \mathbf{F}. \tag{4.10}$$

Matrix $\mathbf{M}_i$ has its special structure that it can be further split into blocks, i.e. $\mathbf{M}_i = \begin{pmatrix} \mathbf{M}_{0,i} & \mathbf{M}_{1,i} \\ \mathbf{0} & \mathbf{0} \end{pmatrix}$, $\mathbf{M}_{0,i}$ is a $(L-1) \times (L-1)$ matrix and $\mathbf{M}_{1,i}$ is a $(L-1) \times N_c$ matrix. Matrix $\mathbf{M}_i$ can be calculated by the multiplication of matrices from (4.10) and this will cause a large computational burden for the receiver. However, the computation can be reduced significantly. Since $\mathbf{D}_i^{-1}$ is a diagonal matrix, it can be decomposed to

$$\mathbf{D}_i^{-1} = \mathbf{F} \cdot \mathbf{A}_i \cdot \mathbf{F}^{-1}, \tag{4.11}$$

where $\mathbf{A}_i$ is a circular matrix. Thus,

$$\mathbf{M}_i = [\ \mathbf{H}_{0,i} \quad \mathbf{H}_{1,i}\ ]^T \cdot \mathbf{F}^{-1} \cdot \mathbf{F} \cdot \mathbf{A}_i \cdot \mathbf{F}^{-1} \cdot \mathbf{F} = [\ \mathbf{H}_{0,i} \quad \mathbf{H}_{1,i}\ ]^T \cdot \mathbf{A}_i. \tag{4.12}$$

Since $\mathbf{A}_i$ is a circular matrix, therefore, by knowing only one column or one row elements of $\mathbf{A}_i$, it is possible to generate the whole circular matrix. We need to point out that there is an interesting property of the Fourier transform matrix $\mathbf{F}$, i.e., the first row and the first column elements are all unity elements. It yields that the first column of $\mathbf{D}_i^{-1} \cdot \mathbf{F}$ can be represented by $[\ \frac{1}{H_i(0)} \quad \cdots \quad \frac{1}{H_i(N_c-1)}\ ]^T$ and $H_i(0), \cdots, H_i(N_c-1)$ are the N_c point Fourier transform of the channel impulse response. Consequently, the first column of $\mathbf{A}_i$ can be calculated by the Fourier transform of vector $[\ \frac{1}{H_i(0)} \quad \cdots \quad \frac{1}{H_i(N_c-1)}\ ]^T$ and so that the computational complexity is reduced to $O(N_c log N_c)$.

According to the definition of $\mathbf{M}_i$, $\mathbf{r}_{i,t}$ and (4.10), formula (4.9) can be rewritten as:

$$\begin{aligned} \mathbf{r}_{i,t} &= [\ \mathbf{M}_{0,i} \quad \mathbf{M}_{1,i}\ ]^T \cdot \bar{\mathbf{r}}_i + [\ \mathbf{M}_{0,i} \quad \mathbf{M}_{1,i}\ ]^T \cdot \mathbf{r}_{i,tail} \\ &= [\ \mathbf{M}_{0,i} \quad \mathbf{M}_{1,i}\ ]^T \cdot \bar{\mathbf{r}}_i + \mathbf{M}_{0,i} \cdot \mathbf{r}_{i,t} \end{aligned} \tag{4.13}$$

Hence,

$$(\mathbf{I} - \mathbf{M}_{0,i}) \cdot \mathbf{r}_{i,t} = [\ \mathbf{M}_{0,i} \quad \mathbf{M}_{1,i}\ ]^T \cdot \bar{\mathbf{r}}_i \tag{4.14}$$

From (4.14), when additive white Gaussian noise exists, the MMSE estimate of $\mathbf{r}_{i,t}$ is given by:

$$\mathbf{r}_{i,t} = \left[(\mathbf{I} - \mathbf{M}_{0,i}) \cdot (\mathbf{I} - \mathbf{M}_{0,i})^H + \frac{\sigma_n^2}{\sigma_{tail}^2}\mathbf{I}\right]^{-1} \cdot (\mathbf{I} - \mathbf{M}_{0,i})^H \cdot [\ \mathbf{M}_{0,i} \quad \mathbf{M}_{1,i}\ ]^T \cdot \bar{\mathbf{r}}_i \tag{4.15}$$

where σ_n^2, σ_{tail}^2 and $\mathbf{I}$ are the noise variance, tail part signal variance and a $(L-1) \times (L-1)$ unitary diagonal matrix, respectively.

However, it is not easy to decide what σ_{tail}^2 should be since a good estimate of the tail part average power is not available as stated previously in Chapter 3. In this Chapter, we derive another approximation to σ_{tail}^2. Suppose the variance of the time domain signal is σ_d^2, channel is normalized and with length equal to L. Denote the normalized average power of each channel tap by $P_{l'}$, $l' = 0, \cdots, L-1$. The total tail part power can be approximated by:

$$P_{tail} = \sigma_d^2 \sum_{l=1}^{L-1} \sum_{l'=1}^{L-l} P_{l'} \tag{4.16}$$

Hence, the average tail part signal power per chip is:

$$\sigma_{tail}^2 = \frac{P_{tail}}{L-1} = \frac{\sigma_d^2 \sum_{l=1}^{L-1} \sum_{l'=1}^{L-l} P_{l'}}{L-1} \tag{4.17}$$

The frequency domain equalisation consists of two steps. In the first step, the required tail part is reconstructed. In the second step, the MMSE equaliser in the frequency domain is given by the following expression:

$$W_i(w) = \frac{H_i^*(w)}{|H_i(w)|^2 + \sigma_n^2/\sigma_d^2 + \alpha}, \ w = 0, \cdots, N_c - 1 \tag{4.18}$$

In (4.18), the real factor α is introduced for the purpose of taking into account unpredictable cyclic reconstruction errors. The reason is that if the condition number $cond(\mathbf{I} - \mathbf{M}_0)$ is large, then the exact solution may change substantially by even a small perturbation in the data due to the additive noise. In the frequency domain, let us define $\tilde{R}_i(w)$ and $X_i(w)$, $w = 0, \cdots, N_c - 1$ as the Fourier transforms of $\tilde{\mathbf{r}}_i$ and $\mathbf{x}_i$, respectively. The equalised $\hat{X}_i(w)$ can be given by:

$$\hat{X}_i(w) = \frac{\tilde{R}_i(w) \cdot H_i^*(w)}{|H_i(w)|^2 + \sigma_n^2/\sigma_d^2 + \alpha}, \ w = 0, \cdots, N_c - 1 \tag{4.19}$$

The equaliser output is finally transformed back to the time domain by inverse Fourier transform. The scrambling code is then removed and the composite signal is despreaded and decoded.

Actually, the reconstructed part is exactly the IBI into the next processing block, thus, we can remove this part from the next block to obtain an IBI free block. Inevitably, this will cause error propagation due to imperfect equalisation; however, the error propagation can be limited within one slot since pilots transmitted every slot are known to the receiver.

4.1.2 Parameters Selection

More freedom in parameter selection is available if non-radix 2 Fourier transforms are adopted. N_c can be selected freely for different situations. However, if we only consider Radix 2 FFT, then N_c, the length of one processing block can only be an integer power of 2.

Note that, matrix inversion and matrix multiplication are involved in every cyclic reconstruction process. This process dominates the computational complexity of the equaliser. Choosing a larger block size, there will be fewer blocks in one slot or one frame and hence fewer cyclic reconstruction processes. Hence, an equaliser selecting a large N_c is more efficient than one with a small N_c in terms of computational complexity. Moreover, larger equaliser length results in smaller processing block numbers, thus, the unpredictable error propagation effect will not be significant. On the other hand, it should be emphasized that because of the channel variation within one block due to high-speed movement, large block length will give raise to the performance degradation (its counterpart in one OFDM system is the induced ICI - inter carrier interference). Usually, we select N_c to be 256 or 512 in order to achieve a good tradeoffs between equaliser performance and error propagations.

In (4.18), the exact calculation of the real factor is fairly complicated if not intractable. Taking $0.1 \leq \alpha \leq 0.2$ results in an acceptable system performance given that the transmitted signal power and the propagation channel are both normalized.

4.1.3 Simulation Results

Figure 4.1 shows the BER performances of the proposed frequency domain equaliser and the equaliser with perfect cyclic reconstruction (assuming the tail part is known to the equaliser).

The terminal is traveling at mobile speed of 50 km/h and 150 km/h. The UMTS Vehicular A Channel model is used in our simulations. In Figure 4.1, $N_c = 512$ is selected for the equaliser. The lower bound performances (system performances with perfect cyclic reconstruction) of equaliser with 64 and 512 FFT size are also given. In Figure 4.2, we present the BER performance of the proposed equaliser with $N_c = 256$. Also shown are the lower bounds for frequency domain equalisers with perfect cyclic reconstruction. We learn from Figure 4.1 that

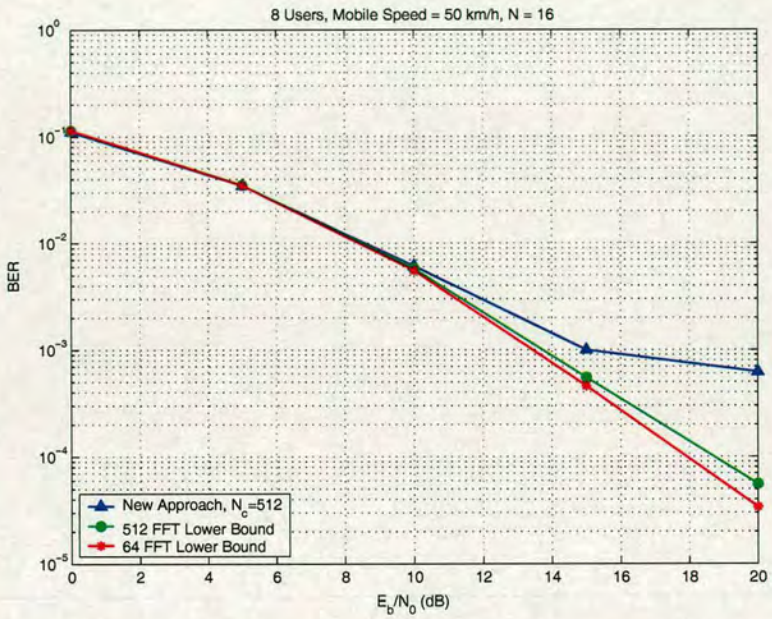

Figure 4.1: *Performance of the new FDE; 8 Users; Mobile speed = 50 km/h; N = 16*

for low speed movement, although under high SNR scenarios the performance of the proposed algorithm is not satisfactory compared with the lower bounds. However, with the aid of forward error correction coding, the area in the figure that of interest is $10^{-2} \leq BER \leq 10^{-1}$. In this area, the performance of the proposed equaliser is acceptable. It can be seen from Figure 4.2 that for high-speed movement, the performance is close to the lower bounds. A system with perfect cyclic reconstruction is equivalent to a cyclic prefix based single carrier system. In an OFDM system, high-speed movements will cause severe ICI; similarly, for single carrier transmission with cyclic prefix, it will also degrade the BER performance significantly. The channel at the beginning of one block and the channel at the end of one block are no longer the same; therefore, the cyclic prefix and its data part are not transmitted though the same channel. The channel within one block can no longer be assumed to be stationary.

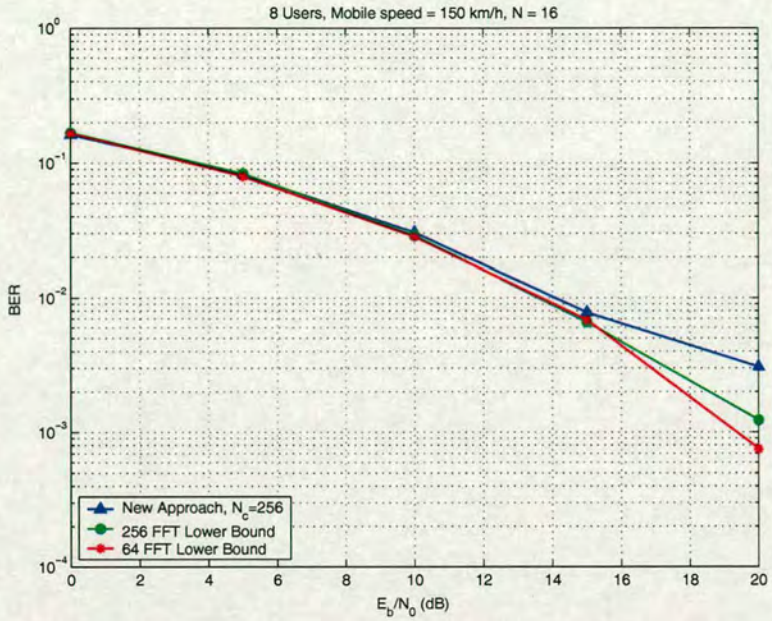

Figure 4.2: *Performance of the new FDE; 8 Users; Mobile speed = 150 km/h; N = 16*

4.1.4 Discussion of Results

In this section, a MMSE frequency domain equaliser based on self cyclic reconstruction is proposed and the BER performance is given. Without the insertion of cyclic prefix at the transmitter, which will change the UMTS signal format, the proposed algorithm exploits the relationship between the required cyclic part and the transmitted signal itself. The estimated cyclic part is then added to the received block signal for doing frequency domain equalisation. Simulation results show the effectiveness of the proposed algorithm.

4.2 FDE Based on Slot Segmentation

In this section, we propose another frequency domain equaliser for UMTS downlink FDD mode. By exploiting the frame and slot structures of the UMTS downlink, the pilots within one slot (for FDD mode) can be used for the required cyclic reconstruction in a FDE. No CP or zero-padding is required at the transmitter, which would change the signal format of the current UMTS system. Furthermore, one slot signal is split into multiple segments for the sake of combating channel variance within one slot. The performance of the proposed MMSE-FDE is studied through simulation.

4.2.1 Slot Segmentation

By the insertion of the CP in OFDM systems, linear channel distortion of the signal results in circular convolution of the transmitted signal and the channel impulse response. With this in mind, it is necessary to reconstruct the resultant effect caused by a virtual CP so that the time and frequency-domain descriptions of the convolution are essentially equivalent and a simple OFDM type FDE can be derived. In the FDD downlink, pilots are pre-inserted in each slot used for channel estimation purpose as shown in Figure 2.6. According to the UMTS specification [101], the pilot sequence can be 64-2048 chips corresponding to different slot formats. Since the shortest pilot sequence still consists of 64 chips which is longer than L (the channel span in chips) in most cases, this prior known information can be used to reconstruct the needed circularity for the FDE. The insertion of CP as in an OFDM system can be avoided and thus the transmitted signal format will not be changed.

The new FDE is performed on a slot (2560 chips) by slot basis. Assuming that the composite channel response $h_i(l)$ is quasi-stationary within the i-th slot and spans over L chips ($L < 64$, i.e. channel span is less than 16.64 μs), we may write the received signal in one block as $r_i(n)$, $0 \leq i \leq 14$, $0 \leq n \leq N_c - 1$ and $N_c = 2560$ is the number of chips within one slot. Finally, we use $x_i(n)$ to denote the corresponding transmitted i-th slot signal. At the receiver, $r_i(n)$ can be written as:

$$r_i(n) = \sum_{l=0}^{L-1} h_i(l)x_i(n-l)u(n-l) + \left(\sum_{l=0}^{L-1} h_{i-1}(l)x_{i-1}(n+N_c-l)(1-u(n-l)) \right) + v_i(n) \tag{4.20}$$

where $u(n)$ represents the unit step function. The second term in (4.20) represents the inter-slot-interference caused by the *(i-1)*-th slot. It is estimated and subtracted from the current slot. Then the slot signal free of inter-slot-interference is given by:

$$\bar{r}_i(n) = r_i(n) - \sum_{l=0}^{L-1} h_{i-1}(l)x_{i-1}(n+N_c-l)(1-u(n-l)) \tag{4.21}$$

Pilot sequences are transmitted at the end of one slot and are known to the receiver. Therefore, pilot signals in the i-th slot can be used to reconstruct the required circularity as shown in (4.22).

$$\tilde{r}_i(n) = \bar{r}_i(n) + \sum_{l=0}^{L-1} h_i(l)x_i(n+N_c-l)(1-u(n-l)) \tag{4.22}$$

Correspondingly, in the frequency domain,

$$\tilde{R}_i(w) \approx H_i(w)X_i(w) + V_i(w) \tag{4.23}$$

where $0 \leq w \leq N_c - 1$, $\tilde{R}_i(w)$, $H_i(w)$, $X_i(w)$ and $V_i(w)$ are the DFT of $\tilde{r}_i(n)$, $h_i(l)$, $x_i(n)$ and $v_i(n)$, respectively. Further defining $W_i(w)$, $0 \leq w \leq N_c - 1$ as the equaliser coefficients in the frequency domain, the MMSE FDE is given by the following expression:

$$W_i(w) = \frac{H_i^*(w)}{|H_i(w)|^2 + \sigma_n^2/\sigma_d^2} \tag{4.24}$$

σ_n^2, σ_d^2 and $H_i^*(w)$ are the variance of the additive Gaussian noise, the variance of the received signal and the conjugate of $H_i(w)$, respectively. The equalised signal is finally transformed back to the time domain by inverse Fourier transform. The scrambling code is removed and the composite signal is despread and detected.

Two sorts of channels are studied in our simulations with their frequency selectivity plotted in Figure 4.3. Computer simulations are carried out at base band for the investigation of the proposed algorithm. BER performance is evaluated for the MMSE FDE in both static spectrally-flat channel (Figure 4.4) and spectrally-deep-fading channel (Figure 4.5). Channel coding is excluded from the study. Perfect knowledge of the channel at the receiver is assumed. In both cases, we use the proposed MMSE FDE, a 32-taps and a 64-taps MMSE time domain equaliser (TDE) [47]. Assuming that the channel is time-invariant within one slot, our simulations show that the proposed MMSE chip level FDE can effectively mitigate inter-chip interferences under channels with or without deep nulls. In fact, the assumption that we made is not reasonable since the channel's stationary assumption cannot be ensured within one slot. Therefore, the time variation of the mobile radio channel is a main obstacle to the proposed FDE. Study of the MMSE-FDE performance in Rayleigh fading channels (UMTS Vehicular A Channel) is presented in this section. Each path is faded independently according to the Rayleigh distribution. As we can see from Figure 4.6, moving at a high speed, the channel within one slot changes very fast and so such a large block frequency domain equaliser results in a worse performance compared with using a short block time domain equaliser. By breaking the 2560 chips slot into a series of disjoint short segments, the time variations of the mobile channel over one segment are sufficiently small and can be neglected. Hence, we can assume that the channel over one segment is static. The whole time-varying channel over one slot can be partitioned into multiple time-invariant channels. A similar approach had been proposed in [102] for OFDM systems.

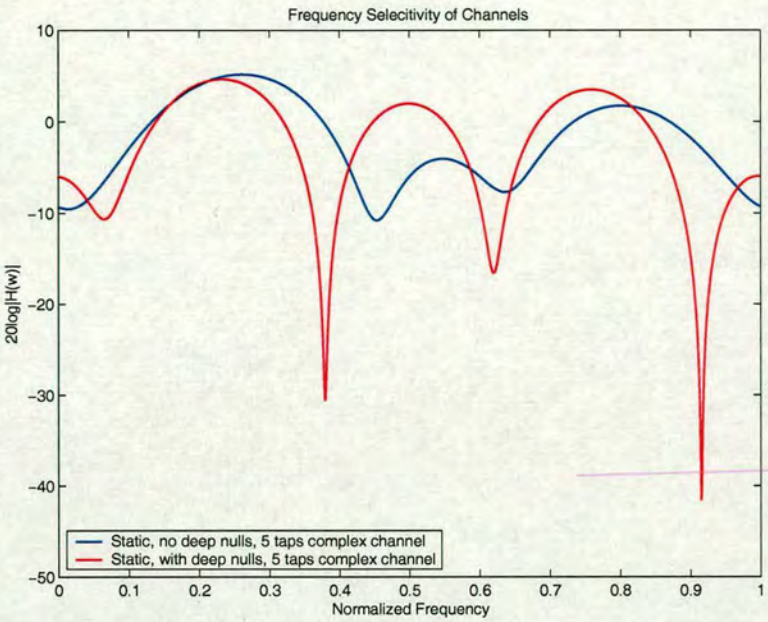

Figure 4.3: *Frequency selectivity of two sorts of channels*

The system performance can be improved greatly, especially in fast fading channels.

To derive the new equalisation scheme, we consider one slot free of interference from the previous slot. The received signal in the i-th slot is expressed as $\bar{\mathbf{r}}_i = [\bar{r}_i(0), ..., \bar{r}_i(N_c - 1)]^T$, $0 \leq i \leq 14$, $N_c = 2560$. We segment $\bar{\mathbf{r}}_i$ into M blocks $\bar{\mathbf{r}}_{i,k}$, with fixed length $P = N_c/M$ and fill zeros to expand them to new N_c elements vectors as:

$$\bar{\mathbf{r}}_{i,k} = [\underbrace{0, ..., 0}_{k \times P}, \underbrace{\bar{r}_i(k \times P), ..., \bar{r}_i((k+1) \times P - 1)}_{P}, \underbrace{0, ..., 0}_{N_c - (k+1) \times P}]^T, \tag{4.25}$$

Hence,

$$\bar{\mathbf{r}}_i = \sum_{k=0}^{M-1} \bar{\mathbf{r}}_{i,k} \tag{4.26}$$

Similarly, the related transmitted signal vector is defined as:

$$\mathbf{x}_{i,k} = [\underbrace{0, ..., 0}_{k \times P}, \underbrace{x_i(k \times P), ..., x_i((k+1) \times P - 1)}_{P}, \underbrace{0, ..., 0}_{N_c - (k+1) \times P}]^T, \tag{4.27}$$

In the frequency domain, M new signal vectors can be written as $\bar{\mathbf{R}}_{i,k}$. Correspondingly, we estimate the mobile channel in one slot at M sampling instance. The channel estimates are $h_i(m; l), m = 384000 * frameindex + 2560 \times slot\,index + (0, \cdots, M-1) \times P - 1, l =$

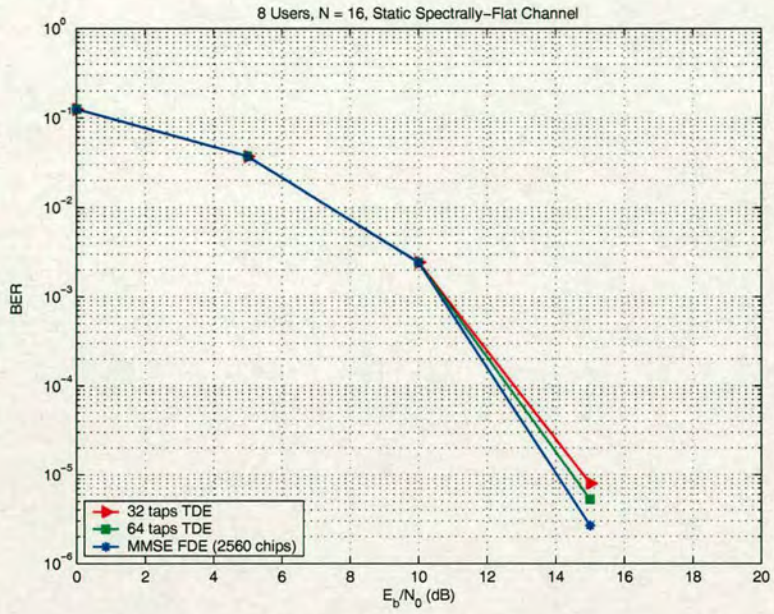

Figure 4.4: *BER versus E_b/N_0 for 8 users, Single cell downlink, Spreading factor=16, Channel without deep nulls*

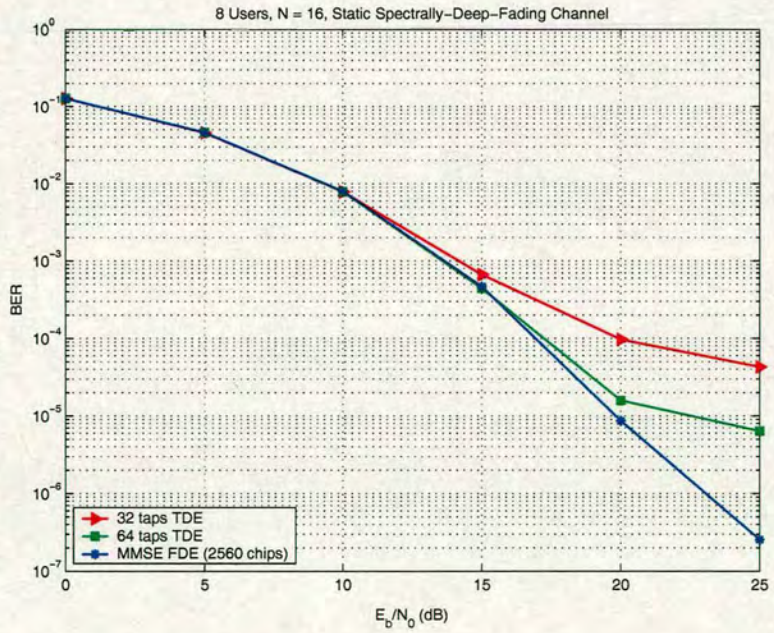

Figure 4.5: *BER versus E_b/N_0 for 8 users, Single cell downlink, Spreading factor=16, Channel with deep nulls*

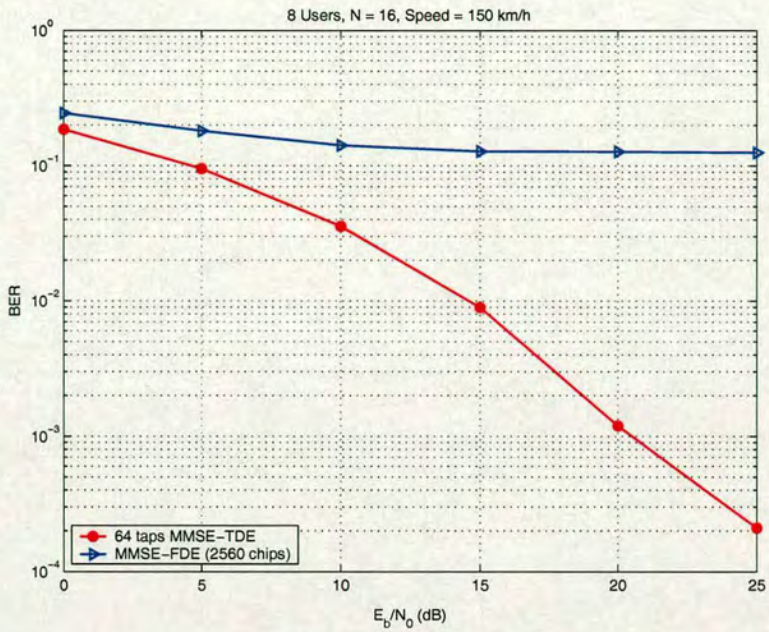

Figure 4.6: *BER versus E_b/N_0 for 8 users, Single cell downlink, Spreading factor=16, UMTS Vehicular A Channel, 2560 chips FDE and 64 taps TDE*

$0, \cdots, L-1$ where L is the order of the channel, and $\mathbf{H}_{i,m}$ is the 2560 length DFT vector of $h_i(m;l)$.The tail part of the convolution process for each block is $[t_{i,k}(0) \cdots t_{i,k}(L-2)]$. Expanded into one slot length with zeros, the tail vector is defined by:

$$\mathbf{t}_{i,k} = \begin{cases} [\underbrace{0,...,0}_{k\times P}, \underbrace{t_{i,k}(0),...,t_{i,k}(L-2)}_{L-1}, \underbrace{0,...,0}_{N_c-k\times P-L+1}]^T, 0 \le k \le M-2 \\ [\underbrace{t_{i,M-1}(0),...,t_{i,M-1}(L-2)}_{L-1}, \underbrace{0,...,0}_{N_c-L+1}]^T, k = M-1 \end{cases} \tag{4.28}$$

The frequency domain counterparts of the tail vectors are denoted by $\mathbf{T}_{i,k}$. The desired transmitted signal in the k-th block can then be recovered by the FDE $\mathbf{W}_{i,k}$ as given in (4.29):

$$\hat{\mathbf{x}}_{i,k} = IDFT\left\{(\bar{\mathbf{R}}_{i,k} + \mathbf{T}_{i,k} - \mathbf{T}_{i,k-1}) \otimes \mathbf{W}_{i,k}\right\} \tag{4.29}$$

where $\otimes$ represents element by element multiplication of two vectors.

Hence, the desired signal vector in the i-th slot is the summation of the M virtual FDE output:

$$\hat{\mathbf{x}}_i = [\hat{x}_i(0), \cdots, \hat{x}_i(N_c-1)]^T = \sum_{k=0}^{M-1} \hat{\mathbf{x}}_{i,k} \tag{4.30}$$

So far we have only the knowledge of $\mathbf{t}_{i,M-1}$ that can be obtained by channel estimate and the pilot information. However, the equation in (4.30) can be written as:

$$\begin{aligned}\hat{\mathbf{x}}_i = \sum_{k=0}^{M-1} \hat{\mathbf{x}}_{i,k} &= \sum_{k=0}^{M-1} IDFT\left\{(\bar{\mathbf{R}}_{i,k} + \mathbf{T}_{i,k} - \mathbf{T}_{i,k-1}) \otimes \mathbf{W}_{i,k}\right\} \\ &= IDFT\left\{\sum_{k=0}^{M-1} (\bar{\mathbf{R}}_{i,k} + \mathbf{T}_{i,k} - \mathbf{T}_{i,k-1}) \otimes \mathbf{W}_{i,k}\right\} \\ &= IDFT\left\{\sum_{k=0}^{M-1} \bar{\mathbf{R}}_{i,k} \otimes \mathbf{W}_{i,k} + \sum_{k=0}^{M-1} (\mathbf{T}_{i,k} - \mathbf{T}_{i,k-1}) \otimes \mathbf{W}_{i,k})\right\} \quad (4.31)\end{aligned}$$

Since channels in the neighboring segments can be considered almost identical. A reasonable assumption is made here that $\mathbf{W}_{i,0} \approx \mathbf{W}_{i,1}, \cdots, \mathbf{W}_{i,M-2} \approx \mathbf{W}_{i,M-1}$ so long as one slot is segmented into adequate large number of blocks. Therefore,

$$\begin{aligned}\hat{\mathbf{x}}_i &= IDFT\{\sum_{k=0}^{M-1} \{\bar{\mathbf{R}}_{i,k} \otimes \mathbf{W}_{i,k} + \mathbf{T}_{i,0} \otimes (\mathbf{W}_{i,0} - \mathbf{W}_{i,1}) + \mathbf{T}_{i,1} \otimes (\mathbf{W}_{i,1} - \mathbf{W}_{i,2}) + \cdots \\ &\quad + \mathbf{T}_{i,M-1} \otimes \mathbf{W}_{i,M-1}\} \\ &\approx IDFT\{\sum_{k=0}^{M-1} \bar{\mathbf{R}}_{i,k} \otimes \mathbf{W}_{i,k} + \mathbf{T}_{i,M-1} \otimes \mathbf{W}_{i,M-1}\} \quad (4.32)\end{aligned}$$

From the above equation, the only task then remaining is to reconstruct the circularity for the *(M-1)*-th block. We then made Monte Carlo simulations to investigate the achievable BER for different selected M value. The uncoded BER results are averaged over different channels (generated according to the UMTS Vehicular A channel model) for varying E_b/N_0. Obviously, the more segments one slot is broken into, the better performance we may get. However, more segments requires more computations. In Figure 4.7 and Figure 4.8, we observe that for small Doppler frequencies f_d, equaliser with small M value, $M = 2$, offers best tradeoff between complexity and performance. For large Doppler frequencies, larger M value, for example $M = 10$, is inevitable.

4.2.2 Computational Complexity Discussion

Similar to the partial transmit sequence (PTS) approaches [103] in OFDM systems (a solution for the inherent peak-to-average problem, PTS can also be used to reduce the ICI in OFDM systems), the input data block is partitioned into disjoint sub-blocks and each sub-block is zero padded to the original block length. The complexity for the proposed algorithm is increased

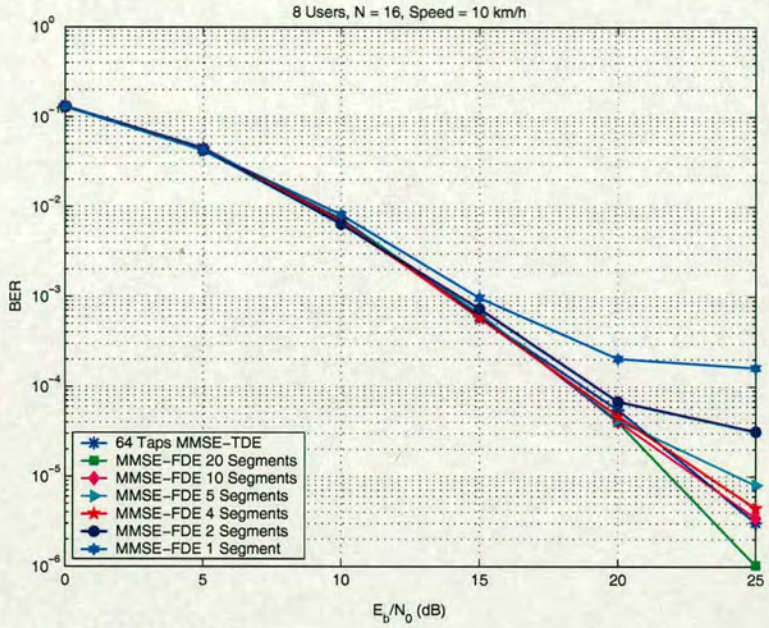

Figure 4.7: *System BER performance, Mobile speed = 10 km/h, f_d=19 Hz*

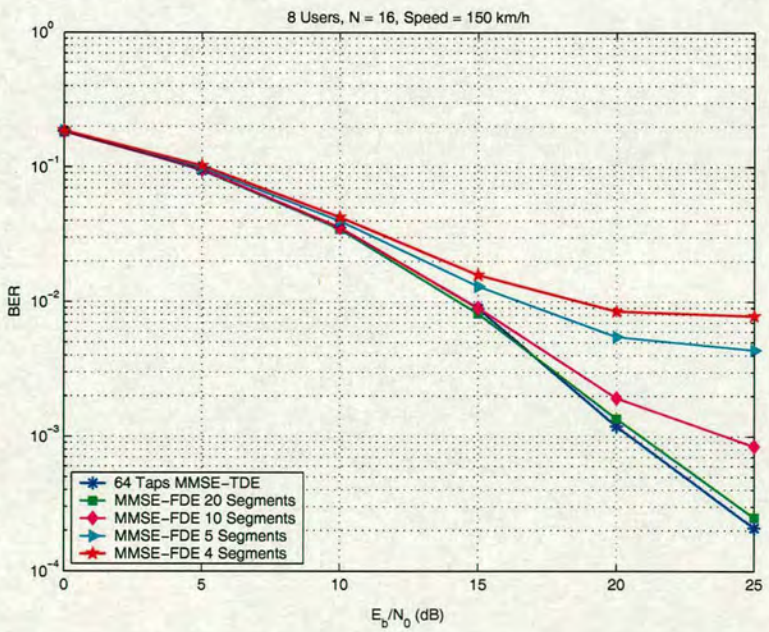

Figure 4.8: *System BER performance, Mobile speed = 150 km/h, f_d=277 Hz*

significantly with the increasing segment number M. However, if the transforms can take advantage of the fact that a large fraction of the input values are zero, the complexity can be reduced greatly. We note that recently there are already some efficient algorithms in calculating partial DFT (input sequence contains many zeros) such as "FFT pruning" [104] and "Transform decomposition" [105]. These algorithms utilize the redundancy in the input to reduce the number of operations below those of the FFT algorithms and have a computational complexity of $O(N_c log_2 P)$ instead of $O(N_c log_2 N_c)$. The algorithm proposed in [106] can further reduce the computational complexity to only $O(N_c + P log_2 P)$. It should be mentioned that the frequency domain equaliser is operated on one slot signal; hence, 2560 chips will be equalised at one time. For those segments where non-zero data are not starting from the beginnings, we may use a time-shift means by simply replacing all the Fourier transform twiddle factors of $W_{N_c}^{k}$ with $W_{N_c}^{k+F}$, where F is the time-shift. This operation will not change the algorithm complexity. In addition, the same receiver architecture can be used for the reception of OFDM signals and reduced the ICI due to channel variance.

4.2.3 Discussion of Results

This section has introduced a MMSE FDE for the UMTS in its downlink transmission and has presented a number of results that demonstrate its effectiveness. One slot signal is segmented into multiple processing blocks in order to combat channel variance within one slot. According the the mobile terminal speed, we can choose a reasonable number of segments to achieve the best tradeoffs between complexity and system performance.

4.3 Hybrid DFE with Variable Length Feedback Filter

4.3.1 Introduction

An alterative approach to OFDM, i.e. single carrier transmission with frequency domain equalisation and time domain decision feedback was proposed recently in [23] and [24]. In these papers, mathematical description of the FFF in the frequency domain and the FBF in the time domain was provided and it was shown that single carrier transmission with a hybrid decision feedback equalisation yields a capacity close to that of OFDM in both indoor and outdoor environments. For simplicity, a one-tap FBF is used in [23] and in [24] the author chose the length of the guard interval between successive blocks as the FBF length. The length is an important

factor for the filter in a variety of aspects: convergence rate, computational complexity, tracking ability and ultimately system performance. But so far, little research work related to this topic has been done. The performance costs for theoretical minimal-length equalisers have been discussed in [107], an algorithm which can adjust the filter length dynamically using a LMS algorithm according to a MSE criterion was proposed in [77]. However, the BER performance is of most concern in a communication system. A length chosen according to a MSE criterion will not necessarily be reasonable in terms of computational complexity. In a DFE, a FFF can to some extent eliminate the channel induced ISI and a feedback filter operates on the outputs of the decision device to further reduce the post-cursor ISI. When the FBF is converged, the taps are approximately the negative values of the residual ISI. Small FBF taps coefficients will not contribute very much to the system performance. Therefore, by observing the power of the FBF tap coefficients, we can remove those unnecessary taps. In this section, we will apply an algorithm based on an MSE criterion to a hybrid DFE and also take into consideration the BER performance, therefore, a more reasonable length can be found. The purpose of adjusting the FBF length is to avoid using excessively long filters which might induce excessively high computational complexity and achieve a good tradeoff between system performance and computations.

4.3.2 System Model

The system model used in this section is given in Figure 4.9. As can be seen in Figure 4.9, the feedforward part is implemented in the frequency domain while the FBF is operating in the time domain. The superscript $(.)^{(n)}$ is used to represent the n-th block since the hybrid DFE works on a block-by-block basis. Other notations introduced in Figure 4.9 are defined as follows:

- $\mathbf{W}^{(n)}$: N_f taps in the FFF vector, $\mathbf{W}^{(n)} = [W_0^{(n)}, \cdots, W_{N_f-1}^{(n)}]^T$
- $\mathbf{R}^{(n)}$: Fourier transform of the received signal, $\mathbf{R}^{(n)} = [R_0^{(n)}, \cdots, R_{N_f-1}^{(n)}]^T$
- $\mathbf{F}^{(n)}$: N_b taps in the FBF vector, $\mathbf{F}^{(n)} = [f_0^{(n)}, \cdots, f_{N_b-1}^{(n)}]^T$
- $\hat{d}_m^{(n)}$: Detected symbol and inputs to the FBF, $m = 1, \cdots, N_f$
- $e_m^{(n)}$: Error signal between equalised and detected symbol, $\mathbf{e}^{(n)} = [e_0^{(n)}, \cdots, e_{N_f-1}^{(n)}]^T$
- $\mathbf{E}^{(n)}$: Frequency domain counterpart of the time domain error signal $\mathbf{e}^{(n)}$

Figure 4.10 shows the specific frame structure that is required by such a hybrid DFE. Such a downstream transmission structure is adopted in both [23] and [24] but with slightly different definitions. Each unique word (UW) is generated by a pseudo-noise process and is the coun-

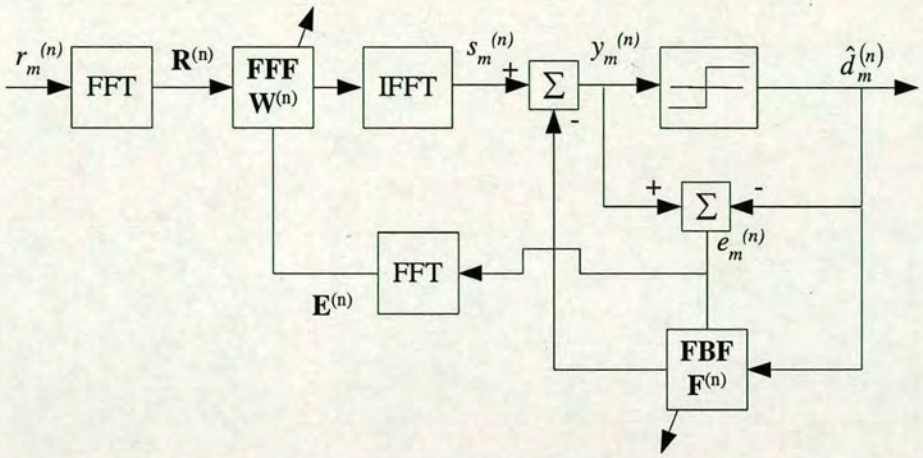

Figure 4.9: *Hybrid DFE system model*

terpart of the cyclic prefix used in an OFDM system. The UW acts as a cyclic prefix for the following block's signal and one block consists of the useful signal and the UW. Such a UW extension is suitable for the hybrid DFE since the first $N_b - 1$ interference symbols on each block signal are generated by the UW signal which is known at the receiver. If the signal data is cyclically extended as in an OFDM system, the DFE is unable to cancel the first $N_b - 1$ interference samples due to lack of the information of the cyclic prefix.

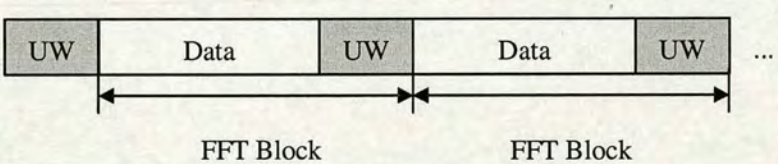

Figure 4.10: *Frame structure*

Let us suppose we are using a hybrid DFE with N_f FFT/IFFT FFF taps and N_b feedback taps. The MMSE-DFE solution is given in [23] and [24]. In this thesis, we focus on the adaptive DFE based on the LMS algorithm. The output signal from the feedforward frequency domain filter is represented by:

$$s_m^{(n)} = IFFT\{\mathbf{R}^{(n)} \otimes \mathbf{W}^{(n)}\}, \; m = 0, 1, \cdots, N_f - 1 \tag{4.33}$$

where $\otimes$ denotes element by element multiplication.

Thus, the n-th block time domain output samples can be expressed as:

$$y_m^{(n)} = s_m^{(n)} - \sum_{k=1}^{N_b} f_k \hat{d}_{m-k}^{(n)}, \; m = 0, \cdots, N_f - 1 \tag{4.34}$$

Detected symbols $\hat{d}_m^{(n)}$ are the decisions being made on the time domain signal $y_m^{(n)}$ and the N_b data symbols of when $m = -N_b, \cdots, -1$ should coincide with the N_b UW symbols. The well-known LMS algorithm can be adopted for both the FFF [56] and the FBF by adjusting tap coefficients in accordance with the error signal $e_m^{(n)}$ defined by:

$$e_m^{(n)} = \hat{d}_m^{(n)} - y_m^{(n)}, \; m = 0, \cdots, N_f - 1 \tag{4.35}$$

The FFF that operates in the frequency domain can be trained as:

$$W_l^{(n+1)} = W_l^{(n)} + \mu E_l^{(n)} R_l^{*(n)}, \; l = 0, \cdots, N_f - 1 \tag{4.36}$$

while the time domain FBF is updated as:

$$f_k^{(n+1)} = f_k^{(n)} - \mu \sum_{m=0}^{N_f-1} e_n(n) \hat{d}_{m-k}^{*(n)}, \; k = 1, \cdots, N_b \tag{4.37}$$

where μ represents the step size.

Equation (4.37) can be written in a vector form:

$$\mathbf{F}^{(n+1)} = \mathbf{F}^{(n)} - \mu \mathbf{D}^{(n)} \mathbf{e}^{(n)} \tag{4.38}$$

where the N_b_by_N_f decision data matrix $\mathbf{D}^{(n)}$ of the n-th block is defined as:

$$\mathbf{D}^{(n)} = \begin{pmatrix} \hat{d}_{-1}^{*(n)} & \hat{d}_{-2}^{*(n)} & \cdots & \hat{d}_{N_f-2}^{*(n)} \\ \vdots & \ddots & \ddots & \vdots \\ \hat{d}_{-N_b}^{*(n)} & \cdots & \hat{d}_{N_f-N_b-2}^{*(n)} & \hat{d}_{N_f-N_b-1}^{*(n)} \end{pmatrix} \tag{4.39}$$

In (4.39), the first N_b decision signals are identical to the N_b UW symbols. From equation (4.38) and (4.39), we note that, when the FBF length is increased by one tap, N_f complex multiplications are required to update the FBF coefficients.

We therefore illustrate the system performance with different FBF lengths. In Figure 4.11, steady state results (via Wiener filtering) are presented. The signal is assumed to be transmitted in an 11 taps fixed additive Gaussian noise channel with tap coefficients $\{0.2049-0.5711j\ -0.0794+0.0257j\ 0.0444+0.2524j\ 0.0358-0.3550j\ -0.0469+0.2139j\ -0.1613+0.0476j\ -0.0901+0.3005j\ 0.0541-0.2421j\ -0.3356+0.0789j\ -0.2184-0.1157j\ 0.0499-0.1157j\}$. The FBF length is increased from 0 (Linear Equaliser case) to 1, 5, 12, 20 and then 32 (The length of the UW is the maximum filter length that is available in the system). It can be seen from Figure 4.11 that the DFE offers an improved performance in a multipath channel over a linear equaliser (LE). The system performance improves with an increasing number of FBF taps. Moreover, there is a threshold value for the number of FBF taps; when the FBF taps reaches the threshold value, as can be seen in Figure 4.11, when the FBF tap length reaches approximately 12, further increasing the FBF taps does not gain much improvement in system performance. On the other hand, unnecessarily long length will increase the computational complexity. Hence, it is desirable to search for the length that offers the best trade-off between complexity and system performance. One adaptive length adjusting algorithm for the hybrid DFE is discussed in the following section.

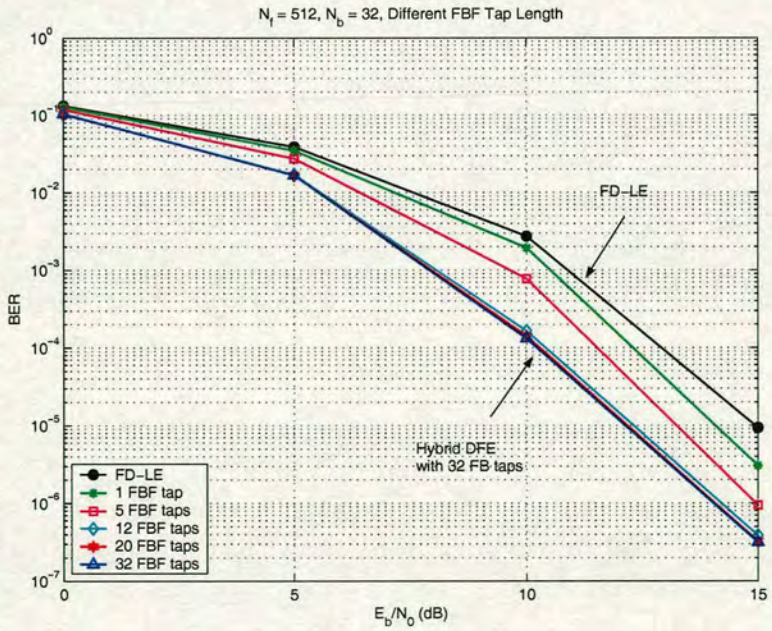

Figure 4.11: *System performances with different FBF length (FD-LE: Frequency domain linear equaliser)*

4.3.3 Length Adjusting Algorithm Based on MSE Criterion

It has been shown in [107] that varying the length of an equaliser can improve performance by adjusting the length according to the channel conditions. In this thesis, we first apply this idea on the feedback section. The total L_{total} ($1 \leq L_{total} \leq UW\ Length$) taps of the FBF is split into L_s concatenated segments of L_t taps each. Combining with the feedforward frequency domain equaliser, each segment in the FBF produces one equalised symbol $y_{m,i}^{(n)}(1 \leq i \leq L_s)$ and hence one error signal $e_{m,i}^{(n)}$ $(1 \leq i \leq L_s)$. From (4.35), similarly, we can write:

$$e_{m,i}^{(n)} = \hat{d}_m^{(n)} - y_{m,i}^{(n)},\ m = 0, \cdots, N_f - 1,\ 1 \leq i \leq L_s \tag{4.40}$$

Since the FFF is operating on a block by block basis, we define the MSE of the n-th block by the following expression.

$$J_i(n) = \frac{\sum_{m=0}^{N_f-1} \|e_{m,i}^{(n)}\|^2}{N_f},\ 1 \leq i \leq L_s \tag{4.41}$$

The output MSE produced by the last two segments are of interest in that they can be used to decide the changing direction of the FBF length as follows. We use $J_{L_s-1}(n)$ and $J_{L_s}(n)$ to denote the MSE corresponding to the $(L_s - 1)$-th and L_s-th segment, respectively. Similar to [77], we derive an adaptive algorithm for a hybrid DFE system:

If $J_{L_s}(n) < \alpha_{up} J_{L_s-1}(n)$,

then add "L_t" extra taps to the FBF, i.e. add one extra segment;

If $J_{L_s}(n) > \alpha_{down} J_{L_s-1}(n)$,

then remove "L_t" taps from the FBF, i.e. remove one segment.

α_{up} and α_{down} are two parameters that control the length adjusting process with $0 < \alpha_{up} < 1$ and $\alpha_{down} \geq 1$. The closer they are to 1, the more frequently the length will change. When one extra segment is added to the FBF, the taps in this new segment are initialized to zeros and when one segment is removed, all the remaining taps maintain their value and the $(L_s - 1)$-th segment becomes the last segment. Since the FBF coefficients are updated on a block by block basis, the segment changes take effect in the new block. Once an extra segment is added, the tap coefficients are set to zeros and by applying the new FBF on the new block, there will not be any differences between $J_{L_s-1}(n)$ and $J_{L_s}(n)$. Therefore, reapplying the updated filter coefficients on the current processing block signal can accelerate the convergence speed.

The performance of the hybrid DFE with variable length FBF is now examined via computer simulations. The multipath channel is assumed to be quasi-static (static within a block) and is modeled as an 11 taps (with total taps power normalized to 1) channel, Channel 1: *h={0.0102+0.2531j, 0.0661-0.1224j, 0.4763-0.1778j, -0.0282-0.0431j, 0.0329-0.2228j, 0.2588+ 0.3816j, -0.2201-0.1689j, 0.0069-0.1322j, 0.0873+0.2061j, 0.2958-0.3436j, 0.1030-0.1770j}*. There are $L_t = 2$ taps within each segment, $N_f = 512$, $N_b = 32$, $\alpha_{up} = 0.995$, $\alpha_{down} = 1$ and $\mu = 0.1$ are the selected parameters. In Figure 4.12, learning curves for one typical simulation run is given. It can be seen that the adaptive algorithm can effectively adjust the FBF length, the filter length is adjusted from either 2 taps or 32 taps. The filter length converges to around 20-22 taps in both cases under the MSE criterion. Figure 4.13 shows the steady state MSE

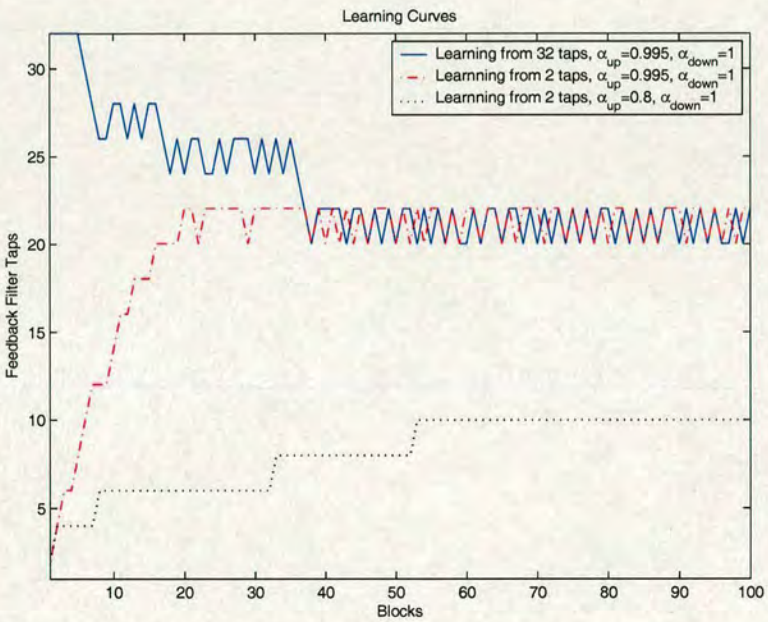

Figure 4.12: *Learning curves of the adaptive algorithm with different initializations,* $E_b/N_0 =$ 20 *dB*

that is achieved by the hybrid DFE with variable length FBF when the signal to noise ratio per bit is 20 dB. With 20 FBF taps, the hybrid DFE reaches its minimum MSE. Using too many taps, besides wasting computations, may increase the MSE owing to algorithm inaccuracies that increase with equaliser length [77]. Therefore, the MSE converge to its minimum when the length is 20 rather than the whole possible value. This fact is well documented in standard adaptive filter textbooks [71]. In Figure 4.14, the BER performance of the system is studied. When the FBF length is converged to an optimal value according to the MSE criterion, the simulation curves for FBF with length 22 and 32 are almost identical. However, when compared

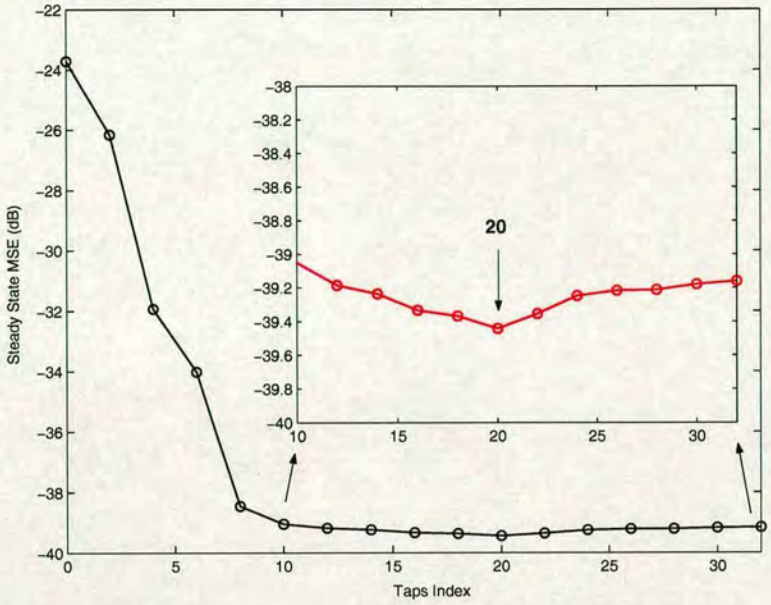

Figure 4.13: *Steady state MSE achieved vs FBF length*

with using FBF with fixed length 2, there is a significant improvement in the BER performance. Figure 4.15 shows the converged FBF coefficients for $E_b/N_0 = 20dB$. It can be seen in Figure 4.15 that the coefficients of taps between 11 and 32 become very small, thus the system performance will not change significantly when we choose only 10 taps. This can be seen from the simulation results given in Figure 4.14. Equalisers longer than 10 taps do not bring any significant advantage to the system performance but will increase the difficulty of convergence and tracking of the LMS algorithm as well as the computational complexity. The reason is that the length of the FBF is adjusted according to the MSE criterion. By applying the MSE criterion in the hybrid DFE may not always bring us to a reasonable length that can achieve good trade-offs between system BER performance and computational complexity. Merely using the MSE criterion results in the algorithm converging to an equaliser with a larger number of taps than is necessary. For example, choosing only 10 taps for the FBF we see an insignificant degradation in the system performance as measured by the BER compared with using 20 taps, the optimal value in terms of the MSE criterion. The extra taps waste computations and the improvement on the system performance is very limited. The reason that the FBF length converge to 20 taps is that we choose $\alpha_{up} = 0.995$ which is a value very close to but less than 1 and hence we can reach the minimum MSE that can be achieved. In other words, the "resolution" of the MSE is rather high, i.e. even a very small difference between $J_{L_s-1}(n)$ and $J_{L_s}(n)$ will lead to a filter length adjustment. In addition, when an α_{up} value close to 1 is chosen, the filter length will

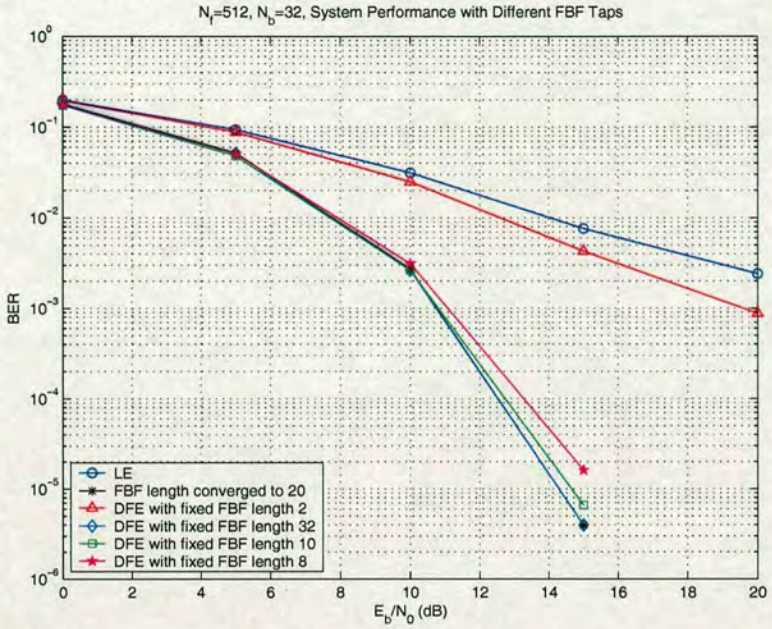

Figure 4.14: *System BER performance with variable FBF length*

change frequently if it starts learning from a small tap value. Consequently, the convergence speed is greatly accelerated and the filter length will converge to an optimal value according to the MSE criterion. However, this value is not always the best selection when we consider the BER performances, i.e., extra taps bring us very limited improvement on system performance. When choosing an α_{up} value less than but not so close to 1, for example $\alpha_{up} = 0.8$, the filter length will converge to a more reasonable value (as can be seen in Figure 4.12, it converges to 10 taps). This is at the expense of slowing down the learning speed. The other problem with the MSE criterion is that with $\alpha_{down} \geq 1$ if we start learning from large taps value, it is hard to converge to the most suitable taps value. Although the hybrid DFE can achieve a minimum steady state MSE with the converged FBF length, there exist some unnecessary taps that do not bring the system much improvement. As an example, in Figure 4.13, the filter length will just oscillate around 20 (at 20, the hybrid DFE achieves a minimum steady state MSE) but the more sensible length, based on a trade-off between complexity and performance is 10. From the above statements and simulation results, it is clear that some new restrictions are required complementary to the MSE criterion in order that the FBF length can converge to a more suitable value.

An interesting phenomenon is also shown in Figure 4.13, using too many taps (any taps beyond 20), besides wasting computations, may increase the MSE owing to algorithm inaccuracies

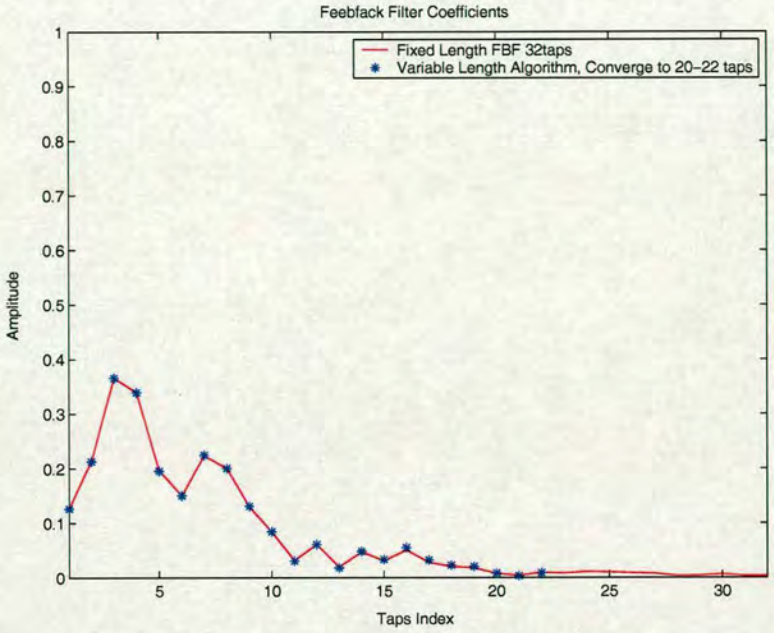

Figure 4.15: *Converged FBF coefficients,* $E_b/N_0 = 20dB$

that increase with equaliser length. These excess taps introduce excess ISI and consequently an excess MSE to the system. This fact is due to the misadjustment nature of the adaptive algorithms and is well documented in [71].

4.3.4 New Criterion

In a DFE, the FBF is being used to eliminate the residual ISI that is not completely removed by the FFF. Unlike a linear equaliser, a DFE has a particular property; in the FBF, when converged, the taps are approximately the negative values of the post-cursor taps of the combined convolution of the channel impulse response and the FFF [41]. Small FBF taps coefficients will not contribute too much to the system performance. Hence, by observing the power of the FBF taps, we can deduce whether we need to add one segment in the FBF or remove one. Usually, the length adjusting algorithms focus on the MSE improvements [77] [74] while in this thesis we also consider the impact of small FBF coefficients on system BER performance. We consider the impact of small FBF coefficients on BER performance rather than linking the FBF length mathematically to the BER. The purpose of adjusting the FBF length is to avoid using excessively long filters, which might induce excessively high computational complexity. Thus we achieve a good tradeoff between system performance and computational complexity. Firstly, we sum up the power of all L_{total} taps in the FBF and the power of the last two taps,

that is:

$$P_1 = \sum_{k=1}^{L_{total}} \|f_k^{(n)}\|^2 \quad P_0 = \|f_{L_{total}}^{(n)}\|^2 + \|f_{L_{total}-1}^{(n)}\|^2 \tag{4.42}$$

Subsequently, we adjust both the parameter α_{up} and the length of the FBF according to the ratio $R = P_0/P_1$. If R is larger than a pre-defined value γ_1, it is clear that we need to increase the FBF length; therefore, we choose a value close to 1 for α_{up} so that the length can be changed frequently and the learning speed is accelerated. Otherwise, we choose a small value for α_{up} to slow down the length changing speed so that it will not converge to an unnecessary long length. If R is below a certain value γ_2 ($\gamma_2 < \gamma_1$), we know that there are already extra long taps existing and then the length is reduced by one tap. Since the tap length is updated once a block, we can only use the instantaneous value of P_1 and P_0. If unfortunately, when the algorithm is not converged and the tap length is reduced one tap by mistake, in the next block, the length can still be adjusted in the right direction. The reason is that when one tap is reduced by mistake, $R > \gamma_1 > \gamma_2$ will result and a new value which is much closer to 1 (for example, 0.995) will be assigned to α_{up}, therefore, a small difference between $J_{L_s-1}(n)$ and $J_{L_s}(n)$ will require the FBF length to increase. The new criterion is very useful while the learning curve converges from a larger FBF length. Otherwise, by merely applying the MSE criterion, the learning curve will stop at an unnecessary long length value.

By applying the MSE criterion as that in [77] and also taking into account the FBF impact on system performance, we propose a new algorithm as depicted in a flowchart shown in Figure 4.16 to control the length of the FBF. Pseudo code shown below illustrates the algorithm based on the new criterion.

1). Initialization

Set the value of α_{up}, α_{down}, γ_1, γ_2, μ, the FBF length L_{total} and $\mathbf{W}^{(n)} = \mathbf{0}$, $\mathbf{F}^{(n)} = \mathbf{0}$

2). LMS algorithm

Use (4.36) and (4.37) to update the FFF and FBF coefficients

3). Length update algorithm, MSE criterion

Calculate $J_{L_s}(n)$ and $J_{L_s-1}(n)$

If $J_{L_s}(n) < \alpha_{up} J_{L_s-1}(n)$,

then add "L_t" extra taps to the FBF, i.e. add one extra segment;

If $J_{L_s}(n) > \alpha_{down} J_{L_s-1}(n)$,

then remove "L_t" extra taps from the FBF, i.e. remove one segment.

4). New criterion applied

Calculate P_0 and P_1

If $P_0/P_1 < \gamma_1$

Set α_{up} a new value α_{up}^1 (for example $\alpha_{up}^1 = 0.9$);

Else

Set α_{up} a new value α_{up}^2 closer to 1, $\alpha_{up}^1 < \alpha_{up}^2 < 1$ (for example $\alpha_{up}^2 = 0.995$);

End

If $P_0/P_1 < \gamma_2\,(\gamma_2 < \gamma_1)$

remove 1 tap from the FBF

End

To illustrate the effectiveness of the new algorithm, we consider the same channel: Channel 1 as mentioned in Section 4.3.3 and apply the new algorithm. We choose $\alpha_{up} = 0.995$, $\alpha_{up}^1 = 0.9$, $\alpha_{up}^2 = 0.995$, $\alpha_{down} = 1$, $\gamma_1 = 0.05$, $\gamma_2 = 0.02$ and $\mu = 0.1$ as the parameters in our algorithm. The FBF length is initialised to 2 taps in one case and 32 taps in the other case. The learning curves of both cases are presented in Figure 4.17 based on one simulation run. The BER performance with 8 taps FBF and 10 taps FBF are both shown in Figure 4.14. We see that by adopting a 10 tap FBF, the BER performance will not degrade as much compared with that FBF with 20 taps or 32 taps. Figure 4.18 shows the learning curve in scenarios when the channel changes from the previous complex one to a real channel, Channel 2: $h = \{0.7605, 0.5024, 0.3320, 0.2193, 0.0957, 0.0418\}$. It is obtained by averaging the learning curves in 100 simulation runs. During the first 50 blocks, signals are transmitted through Channel 1 (Channel 2) and at the 51st block, the environment changes to Channel 2 (Channel 1). It is clear from Figure 4.18 that the new algorithm tracks the channel change successfully

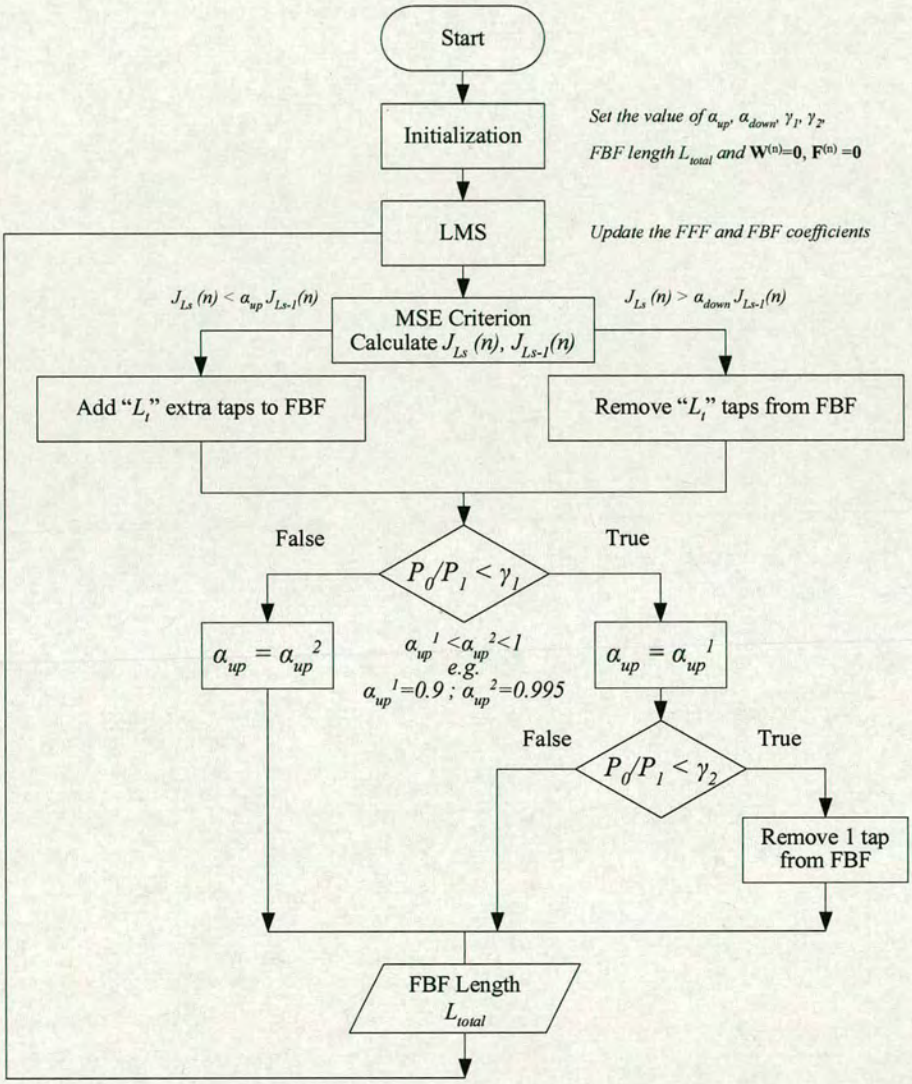

Figure 4.16: *Flowchart of the new algorithm*

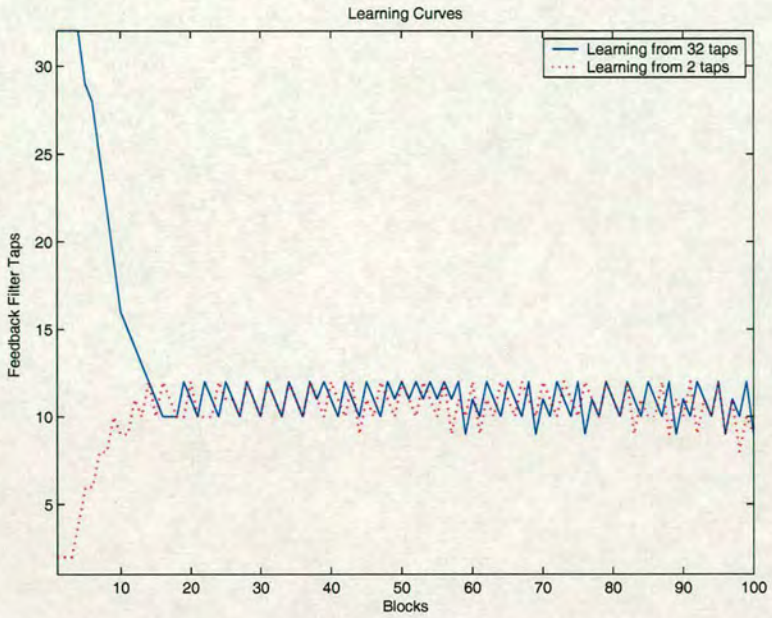

Figure 4.17: *Learning curves with the new algorithm*

in both scenarios.

4.3.5 Discussion of Results

Usually, hybrid DFEs have a fixed feedback length, either 1 or the length of the guard interval between successive blocks. In this thesis, a hybrid DFE with variable length FBF was proposed and evaluated. The purpose of adjusting the FBF length is to avoid using excessively long filters, which might induce excessively high computational complexity. The algorithm is based on the length adjustment of the FBF according to MSE criterion, and the impact of small FBF coefficients on system BER performance was also taken into consideration. We show that the proposed algorithm provides a sub-optimal length for the FBF and this filter length is more reasonable than the MMSE optimal one regarding system performance. Although the new FBF length is not the optimal one in terms of the MSE criterion, it achieves a good tradeoff between the MSE and the BER performance. The desired system performance is achieved with a reduced computational complexity. Simulation results show that it is also able to track channel changes successfully.

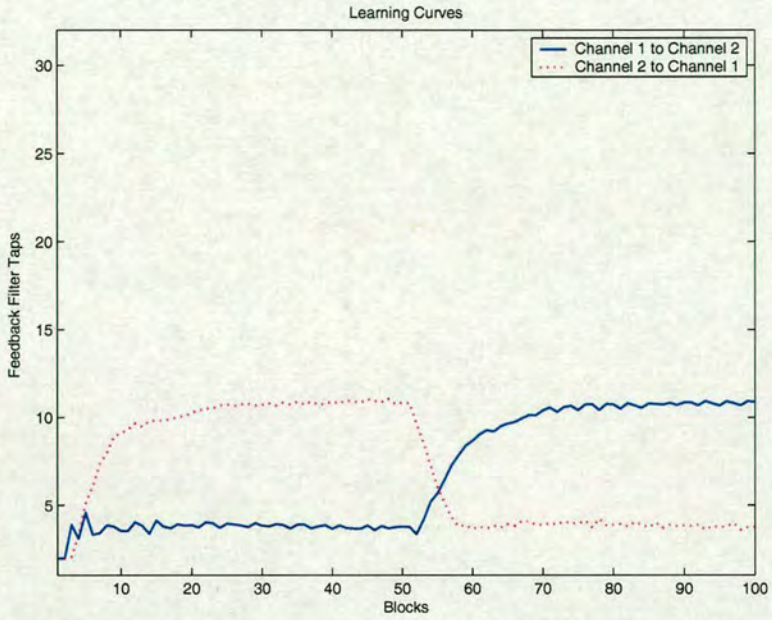

Figure 4.18: *Learning curves, Channel changes (Y axis feedback filter taps)*

4.4 Conclusions

The two FDE for UMTS in this chapter are extensions to the work reported in Chapter 3. In the previous chapter, a high power common pilot channel is deployed in the system for channel estimation and cyclic reconstruction purposes. However, this is not compatible with the current HSDPA system since only about 10%-20% signal power is allocated to the pilot channel. In this new chapter, the requirement of high power pilot channel is no longer necessary; hence, it can be successfully adopted for HSDPA systems.

In the second part, a hybrid DFE with varying length FBF is proposed. The equaliser is an adaptive DFE with a feedforward filter implemented in the frequency domain with its length fixed by the FFT/IFFT size and a feedback filter in the time domain. The FBF length is adjusted according to the achieved MSE. In addition, the impact of small FBF coefficients on system performance is taken into account so that a shorter filter length results. Computer simulations show that the proposed approach is capable of adjusting the feedback filter length to a satisfactory level in terms of MSE and system performance and is able to track channel changes successfully.

Chapter 5
Bandwidth Efficient Single Carrier Systems with Frequency Domain Equalisation

As in an OFDM system, the inserted CP will reduce the bandwidth efficiency in a SC-FDE system. In this chapter, MMSE Turbo equalisation and cyclic reconstruction are combined together to eliminate the normally required cyclic prefix for a SC-FDE system. The proposed method achieves much better performance than the RISIC approach by utilizing soft decoded information and introducing turbo equalisation. The performance of the proposed scheme is studied through simulations.

The system model is outlined in Section 5.2. Existing algorithms trying to remove the inserted CP are described in Section 5.3. In Section 5.4, we give a brief introduction to turbo codes and turbo equalisation. A combined turbo equalisation and cyclic reconstruction scheme is then proposed in Section 5.5. The simulation results are then given in Section 5.6. Finally, we discuss the computational complexity issue in Section 5.7 and draw conclusions in Section 5.8.

5.1 Introduction

Like an OFDM system, the drawback of the CP inserted in a single carrier system is that it reduces the bandwidth efficiency. The RISIC algorithm is proposed in [90] to solve this problem. In the RISIC algorithm, the missing CP is regarded as bursty distortion in a time domain block and the amount of distortion is diminished in an iterative process with hard decision being made in the frequency domain. However, in channels with deep nulls or long delays, the RISIC fails to achieve satisfactory system performance, which will be shown in later simulations. After that, the RISIC approach has been extended by other researchers in [108] and [91]. In [91], soft decoding information has been used for cyclic reconstruction. This extension of RISIC is of interest in this thesis and its performance is compared with the new combined iterative equalisation and cyclic reconstruction algorithm.

Turbo equalisation has been a hot topic for the past few years [109]. The turbo concept has been widely studied in equalisation, estimation and detection. One drawback of this approach is the increasing complexity with each iterative process. In order to overcome this problem and make it more practical, various sub-optimal methods using MMSE equaliser instead of the maximum *a posteriori* (MAP) equaliser have been proposed [110] [111] [112]. It has been shown that the MMSE turbo equaliser is a suboptimal solution capable of removing the ISI effectively with much less computational complexity.

In this chapter, a MMSE turbo equalisation algorithm and cyclic reconstruction through an iterative process are combined to form a new scheme.

5.2 Conventional SC-FDE System Model

A convolutionally coded single carrier system is studied. Transmitted signals are BPSK modulated, convolutionally coded, interleaved and divided into successive blocks. Each signal block is then cyclically extended and transmitted through mobile channels. Assuming that the composite channel response $h_i(l)$ is stationary within the i-th block and spans over L symbols, we may write the received signal in one block as $r_i(n)$, $0 \leq n \leq N_c - 1$ where N_c is the number of symbols within one block. Finally, we use $x_i(n)$ to denote the corresponding transmitted convolutionally coded signal. At the receiver, the CP is removed and the i-th block signal $r_i(n)$ can be written as:

$$r_i(n) = h_i(n) \odot x_i(n) + v_i(n) \tag{5.1}$$

where $\odot$ and $v_i(n)$ represents circular convolution and a discrete zero mean white Gaussian noise process with variance σ_n^2, respectively.

Correspondingly, in the frequency domain,

$$R_i(w) = H_i(w)X_i(w) + V_i(w) \tag{5.2}$$

where $0 \leq w \leq N_c - 1$, $R_i(w)$, $H_i(w)$, $X_i(w)$ and $V_i(w)$ are the DFT of $r_i(n)$, $h_i(l)$, $x_i(n)$ and $v_i(n)$, respectively. Further defining $W_i(w)$, $0 \leq w \leq N_c - 1$ as the equaliser coefficients in the frequency domain, the MMSE equaliser in the frequency domain that minimizes the cost

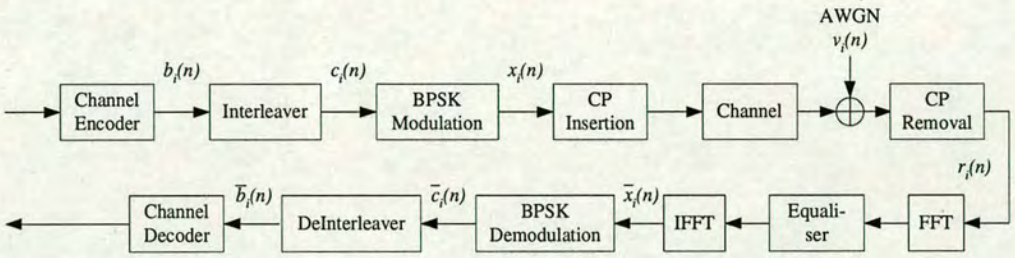

Figure 5.1: *Coded single carrier system with frequency domain equalisation*

function:

$$J = E\left\{\frac{1}{N_c}\sum_{w=0}^{N_c-1}|W_i(w)H_i(w)X_i(w) + W_i(w)V_i(w) - X_i(w)|^2\right\} \tag{5.3}$$

is given by the following expression:

$$W_i(w) = \frac{H_i^*(w)}{|H_i(w)|^2 + \sigma_n^2/\sigma_d^2} \tag{5.4}$$

σ_n^2, σ_d^2 and $H_i^*(w)$ are the variance of the additive Gaussian noise, the variance of the received signal and the conjugate of $H_i(w)$, respectively. It is derived by setting the gradient of "J" with respect to the equaliser coefficients $W_i(w)$ to zero.

The equalisation process can be performed by multiplying the signal spectrum $R_i(w)$ by $W_i(w)$. Outputs from the equaliser are transformed back to the time domain by IDFT. The equalised signal can be written as:

$$\bar{x}_i(n) = IDFT\{R_i(w)\cdot W_i(w)\}\,,\ 0 \le n \le N_c - 1\,,\ 0 \le w \le N_c - 1 \tag{5.5}$$

The transmitted information is then obtained by deinterleaving, decoding and demodulating $\bar{x}_i(n)$. The whole process can be summarised in Figure 5.1.

5.3 Existing Cyclic Reconstruction Methods

5.3.1 SC-FDE without CP

In this chapter, our purpose is to develop a bandwidth efficient SC-FDE, therefore, we first study a single carrier system without CP. When there is no CP inserted, the channel distortion

becomes a linear convolution on the transmitted signal and IBI exists, i.e., interference caused by the preceding block can not be eliminated and will affect the current block. Thus, we rewrite (5.1) as:

$$r_i(n) = \sum_{l=0}^{L-1} h_i(l)x_i(n-l)u(n-l) + \left(\sum_{l=0}^{L-1} h_{i-1}(l)x_{i-1}(n+N_c-l)(1-u(n-l)) \right) + v_i(n) \tag{5.6}$$

where $u(.)$ represents the unit step function. The second term in (5.6) represents the IBI term caused by the *(i-1)*-th block. It can be estimated and subtracted from the current block. Then a block signal free of IBI is given by:

$$\bar{r}_i(n) = r_i(n) - \sum_{l=0}^{L-1} h_{i-1}(l)x_{i-1}(n+N_c-l)(1-u(n-l)) \tag{5.7}$$

We need to reconstruct the required circularity so that the time and frequency-domain descriptions of the convolution are essentially equivalent. If the last part of the transmitted signal is known, then it can be used for cyclic reconstruction as shown in (5.8).

$$\tilde{r}_i(n) = \bar{r}_i(n) + \sum_{l=0}^{L-1} h_i(l)x_i(n+N_c-l)(1-u(n-l)) \tag{5.8}$$

Correspondingly, in the frequency domain,

$$\tilde{R}_i(w) = H_i(w)X_i(w) + V_i(w) \tag{5.9}$$

Unfortunately, perfect cyclic reconstruction is not possible since the last part of the signal is not available at the receiver. The RISIC scheme [90] employs an iterative cyclic reconstruction based on hard detection, and this is discussed together with its extension [91].

5.3.2 RISIC and Its Extension

The RISIC algorithm proceeds as follows:

Step 1. Tail cancellation based on decision on the previous block as in (5.7), the residual ISI is calculated and subtracted;

Step 2. $\bar{r}_i(n)$ obtained in Step 1 are converted to the frequency domain using FFT and equalised (ZF or MMSE equalisation);

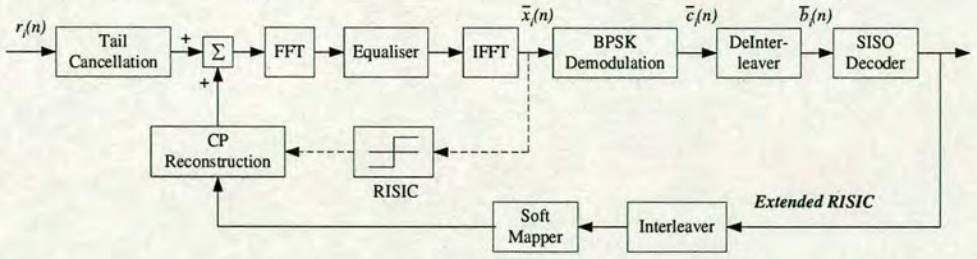

Figure 5.2: *RISIC scheme and its extended version*

Step 3. The equalised signal is transformed back to the time domain by IFFT;

Step 4. Hard decisions are made on the time domain signal to give an estimated $\tilde{x}_i^I(n)$. *I is denoted by an iteration number with an initial value of I=1;*

Step 5. If $I = I_{end}$ *where* I_{end} *is a predefined iteration number, stop;*

Step 6.Reconstruct the effect of the missing CP by (5.8);

Step 7. $\tilde{r}_i(n)$ *are converted to the frequency domain using FFT and equalised (ZF or MMSE equalisation);*

Step 8. $I = I + 1$ *and jump to Step 3.*

The scheme reported in [91] is an extended version of RISIC that exploits the power of the FEC for cyclic reconstruction to obtain more reliable estimates of the missing CP. Instead of making hard decisions like RISIC, the new approach utilizes soft-input soft-output (SISO) decoder to generate soft information for cyclic reconstruction. The equalised signal is first converted into the log-likelihood ratio (LLR) values and fed into the SISO decoder. The outputs of the SISO decoder are then mapped to soft decisions and used for cyclic reconstruction. This soft decoding approach achieves better performance than the RISIC with the ZF equaliser and channels with moderate nulls. The structure of the RISIC scheme and its extended version is given in Figure 5.2.

5.4 Turbo Iterative Equalisation

In this section, we discuss the basic idea of turbo equalisation, an iterative equalisation scheme that achieves significant system performance gain for communication systems.

5.4.1 Turbo Codes

Turbo codes were first proposed in 1990s [113] [114] and proved to be an efficient and powerful coding scheme. Turbo code consists of two or more components which are normally convolutional encoders. Unlike the decoding process of any traditional concatenated codes, for turbo codes, soft information is exchanged between/among component decoders to fully exploit the information learned by each decoders. The soft information is the so-called extrinsic information representing extra knowledge gleaned from the decoding process, it is typically calculated as a LLR with its polarity determining the sign of the bit and its amplitude representing the probability of a correct decision. The symbol by symbol MAP algorithm [115] is an optimal decoding way for turbo codes, however, too complex to be used in practice. Since the discovery of turbo codes, several decoding techniques had been proposed aiming at reducing the complexity of the optimal MAP algorithm (the Max-Log-MAP algorithm [116]) or finding alternatives (soft-output Viterbi algorithm (SOVA) [117]).

5.4.2 Turbo Equalisation

The iterative turbo decoding concept has evoked a joint equalisation and decoding structure, namely Turbo equalisation [118], where a SISO detector/equaliser and a soft decoder mutually exchange the extrinsic soft information. In the original scheme proposed in [118], the SISO equaliser is a MAP detector. The high complexity of such a MAP-based turbo equalisation prevent it from practical uses, especially for systems with high level modulation and long delay spreads [110] [111]. Therefore, low complexity linear SISO had been studied such as an ISI canceller [112] and MMSE equaliser [110] [111] [119]. In this section, MAP detector assisted Turbo equalisation is briefly introduced.

The symbol by symbol MAP detection algorithm [115] can be used not just for decoding but also for equalisation [118] [109]. Given a received sequence $\mathbf{r}$, the goal of the MAP algorithm is to deliver the conditional LLR $L(x_k|\mathbf{r})$ defined as:

$$L(x_k|\mathbf{r}) = ln\frac{P(x_k=+1|\mathbf{r})}{P(x_k=-1|\mathbf{r})} = ln\frac{\sum_{\forall(s',s),x_k=+1} p(s',s,\mathbf{r})}{\sum_{\forall(s',s),x_k=-1} p(s',s,\mathbf{r})} \tag{5.10}$$

where s' denotes the previous state, i.e. state at time $k-1$, s represents the current state, i.e. state at time k. At each time instant, the index pair (s',s) corresponding to all valid transitions from state s' to state s can uniquely determine an input symbol x_k and a channel output symbol

v_k. The noise free input-output relationship is represented as:

$$v_k = \sum_{l=0}^{L-1} h_l x_{k-l} \tag{5.11}$$

For a memoryless channel, the joint probability $p(s', s, \mathbf{r})$ can be decomposed into three independent terms:

$$p(s', s, \mathbf{r}) = \underbrace{p(s', r_1, \cdots, r_{k-1})}_{\alpha_{k-1}(s')} \cdot \underbrace{P(s|s') \cdot p(r_k|s', s)}_{\gamma_k(s',s)} \cdot \underbrace{p(r_{k+1}, \cdots, r_N|s)}_{\beta_k(s)} \tag{5.12}$$

The forward recursion of the MAP algorithm is given by:

$$\alpha_k(s) = \sum_{s'} \gamma_k(s', s) \cdot \alpha_{k-1}(s') \tag{5.13}$$

with an initial value $\alpha_0(s) = P(s_{start} = s)$. The backward recursion can be computed as:

$$\beta_{k-1}(s') = \sum_{s} \gamma_k(s', s) \cdot \beta_k(s) \tag{5.14}$$

with an initial value $\beta_{N_c}(s) = 1$ for all s.

For every valid pair (s', s), the transition probability $\gamma_k(s', s)$ can be computed as:

$$\gamma_k(s', s) = P(x_k) \cdot p(r_k|v_k) \tag{5.15}$$

Given the LLR $L(x_k) = ln\frac{P(x_k=+1)}{P(x_k=-1)}$, we can calculate the probability that $x_k = +1$ or $x_k = -1$ as:

$$P(x_k = \pm 1) = \left(\frac{e^{-L(x_k)/2}}{1 + e^{-L(x_k)}}\right) \cdot e^{\pm L(x_k)/2} \tag{5.16}$$

Since $r_k = v_k + n_k$, noise samples n_k are additive white Gaussian noise with variance σ_n^2, the $p(r_k|v_k)$ term in (5.15) is given by:

$$p(r_k|v_k) = \frac{1}{\sqrt{2\pi\sigma_n^2}} e^{\frac{-(r_k - v_k)^2}{2\sigma_n^2}} \tag{5.17}$$

From (5.13), (5.14), (5.15) and the decomposition of $p(s', s, \mathbf{r})$ in (5.12), the conditional LLR $L(x_k|\mathbf{r})$, also called *a posteriori* information, can be computed as in (5.10). Equations (5.10)

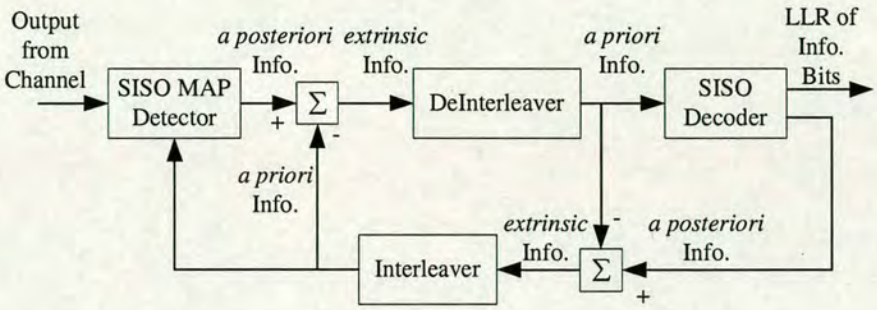

Figure 5.3: *MAP assisted Turbo equaliser structure*

to (5.17) are from [115]. A MAP assisted Turbo equaliser structure is illustrated in Figure 5.3. According to [109], the output *a posteriori* from the MAP equaliser can be split into the extrinsic LLR $L_{ext}(x_k|\mathbf{r})$ and the intrinsic LLR $L(x_k)$, therefore, we can compute the extrinsic information delivered by the MAP detector as:

$$L_{ext}(x_k|\mathbf{r}) = L(x_k|\mathbf{r}) - L(x_k) \tag{5.18}$$

The soft extrinsic information $L_{ext}(x_k|\mathbf{r})$ is deinterleaved and input to the SISO MAP decoder as soft *a posteriori* information. In a similar way to Turbo decoding, the SISO MAP decoder generates its soft extrinsic information, interleaves and feeds it back to the equaliser as *a posteriori* LLR $L(x_k)$. Thus, this fulfils an entire iteration. The process repeats for the desired number of iterations, after which the SISO decoder outputs a hard decision of the uncoded data.

5.5 Combined Turbo Equalisation and Cyclic Reconstruction

Turbo equalisation based on MMSE criterion has been widely studied in [110] [111] [112]. The channel equaliser can be considered as one component part in a concatenated turbo structure. Extrinsic posteriori information from the SISO decoder is utilized to generate "soft bits" as a-priori information for the MMSE SISO detector. Using the standard BCJR algorithm [115] as the SISO decoder, in turbo equalisation, not only the LLRs of information bits are calculated but also the LLR of every coded bit. Since turbo equalisation and cyclic reconstruction are both conducted in an iterative manner, in a new structure as in Figure 5.4, they are jointly combined in one iteration process. With a slight increase in computational complexity compared to the extended RISIC (For both systems, the complexity is dominated by the MAP decoder), the

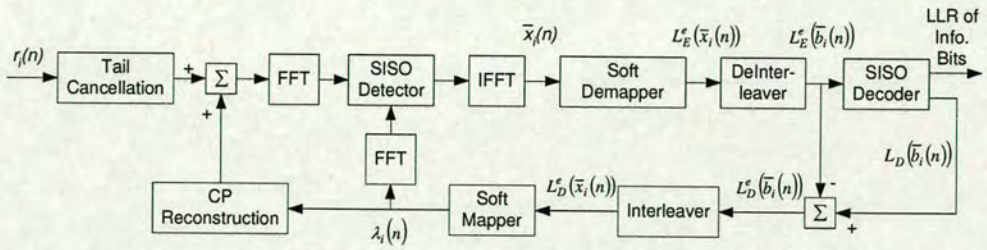

Figure 5.4: *Combined turbo equalisation and cyclic reconstruction*

improvement in system performance that can be achieved is significant.

5.5.1 Turbo equalisation for SC-FDE

In this chapter, we employ a MMSE turbo equaliser for SC-FDE developed in [119]. We rewrite (5.1) in its vector format:

$$\tilde{\mathbf{r}}_i = \mathbf{H}_{c,i}\mathbf{x}_i + \mathbf{v}_i \tag{5.19}$$

where $\tilde{\mathbf{r}}_i = [\tilde{r}_i(0), \cdots, \tilde{r}_i(N_c-1)]^T$, $\mathbf{x}_i = [x_i(0), \cdots, x_i(N_c-1)]^T$, $\mathbf{v}_i = [v_i(0), \cdots, v_i(N_c-1)]^T$ and $\mathbf{H}_{c,i}$ is a circular channel matrix that can be diagonalized by Fourier transform (the superscript i indicates it is a channel matrix for the i-th block) and is assumed perfectly known at the receiver. In the time domain, we have the detected $\bar{\mathbf{x}}_i = [\bar{x}_i(0), \cdots, \bar{x}_i(N_c-1)]^T$.

Using the approximate implementation of the MMSE turbo equalisation as in [110], the time domain equaliser $\mathbf{c}_i$ is computed at $n = 0$ under the assumption that there is no *a priori* information for $\mathbf{x}_i$, i.e. the elements of $\mathbf{x}_i$ are equally +1 or -1.

$$\mathbf{c}_i = (\frac{\sigma_n^2}{\sigma_d^2}\mathbf{I}_{N_c} + \mathbf{H}_{c,i}{\mathbf{H}_{c,i}}^H)^{-1}\mathbf{H}_{c,i}\mathbf{u} \tag{5.20}$$

where $\mathbf{u} = [1, 0, 0, \cdots, 0]^T$.

As can be seen in Figure 5.4, in an iterative equalisation, extrinsic information $L_D^e(\bar{b}_i(n))$ is delivered to the interleaver by the SISO decoder. The reordered $L_D^e(\bar{x}_i(n))$ is used to generate the soft bits of $x_i(n)$ as:

$$\lambda_i(n) = E\{x_i(n)\} = P(x_i(n) = +1) - P(x_i(n) = -1) = \tanh(\frac{1}{2}L_D^e(\bar{x}_i(n))) \tag{5.21}$$

The extrinsic information delivered by the SISO detector is based upon the received signal $\mathbf{r}_i$ and $\lambda_i(m), m \neq n$, the priori information about the code bits other than the n-th bit. Given $\lambda_i(m), m \neq n$, we can obtain,

$$\bar{x}_i(n) = E\{x_i(n)\} + \mathbf{c}_i^H \left(\mathbf{r}_i - E\{\mathbf{r}_i\}\right) = \mathbf{c}_i^H \left(\mathbf{r}_i - \mathbf{H}_{c,i}\vec{\lambda}_i + \lambda_i(n)\mathbf{H}_{c,i}\mathbf{u}\right) \tag{5.22}$$

where $\vec{\lambda}_i = [\lambda_i(0), \cdots, \lambda_i(N_c - 1)]^T$.

The detector for a SC-FDE is given by $\mathbf{W}_i = diag\{W_i(0), \cdots, W_i(N_c - 1)\}$ in the frequency domain and an equivalent circular equaliser matrix $\mathbf{W}_{c,i}$ in the time domain. Hence,

$$\bar{\mathbf{x}}_i = \mathbf{W}_{c,i}\mathbf{r}_i - \mathbf{W}_{c,i}\mathbf{H}_{c,i}\vec{\lambda}_i + \mathbf{c}_i^H\mathbf{H}_{c,i}\mathbf{u}\vec{\lambda}_i \tag{5.23}$$

The relationship between the time domain equaliser coefficients and the frequency domain equaliser coefficients can be described as:

$$[W_i(0), \cdots, W_i(N_c - 1)]^H = \mathbf{F}\mathbf{c}_i \tag{5.24}$$

where $\mathbf{F}$ is the Fourier transform matrix. We define $\mathbf{H}_i$ in the frequency domain as:

$$\mathbf{H}_i = diag\{H_i(0), \cdots, H_i(N_c - 1)\} = diag\{\mathbf{F}[h_i(0), \cdots, h_i(L-1), \mathbf{0}_{1\_by\_N_c-L}]\} \tag{5.25}$$

$\bar{\mathbf{X}}_i$ can be obtained by applying the DFT on $\bar{\mathbf{x}}_i$ as:

$$\begin{aligned}
\bar{\mathbf{X}}_i &= \mathbf{F}\bar{\mathbf{x}}_i \\
&= \mathbf{F}\mathbf{W}_{c,i}\mathbf{r}_i - \mathbf{F}\mathbf{W}_{c,i}\mathbf{H}_{c,i}\vec{\lambda}_i + \mathbf{F}\mathbf{c}_i^H\mathbf{H}_{c,i}\mathbf{u}\vec{\lambda}_i \\
&= \mathbf{F}\mathbf{W}_{c,i}\mathbf{r}_i - \mathbf{F}\mathbf{W}_{c,i}\mathbf{H}_{c,i}\vec{\lambda}_i + \mathbf{F}((\mathbf{H}_{c,i})^H\mathbf{c}_i)^H\mathbf{I}\mathbf{u}\vec{\lambda}_i \\
&= \mathbf{F}\mathbf{W}_{c,i}\mathbf{r}_i - \mathbf{F}\mathbf{W}_{c,i}\mathbf{H}_{c,i}\vec{\lambda}_i + \mathbf{F}\left((\mathbf{H}_{c,i})^H\mathbf{c}_i\right)^H\left(\frac{1}{N_c}\mathbf{F}^H\mathbf{F}\right)\mathbf{u}\vec{\lambda}_i \\
&= \mathbf{F}\mathbf{W}_{c,i}\mathbf{r}_i - \mathbf{F}\mathbf{W}_{c,i}\mathbf{H}_{c,i}\vec{\lambda}_i + \frac{1}{N_c}\mathbf{F}\left(\mathbf{F}(\mathbf{H}_{c,i})^H\mathbf{c}_i\right)^H\mathbf{F}\mathbf{u}\vec{\lambda}_i \\
&= \mathbf{F}\mathbf{W}_{c,i}\mathbf{F}^{-1}\mathbf{F}\mathbf{r}_i - \mathbf{F}\mathbf{W}_{c,i}\mathbf{F}^{-1}\mathbf{F}\mathbf{H}_{c,i}\mathbf{F}^{-1}\mathbf{F}\vec{\lambda}_i + \frac{1}{N_c}\mathbf{F}\mathbf{c}_i^H\mathbf{F}^H\mathbf{H}_i\mathbf{F}\mathbf{u}\vec{\lambda}_i \\
&= \mathbf{W}_i\mathbf{F}\mathbf{r}_i - diag\{W_i(0)H_i(0), \cdots, W_i(N_c-1)H_i(N_c-1)\}\mathbf{F}\vec{\lambda}_i \\
&\quad + \frac{1}{N_c} \cdot \sum_{w=0}^{N_c-1}[W_i(w)H_i(w)] \cdot \mathbf{F}\vec{\lambda}_i
\end{aligned} \tag{5.26}$$

The properties $\mathbf{F}^H = N_c \cdot \mathbf{F}^{-1}$ and $\mathbf{Fu} = \underbrace{[1, \cdots, 1]}_{N_c}^T$ are used in the derivation of (5.26). From (5.20), we can derive $\mathbf{W}_i$ in the frequency domain as:

$$W_i(w) = \frac{H_i^*(w)}{|H_i(w)|^2 + \sigma_n^2/\sigma_d^2} \tag{5.27}$$

which is the same as (5.4). $\bar{\mathbf{X}}_i$ is transformed back to the time domain detected signal $\bar{\mathbf{x}}_i$ via IDFT.

As in [112], we assume the output of the MMSE equaliser as the output from an equivalent AWGN channel with $\mathbf{x}_i$ as its input:

$$\bar{x}_i(n) = \varphi(n)x_i(n) + \eta(n)\,,\ n = 0, \cdots, N_c - 1 \tag{5.28}$$

where $\varphi(n)$ is an equivalent fading factor, $\eta(n)$ is AWGN with zero mean and variance σ^2.

$$\begin{aligned} \varphi = \varphi(n) &= E\{\bar{x}_i(n)x_i(n)\} \approx \mathbf{c}_i^H \mathbf{H}_{c,i}\mathbf{u} = \frac{1}{N_c} \cdot \sum_{w=0}^{N_c-1} [W_i(w)H_i(w)] \\ \sigma^2 &= var\{\bar{x}_i(n)\} = \frac{1}{N_c} \cdot \sum_{n=0}^{N_c-1} |\bar{x}_i(n) - \varphi \cdot sign(\bar{x}_i(n))|^2 \end{aligned} \tag{5.29}$$

The probability of the equaliser output $\bar{x}_i(n)$ is:

$$P(\bar{x}_i(n)|x_i(n) = \pm 1) = \frac{1}{\sigma\sqrt{2\pi}} \cdot exp(-\frac{1}{2\sigma^2}(\bar{x}_i(n) \mp \varphi)^2) \tag{5.30}$$

Therefore, the LLR of $\bar{x}_i(n)$ is given by:

$$\begin{aligned} L_E^e(\bar{x}_i(n)) &= L(\bar{x}_i(n)|x_i(n)) = ln\left(\frac{P(\bar{x}_i(n)|x_i(n) = +1)}{P(\bar{x}_i(n)|x_i(n) = -1)}\right) \\ &= ln\left(\frac{exp(-\frac{1}{2\sigma^2}(\bar{x}_i(n) - \varphi)^2)}{exp(-\frac{1}{2\sigma^2}(\bar{x}_i(n) + \varphi)^2)}\right) \\ &= \left(-\frac{1}{2\sigma^2}(\bar{x}_i(n) - \varphi)^2\right) - \left(-\frac{1}{2\sigma^2}(\bar{x}_i(n) + \varphi)^2\right) \\ &= \frac{2\varphi}{\sigma^2}\bar{x}_i(n) \end{aligned} \tag{5.31}$$

For the first iteration, no *a-priori* information from the decoder is available, from [119] [112], $L_E^e(\bar{x}_i(n)) = \frac{2}{1-\varphi^2}\bar{x}_i(n)$.

Given the received signal $\tilde{\mathbf{r}}_i$, *a priori* information $[L_D^e(\bar{x}_i(0)), \cdots, L_D^e(\bar{x}_i(N_c-1))]^T$ and perfect channel estimates $h_i(l)$, we summarise the frequency domain turbo equalisation algorithm as follows:

1. $\tilde{\mathbf{R}}_i = \mathbf{F}\tilde{\mathbf{r}}_i$, $[H_i(0), \cdots, H_i(N_c-1)]^T = \mathbf{F}[h_i(0), \cdots, h_i(L-1), \mathbf{0}_{1\_by\_N_c-L}]^T$,
   $\varphi = \frac{1}{N_c} \cdot \sum_{w=0}^{N_c-1} (\frac{H_i(w)H_i^*(w)}{|H_i(w)|^2+\sigma_n^2/\sigma_d^2})$
   $\sigma^2 = var\{\bar{x}_i(n)\} = \frac{1}{N_c} \cdot \sum_{n=0}^{N_c-1} |\bar{x}_i(n) - \varphi \cdot sign(\bar{x}_i(n))|^2$

2. If a priori information $[L_D^e(\bar{x}_i(0)), \cdots, L_D^e(\bar{x}_i(N_c-1))]^T$ is available, then go to 3). For the first iteration,
   $\bar{\boldsymbol{X}}_i = [\bar{X}_i(0), \cdots, \bar{X}_i(N_c-1)]^T$, $\bar{X}_i(w) = W_i(w)\tilde{R}_i(w)$, $w = 0, \cdots, N_c-1$
   $\bar{\boldsymbol{x}}_i = [\bar{x}_i(0), \cdots, \bar{x}_i(N_c-1)]^T = \boldsymbol{F}^{-1}\bar{\boldsymbol{X}}_i$, $L_E^e(\bar{x}_i(n)) = \frac{2}{1-\varphi^*}\bar{x}_i(n)$, $n = 0, \cdots, N_c-1$

3. Calculate soft bits, $\lambda_i(n) = \tanh(\frac{1}{2}L_D^e(\bar{x}_i(n)))$, $n = 0, \cdots, N_c-1$
   $\vec{\Lambda}_i = [\Lambda_i(0), \cdots, \Lambda_i(N_c-1)]^T = \boldsymbol{F}\vec{\lambda}_i$
   $\bar{X}_i(w) = W_i(w)\tilde{R}_i(w) + (\varphi - \frac{H_i(w)H_i^*(w)}{|H_i(w)|^2+\sigma_n^2/\sigma_d^2})\Lambda_i(w)$, $w = 0, \cdots, N_c-1$
   $\bar{\boldsymbol{x}}_i = [\bar{x}_i(0), \cdots, \bar{x}_i(N_c-1)]^T = \boldsymbol{F}^{-1}\bar{\boldsymbol{X}}_i$, $L_E^e(\bar{x}_i(n)) = \frac{2\varphi}{\sigma^2}\bar{x}_i(n)$, $n = 0, \cdots, N_c-1$

5.5.2 SISO Channel Decoder and Cyclic Reconstruction

The extrinsic information $[L_E^e(\bar{x}_i(0)), \cdots, L_E^e(\bar{x}_i(N_c-1))]^T$ is deinterleaved and delivered to the SISO decoder as $[L_E^e(\bar{b}_i(0)), \cdots, L_E^e(\bar{b}_i(N_c-1))]^T$. For brevity, the details of the BCJR algorithm are omitted. Log-MAP and Max-Log-MAP algorithms can be used to reduce complexity [120] [121]. Unlike the decoder in a parallel turbo decoder, the SISO decoder here uses $[L_E^e(\bar{b}_i(0)), \cdots, L_E^e(\bar{b}_i(N_c-1))]^T$ as its input and delivers the required LLRs for not only the information bits but also all the coded bits. Only for the last iteration will the SISO decoder generate LLRs for the information bit and feed them to a hard decision device. The hard decision device will decide if the transmitted bit is +1 or -1 based on the sign of the LLRs. The extrinsic LLRs of the coded bits are given by subtracting $[L_E^e(\bar{b}_i(0)), \cdots, L_E^e(\bar{b}_i(N_c-1))]^T$ from the output of the SISO decoder $[L_D(\bar{b}_i(0)), \cdots, L_D(\bar{b}_i(N_c-1))]^T$, as shown in Figure 5.4 and (5.32),

$$L_D^e(\bar{b}_i(n)) = L_D(\bar{b}_i(n)) - L_E^e(\bar{b}_i(n)), \; n = 0, \cdots, N_c-1 \tag{5.32}$$

Hereafter $[L_D^e(\bar{x}_i(n))$ is obtained by reinterleaving $[L_D^e(\bar{b}_i(n))$.

Soft bits generated by $[L_D^e(\bar{x}_i(0)), \cdots, L_D^e(\bar{x}_i(N_c-1))]^T$ are used as *a-priori* information for the MMSE turbo equaliser as stated in the previous subsection. They are also utilized in the cyclic reconstruction block to compensate for the effect of omitting the CP. The advantage of using soft bits for cyclic reconstruction is that the LLRs $[L_D^e(\bar{x}_i(0)), \cdots, L_D^e(\bar{x}_i(N_c-1))]^T$ gives the probability of a coded bit to be +1 or -1, therefore, cyclic reconstruction is more reliable since coded bits with small probabilities will not contribute much to the reconstructed part. For example, in an extreme case, the soft bit $\lambda_{i,n}$ is equal to ± 1 if $L_D^e(\bar{x}_i(n)) = \pm\infty$ or 0 elsewhere. Then, the incorrect bits will not be used in the cyclic reconstruction and error propagation is avoided. The whole process of the new proposed scheme is summarised as follows:

Step 1. Tail cancellation based on decision on the previous block as in (5.7),

Step 2. $\bar{r}_i(n)$ *obtained in Step 1 are converted to the frequency domain using FFT,*

Step 3. If it is the first iteration, $\bar{X}_i(w) = W_i(w)\bar{R}_i(w)$*, else go to Step 4.*

Step 4. Equalised signal $\bar{X}_i(w) = W_i(w)\tilde{R}_i(w) + (\varphi - \frac{H_i(w)H_i^*(w)}{|H_i(w)|^2+\sigma_n^2/\sigma_d^2})\Lambda_i(w)$, $\vec{\Lambda}_i = \boldsymbol{F}\vec{\lambda}_i$

Step 5. Transform $\bar{\boldsymbol{X}}_i$ *back to the time domain signal* $\bar{x}_i(n)$ *and calculate* φ *and* σ^2*. If I=1,* $L_E^e(\bar{x}_i(n)) = \frac{2}{1-\varphi^*}\bar{x}_i(n)$*, else* $L_E^e(\bar{x}_i(n)) = \frac{2\varphi}{\sigma^2}\bar{x}_i(n)$, $n = 0, \cdots, N_c-1$

Step 6. Deinterleave $L_E^e(\bar{x}_i(n))$ *for the SISO channel decoder. Compute the a posteriori LLRs for the information bits and the coded bits. If* $I = I_{end}$*, go to Step 11.*

Step 7. Calculate extrinsic information $L_D^e(\bar{b}_i(n))$

Step 8. Interleave $L_D^e(\bar{b}_i(n))$ *to get* $L_D^e(\bar{x}_i(n))$*. Calculate soft bits,* $\lambda_i(n) = \tanh(\frac{1}{2}L_D^e(\bar{x}_i(n)))$

Step 9. Reconstruct the effect of the missing CP:

$$\tilde{r}_i(n) = \bar{r}_i(n) + \sum_{l=0}^{L-1} h_i(l)\lambda_i(n+N_c-l)(1-u(n-l))$$

Step 10. I=I+1 and jump to Step 4

Step 11. Hard decisions are made on the LLRs for the information bits.

Comparing the structure of the new scheme and the extended RISIC, we notice that extra computations are only required for the FFT operations that convert the time domain soft bits $\lambda_i(n)$

into its frequency domain counterpart $\Lambda_i(w)$.

5.6 Simulation Results

A coded SC-FDE system with 64 BPSK symbols in each block is first studied. For the FEC code, a 1/2 rate convolutional code with constraint length of 3, the generator polynomials are $x^2 + x + 1$ and $x^2 + 1$. Coded data are randomly interleaved within one block. No CP is transmitted in our simulations and the missing effect of the CP is reconstructed by the extended RISIC and our new scheme. Simulations assume perfect knowledge of the channel impulse response. Three kinds of discrete time-invariant channels are used in our simulations:

$$\mathbf{h}1 = [0.7503, 0.2651, -0.4328, 0.4136, -0.0918]^T;$$

$$\mathbf{h}2 = [0.227, 0.460, 0.688, 0.460, 0.227]^T;$$

$$\mathbf{h}3 = [0.04, -0.05, 0.07, -0.21, -0.5, 0.72, 0.36, 0, 0.21, 0.03, 0.07]^T;$$

Channel $\mathbf{h}2$, $\mathbf{h}3$ are proposed by Proakis in [41] for evaluation purposes. There are two deep nulls in the spectrum of channel $\mathbf{h}2$ whilst channel $\mathbf{h}1$ and $\mathbf{h}3$ are channels with moderate nulls. The channel power has been normalized to unity and the average transmitted signal power $\sigma_d^2 = 1$. The frequency selectivity of theses channels is given in Figure 5.5. In each simulation, turbo equalisation performance for SC-FDE with CP is also given for comparisons. Figure 5.6 shows the bit error rate curves of SC-FDE with CP (in our simulations, the CP length is chosen to be 1/4 of the FFT size), extended RISIC for SC-FDE without CP and combined turbo equalisation and cyclic reconstruction scheme. Simulation results with no iteration, after first iteration and after 2-3 iterations are also shown. It can be seen from Figure 5.6 that both the extended RISIC and the new combined scheme can effectively reconstruct the missing CP under channel $\mathbf{h}1$ with moderate nulls and moderate delay spread. However, the extended RISIC is not effective for MMSE equaliser, as can be seen in Figure 5.6, 5.7, 5.8. With the iteration number increasing, very little improvement is obtained. This fact is also described in [91]. System performances for channel $\mathbf{h}2$ are given in Figure 5.7. In such a channel with deep frequency nulls, the new scheme offers significant improvement over the extended RISIC algorithm. Figure 5.8 compares the extended RISIC and the new scheme when $\mathbf{h}3$ is used. Although the new scheme still outperforms the extended RISIC algorithm, both of them can not achieve satisfactory performance. This is because the SISO decoder can not effectively

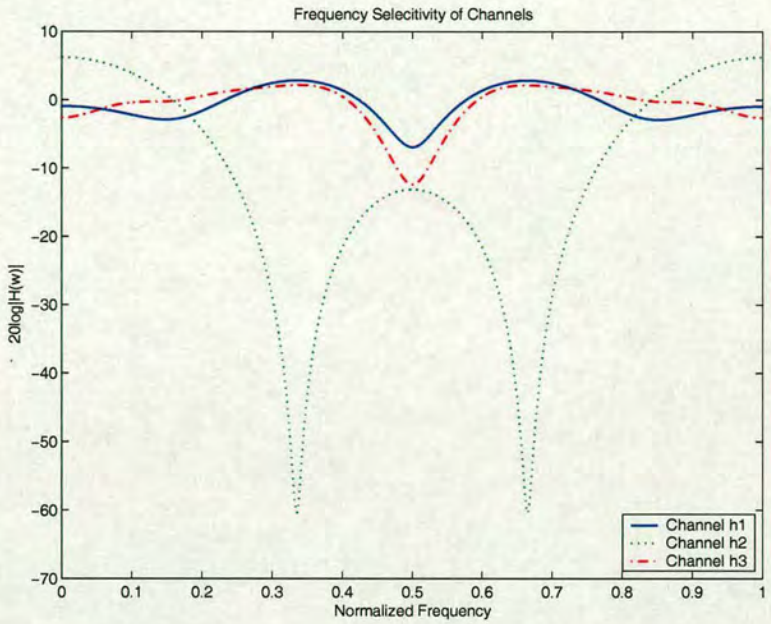

Figure 5.5: *Frequency selectivity of channels*

deliver reliable extrinsic information since the delay spread of **h**3 is too long compared with the interleaver size. To improve the system performance of the new scheme over such channels with long delay spread, one can increase the interleaver size or in this case, the block size since we interleave symbols within one block. In Figure 5.9, the data symbol per block is changed from 64 to 128. Therefore, since the interleaver has a size equal to the block size, the SISO decoder in this case can feed back more reliable information about the coded bits and improve system performance.

5.7 Complexity Analysis

In this section, we discuss the complexity issue in regarding complexity vs. processing block size (N_c). The complexity of time domain equaliser, frequency domain equaliser with CP, extended RISIC and the new algorithm are investigated and compared. For simplicity, only those computations that dominate the complexities are considered; computations like additions, interleaving, deinterleaving and short convolutions are omitted. v is the constraint length of the convolutional codes.

- TDE: For a TDE, Cholesky decomposition is used to reduce the complexity of matrix inversion. The total computational complexity per data symbol is in the order of $O(N_c^2 +$

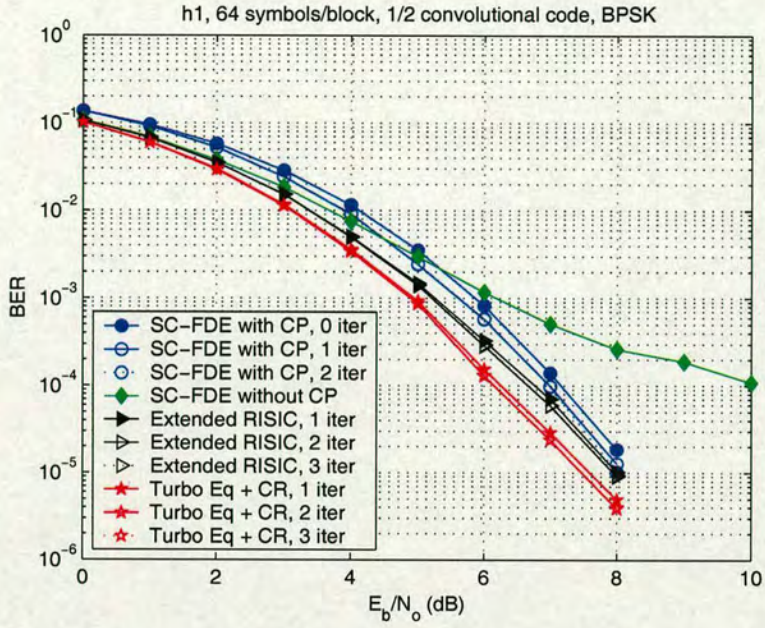

Figure 5.6: *Performances for channel h1; CR: Cyclic reconstruction*

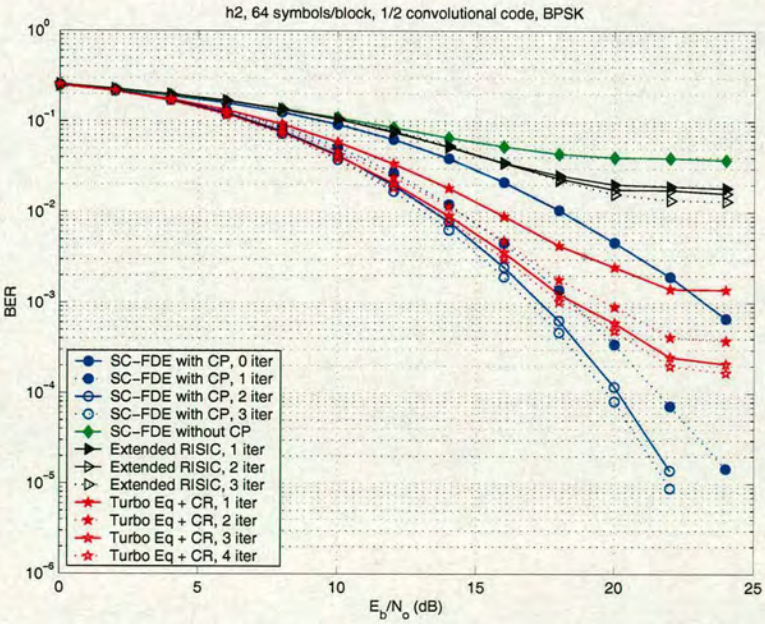

Figure 5.7: *Performances for channel h2; CR: Cyclic reconstruction*

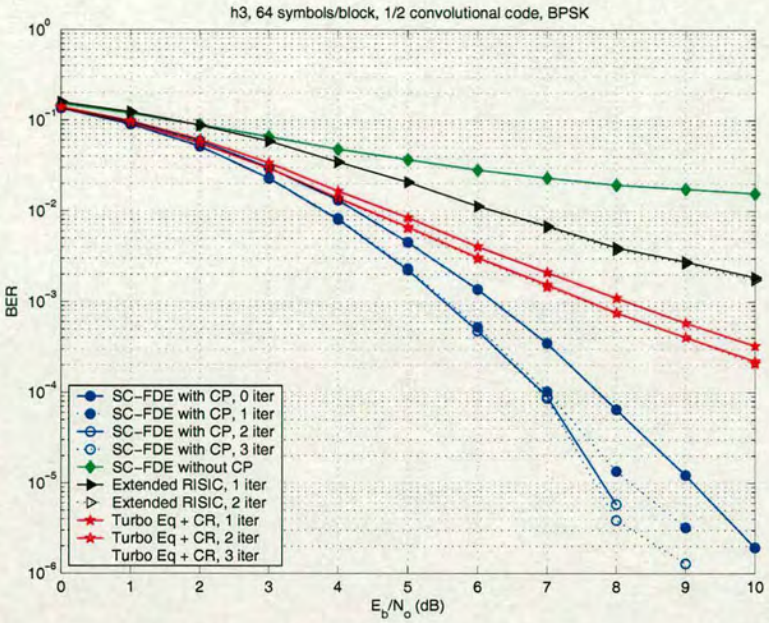

Figure 5.8: *Performances for channel h3; CR: Cyclic reconstruction*

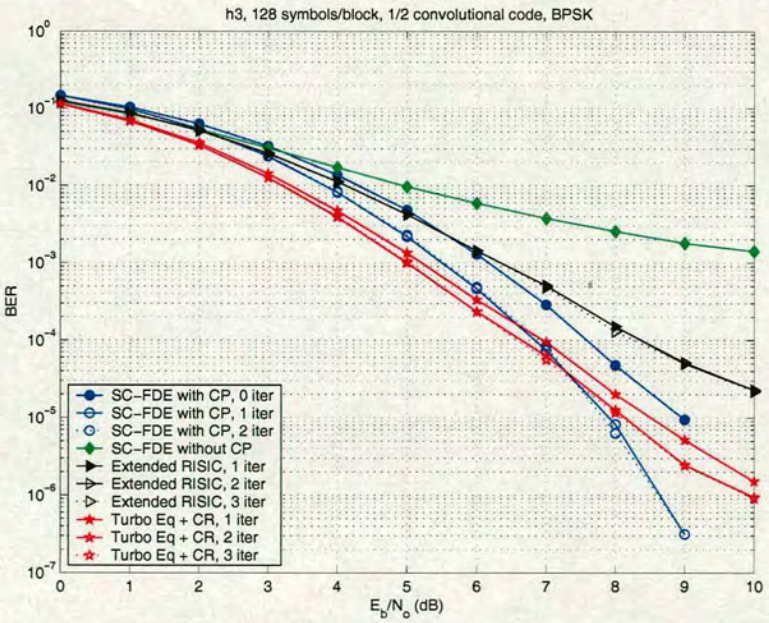

Figure 5.9: *Performances for channel h3, FFT size =128; CR: Cyclic reconstruction*

2^{v-1}).

- FDE with CP: The total computational complexity per data symbol is in the order of $O(log_2 N_c + 2^{v-1})$.
- Extended RISIC: While using I iterations, with MAP soft decoding operation in each iteration, the total computational complexity per data symbol is in the order of $O(I \cdot log_2 N_c + I \cdot 2^{v-1})$.
- New algorithm: The new scheme combining turbo equalisation and cyclic reconstruction uses a similar structure to that of the extended RISIC. Compared with the extended RISIC, extra major computation burden is one FFT operation per iteration. Therefore, the total computational complexity per data symbol is in the order of $O((I+1) \cdot log_2 N_c + I \cdot 2^{v-1})$.

5.8 Conclusions

In this chapter, a new combined turbo equalisation and cyclic reconstruction scheme is proposed for a SC-FDE without CP. Two iterative processes are jointly integrated in one structure to compensate for the effect of the missing CP and achieve significant improvements with only a slight increase in computation compared with the extended RISIC method. The same idea is extended for OFDM systems and is presented in [122].

Chapter 6
Channel Estimation and Interference Cancellation

In this chapter, an iterative channel estimation approach is proposed for WCDMA and CP-CDMA systems. Code-multiplexed pilots are used for channel estimation to maintain bandwidth efficiency in both systems. For WCDMA systems, the proposed method reconstructs received waveforms for each user and removes them from the received signal hence the channel estimation accuracy is improved via another correlation process. The algorithm is modified and used in CP-CDMA systems; the sum of data channels and the pilot channel is reconstructed for channel estimation. The proposed method achieves significant improvement in both systems compared to the conventional correlation approach. Simulation results demonstrate good estimation capability with an allocation of only 10% of the whole power to the pilot channel (A pilot channel with 10% of the whole transmitted power is used in HSDPA [100]). In addition, we propose an integrated channel estimator and PIC detector. The interference contributed by different data channels as well as the pilot channel are regenerated and subtracted from the received signal at the final stage. The channel estimation error reduces at each iteration and the PIC at the last stage enable further BER performance improvement to be achieved for the system.

Joint Iterative channel estimation and PIC algorithms are proposed for WCDMA systems and CP-CDMA systems in Section 6.2 to Section 6.5 and Section 6.6 to Section 6.10, respectively. Finally, we conclude this chapter in Section 6.11.

6.1 Introduction

Channel estimation is a major issue for reliable transmission in both WCDMA and CP-CDMA systems. The system performance of WCDMA with imperfect channel estimation has been widely studied in recent years [40] [45]. Usually, there are two types of pilots used in the downlink of WCDMA systems: time-multiplexed pilots [123] and code-multiplexed pilots [124].

The time-multiplexed pilots inevitably require extra bandwidth and hence reduce bandwidth efficiency. Inserting code-multiplexed pilots is an effective means to solve this problem by assigning a pilot signal an individual pseudorandom sequence [40]. This only consumes extra power on sending a known pilot sequence while no bandwidth spreading is necessary. The pilot channel is superimposed on the data channel and continuously transmitted through the same mobile propagation channel. In practice, the correlation method is a simple technique for channel estimation [40] [125]. However, the distorted autocorrelation property due to channel impairments degrades its performance hence, a high power code-multiplexed pilot sequence is required for better channel estimates. It introduces high MAI to the data channels. In this chapter, we demonstrate that with our new approach, good performance can be achieved while only a small amount of power (10% the whole transmit power) is allocated to the pilot channel.

Performance of CDMA based systems is dominated by the amount of interference generated by the simultaneous presence of users. PIC appears as a simple interference suppression scheme, which subtract interferences from users other than the desired one simultaneously without too much delay [126]. In this chapter, PIC and channel estimation are combined in an iterative process to form a new scheme.

6.2 WCDMA System with Code-Multiplexed Pilot Channel

In WCDMA systems, a code-multiplexed signal is continuously transmitted from each base station. It is broadcast over the entire cell and used as a phase reference for downlink channels. This channel plays a vital role in the cell searching of mobile station and channel estimation. In this chapter only the uncoded downlink scenario is considered: all signals are transmitted symbol and chip synchronously through the same mobile radio channel, perfect synchronization is assumed. Consider K-user's traffic that is QPSK modulated before spreading. The complex envelope of the transmitted signal due to the k-th user is given in (2.4) and reprinted here:

$$d_k(t) = \sqrt{E_k} \sum b_k^{(m)} s_k(t - mT), \tag{6.1}$$

where T denotes the symbol interval; E_k, $b_k^{(m)}$ and $s_k(t)$ denote the average power of the k-th user, the m-th symbol of the k-th user and the spreading chip waveform of the k-th user given by the convolution of spreading sequence and the chip waveform, respectively. The total average data channel power can be represented as $E_d = \sum_{k=1}^{K} E_k$.

After spreading, user data is summed together with the code-multiplexed pilot $p(t)$ which is used to provide phase reference information for data channels. Let E_p be the average power allocated to the pilot channel. We use "g" to denote the power ratio of the pilot channel to the whole signal power where $g = E_p/(E_d + E_p)$. The transmitted signal being scrambled by a long code $c(t)$ can be written as:

$$\begin{aligned} x(t) &= c(t)\Big[\sum_{k=1}^{K} d_k(t) + \sqrt{E_p}p(t)\Big] \\ &= c(t)\Big[\sum_{k=1}^{K} \sqrt{E_k}\sum b_k^{(m)} s_k(t - mT) + \sqrt{E_p}p(t)\Big]. \end{aligned} \tag{6.2}$$

The period of one chip is denoted by T_c. All signals that arrive at the receiver from the same basestation have passed through an identical complex channel. The complex FIR filter $h(\tau; t)$ with order L is a composite successive convolution of the transmitter filter, the mobile radio channel and the receiver filter. The definition of $h(\tau; t)$ can be rewritten as:

$$h(\tau; t) = \sum_{l=0}^{L-1} h_l(t)\delta(\tau - \tau_l T_c) \tag{6.3}$$

we further assume that $\sum_{l=0}^{L-1} E\left\{|h_l(t)|^2\right\} = 1$.

At the receiver, the received signal can be represented in an equivalent lowpass form as:

$$\begin{aligned} r(t) &= \sum_{l=0}^{L-1} h_l(t)c(t - \tau_l T_c)\Big[\sum_{k=1}^{K} \sqrt{E_k}\sum b_k^{(m)} s_k(t - mT - \tau_l T_c) \\ &+ \sqrt{E_p}p(t - \tau_l T_c)\Big] + v(t) \end{aligned} \tag{6.4}$$

where $v(t)$ is the complex-valued lowpass equivalent AWGN.

Let N be the spreading factor for both user data channels and the pilot channel, thus, the symbol duration T is N times the chip period or the sample interval T_c. The received signal in (6.4)

can be represented in its discrete form:

$$\begin{aligned} r(mN+n) &= \sum_{l=0}^{L-1} h_l(mN+n)c(mN+n-\tau_l) \\ &\times \Big[\sum_{k=1}^{K} \sqrt{E_k} b_k^{(m)} s_k(n-\tau_l) + \sqrt{E_p} p(mN+n-\tau_l)\Big] \\ &+ v(mN+n) \end{aligned} \tag{6.5}$$

where $0 \leq n \leq N-1$. The sampled input signal to the l-th Rake receiver finger is descrambled as:

$$r_l(mN+n) = h_l(mN+n)\Big[\sum_{k=1}^{K} \sqrt{E_k} b_k^{(m)} s_k(n) + \sqrt{E_p} p(mN+n)\Big] + \eta_l(mN+n) \tag{6.6}$$

In (6.6), $\eta_l(mN+n)$ accounts for a mixture of additive Gaussian noise, multipath interference and multiple access interference.

We use $\hat{h}_l(mN+n)$ to denote the channel estimates, then the L resolved signals are multiplied by the complex conjugates of $\hat{h}_l(mN+n)$ and maximum ratio combined in the Rake receiver. Consequently, the output at the $mN+n$ sample interval can be represented as:

$$y(mN+n) = \sum_{l=0}^{L-1} r_l(mN+n)\hat{h}_l^*(mN+n) \tag{6.7}$$

Finally, despreading and demapping are performed on $y(mN+n)$ to recover the user data symbol.

6.3 Iterative Channel Estimation

Channel estimation plays an important role in the receiver especially for a Rake receiver. The system performance strongly depends on the estimate of the channel impulse response. In this section, we review a popularly used conventional channel estimator and subsequently propose a new iterative approach.

6.3.1 Correlation Method

The correlation method had been widely adopted for the design of Rake receivers [40] [125]. In [45], a symbol level estimator is detailed and is briefly reviewed here. Suppose that s_p is the spreading sequence assigned to the pilot channel, the pilot term $p(mN+n)$ in (6.6) can be rewritten as:

$$p(mN+n) = S_{pilot} s_p(n) \tag{6.8}$$

where S_{pilot} denotes the pilot symbol, usually all "1" or "$\frac{1+j}{\sqrt{2}}$". Using the orthogonal property of the spreading codes and assuming the pilot signature sequence is uncorrelated with the noise term $\eta_l(mN+n)$ in (6.6), if $S_{pilot} = 1$, the m-th pilot symbol at the l-th finger $\hat{S_{pilot,l}}^m$ can be recovered as in [45]:

$$\hat{S_{pilot,l}}^m = \frac{1}{N} \sum_{n=0}^{N-1} r_l(mN+n) s_p(n) \tag{6.9}$$

if $S_{pilot} = \frac{1+j}{\sqrt{2}}$, then $\hat{S_{pilot,l}}^m$ will be detected as:

$$\hat{S_{pilot,l}}^m = \frac{1}{N} \sum_{n=0}^{N-1} r_l(mN+n) s_p(n) (\frac{1-j}{\sqrt{2}}) \tag{6.10}$$

From (6.6), we can express the pilot symbol $\hat{S_{pilot,l}}^m$ as:

$$\hat{S_{pilot,l}}^m = \sqrt{E_p}|S_{pilot}|^2 \cdot \frac{1}{N} \sum_{n=0}^{N-1} \hat{h}_l(mN+n) = \sqrt{E_p}|S_{pilot}|^2 \hat{h}_l^m \tag{6.11}$$

Usually we assume that the channel is invariant within an M symbol observation window, i.e. $N_w = M \times N$ chips. Hence, applying an averaging filter, we obtain the channel estimate $\hat{h}_l$ for this observation period as:

$$\hat{h}_l = \sum_{m}^{m+M-1} \hat{h}_l^m = \frac{1}{\sqrt{E_p}|S_{pilot}|^2} \sum_{m}^{m+M-1} \hat{S_{pilot,l}}^m \tag{6.12}$$

The correlation method is simple, however, its estimation performance degrades due to the non-ideal autocorrelation properties and has significant influence on the BER performance of the system.

6.3.2 Iterative Method

A novel iterative channel estimator for WCDMA systems is investigated in this section. $\hat{h}_l$ obtained by the correlation method is used as an initial channel estimate for the system. We consider an uncoded system and only hard detection, consequently, estimates of K users' transmitted symbols $\tilde{b}_k^{(m)}$ can be obtained by despreading as:

$$\tilde{b}_k^{(m)} = \frac{1}{N} \sum_{n=0}^{N-1} y(mN+n) s_k(n) \tag{6.13}$$

Hard detection is performed on $\tilde{b}_k^{(m)}$ and hence $\hat{b}_k^{(m)}$ is obtained. Similar to a PIC scheme, we regenerate the channel distorted waveforms of the k-th user as:

$$\hat{r}_k(mN+n) = \sqrt{E_k} \sum_{l=0}^{L-1} \hat{h}_l(mN+n) c(mN+n-\tau_l) \times \hat{b}_k^{(m)} s_k(n-\tau_l) \tag{6.14}$$

Then, the reconstructed channel distorted waveforms of all the user channels other than the pilot channel are removed from the composite signal $r(mN+n)$ as:

$$\hat{r}(mN+n) = r(mN+n) - \sum_{k=1}^{K} \hat{r}_k(mN+n) \tag{6.15}$$

Hence, the good autocorrelation property of the pilot channel can be recovered given perfect channel estimates and correctly detected user symbols. Applying the correlation method on the signal $\hat{r}(mN+n)$, channel estimates are refined and system BER performance is enhaced.

In this thesis, a different view from the chip level is given on the correlation method. Since user data is treated as an independent signal and the aggregation can be considered to be an additive noise on the pilot channel, under the assumption that the pilot sequence is uncorrelated with the data channels and the additive Gaussian white noise, we can derive that:

$$E\left\{ \begin{bmatrix} \hat{r}(mN+n) \\ \vdots \\ \hat{r}(mN+n+L-1) \end{bmatrix} p^*(mN+n) c^*(mN+n) \right\} = \sqrt{E_p} |S_{pilot}|^2 \begin{bmatrix} \hat{h}_0^{Iter} \\ \vdots \\ \hat{h}_{L-1}^{Iter} \end{bmatrix} \tag{6.16}$$

where $\hat{h}_l^{Iter}$ is the new channel estimate. Thus, the complex channel coefficients can be determined up to a fixed scaling factor. The expectation operation is a useful means to combat both the AWGN and the MAI, which can be treated as additive noise. The correlation method

in [45] and the one presented in (6.16) are essentially equal.

6.4 Joint Channel Estimation and Parallel Interference Cancellation

Multiple access interference cancellation can be achieved in a PIC stage. A multistage PIC cancels the MAI estimated with the hard decisions made in the previous stage. Since the proposed new channel estimator has a similar structure to a parallel interference cancellation, we can easily integrate these two together so that the system BER performance can be further improved with only a slight increase in computation complexity.

After performing the iterative channel estimation in Section 6.3, interference from the interfering *K-1* users and the parallel pilot channel are regenerated given the new channel estimates $\hat{h}_l^{Iter}$. Let the u-th user be the desired user and the composite signal excluding the u-th user's information can be regenerated as:

$$\begin{aligned} \check{r}(mN+n) &= \sum_{l=0}^{L-1} \hat{h}_l^{Iter}(mN+n)c(mN+n-\tau_l) \\ &\times \Big[\sum_{k=1,k\neq u}^{K} \sqrt{E_k}\hat{b}_k^{(m)} s_k(n-\tau_l) + \sqrt{E_p}p(mN+n-\tau_l) \Big] \end{aligned} \tag{6.17}$$

Subsequently, $\check{r}(mN+n)$ is subtracted from the received signal $r(mN+n)$ as:

$$\dot{r}(mN+n) = r(mN+n) - \check{r}(mN+n) \tag{6.18}$$

A Rake receiver is then applied to the MAI cleared signal for a second time and the output is despread and hard-decision detected. Compared with a conventional PIC scheme, the new joint structure requires extra computations mainly on another correlation process and for interference regeneration. It is known that PIC is quite sensitive to channel estimation errors and with a bad initial channel estimate, the PIC would increase the amount of interference rather than cancel it. Adopting the new joint channel estimation and PIC structure, better channel estimates can be obtained for the PIC. With a slight increase in computational complexity, the improvement in system performance that can be achieved is significant.

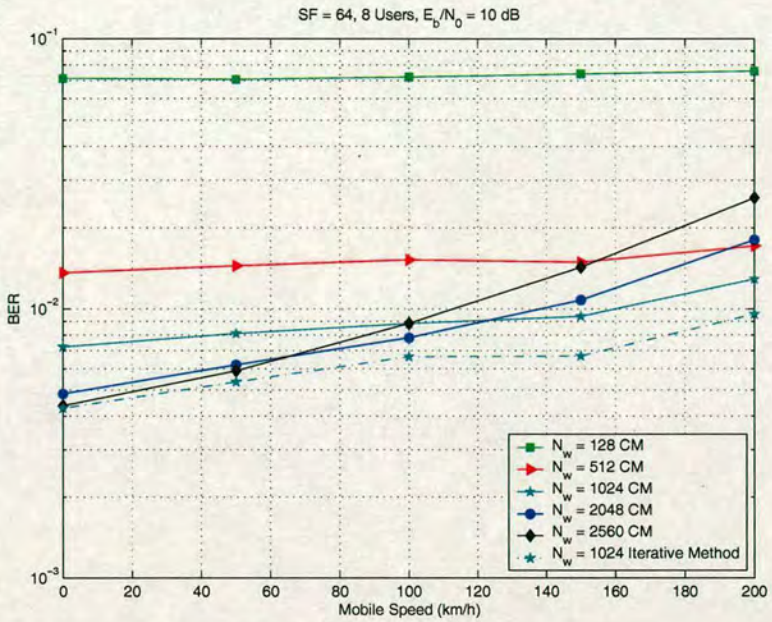

Figure 6.1: *System BER performance versus Varying mobile speed, SF=64, 8 Active users, $E_b/N_0 = 10dB$, CM: Correlation Method*

6.5 Simulation Results

Computer simulations are carried out at baseband. One pilot channel is code-multiplexed with dedicated data channels. 10% of the whole power is allocated to the pilot channel. The UMTS Vehicular A channel model [46] is used for BER evaluation in our simulation.

Figure 6.1 shows the numerical results of system performances when mobile terminal is moving at different speed. 8 active users are simulated with a spreading factor of 64 and the SNR per bit is fixed at 10 dB. Imperfect channel estimation is considered (channel is estimated based on the pilot channel). Both the correlation method and the new iterative estimation approach are evaluated. It can be seen from Figure 6.1 that $N_w = 1024$ is a suitable window size for both estimators. It achieves a good BER performance compared to choosing a smaller window size and keeps the performance more stable than choosing a larger window size. We can also see from the figure that the new iterative approach outperforms the conventional correlation method.

Figure 6.2 and Figure 6.3 demonstrate the performance of the two estimators with different numbers of active users. Mobile terminal is assumed moving at a speed of 30 km/h and 150 km/h. At a required target BER of 2×10^{-2}, using the new method can support 5 more users

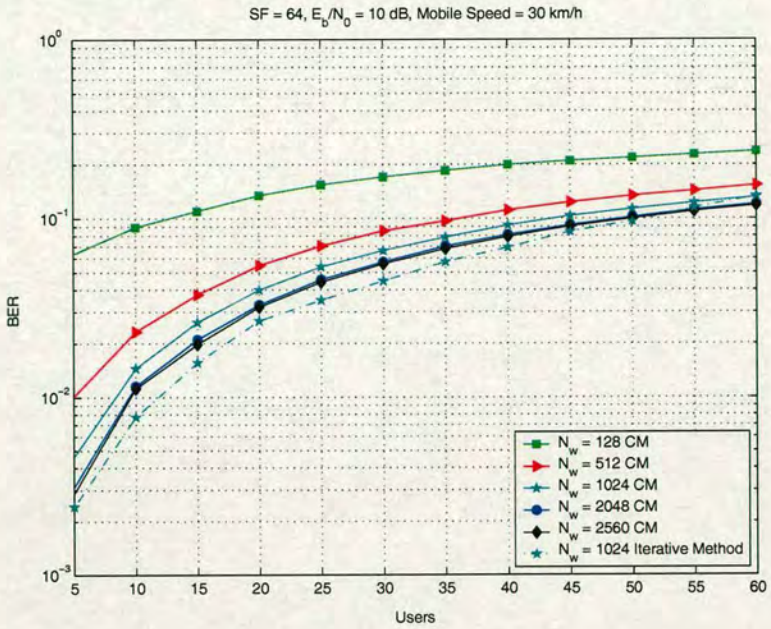

Figure 6.2: *System BER performance versus Different number of users, SF=64,* $E_b/N_0 = 10$*dB, Mobile Speed=30 km/h, CM: Correlation Method*

than the conventional one with a fixed window size $N_w = 1024$.

In Figure 6.4 and Figure 6.5, we present the BER performance of different detectors with a mobile speed of 30 km/h and 150 km/h. The spreading factor is 16 and 10 active users are simulated to study their performance in such a high load scenario. The Rake performance is dominated by the MAI and with such a high loading this results in saturation at a fairly high error rate.

Figure 6.6 demonstrates the system improvements with PIC. A joint iterative channel estimator and PIC method achieves a 3 dB gain at the BER of 10^{-1} compared with a conventional correlation method with PIC. Since PIC is very sensitive to channel estimation errors, the iterative estimation scheme offers good channel estimates and hence improvements on system performance. The conventional CM + PIC introduces more interference to the system due to bad channel estimation accuracy and hence worse BER performance. Figure 6.6 also demonstrates the effectiveness of the joint scheme in a low load scenario when mobile terminal is moving at different speeds. The proposed joint scheme consistently outperforms the other three and achieves good BER performance.

As depicted in Figure 6.7 and Figure 6.8, in a high load environment, none of the four receiver

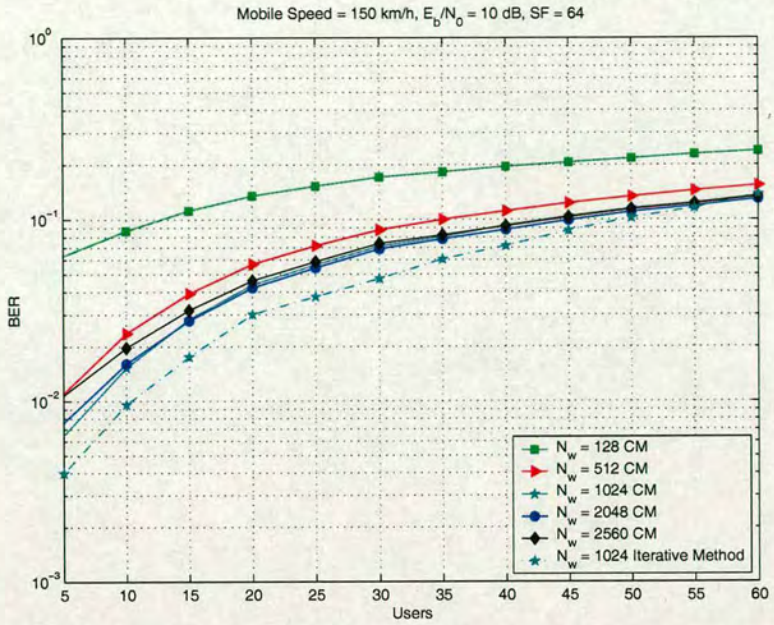

Figure 6.3: *System BER performance versus Different number of users, SF=64,* $E_b/N_0 = 10$*dB, Mobile Speed=150 km/h, CM: Correlation Method*

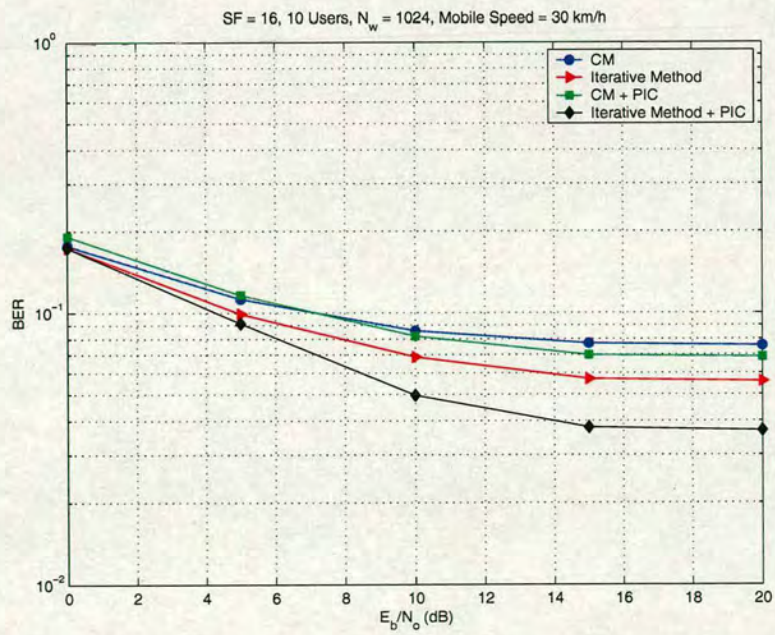

Figure 6.4: *System BER performance with different detectors, SF=16, 10 Active users, Mobile Speed=30 km/h, CM: Correlation Method*

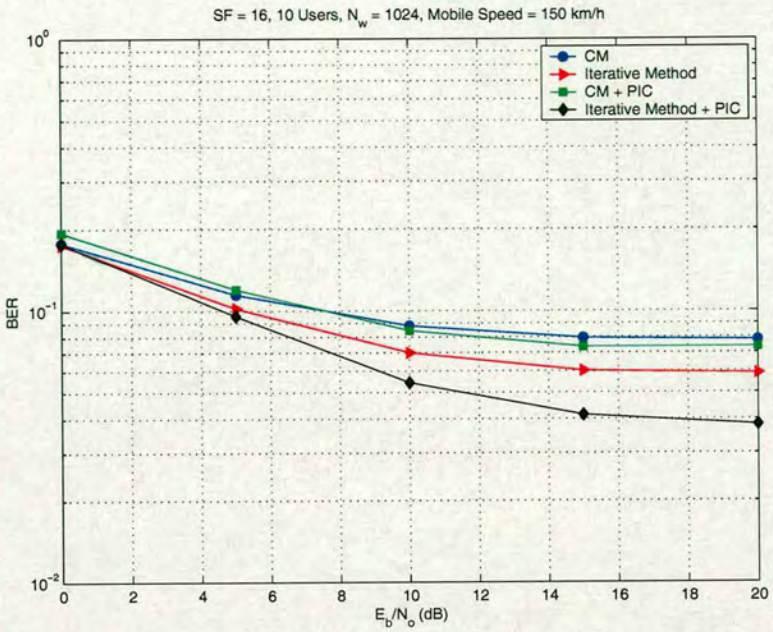

Figure 6.5: *System BER performance with different detectors, SF=16, 10 Active users, Mobile Speed=150 km/h, CM: Correlation Method*

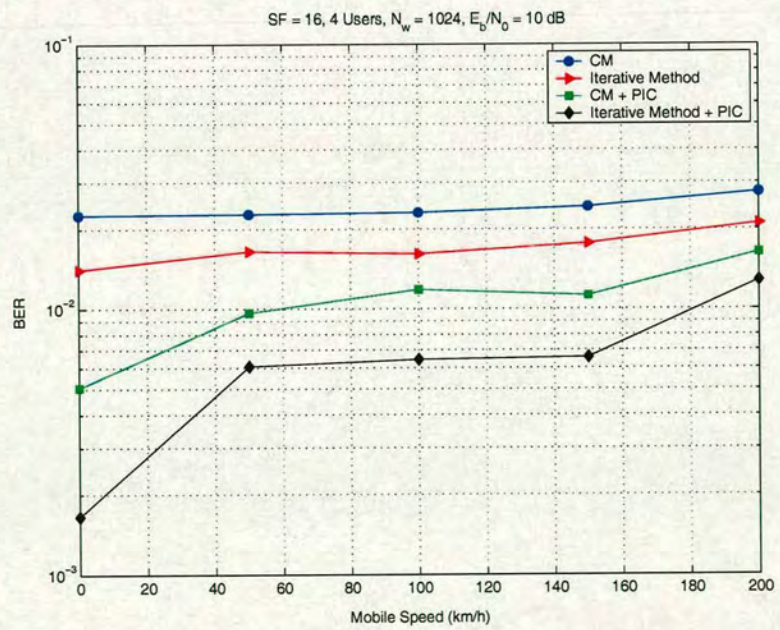

Figure 6.6: *System BER performance versus Varying mobile speed, SF=16, 4 Active users,* $E_b/N_0 = 10dB$*, CM: Correlation Method*

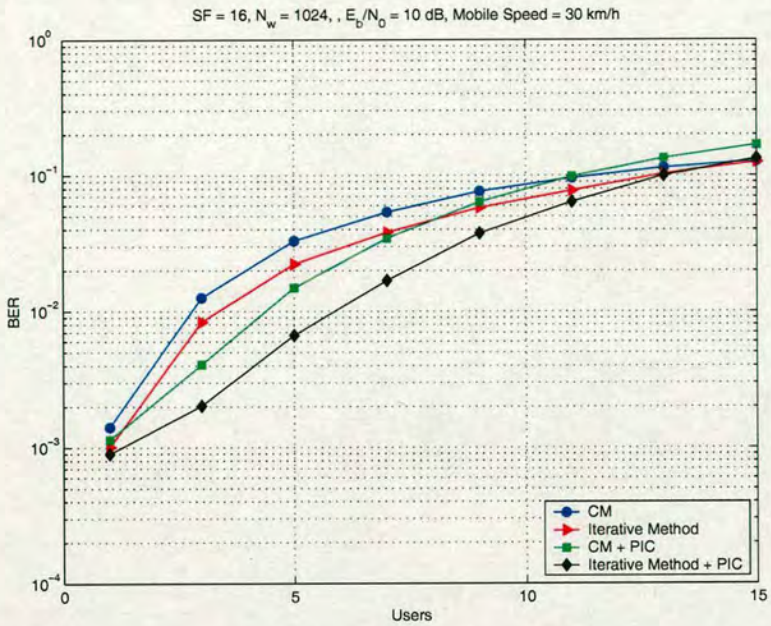

Figure 6.7: *System BER performance versus Different number of users, SF=16, $E_b/N_0 = 10dB$, Mobile Speed=30 km/h, CM: Correlation Method*

can achieve good performance. Actually, with the increasing number of users, the performances tend towards the same due to bad channel estimation. Nonetheless, when the number of active users is low, we can still see the enhancement on performance. Interestingly, it can be observed from the results that when there are more than 7 active users in this scenario, even a Rake receiver with the iterative channel estimator only achieves better performance than the CM + PIC scheme. This is because that the CM fails to provide good estimates and hence the PIC introduces more interference.

6.6 CP-CDMA System Model and Equalisation

In this section, the scheme proposed in Section 6.3 is modified for a CP-CDMA system. The transmitted signal is generated according to (6.1) and (6.2). The scrambled signal is split into successive data blocks with N_c chips in one block. Unlike MC-CDMA or MC-DS-CDMA, the CP-CDMA system is a single carrier DS-CDMA system. With the introduced cyclic prefix concept, a block is cyclic extended to $N_c + N_{CP}$ chips with the last N_{CP} chips inserted at the beginning of the block. Note that the length of the CP N_{CP} should be no less than the maximum delay of the mobile propagation channel. The transmitted block signal is illustrated in Figure 6.9.

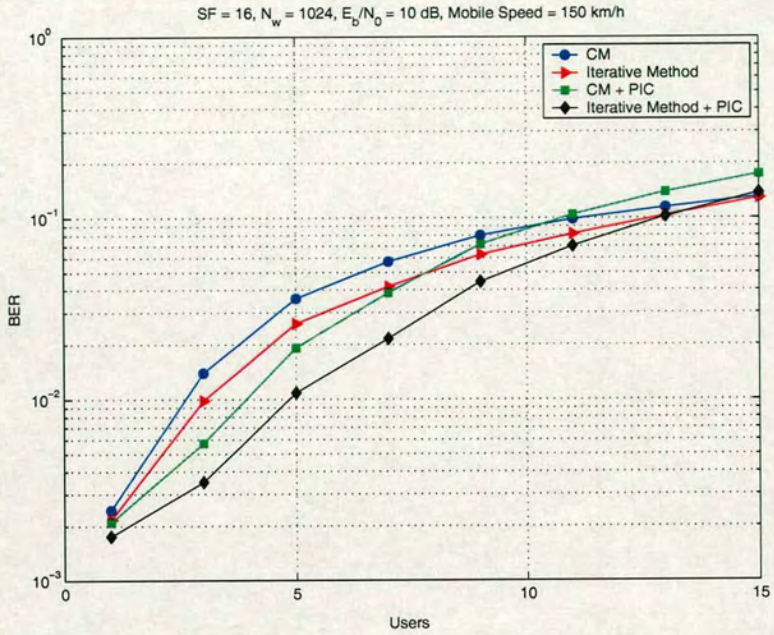

Figure 6.8: *System BER performance versus Different number of users, SF=16, E_b/N_0 = 10dB, Mobile Speed=150 km/h, CM: Correlation Method*

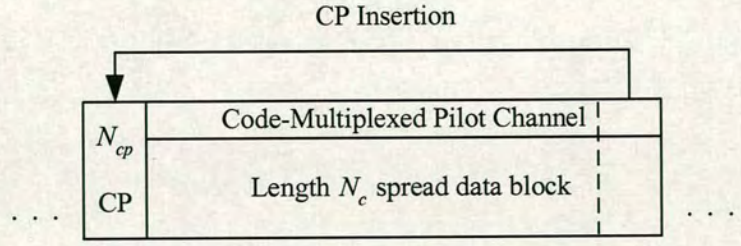

Figure 6.9: *CP-CDMA block signal*

At the receiver, perfect synchronisation is assumed and the CP is discarded before equalisation. For such a system, it is convenient to perform block based processing at the receiver. We write the received signal in one block as $r_i(n)$, $0 \leq n \leq N_c - 1$, where i is the block index. $x_i(n)$ denotes the corresponding transmitted block signal. Therefore, assuming that the composite channel response $h_i(l)$ is quasi-static within the i-th block and is normalized. The relation between $r_i(n)$ and $x_i(n)$ can be written as:

$$r_i(n) = x_i(n) \odot h_i(n) + v_i(n), \tag{6.19}$$

where $v_i(n)$ is additive Gaussian noise and "$\odot$" denotes circular convolution. Due to the inserted CP, the distortion of the channel is considered as a multiplication in the frequency domain. Thus, in the frequency domain,

$$R_i(w) = H_i(w)X_i(w) + V_i(w)\,,\ 0 \leq w \leq N_c - 1 \tag{6.20}$$

where $R_i(w)$, $H_i(w)$, $X_i(w)$ and $V_i(w)$ are the Fourier transforms of $r_i(n)$, $h_i(n)$, $x_i(n)$ and $v_i(n)$, respectively.

The minimum mean square error (MMSE) equaliser $W_i(w)$ in the frequency domain is given by the following expression [63]:

$$W_i(w) = \frac{H_i^*(w)}{|H_i(w)|^2 + \sigma_n^2/\sigma_d^2} \tag{6.21}$$

σ_n^2, σ_d^2 and $H_i^*(w)$ are the variance of the additive white Gaussian noise, the variance of the received signal and the conjugate of $H_i(w)$, respectively. Consequently, the equalised signal is converted back to the time domain as:

$$\hat{x}_i(n) = \frac{1}{N_c} \cdot \sum_{w=0}^{N_c-1} W_i(w)R_i(w)e^{j2\pi nw/N_c} \tag{6.22}$$

after which, descrambling, despreading and demapping are performed.

6.7 Iterative Channel Estimation

Although the same correlation method can be used for CP-CDMA systems; however, in this section, we develop a novel iterative channel estimator. $\hat{\mathbf{h}}_i^{CORR}$ obtained from the correlation

method is used as an initial channel estimate for the system. The received signal is equalised in the frequency domain and transformed back to the time domain by IFFT. The scrambling code is then removed and the composite signal is despread and detected. In this chapter, we consider uncoded systems and only hard detection. Consequently, estimates of K users' transmitted symbols $\hat{b}_{i,k}^{(m)}$, $0 \leq m \leq N_c/N - 1$ (N is the spreading factor, single rate is assumed) can be obtained. The idea of iterative channel estimation is that initially an estimate is made based on the parallel pilot channel and then refined by using both pilots and reconstructed user symbols. Once the detector outputs the estimates of users' symbols, they are respread, rescrambled and summed with the code-multiplexed pilots as virtual pilots, which then enhances the estimation performance.

The whole process is summarised as follows:

Step 1. Correlation method is used to deliver initial channel estimates $\hat{\boldsymbol{h}}_i^{CORR}$.

Step 2. The received signal is equalised in the frequency domain and transformed back to the time domain by IFFT. The scrambling code is then removed and the composite estimated signal $\hat{x}_i(n)$ *is despread and hard detected.*

Step 3. K users' transmitted symbols $\hat{b}_{i,k}^{(m)}$ *are respread and rescrambled. The scrambled code-multiplexed pilots are added to form an estimated composite signal* $\tilde{x}_i(n)$.

Step 4. $\tilde{x}_i(n)$ *is converted to* $\tilde{X}_i(w)$ *in the frequency domain and used for channel estimation together with the received frequency domain signal* $R_i(w)$. *In the estimator, the reconstructed composite signal* $\tilde{X}_i(w)$ *is treated as a pilot signal. A refined channel estimate can be obtained in the frequency domain as:* $\tilde{H}_i(w) = \frac{R_i(w)X_i^*(w)}{|X_i(w)|^2+\sigma_n^2/\sigma_d^2}$

Step 5. The result from step 4 is converted to time domain and only the first L values are kept to form the channel estimate $\tilde{\boldsymbol{h}}_i = [\tilde{h}_i(0), \cdots, \tilde{h}_i(L-1)]^T$.

Step 6. $\tilde{\boldsymbol{h}}_i$ *is used for equalisation. Go to step 2 or stop here.*

Figure 6.10 shows the system structure with our iterative channel estimation method.

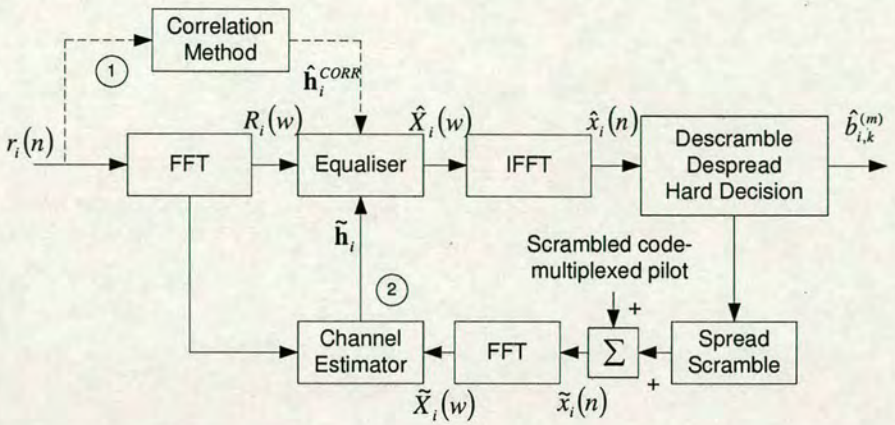

Figure 6.10: *Iterative Channel Estimation for CP-CDMA*

6.8 Joint Channel Estimation and Parallel Interference Cancellation

In a similar manner as to what has been done for WCDMA systems, the iterative channel estimation and the PIC can be jointly combined to enhance system performance. The received signal $r_i(n)$ is first converted into the frequency domain and passed into a equaliser. The output from the equaliser at the I-th stage $\hat{X}_i^I(w)$, $I = 1, \cdots, I_{end}$ is then IFFT back to the time domain and hard decisions on the user's transmitted symbols $\hat{b}_{i,k}^{I,(m)}$ are made. For convenience, we rewrite the transmitted i-th block signal in vector formats. Let $\mathbf{s}_k = [s_k(0), \cdots, s_k(N-1)]$ be the spreading code vector for user k and there are N_c/N user symbols in one block, the discrete transmitted scrambled signal can be written as:

$$\mathbf{x}_i = diag\{c(0), \cdots, c(N_c-1)\} \times \left[\sum_{k=1}^{K}\sqrt{E_k}b_{i,k}^{(0)}\mathbf{s}_k + \sqrt{E_p}\mathbf{p}_0, \cdots, \sum_{k=1}^{K}\sqrt{E_k}b_{i,k}^{(N_c/N-1)}\mathbf{s}_k + \sqrt{E_p}\mathbf{p}_{N_c/N-1}\right]^T \quad (6.23)$$

where $\mathbf{p}_m = [p(m \times N), \cdots, p(m \times N + N - 1)]^T$, $0 \leq m \leq N_c/N - 1$.

At the receiver, after removal of the cyclic prefix, the received block signal can be expressed as:

$$\mathbf{r}_i = \mathbf{H}_{c,i}\mathbf{x}_i + \mathbf{v}_i \quad (6.24)$$

where $\mathbf{v}_i$ is a Gaussian noise vector and $\mathbf{H}_{c,i}$ is an N_c by N_c circular matrix defined by:

$$\mathbf{H}_{c,i} = \begin{bmatrix} h_i(0) & & & & h_i(L-1) & \cdots & h_i(1) \\ \vdots & h_i(0) & & & & \ddots & \vdots \\ \vdots & \vdots & \ddots & & & & h_i(L-1) \\ h_i(L-1) & \vdots & \vdots & h_i(0) & & & \\ & h_i(L-1) & \vdots & \vdots & h_i(0) & & \\ & & \ddots & \vdots & \vdots & \ddots & \\ 0 & & & h_i(L-1) & h_i(L-2) & \cdots & h_i(0) \end{bmatrix} \tag{6.25}$$

Circulant matrix $\mathbf{H}_{c,i}$ can be efficiently diagonalized by Fourier transform and inverse Fourier transform, hence, (6.24) can be expressed in the frequency domain as:

$$\mathbf{R}_i = diag\left\{H_i(0), \cdots, H_i(N_c-1)\right\}\mathbf{X}_i + \mathbf{V}_i \tag{6.26}$$

where $\mathbf{R}_i$, $\mathbf{X}_i$ and $\mathbf{V}_i$ are the DFT of $\mathbf{r}_i$, $\mathbf{x}_i$ and $\mathbf{v}_i$, respectively.

At each stage, the estimated user symbols $\hat{b}_{i,k}^{I,(m)}$ are used together with code-multiplexed pilots to generate virtual pilots for channel estimation; the I-th stage regenerated transmitted signal can be expressed by:

$$\begin{aligned}\tilde{\mathbf{x}}_i^I = & diag\{c(0), \cdots, c(N_c-1)\} \times \\ & \left[\sum_{k=1}^{K}\sqrt{E_k}\hat{b}_{i,k}^{I,(0)}\mathbf{s}_k + \sqrt{E_p}\mathbf{p}_0, \cdots, \sum_{k=1}^{K}\sqrt{E_k}\hat{b}_{i,k}^{I,(N_c/N-1)}\mathbf{s}_k + \sqrt{E_p}\mathbf{p}_{N_c/N-1}\right]^T\end{aligned} \tag{6.27}$$

After performing the iterative channel estimation, $\tilde{\mathbf{h}}_i^I = [\tilde{h}_i^I(0), \cdots, \tilde{h}_i^I(L-1)]^T$with its frequency domain counterpart $diag\{\tilde{H}_i^I(0), \cdots, \tilde{H}_i^I(N_c-1)\}$ are used for system equalisation and interference cancellation. Let the u-th user be the desired user and the estimated composite signal excluding the u-th user's information can be regenerated as:

$$\begin{aligned}\dot{\tilde{\mathbf{x}}}_i^I = & diag\{c(0), \cdots, c(N_c-1)\} \times \\ & \left[\sum_{k=1,k\neq u}^{K}\sqrt{E_k}\hat{b}_{i,k}^{I,(0)}\mathbf{s}_k + \sqrt{E_p}\mathbf{p}_0, \cdots, \sum_{k=1,k\neq u}^{K}\sqrt{E_k}\hat{b}_{i,k}^{I,(N_c/N-1)}\mathbf{s}_k + \sqrt{E_p}\mathbf{p}_{N_c/N-1}\right]^T\end{aligned} \tag{6.28}$$

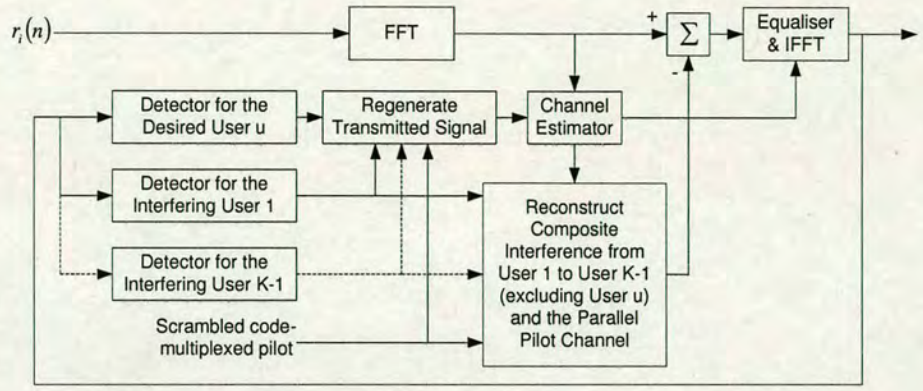

Figure 6.11: *Combined channel estimation and parallel interference cancellation structure*

Parallel interference cancellation can be performed at the I-th stage as follows:

$$\mathbf{r}_i^I = \mathbf{r}_i - \tilde{\mathbf{H}}_{c,i}^I \dot{\tilde{\mathbf{x}}}_i^I \tag{6.29}$$

where $\tilde{\mathbf{H}}_{c,i}^I$ is a circular matrix with elements taken from $\tilde{\mathbf{h}}_i^I$. This can be done in the frequency domain as:

$$\mathbf{R}_i^I = \mathbf{R}_i - diag\left\{\tilde{H}_i^I(0), \cdots, \tilde{H}_i^I(N_c - 1)\right\} \cdot \dot{\tilde{\mathbf{X}}}_i^I \tag{6.30}$$

where $\mathbf{R}_i^I$ and $\dot{\tilde{\mathbf{X}}}_i^I$ are the Fourier transforms of $\mathbf{r}_i^I$ and $\dot{\tilde{\mathbf{x}}}_i^I$, respectively.

Figure 6.11 shows how we can combine the iterative channel estimation and PIC within one structure. In each iteration cycle, K users' signals are regenerated and summed with the pilot channel for channel estimation purpose. Meanwhile, interference from the interfering *K-1* users and the parallel pilot channel are constructed and subtracted from the received composite signal, hence, interference can be reduced through each iteration. We should point out that the PIC processing is done in a different manner to the conventional approach. Since we simulate the downlink scenario in this thesis, for simplicity, only a single stage PIC is considered. There may be more than one time iteration, but only a single stage PIC is required for the system.

6.9 Simulation Results

Computer simulations are carried out at baseband. The chip rate is 3.84 Mchips/s. Walsh codes with length 16 are used as channelization codes and a 512 Gold code segment is used as the

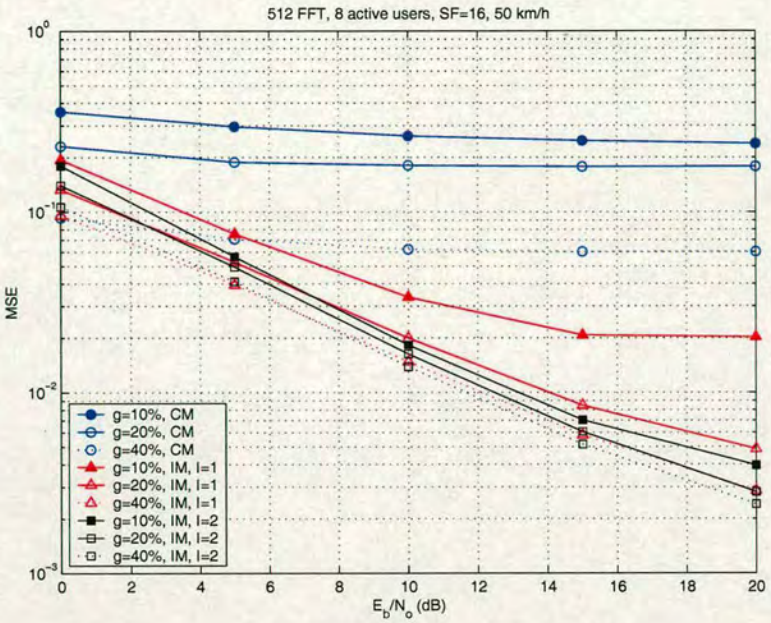

Figure 6.12: *Channel Estimation MSE versus E_b/N_o, g=10%, 20%, 40%. I: Number of Iterations. CM: Correlation Method, IM: Iterative Method*

scrambling code. One pilot channel is code-multiplexed with dedicated data channels. The block size is 512 excluding the 16 chips CP. In our simulations, the terminal is assumed to be moving at 50 km/h, and the carrier frequency is 2 GHz. The UMTS Vehicular A channel model is used for BER evaluation in our simulation. The CP duration 4.16 μs is selected to be larger than the longest channel delay spread 2.51 μs.

To evaluate the estimator performance, we compute the Mean Square Error (MSE) for both the correlation method and the new iterative procedure:

$$MSE(\tilde{\mathbf{h}}_i) = E\left\{\sum_{l=0}^{L-1} |h_i(l) - \tilde{h}_i(l)|^2\right\} \tag{6.31}$$

In Figure 6.12, we show the MSE curves of channel estimation versus signal to noise ratio per bit with varying pilot power, i.e. g=10%, 20% and 40%. From the simulation results presented, it follows that by using the correlation method, the higher the pilot power is, the better the channel estimates. In other words, if the value of 'g' is large, the channel estimation quality is good. However, this will lead to a large MAI with large error probability, which will be shown in Figure 6.13. We also observe that the new iterative scheme can effectively reduce channel estimation errors in comparison with the correlation method. Figure 6.13 shows the

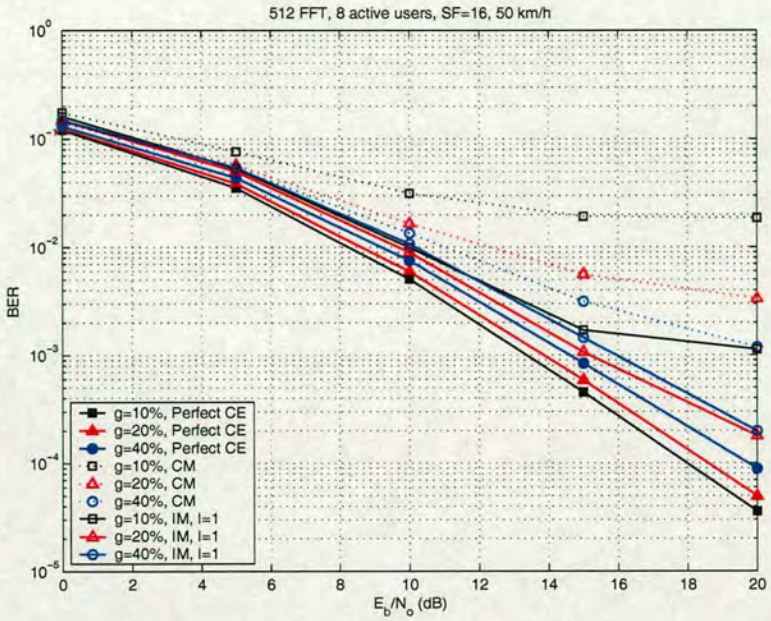

Figure 6.13: *Simulated BER performances, g=10%, 20%, 40%. CM: Correlation Method, IM: Iterative Method, Perfect CE: Perfect Channel Estimation*

numerical results of system performances. Imperfect channel estimation is considered (channel is estimated based on the pilot channel). Both the correlation method and the new iterative estimation approach are evaluated. The value of 'g' is chosen to be 10%, 20% and 40%. Ideal channel estimation is also used in our simulation as a reference result to compare BER performance results from the two channel estimation approaches. From Figure 6.13, we can see that under the perfect channel knowledge assumption, allocating more power to pilots (larger 'g') introduces more interference to the system and hence worse BER performance. Using the correlation method for channel estimation, the higher the pilot power is, the better the channel estimates can be achieved. However, this will lead to a large MAI with large error probability. Although a pilot channel with only 10%, 20% of the whole signal power induces less interference, the BER performance is worse than that with g=40%. This is because that when the power ratio of the pilots over the whole signal power is small, the channel estimation is poor so that the system performance is degraded. The BER performance with the new iterative channel estimation scheme are also shown with g=10%, 20% and 40%. Notice that with only a small amount of power allocated to the pilots, good performance can still be achieved via this structure. This is important for practical systems since usually only around 10% power can be allocated to the pilot channel, for example, g=10% in HSDPA [100]. Transmitting a small portion of power on the pilot makes the system power efficient and since parallel code-multiplexed

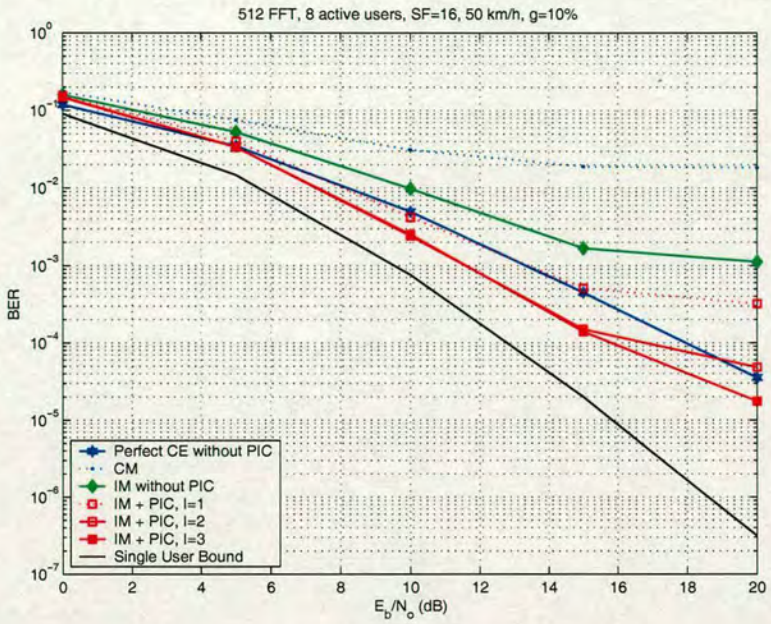

Figure 6.14: *Simulated BER performances with channel estimations and PIC, 8 active user, CM: Correlation Method, IM: Iterative Method, Perfect CE: Perfect Channel Estimation.*

pilots are used, bandwidth efficiency can be maintained.

Figure 6.14 demonstrates the system improvements with PIC. The single user situation (no MAI) with perfect channel estimation and MMSE-FDE is also simulated as reference results with the name "single user bound". After interference cancellation, the BER performance is enhanced significantly, especially when the number of active users is large. This shows that the other user interference as well as interference from pilot channel has considerable impact on such multiuser system performance. As we had mentioned in above section, the PIC is performed only at the last stage since we use it only for the desired user. When I=1, decisions $\hat{b}_{i,k}^{1,(m)}$ are made based on the equaliser with the channel estimates obtained by the correlation method and are used for interference regeneration. Since the initial channel impulse response estimates are bad, interference regeneration based on $\hat{b}_{i,k}^{1,(m)}$ is not so accurate. Consequently, with $I > 1$ we have more reliable estimates $\hat{b}_{i,k}^{I,(m)}$ and hence better PIC performance. Starting from the correlation method, the new scheme improves the performance of channel estimation and signal detection iteratively. However, PIC cannot decrease the BER with more iterations.

Figure 6.15 repeats the experiment for 4 active users; the advantages of the proposed scheme are still evident.

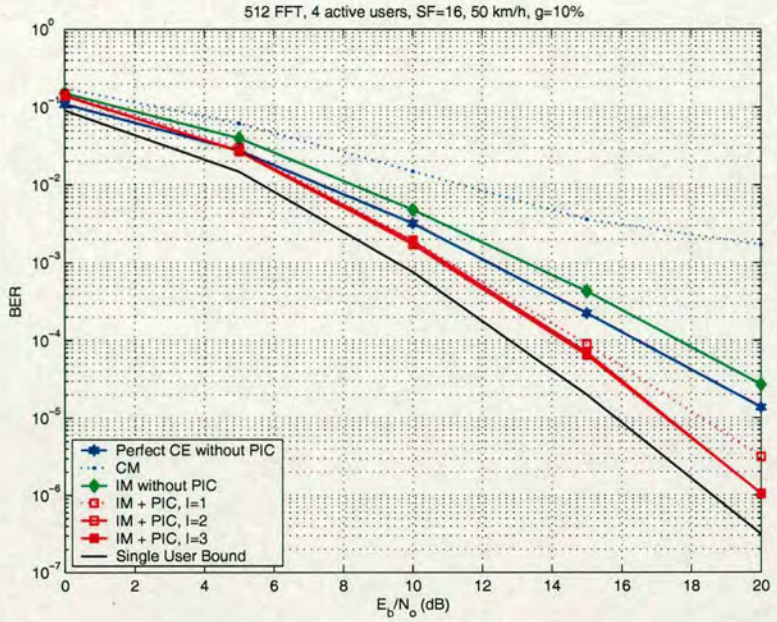

Figure 6.15: *Simulated BER performances with channel estimations and PIC, 4 active users, CM: Correlation Method, IM: Iterative Method, Perfect CE: Perfect Channel Estimation.*

6.10 Further Improvement

The channel estimation scheme discussed above can be further enhanced based on the fact that the channel will not change significantly across blocks. We use the refined channel estimates in the i-th block as an initial estimates for the $(i+1)$-th block instead of using the correlation method. By doing so, we can save computations because the correlation method is applied at the first block only. On the other hand, we have better initial estimates for successive blocks. Figure 6.16 and Figure 6.17 demonstrate that the new scheme is able to offer further improvement on system performance.

In both situations, whether PIC is used or not, we show that system performance is enhanced, in the meanwhile, computations are saved.

6.11 Conclusions

In this chapter a new iterative channel estimation method was studied for WCDMA systems and modified and extended for CP-CDMA systems. The new approach was evaluated through simulations and compared with the conventional correlation method in terms of BER perfor-

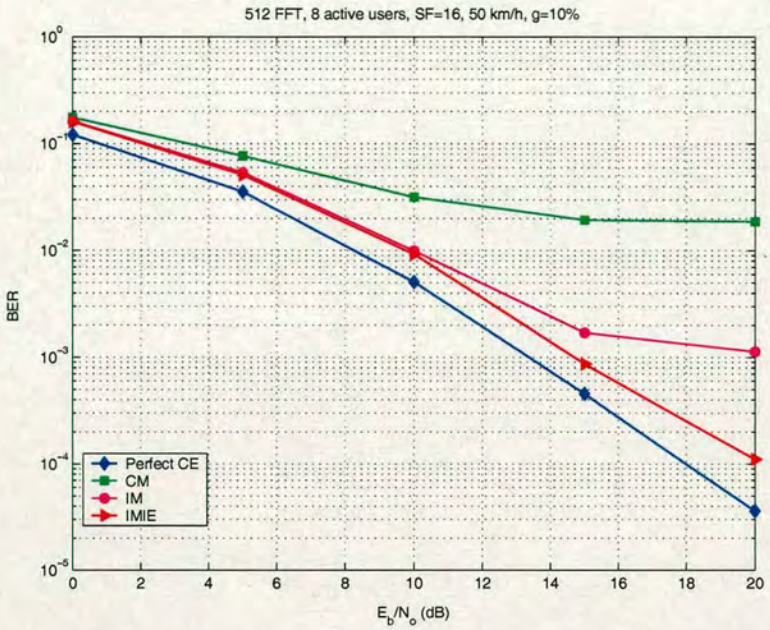

Figure 6.16: *Simulated BER performances with channel estimations, 8 active users, CM: Correlation Method, IM: Iterative Method, Perfect CE: Perfect Channel Estimation, IMIE: Iterative Method with Initial Estimates.*

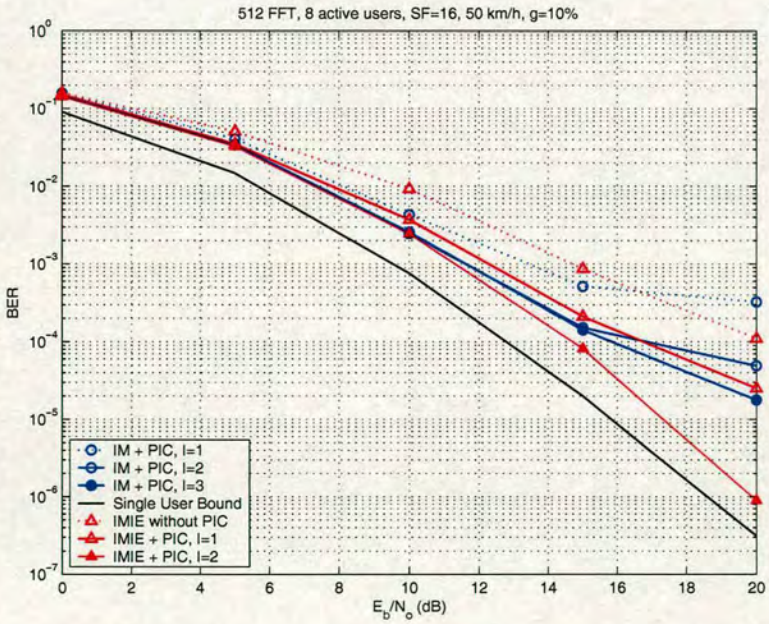

Figure 6.17: *Simulated BER performances with channel estimations and PIC, 8 active users, CM: Correlation Method, IM: Iterative Method, Perfect CE: Perfect Channel Estimation, IMIE: Iterative Method with Initial Estimates.*

mances. Our results verify the effectiveness of the new method. Moreover, parallel interference cancellation is introduced into the iterative structure. The proposed joint scheme shows good channel estimation accuracy and significant improvements with respect to an equaliser with the conventional correlation method.

Chapter 7
Conclusions and Further Work

7.1 Conclusions

Recent advances in wireless communications and multimedia data communications have urged the development of low-cost and low power multi-mode receivers that are capable of accessing different networks while providing mobility and reliability over mobile radio channels.

When talking about multi-mode terminals, people may be familiar with receiver architectures and supporting software that operate in multiple modes and multiple bands coping with GSM and CDMA signals. The progress from GSM to 3G has increased this requirement on cellular transmitters [86].

To design a multi-mode receiver which is in a position to handle multiple protocol standards, an apparent problem is that wireless network protocols operate in different radio frequency bands. A multi-mode approach in which a single-chipset can be unconditionally reconfigured and can switch from one service operating at a frequency to another service operating at another frequency has been proposed in 2001, mainly concentrating on the front-end design [127].

The main target of this work is to develop multi-mode terminals from the algorithm viewpoint, reducing receiver complexity by taking advantages of the commonalities among different specifications and receiver requirements.

Chapter 2 began with a brief introduction of the basic principles of multi-carrier transmissions. A review of three OFDM based standards are then presented. Comparing the architectures of the three systems, the strong resemblance among their physical layer is observed and a generic OFDM transceiver architecture is discussed. Spread spectrum system is then introduced since it is the fundamental of UMTS which is another main concern in this thesis. Single carrier systems with frequency domain equalisation attract more and more interests as an alternative solution to OFDM. It avoids the inherent PAPR problem and it is less sensitive to carrier frequency offsets and phase noise. A description of the SC-FDE is given in this chapter. A short tutorial on adaptive filters and the concept of varying length equaliser are described next.

Equaliser reconfiguration is motivated by looking at not only how to reduce MMSE but also at how to reduce computational complexity without significant performance degradation. In this chapter, a sigma-delta modulation based sampling rate conversion scheme was suggested. The sampling architecture allows the use of a common clock in the multi-mode receiver. Simulation result shows that for the DVB-T system a 40 MHz clock rate with linear interpolation can provide good time alignment. Therefore, 40 MHz can be chosen as a best compromise between the system performance and hardware expenses for such a multi-mode receiver since the other standards, i.e. DAB and UMTS have a lower sampling rate than DVB-T. Moreover, higher sampling rate if possible and with not too much power consumption can definitely improve the system performance and also enable a fractional spaced equalisation which is more robust than classical equalisers. A receiver architecture combining SRC and OFDM symbol synchronisation is also proposed in this chapter.

Chapter 3 addressed a CPICH based frequency domain equaliser for UMTS FDD mode. This is an extension of work on chip level equalisation into the frequency domain. The high power CPICH transmitted for channel estimation and synchronsation is utilized for approximate cyclic reconstruction. Simulation results demonstrate that the proposed scheme outperforms the existing "overlap-cut" algorithm. Equalising WCDMA signals in the frequency domain enables a multi-mode receiver to reuse the powerful FFT/IFFT processing blocks normally found in OFDM systems. It provides the UMTS system with a simple equalisation structure which was identical to that for OFDM systems. Therefore, two kinds of systems happily coexist together. Additionally, we proposed a MMSE interference cancellation solution in the frequency domain. The CPICH based FDE for UMTS FDD requires a high power pilot channel for both good channel estimates and effective cyclic reconstruction. It was shown that the interference caused can be suppressed prior to spreading.

In Chapter 4, further developments on FDE algorithms enabling multi-mode operation were discussed. Two alternative frequency domain equalisers for WCDMA are derived. One is based on self cyclic reconstruction and the other one is based on slot segmentation. Simulation results verify the effectiveness of these two approaches by comparing to the time domain equaliser. Most importantly, unlike the FDE in Chapter 3, these two algorithms do not require a high power pilot channel. Furthermore, a hybrid DFE with varying length feedback filter is presented. This kind of DFE uses feedforward filtering in the frequency domain while the feedback part is operating in the time domain. The algorithm adjusts feedback filter length in order

to save unnecessary computational complexity. The impact of small feedback filter coefficients on system BER performance is considered and a more reasonable filter length than the MMSE optimal one regarding system performance is provided. Although the new FBF length is not the optimal one in terms of the MSE criterion, it achieves a good balance between the MSE and the system performance. The proposed algorithm is also able to track channel changes successfully as can be seen from the simulation results.

In Chapter 5, MMSE Turbo equalisation and cyclic reconstruction are jointly combined in one iteration process since they are both conducted in an iterative manner. The proposed scheme can effectively remove the normally inserted cyclic prefix in a SC-FDE. Meanwhile, MMSE equalisation has advantages over traditional MAP detectors if low complexity processing is required. With a slight increase in computational complexity compared to the extended RISIC, the system performance can be improved. The same idea is extended for OFDM systems and is published in [122].

Chapter 6 deals with channel estimation and parallel interference cancellation for both WCDMA and CP-CDMA systems. The new channel estimators differ from each other, however, with the same basic idea behind them. For WCDMA systems, the received waveforms for each user are reconstructed and removed from the received signal hence the channel estimation accuracy is improved via another correlation process. For CP-CDMA systems, the sum of data channels and the pilot channel is reconstructed and is treated as a new compound pilot. With the reconstructed virtual pilot and the received signal, new channel estimates can be computed. Simulation results verify the effectiveness of the new scheme with only 10% transmitted power allocated to the code-multiplexed pilot channel. Therefore it is compatible with systems like HSDPA where only a small amount of power is transmitted through the pilot channel. Moreover, parallel interference cancellation is introduced into the iterative estimation structure; interference is reduced prior to despreading and system performance is significantly improved.

In this thesis, all algorithms and architectures were developed within the framework of multimode terminals; OFDM based systems, WCDMA systems, SC-FDE and CP-CDMA systems were taken into account.

7.2 Suggestions for Further Work

There are a few options for us to consider how to proceed:

- The new work will still focus on frequency domain processing for systems normally handled in the time domain or time domain processing for systems normally dealt with in the frequency domain. This is the key idea of architectures for multi-mode baseband terminals. For examples, frequency domain equalisation for UMTS and time domain processing for OFDM or MC-CDMA. The importance and advantage of this is that same processing structure can be reused or shared for receivers of different systems.

- MC-CDMA and MC-DS-CDMA are important areas and so would be another good direction. Since a multi-mode terminal is anticipated to cope with not only existing standards and also future evolutions, these two systems should be considered in a multi-mode receiver.

- The current work on channel estimation needs extending. An obvious area is to extend it for MC-CDMA and MC-DS-CDMA systems. Further work should investigate the combination of time-multiplexed pilots and code-multiplexed pilots for channel estimation purposes. A comparison with other approaches will also be studied. Moreover, the channel estimation problem for OFDM systems needs to be investigated.

- In this thesis, our main contribution has been various cyclic prefix or virtual cyclic prefix reconstruction approaches. More work can be done on this topic, e.g. a combination of iterative cyclic prefix reconstruction and channel estimation, cyclic prefix reconstruction in a space time block coded system. In the context of UMTS, joint channel estimation, cyclic reconstruction and parallel interference cancellation will be considered.

- Varying length filters may be of interest in this work due to its flexible structure. Lots of areas on applications to WCDMA systems and SC-FDE systems remain untouched. More efforts are needed to develop reconfigurable structures for equalisation in mobile receivers that can offer satisfactory performance with a low computational complexity.

In this thesis, our research work concentrated on merely a multi-mode receiver handling only one system at one time. As for the further study, simultaneously receiving two or more than two types of signals will be considered. Fast synchronisation and identification of signals and information of all available programs and services should be given to users, allowing the users to be made aware of what available on the other services. The multi-mode receiver is desired to switch among different standards, be capable of running a searching or tracking process at the back of the current working system. A possible solution is to maintain synchronisation to

each system and decode only the service management data, unless the terminal is requested to switch to a specific network.

References

[1] S. Redl, M. W. Oliphant, and M. K. Weber, "An introduction to GSM." Artech House, March 1995.

[2] A. Bahai and B. Saltzberg, "Multi-carrier digital communications - theory and applications of OFDM." Kluwer Academic/Plenum Publishers, 1999.

[3] L. Hanzo, L.-L. Yang, E.-L. Kuan, and K. Yen, "Single- and multi-carrier DS-CDMA." John Wiley & Sons, Ltd, 2003.

[4] A. Chouly, A. Brajal, and S. Jourdan, "Orthogonal multicarrier techniques applied to direct sequence spread spectrum CDMA systems," in *Proceedings of the IEEE Global Telecommunications Conference*, pp. 1723–1728, Nov./Dec. 1993.

[5] S. Kondo and L. Milstein, "On the use of multicarrier direct sequence spread spectrum systems," in *Proceedings of the IEEE Military Communications Conference*, pp. 52–56, Oct. 1993.

[6] N. Yee, J.-P. Linnartz, and G. Fettweis, "Multi-carrier CDMA for indoor wireless radio networks," in *Proceedings of the International Symposium on Personal, Indoor and Mobile Radio Communications*, pp. 109–113, Sept. 1993.

[7] ETSI, "UMTS (TR-101 112), V 3.2.0," April 1998.

[8] ETSI EN 300 744 V1.4.1 (2001-01), "Digital video broadcasting (DVB); framing structure, channel coding and modulation for digital terrestrial television."

[9] ETSI EN 300 401 V1.3.3 (2001-05), "Radio broadcasting systems; digital audio broadcasting (DAB) to mobile, portable and fixed receivers."

[10] N. Prasad and H. Teunissen, "A state-of-the-art of HIPERLAN/2," in *Proceedings of the 50th IEEE Vehicular Technology Conference*, vol. 5, pp. 2661–2666, Sept. 1999.

[11] H. Harada, Y. Kamio, and M. Fujise, "Multimode software radio system by parameter controlled and telecommunication component block embedded digital signal processing hardware," *IEICE Transactions on Communications*, vol. E83-B, pp. 1217–1228, June 2000.

[12] H. Harada and M. Fujise, "A new small-size multi-mode and multi-task software radio prototype for future intelligent transport systems," *IEICE Transactions on Communications*, vol. E85-B, pp. 2703–2715, Dec. 2002.

[13] Y. Li, S. McLaughlin, D. G. M. Cruickshank, and C. Williams, "New physical layer architecture for future multi-mode mobile communication systems," in *The 12th Wireless World Research Forum (WWRF), Toronto*, Nov. 2004.

[14] Y. Li(co-author), "Personal area technologies for internetworked services," *IEEE Communications Magazine*, vol. 42, pp. S15–S26, Dec. 2004.

[15] Y. Li, S. McLaughlin, and D. G. M. Cruickshank, "Cyclic-prefix CDMA system with chip based equalization and interference cancellation," in *Proceedings of the International Symposium on Personal, Indoor and Mobile Radio Communications*, Sept. 2005.

[16] Y. Li, S. McLaughlin, and D. G. M. Cruickshank, "UMTS FDD frequency domain equalization based on self cyclic reconstruction," in *IEEE International Conference on Communications*, vol. 3, pp. 2122–2126, May 2005.

[17] Y. Li, S. McLaughlin, and D. G. M. Cruickshank, "UMTS FDD frequency domain equalization based on slot segmentation," in *Proceedings of the 61st IEEE Vehicular Technology Conference*, May 2005.

[18] Y. Li, X. Wei, D. G. M. Cruickshank, and S. McLaughlin, "Hybrid DFE with variable length feedback filter," *accepted by IEE Proceedings - Communications.*

[19] Y. Li, S. McLaughlin, and D. G. M. Cruickshank, "Bandwidth efficient single carrier systems with frequency domain equalization," *Electronics Letters*, vol. 41, pp. 857–858, July 2005.

[20] Y. Li, S. McLaughlin, and D. G. M. Cruickshank, "Joint channel estimation and parallel interference cancellation for WCDMA," in *submitted to the Proceedings of the 63rd IEEE Vehicular Technology Conference.*

[21] Y. Li, S. McLaughlin, and D. G. M. Cruickshank, "Channel estimation and interference cancellation in CP-CDMA systems," *submitted to IEE Proceedings - Communications.*

[22] H. Sari, G. Karam, and I. Jeanclaude, "Transmission techniques for digital terrestrial TV broadcasting," *IEEE Communications Magazine*, vol. 33, pp. 100–109, Feb. 1995.

[23] D. Falconer, S. Ariyabistakul, A. Benyamin-Seeyar, and B. Eidson, "Frequency domain equalization for single-carrier broadband wireless systems," *IEEE Communications Magazine*, pp. 58–66, April 2002.

[24] N. Benvenuto and S. Tomasin, "On the comparison between OFDM and single carrier modulation with a DFE using a frequency-domain feedforward filter," *IEEE Transactions on Communications*, vol. 50, pp. 947–955, June 2002.

[25] R. Chang, "Synthesis of band-limited orthogonal signals for multichannel data transmission," *Bell Systems Technical Journal*, vol. 46, pp. 1775–1796, Dec. 1966.

[26] S. Weinstein and P. Ebert, "Data transmission by frequency-division multiplexing using the discrete fourier transform," *IEEE Transactions on Communications*, vol. 19, pp. 628–634, Oct. 1971.

[27] W. Zou and Y. Wu, "COFDM: an overview," *IEEE Transactions on Broadcasting*, vol. 41, pp. 1–8, Mar. 1995.

[28] R. Prasad, "Universal wireless personal communications." Artech House Boston/London, 1998.

[29] T. Keller and L. Hanzo, "Adaptive multicarrier modulation: a convenient framework for time-frequency processing in wireless communications," *Proceedings of the IEEE*, vol. 88, pp. 611–640, May 2000.

[30] The World DAB Forum, "http://www.worlddab.org/."

[31] BBC Research and Development, "http://www.bbc.co.uk/rd/."

[32] EUREKA -147 Project, "Digital audio broadcasting."

[33] ETSI TR 101 190 V1.1.1 (1997-12), "Digital video broadcasting (DVB); implementation guidelines for DVB terrestrial services; transmission aspects."

[34] DVB - Digital Video Broadcasting, "http://www.dvb.org/."

[35] ETSI TR 101 683 V1.1.1 (2000-02), "Broad radio access networks (BRAN); HIPERLAN type 2; system overview."

[36] ETSI TS 101 475 V1.3.1 (2001-12), "Broadband radio access networks (BRAN); HIPERLAN type 2; physical (PHY) layer."

[37] Hiperlan 2 Global Forum, "http://www.hiperlan2.com/."

[38] M. Barnard and S. McLaughlin, "Reconfigurable terminals for mobile communication systems," *Electronics & Communication Engineering Journal*, vol. 12, pp. 281–292, Dec. 2000.

[39] X. Wu, B. Jiang, and Q. Yin, "Software-defined radio based baseband discrete model for orthogonal frequency division multiplexing CDMA systems," in *Proceedings of the 53rd IEEE Vehicular Technology Conference*, vol. 2, pp. 771–775, May 2001.

[40] A. Viterbi, "CDMA principles of spread spectrum communication." Addison-Wesley Publishing Company, April 1995.

[41] J. Proakis, "Digital communications." McGraw-Hill, 3rd edition, 1995.

[42] K. Fazel and S. Kaiser, "Multi-carrier and spread spectrum systems." John Wiley and Sons Ltd., 2003.

[43] B. Sklar, "Rayleigh fading channels in mobile digital communication systems part I: characterization," *IEEE Communications Magazine*, vol. 35, pp. 90–100, July 1997.

[44] W. Jakes, "Microwave mobile communications." Wiley Publishing House, 1974.

[45] S. Ko and H. Choi, "Performance analysis of channel estimators for forward link W-CDMA under multipath rayleigh fading channels," *IEICE Transactions on Communications*, vol. E86-B, pp. 1212–1223, April 2003.

[46] ETSI TR 101 112 V3.2.0 (1998-04), "Universal mobile telecommunications system (UMTS); selection procedures for the choice of radio transmission technologies of the umts."

[47] K. Hooli, M. Juntti, M. Heikkila, P. Komulainen, M. Latva-aho, and J. Lilleberg, "Chip-level channel equalization in WCDMA downlink," *EURASIP Journal on Applied Signal processing*, vol. 8, pp. 757–770, 2002.

[48] T. Krauss, W. Hillery, and M. Zoltowksi, "MMSE equalization for forward link in 3G CDMA: Symbol-level versus chip-level," in *Proceedings of the 10th IEEE Workshop on Statistical Signal and Array Processing*, pp. 18–22, Aug. 2000.

[49] S. Verdu, "Multiuser detection." Cambridge University Press, 1998.

[50] K. Hooli, M. Latva-aho, and M. Juntti, "Performance evaluation of adaptive chip-level channel equalizers in WCDMA downlink," in *IEEE International Conference on Communications*, vol. 6, pp. 1974–1979, 2001.

[51] A. Baynast, P. Radosavljevic, and J. Cavallaro, "Chip-level LMMSE equalization for downlink MIMO CDMA in fast fading environments," in *IEEE Global Telecommunications Conference*, vol. 4, pp. 2552–2556, Nov. 2004.

[52] L. Mailaender, "Adaptive frequency-domain chip equalization for the MIMO CDMA downlink," in *Proceedings of the 60th IEEE Vehicular Technology Conference*, vol. 3, pp. 1766–1770, Sept. 2004.

[53] J. Choi, S. Kim, and C. Lim, "Receivers with chip-level decision feedback equalizer for CDMA downlink channels," *IEEE Transactions on Wireless Communications*, vol. 3, pp. 300–315, Jan. 2004.

[54] E. Dahlman, P. Beming, J. Knutsson, F. Ovesj, M. Persson, and C. Roobol, "WCDMA-the radio interface for future mobile multimedia communications," *IEEE Transactions on Vehicular Technology*, vol. 47, pp. 1105–1118, Apr. 1998.

[55] H. Holma and A. Toskala, "WCDMA for UMTS." Wiley Publishing House, 2001.

[56] M. Clark, "Adaptive frequency-domain equalization and diversity combining for broadband wireless communications," *IEEE Journal on Select Areas in Communications*, vol. 16, pp. 1385–1395, 8 1998.

[57] M. Huemer, L. Reindl, A. Springer, and R. Weigel, "Frequency domain equalization of linear polyphase channels," in *Proceedings of the IEEE Vehicular Technology Conference*, pp. 1698–1702, May 2000.

[58] K. Takeda, T. Itagaki, and F. Adachi, "Joint use of frequency-domain equalization and transmit/receiv antenna diversity for single carrier transmissions," *IEICE Transactions on Communications*, vol. E87-B, pp. 1946–1953, July 2004.

[59] J. Coon, J. Siew, M. Beach, A. Nix, S. Armour, and J. McGeehan, "A comparison of MIMO-OFDM and MIMO-SCFDE in WLAN environments," in *2003 IEEE Global Telecommunications Conference*, vol. 6, pp. 3296–3301, Dec. 2003.

[60] J. Coon, S. Armour, M. Beach, and J. McGeehan, "Adaptive frequency-domain equalization for single-carrier multiple-input multiple-output wireless transmissions," *IEEE Transactions on Signal Processing*, vol. 53, pp. 3247–3256, Aug. 2005.

[61] M. Yee, M. Sandell, and Y. Sun, "Comparison study of single-carrier and multi-carrier modulation using iterative based receiver for MIMO system," in *Proceedings of the 59th IEEE Vehicular Technology Conference*, vol. 3, pp. 1275–1279, May 2004.

[62] IEEE 802.16.3 Task Group, "SC-FDE PHY layer system proposal for sub 11 GHz BWA (an OFDM compatible solution)." http://www.wirelessman.org/tg3/contrib/802163p-01_31r2.pdf, March 2001.

[63] K. Baum, T. Thomas, F. Vook, and V. Nangia, "Cyclic-prefix CDMA: an improved transmission method for broadband DS-CDMA cellular systems," in *IEEE Wireless and Communications and Networking Conference*, vol. 1, pp. 183–188, 2002.

[64] P. Lin and T. Chiueh, "Low complexity frequency-domain despreading for cyclic-prefix CDMA systems," *IEEE Communications Letters*, vol. 8, pp. 339–341, June 2004.

[65] F. Vook, T. Thomas, and K. Baum, "Cyclic-prefix CDMA with antenna diversity," in *Proceedings of the 55th IEEE Vehicular Technology Conference*, vol. 2, pp. 1002–1006, 2002.

[66] F. Adachi, D. Garg, S. Takaoka, and K. Takeda, "Broadband CDMA techniques," *IEEE Wireless Communications*, vol. 12, pp. 8–18, Apr. 2005.

[67] F. Adachi and K. Takeda, "Bit error rate analysis of DS-CDMA with joint frequency domain equalization and antenna diversity combining," *IEICE Transactions on Communications*, vol. E87-B, pp. 2991–3002, Oct. 2004.

[68] S. Qureshi, "Adaptive equalization," *Proceeding of the IEEE*, vol. 73, pp. 1349–1387, 1985.

[69] C. Cowan and P. Grant, "Adpative filters." Prentice-Hall, 1985.

[70] B. Mulgrew and C. Cowan, "Adpative filters and equalisers." Kluwer Academic Publishers, 1988.

[71] S. Haykin, "Adaptive filter theory." Prentice Hall, 4th edition, 2001.

[72] K. Wesolowski, C. Zhao, and W. Rupprecht, "Adaptive LMS transversal filters with controlled length," *IEE Proceedings on Radar and Signal Processing*, vol. 139, pp. 233–238, June 1992.

[73] F. Riera-Palou, J. Noras, and D. G. M. Cruickshank, "Variable length equalizers for broadband mobile systems," in *Proceedings of the 52nd IEEE Vehicular Technology Conference*, vol. 5, pp. 2478–2485, Sept. 2000.

[74] X. Wei, D. G. M. Cruickshank, B. Mulgrew, and F. Riera-Palou, "Performance of equalizers with dynamic length," in *Proceedings of the 59th IEEE Vehicular Technology Conference*, vol. 1, pp. 545–549, May 2004.

[75] Y. Gong and C. Cowan, "Structure adaptation of linear MMSE adaptive filters," *IEE Proceedings on Vision, Image, and Signal Processing*, vol. 151, pp. 271–277, August 2004.

[76] Z. Pritzker and A. Feuer, "Variable length stochastic gradient algorithm," *IEEE Transactions on Signal Processing*, vol. 39, pp. 997–1001, April 1991.

[77] F. Riera-Palou, J. Noras, and D. G. M. Cruickshank, "Linear equalisers with dynamic and automatic length selection," *IEE Electronic Letters*, vol. 37, pp. 1553–1554, Dec 2001.

[78] X. Wei, D. G. M. Cruickshank, and B. Mulgrew, "Varying length equalizer for WCDMA system," in *Proceedings of the 3rd IEEE International Symposium on Signal Processing and Information Technology, 2003*, pp. 355 – 358, Dec. 2003.

[79] Y. Gu, K. Tang, H. Cui, and W. Du, "LMS algorithm with gradient decent filter length," *IEEE Signal Processing Letters*, vol. 11, pp. 305–307, Mar. 2004.

[80] Y. Gong and C. Cowan, "A LMS style variable tap-length algorithm for structure adaptation," *IEEE Transactions on Signal Processing*, vol. 53, pp. 2400–2407, July 2005.

[81] F. Gardner, "Interpolation in digital modems-part I: fundamentals," *IEEE Transactions on Communications*, vol. 41, pp. 501–507, March 1993.

[82] L. Erup, F. Gardner, and R. Harris, "Interpolation in digital modems-part II: Implementation and performance," *IEEE Transactions on Communications*, vol. 41, pp. 998–1008, June 1993.

[83] J. Candy and G. Temes, "Oversampling delta-sigma data converters - theory, design and simulation." The institute of electrical and electronics engineering, 1992.

[84] J. Heiskala and J. Terry, "OFDM wireless LANs: A theoretical and practical guide." Sams, Dec. 2001.

[85] T. Pollet, P. Spruyt, and M. Moeneclaey, "The BER performance of OFDM systems using non-synchronized sampling," in *Proceedings of the IEEE GLOBECOM'94*, pp. 253–257, Nov. 1994.

[86] L. Robinson, P. Aggarwal, and R. Surendran, "Direct modulation multimode transmitter," in *3G Mobile communication technologies*, pp. 206–210, May 2002.

[87] A. Doufexi, E. Tameh, A. Nix, S. Armour, and A. Molina, "Hotspot wireless LANs to enhance the performance of 3G and beyond cellular networks," *IEEE Communications Magazine*, vol. 41, pp. 58–65, July 2003.

[88] F. Adachi, "Effects of orthogonal spreading and rake combining on DS-CDMA forward link in mobile radio," *IEICE Transactions on Communications*, vol. E80-B, pp. 1703–1712, Jan. 1997.

[89] M. Hunukumbure, M. Beach, and B. Allen, "Downlink orthogonality factor in UTRA FDD systems," *Electronics Letters*, vol. 38, pp. 196–197, Feb. 2002.

[90] D. Kim and G. Stüber, "Residual ISI cancellation for OFDM with applications to HDTV broadcasting," *IEEE Journal on Select Areas in Communications*, vol. 16, pp. 1590–1599, 8 1998.

[91] T. Hwang and Y. Li, "Iterative cyclic prefix reconstruction for coded single-carrier systems with frequency-domain equalization (sc-fde)," in *Proceedings of the IEEE Vehicular Technology Conference*, vol. 3, pp. 1841–1845, 2003.

[92] A. McCormick, P. Grant, and J. Thompson, "Hybrid uplink multi-carrier CDMA interference cancellation receiver," *IEE Proceedings Communications*, vol. 148, pp. 119–124, Apr. 2001.

[93] A. Oppenheim and R. Schafer, "Digital signal processing." Prentice-Hall, 1975.

[94] G. Clark, S. Mitra, and S. Parker, "Block implementation of adaptive digital filters," *IEEE Transactions on Signal Processing*, vol. 29, pp. 744–752, June 1981.

[95] E. Ferrara, "Fast implementations of LMS adaptive filters," *IEEE Transactions on Signal Processing*, vol. 28, pp. 474–475, Aug. 1980.

[96] M. Vollmer, M. Haardt, and J. Gotze, "Comparative study of joint detection techniques for TD-CDMA based mobile radio systems," *IEEE Journal on Select Areas in Communications*, vol. 19, pp. 1461–1475, 8 2001.

[97] R. Machauer and F. Jondral, "FFT-speed and windowed multiuser detector for UTRA-FDD high rate data mode," in *IEEE 7th International Symposium on Spread Spectrum Techniques and Applications*, vol. 3, pp. 712–716, Sept 2002.

[98] I. Martoyo, T. Weiss, F. Capar, and F. Jondral, "Low complexity CDMA downlink receiver based on frequency domain equalization," in *Proceedings of the IEEE Vehicular Technology Conference*, vol. 2, pp. 987 – 991, October 2003.

[99] J. Cioffi and J. Bingham, "A data-driven multitone echo canceller," *IEEE Transactions on Communications*, vol. 42, pp. 2853–2869, Oct. 1994.

[100] M. Harteneck and C. Luschi, "Practical implementation aspects of MMSE equalisation in a 3GPP HSDPA terminal," in *Proceedings of the 59th IEEE Vehicular Technology Conference*, vol. 1, pp. 445–449, May 2004.

[101] 3GPP TS 25.211, "Physical channels and mapping of transport channels onto physical channels (FDD)."

[102] X. Dai and X. Xie, "Adaptive blind equalization of the time-and frequency-selective OFDM system based on the local approximation," in *IEEE International Conference on Neural Networks and Signal Processing*, vol. 2, pp. 1402–1405, 2003.

[103] S. Kang, J. Kim, and E. Joo, "A novel subblock partition scheme for partial transmit sequence OFDM," *IEEE Transaction on Broadcasting*, vol. 45, pp. 333–338, Sept. 1999.

[104] J. Markel, "Fft pruning," *IEEE Transaction on Audio and Electroacoustics*, vol. 19, pp. 305–311, Dec. 1971.

[105] H. Sorensen and C. Burrus, "Efficient computation of the DFT with only a subset of input or output points," *IEEE Transaction on Signal Processing*, vol. 41, pp. 1184–1200, Mar. 1993.

[106] S. He and M. Torkelson, "Computing partial DFT for comb spectrum evaluation," *IEEE Signal Processing Letters*, vol. 3, pp. 173–175, 1996.

[107] M. Larimore, S. Wood, and J. Treichler, "Performance costs for theoretical minimal-length equalizers," in *IEEE International Conference on Acoustics Speech and Signal Processing*, vol. 3, pp. 2477–2480, 1997.

[108] J. Kim, J. Kang, and E. Powers, "A bandwidth efficient OFDM transmission scheme," in *International Conference on Acoustics, Speech, and Signal Processing*, vol. 3, pp. 2329–2332, 2002.

[109] R. Koetter, A. Singer, and M. Tüchler, "Turbo equalization," *IEEE signal processing magazine*, vol. 21, pp. 67–80, Jan. 2004.

[110] M. Tüchler, R. Koetter, and A. Singer, "Turbo equalization: principles and new results," *IEEE Transactions on Communications*, vol. 50, pp. 754–767, May 2002.

[111] M. Tüchler, A. Singer, and R. Koetter, "Minimum mean square error equalization using a priori information," *IEEE Transactions on Signal Processing*, vol. 50, pp. 673–683, Mar. 2002.

[112] D. Reynolds and X. Wang, "Low-complexity turbo-equalization for diversity channels," *Signal Processing*, vol. 81, pp. 989–995, 2001.

[113] C. Berrou, A. Glavieux, and P. Thitimajshima, "Near shannon limit error-correcting coding and decoding: Turbo-codes," in *IEEE International Conference on Communications*, vol. 2, pp. 1064–1070, May 1993.

[114] C. Berrou and A. Glavieux, "Near optimum error correcting coding and decoding: turbo-codes," *IEEE Transactions on Communications*, vol. 10, pp. 1261–1271, Oct. 1996.

[115] L. Bahl, J. Cocke, F. Jelinek, and J. Raviv, "Optimal decoding of linear codes for minimizing symbol error rate," *IEEE Transaction on Information Theory*, vol. IT-20, pp. 284–287, Mar. 1974.

[116] P. Robertson, E. Villebrun, and P. Hoeher, "A comparison of optimal and sub-optimal MAP decoding algorithms operating in the log domain," in *IEEE International Conference on Communications*, vol. 2, pp. 18–22, June 1995.

[117] J. Hagenauer and L. Papke, "Decoding 'turbo'-codes with the soft output viterbi algorithm (SOVA)," in *IEEE International Symposium on Information Theory*, p. 164, June 1994.

[118] C. Douillard, M. Jezequel, C. Berrou, A. Picart, P. Didier, and A. Glavieux, "Iterative correction of intersymbol interference: turbo-equalization," *European Transactions on Telecommuications*, vol. 6, pp. 507–511, 1995.

[119] M. Tuchler and J. Hagenauer, "Linear time and frequency domain turbo equalization," in *Proceedings of the 53rd IEEE Vehicular Technology Conference*, pp. 1449–1453, May 2001.

[120] P. Robertson and P. Hoeher, "Optimal and sub-optimal maximum a posteriori algorithms suitable for turbo decoding," *European Transactions on Telecommunications*, vol. 8, pp. 119–125, March-April 1997.

[121] J. Hagenauer, E. Offer, and L. Papke, "Iterative decoding of binary block and convolutional codes," *IEEE Transaction on Information Theory*, vol. 42, pp. 429–445, Mar. 1996.

[122] Y. Li, S. McLaughlin, and D. G. M. Cruickshank, "OFDM system with cyclic prefix reconstruction and MMSE Turbo equalization," in *Proceedings of the 62nd IEEE Vehicular Technology Conference*, Sept. 2005.

[123] P. Schramm and R. Müller, "Pilot symbol assisted BPSK on rayleigh fading channels with diversity: performance analysis and parameter optimization," *IEEE Transactions on Communications*, vol. 46, pp. 1560–1563, Dec. 1998.

[124] P. Schramm, "Analysis and optimisation of pilot-channel-assisted BPSK for DS-CDMA systems," *IEEE Transactions on Communications*, vol. 46, pp. 1122–1124, Sep. 1998.

[125] N. Benvenuto, E. Costa, and E. Obetti, "Performance comparison of chip matched filter and RAKE receiver for WCDMA systems," in *GLOBECOM 2001*, pp. 3060–3064, 2001.

[126] D. Koulakiotis and A. Aghvami, "Data detection techniques for DS/CDMA mobile systems: a review," *IEEE Personal Communications*, pp. 24–34, June 2000.

[127] M. Madihian, "A band selection/switching technique for multi-mode wireless front-end transceivers," in *Proceedings of the 2001 IEEE Microwave and Optoelectronics Conference*, vol. 1, pp. 257–260, 2001.

Appendix A
Derivation of the feedback filter $G_i(w)$

To derive the filter coefficients for the CPICH interference canceller, a cost function J is defined in (3.15) and is rewritten as:

$$J = \frac{1}{N_c}\sum_{w=0}^{N-1}[\sigma^2_{residual}|1 - H_i(w)W_i(w)|^2 + \sigma^2_n|W_i(w)|^2 + \sigma^2_p|G_i(w) - H_i(w)W_i(w)|^2] \tag{A.1}$$

Let $J_1 = \sigma^2_{residual}|1-H_i(w)W_i(w)|^2$, $J_2 = \sigma^2_n|W_i(w)|^2$ and $J_3 = \sigma^2_p|G_i(w)-H_i(w)W_i(w)|^2$, respectively. Inserting $W_i(w) = \frac{(\sigma^2_{residual}+\sigma^2_p G_i(w))H^*_i(w)}{\sigma^2_n+(\sigma^2_{residual}+\sigma^2_p)|H_i(w)|^2}$ into (A.1), this results in

$$J_1 = \sigma^2_{residual}|\frac{\sigma^2_n + \sigma^2_p|H_i(w)|^2 - \sigma^2_p|H_i(w)|^2 G_i(w)}{\sigma^2_n + (\sigma^2_{residual} + \sigma^2_p)|H_i(w)|^2}|^2 \tag{A.2}$$

The gradient of J_1 with respect to $G_i(w)$ is:

$$\nabla_{G_i(w)}J_1 = \frac{\sigma^2_{residual}[-(\sigma^2_n + \sigma^2_p|H_i(w)|^2)|H_i(w)|^2 + \sigma^4_p|H_i(w)|^4 G^*_i(w)]}{(\sigma^2_n + (\sigma^2_{residual} + \sigma^2_p)|H_i(w)|^2)^2} \tag{A.3}$$

$$J_2 = \sigma^2_n|\frac{(\sigma^2_{residual} + \sigma^2_p G_i(w))H^*_i(w)}{\sigma^2_n + (\sigma^2_{residual} + \sigma^2_p)|H_i(w)|^2}|^2 \tag{A.4}$$

The gradient of J_2 with respect to $G_i(w)$ is:

$$\nabla_{G_i(w)}J_2 = \frac{\sigma^2_n(\sigma^2_{residual}\sigma^2_p + \sigma^4_p G^*_i(w))|H_i(w)|^2}{(\sigma^2_n + (\sigma^2_{residual} + \sigma^2_p)|H_i(w)|^2)^2} \tag{A.5}$$

$$J_3 = \sigma^2_p|\frac{(\sigma^2_n + \sigma^2_{residual}|H_i(w)|^2)G_i(w) - \sigma^2_{residual}|H_i(w)|^2}{\sigma^2_n + (\sigma^2_{residual} + \sigma^2_p)|H_i(w)|^2}|^2 \tag{A.6}$$

The gradient of J_3 with respect to $G_i(w)$ is:

$$\nabla_{G_i(w)}J_3 = \frac{-\sigma^2_p(\sigma^2_n + \sigma^2_{residual}|H_i(w)|^2)\sigma^2_{residual}|H_i(w)|^2 + \sigma^2_p(\sigma^2_n + \sigma^2_{residual}|H_i(w)|^2)^2 G^*_i(w)}{(\sigma^2_n + (\sigma^2_{residual} + \sigma^2_p)|H_i(w)|^2)^2} \tag{A.7}$$

Let $\nabla_{G_i(w)} J = 0$, then $\nabla_{G_i(w)}(J_1 + J_2 + J_3) = 0$, i.e.

$$\begin{aligned}
&\sigma^2_{residual}[-(\sigma^2_n + \sigma^2_p|H_i(w)|^2)|H_i(w)|^2 + \sigma^4_p|H_i(w)|^4 G^*_i(w)] \\
&+\sigma^2_n(\sigma^2_{residual}\sigma^2_p + \sigma^4_p G^*_i(w))|H_i(w)|^2 \\
&-\sigma^2_p(\sigma^2_n + \sigma^2_{residual}|H_i(w)|^2)\sigma^2_{residual}|H_i(w)|^2 + \sigma^2_p(\sigma^2_n + \sigma^2_{residual}|H_i(w)|^2)^2 G^*_i(w) \\
&= 0
\end{aligned} \tag{A.8}$$

Equation (A.8) can then be written as:

$$\begin{aligned}
G^*_i(w) &= \frac{\sigma^4_p\sigma^2_{residual}|H_i(w)|^4 + \sigma^2_p(\sigma^2_n + \sigma^2_{residual}|H_i(w)|^2)\sigma^2_{residual}|H_i(w)|^2}{\sigma^2_{residual}\sigma^4_p|H_i(w)|^4 + \sigma^2_n\sigma^4_p|H_i(w)|^2 + \sigma^2_p(\sigma^2_n + \sigma^2_{residual}|H_i(w)|^2)^2} \\
&= \frac{\sigma^2_{residual} \cdot |H_i(w)|^2}{\sigma^2_{residual} \cdot |H_i(w)|^2 + \sigma^2_n}
\end{aligned} \tag{A.9}$$

From (A.9) it is known that $G^*_i(w)$ is a real term. Therefore,

$$G_i(w) = \frac{\sigma^2_{residual} \cdot |H_i(w)|^2}{\sigma^2_{residual} \cdot |H_i(w)|^2 + \sigma^2_n} = \frac{|H_i(w)|^2}{|H_i(w)|^2 + \sigma^2_n/\sigma^2_{residual}} \tag{A.10}$$

Appendix B
Publications

B.1 Publications

The following papers describing what reported in this thesis have been published or accepted for publication:

B.1.1 Journal

- **Yushan Li**, Xusheng Wei, David G. M. Cruickshank, Steve McLaughlin, "Hybrid DFE with Variable Length Feedback Filter", IEE Proceedings - Communications, accepted for publication.
- **Yushan Li**, Steve McLaughlin, David G. M. Cruickshank, "Bandwidth Efficient Single Carrier Systems with Frequency Domain Equalization", Electronics Letters, Vol. 41, No. 15, July 2005, pp. 857-858.
- **Yushan Li** (co-author), "Personal area technologies for internetworked services", IEEE Communications Magazine, Vol. 42, Issue: 12, Dec. 2004, pp. S15- S26.

B.1.2 Conferences

- **Yushan Li**, Steve McLaughlin, David G. M. Cruickshank, "Cyclic-Prefix CDMA System with Chip Based Equalization and Interference Cancellation", Proceedings of the 2005 IEEE International Symposium on Personal, Indoor and Mobile Radio Communications, Sept. 2005, Berlin, Germany
- **Yushan Li**, Steve McLaughlin, David G. M. Cruickshank, "OFDM Systems with Cyclic prefix Reconstruction and MMSE Turbo Equalisation", Proceedings of the 62nd IEEE Vehicular Technology Conference, Sept. 2005, Dallas, USA.

- **Yushan Li**, Steve McLaughlin, David G. M. Cruickshank, "UMTS FDD Frequency Domain Equalization Based on Self Cyclic Reconstruction", IEEE International Conference on Communications, 16-20 May 2005, Vol.3, pp. 2122-2126, Seoul, South Korea.
- **Yushan Li**, Steve McLaughlin, David G. M. Cruickshank, "UMTS FDD Frequency Domain Equalization Based on Slot Segmentation", Proceedings of the 61st IEEE Vehicular Technology Conference, May 2005, Stockholm, Sweden.
- **Yushan Li**, Steve McLaughlin, David G. M. Cruickshank, Chris Williams, "New Physical Layer Architecture for Future Multi-Mode Mobile Communication Systems" in 12th Wireless World Research Forum (WWRF), Toronto, Nov. 2004.
- Emad A. Al-Susa, David G. M. Cruickshank, Steve McLaughlin, **Yushan Li**, "Capacity Evaluation of a Multi-Cellular System Based on Adaptive Multi-carrier Turbo-coded Transmission", Proceeding of the 6th International Symposium on Wireless Personal Multimedia Communications, Oct. 2003, Yokosuka, Japan.

B.2 Papers under review

Two papers have been submitted for publication and are currently under review.

- **Yushan Li**, Steve McLaughlin, David G. M. Cruickshank, Xusheng Wei, "Multi-Mode Terminals", submitted to IEEE Vehicular Magazine in Dec. 2005.
- **Yushan Li**, Steve McLaughlin, Xusheng Wei, "Joint Channel Estimation, Chip Level Equalization and Parallel Interference Cancellation for WCDMA", submitted to IEEE Transactions on Vehicular Technology in Nov. 2005.
- **Yushan Li**, Steve McLaughlin, David G. M. Cruickshank, "Joint Channel Estimation and Parallel Interference Cancellation for WCDMA", submitted to the 63rd IEEE Vehicular Technology Conference in Sept. 2005.
- **Yushan Li**, Steve McLaughlin, David G. M. Cruickshank, "Channel Estimation and Interference Cancellation in CP-CDMA Systems", submitted to IEE Proceedings - Communications in July 2005, temporally accepted for publication, revised paper submitted in Dec. 2005.

Appendix C
Selected Publications

Multi-Mode Terminals

Yushan Li, Steve McLaughlin, David G. M. Cruickshank, Xusheng Wei
Institute for Digital Communications, School of Engineering and Electronics,
University of Edinburgh, King's Buildings, Mayfield Road,
Edinburgh EH9 3JL, UK.

Abstract

Wireless communications is rapidly moving towards so called 4G wireless systems. This has led to an increasing demand to develop integrated mobile terminals which have multi-mode capabilities, i.e. multiple communication systems which can coexist. Attention of this paper is focused on the coexistence of multiple communication systems via a simple structure. Algorithms and architectures are developed within the framework of multi-mode terminals. This is in contrast to software-defined radios, the term multi-mode in this paper is limited to a set of standards and a receiver is expected to handle different systems with low hardware complexity. Dedicated hardware is shared and reused by different systems. Existing specifications DAB, DVB-T, HIPERLAN-2 and UMTS are considered in this paper. They can be classified into two categories: multi-carrier systems and single-carrier systems. This paper considers multi-mode terminals from both the algorithm and the architecture viewpoint, reducing receiver complexity by taking advantage of the commonalities among different specifications and receiver requirements. As an example, a joint channel estimation, chip-level frequency domain equalization and parallel interference cancellation structure for WCDMA is presented.

I. Introduction

The most significant concern in the wireless personal communication area is the desire for mobility and flexibility in communications and the demand for real time high data rate transmission. Future wireless multimedia communication systems will be designed with the focus on satisfying user's requirements. In mobile communications, there is an increasing demand to develop more sophisticated integrated mobile terminals with multi-mode capabilities. Today, voice, text, audio and video communications, wireless networks and Internet are beginning to interact more and more with each other [1]. Thus, future wireless

systems, so called 4G will need to consider be a multi-functional integrated broadband mobile communication system. A schematic graph of such an integrated network is shown in Figure 1.

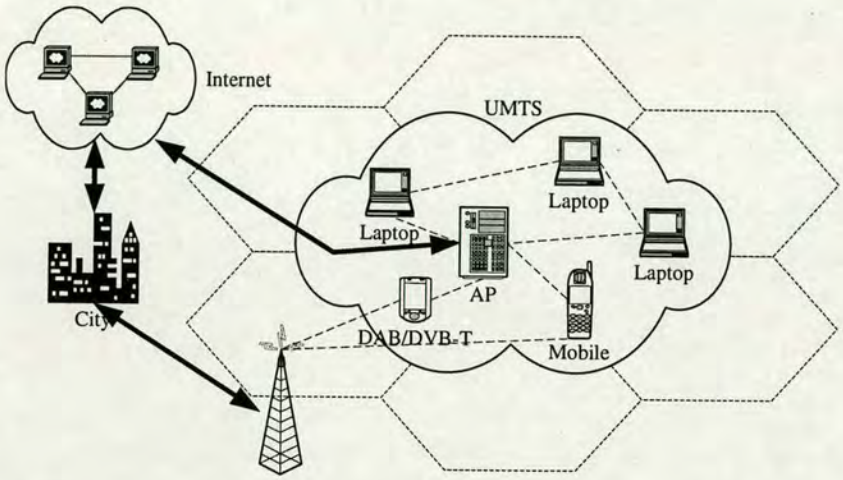

Fig. 1. Integrated network, UMTS, DAB, DVB-T, WLAN

To support this goal, it will be necessary to determine suitable structures for multi-mode terminals that maximize flexibility without an excessive compromise in performance. In this paper, only existing communication systems, Digital Video Broadcasting - Terrestrial (DVB-T) [2], Digital Audio Broadcasting (DAB) [3] and High Performance Radio Local Area Network-type 2 (HIPERLAN-2) [4] are considered in combination with Universal Mobile Telecommunications System (UMTS) [5]. These are the most prominent solutions for broadband transmission of multimedia signals and future wireless network connections that are currently meeting the requirements of many consumers. These standards are receiving a great deal of attention with an increasing requirement for one receiver to cope with these multiple services. By investigating algorithmic structural commonalities among physical layer implementations, based on the design of some new receiver architectures, the foundations for a multi-mode receiver can be achieved.

Most recent work in this area has been from a software-defined radio (SDR) perspective as evidenced in [6][7]. The general assumption underpinning this is the presence of powerful digital processing units, such as programmable digital signal processors (DSPs) and field programmable gate arrays (FPGAs). Obviously, these processors provide more flexibility than dedicated DSPs, however, dedicated DSPs are usually faster

and consume less power than general-purpose processors. Power consumption is an important issue in battery powered handsets. Consequently, the term multi-mode used in this paper is distinct from SDR, in that it is limited to a set of standards and is expected to handle different systems with low hardware complexity. The assumption is that a SDR inspired controlling framework will still be required. This can be done by discovering the commonalities in standards definition and processing requirements and thus sharing dedicated hardware between the different systems.

Code division multiple access (CDMA) and Orthogonal frequency division multiplexed (OFDM) are currently the two dominant air interfaces in the consumer market. They can be viewed as representatives for single-carrier systems and multi-carrier systems, respectively. Significant research efforts have been carried out on the integration of these two techniques [12]. In this paper, the implementation of multi-mode terminals is considered from two aspects, a multi-mode receiver for multi-carrier systems and a multi-mode receiver capable of handling both single-carrier and multi-carrier systems. Finally, a joint channel estimation, chip level frequency domain equalization (FDE) and parallel interference cancellation (PIC) structure is proposed as an example.

II. Muti-Mode Terminal Implementation: Multi-Carrier Systems

In the 1990s, OFDM was successfully deployed for high data rate broadband communications. OFDM is one type of high data rate transmission technique used over wireless channels. The frequency response of most wireless channels is not flat, thus, the key point of OFDM is to divide the given channel into several orthogonal sub-channels in the frequency domain. Data streams are modulated on multi-carriers and then several sub-carriers are transmitted in parallel simultaneously. Therefore, although the overall channel is non-flat with a frequency selective characteristic, every sub-channel can be considered flat fading. In theory, sub-carriers are orthogonal to each other and mutually overlapped which leads to a reduction of adjacent carrier interference as well as full use of the available spectrum.

In the future, user demands will be the major concern of service providers and industrial organizations. DAB, DVB-T and HIPERLAN-2 are three major broadband wireless access specifications employing

OFDM. Generally speaking, the implementation of multi-mode terminals regarding these OFDM based systems is not complicated since they share the same air interface. A comparison of DAB, DVB-T and HIPERLAN-2 standards, including key features was presented in [8]. These specifications show significant commonalities with baseline systems. Comparing the architectures of three standards, it is quite obvious that a strong resemblance among their receiver architectures exists. Making good use of those commonalities, common hardware blocks can be reused and thus a multi-mode receiver is implemented with reduced hardware expenses. In practice, this is not simply mixing them together since each mode has its own operating frequency, bandwidth, data rate, and spectrum specifications, etc; Figure 2 shows a generic OFDM transceiver.

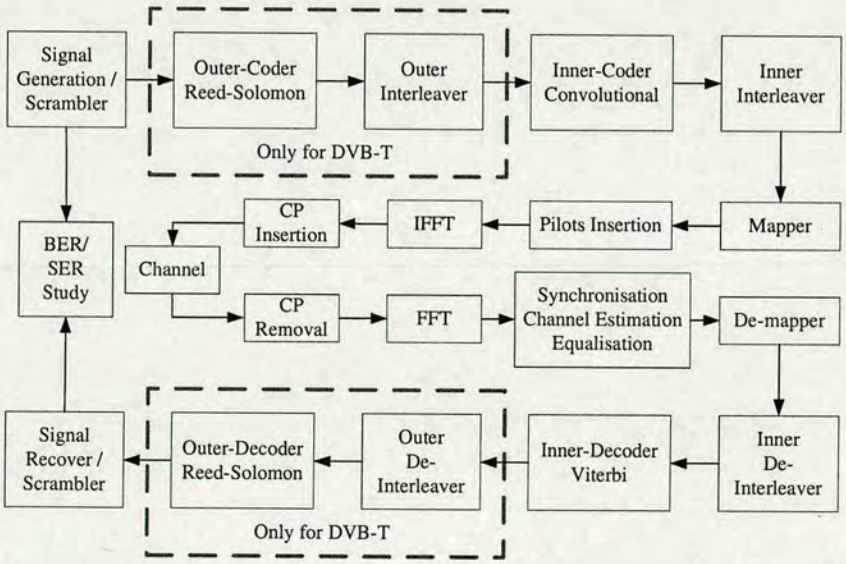

Fig. 2. A generic OFDM transceiver block diagram (For DAB/DVB-T/HIPERLAN-2)

For a multi-mode digital communication receiver, it is required that the terminal must be able to handle various communications standards. Generally, different chip/sample/symbol rates are specified in different standards. An obvious simplistic solution is to adopt different dedicated clocks for different standards, however, it would be costly and cumbersome. The terminal size would be greatly enlarged as the number of standards would increase. The three systems considered here deploy three different sampling rates, 9.143 MHz for DVB-T, 2.048 MHz for DAB and 20 MHz for HIPERLAN-2, respectively. Sampling rate

adaptation is the first key issue to be considered for a multi-mode receiver even before synchronization. Since the sampling rate of HIPERLAN-2 is the highest among the sampling rates of the three investigated standards, a possible solution for this sampling rate conversion problem might be based on the over-sampling of HIPERLAN-2 and then approximating sample data or sampling instants for DAB and DVB-T. The reason for doing so is twofold,

1. 20 MHz is the highest signalling rate among the targeted systems; the multi-mode receiver should be able to handle the highest signalling rate system;

2. No fractional sampling rate conversion is required for the HIPERLAN-2 system except a simple decimation process.

In [9], Sigma-Delta modulation and linear interpolation are deployed in the receiver for sampling rate adaptation purposes. A new sampling rate is adopted in the multi-mode receiver, which is a integer multiple of 20 MHz (the sampling rate of HIPERLAN-2). A new proposed structure can integrate the three OFDM based systems by a single system clock effectively and in addition, bring advantages to symbol synchronization of the OFDM systems. The receiver architecture is shown in Figure 3.

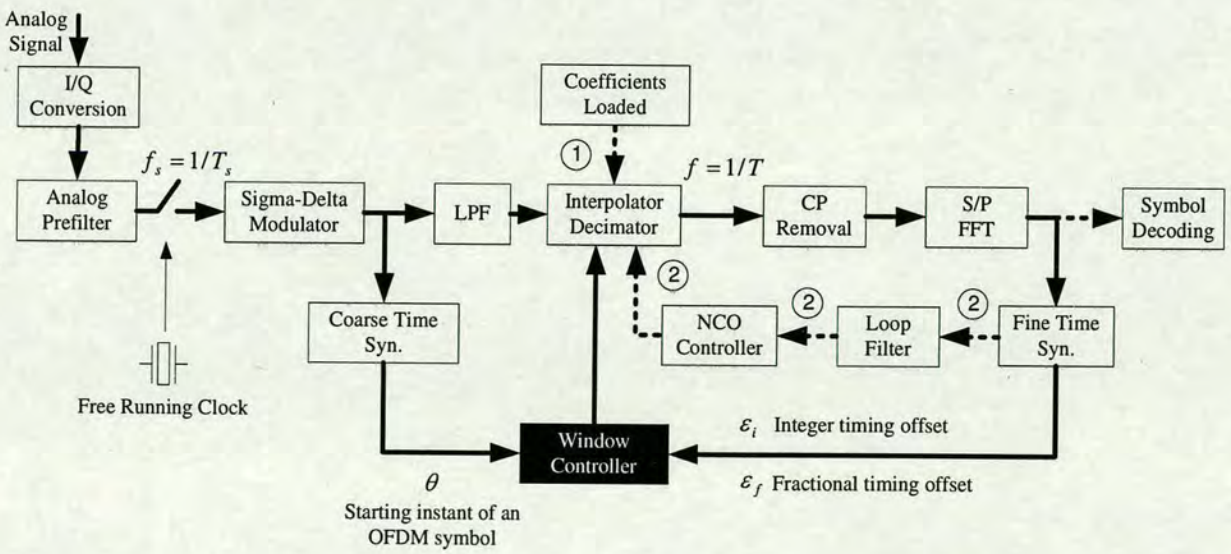

Fig. 3. Proposed multi-mode OFDM receiver architecture

First, the analogue signals are sampled at a sampling frequency much higher than its signalling

rate. Signals sampled at a high frequency are pushed to a Sigma-Delta modulator and then, a low pass filter (LPF) preceding the interpolation and decimation block is used for anti-aliasing purpose and quantization noise attenuation. Generally, an OFDM system achieves symbol synchronization by adjusting the FFT position, including coarse synchronization and fine synchronization. Before the interpolation and decimation block, the receiver works under the coarse symbol-acquiring mode. The symbol starting instant θ can be coarsely determined by CP based pre-FFT approaches [10]. The starting position of an OFDM symbol and the FFT window position can be determined and set. The sampling rate of the Interpolator/Decimator output approximates the targeted system signalling rate, $1/T$. Afterwards, post-FFT fine symbol synchronization is carried out. The residual timing offset is estimated though pilots in the frequency domain and then compensated for the fine symbol synchronization purpose. Based on the high sampling rate before the interpolator, it is now easy to adjust the starting instant of an OFDM symbol by fractional offsets, which is not a simple task for conventional OFDM receivers sampled at the symbol rate. The timing error can be compensated by the feedback from the error estimation every OFDM symbol.

Figure 4 shows the performance of a multi-mode receiver with different sampling rates deployed in the Sigma-Delta modulation block. The mean squared error (MSE) of the uncoded data in the frequency domain against E_b/N_0 is plotted, a DVB-T receiver is considered in the simulation. Since the other standards (DAB & UMTS) have lower sample rate requirements than DVB-T, if a sampling rate is selected that is suitable for DVB-T, then it should also be suitable for DAB & UMTS in terms of using linear interpolation. 40 MHz would appear a good initial choice as the best compromise between the system performance and hardware expense.

If it is possible to have higher sampling frequency with not too much power consumption, this will definitely improve the system performance and also enable a fractional spaced equalization (FSE) which is less sensitive to sample timing.

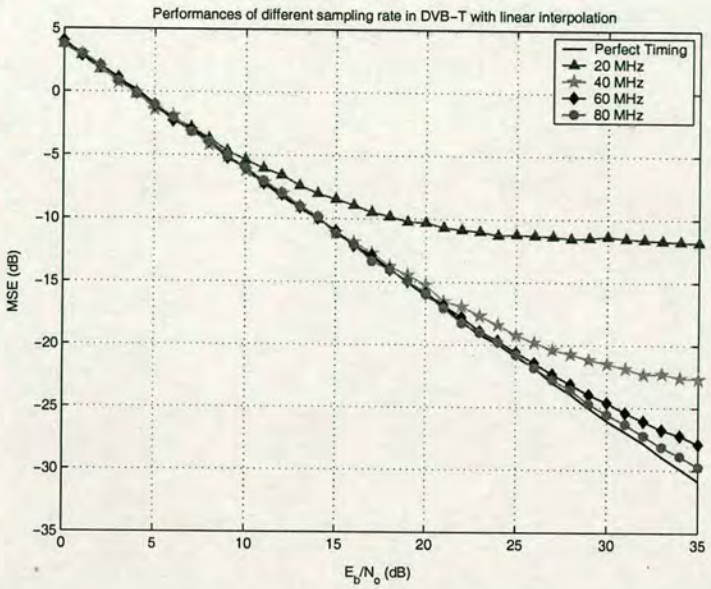

Fig. 4. Performances of different sampling rate in DVB-T with interpolation

III. Multi-Mode Terminal Implementation: Single-Carrier Systems + Multi-Carrier Systems

Significant research efforts has been carried out on the integration of single-carrier CDMA and OFDM techniques [12]. The combination of direct sequence CDMA (DS-CDMA) and multi-carrier modulation has been proposed; multi-carrier CDMA (MC-CDMA) and multi-carrier DS-CDMA (MC-DS-CDMA) are two different realizations [14][12]. However, in this paper, only the combination of current single-carrier DS-CDMA systems and the previous discussed OFDM based systems is considered.

In a DS-CDMA downlink scenario, all signals are transmitted symbol and chip synchronously through the same mobile radio channel. The general principle behind DS-CDMA is its spectrum spreading [11][12]. The information signal with bandwidth is spread over a wideband pseudo-noise (PN) sequence. After spreading, user data is summed together for transmission in a mobile channel with L multi-paths. At the receiver end, L resolved signals are multiplied by the complex conjugates of the channel taps and maximum ratio combined (MRC) in a RAKE receiver. Finally, despreading and demapping are performed on the output of the RAKE receiver to recover the user data symbol. The block diagram of a transmitter and a RAKE receiver is shown in Figure 5.

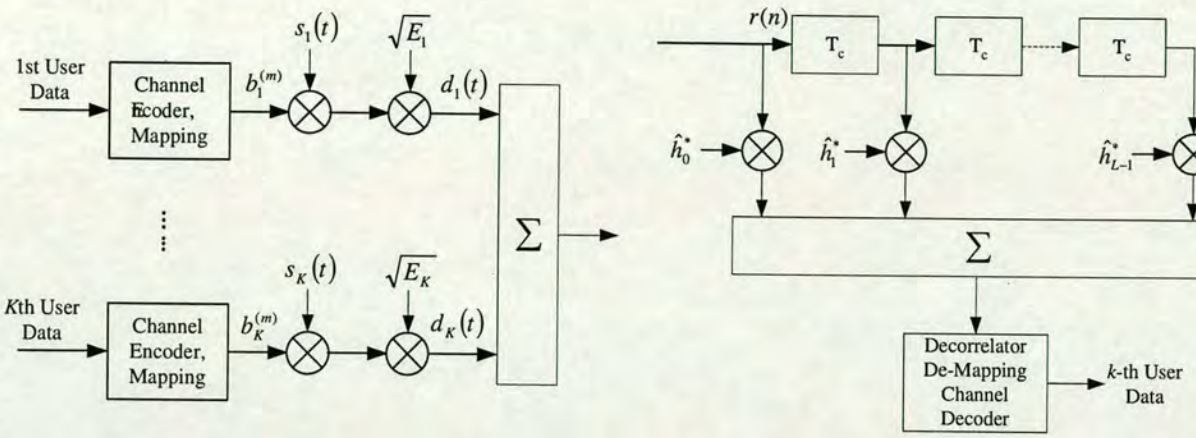

(a) DS-CDMA transmitter block diagram

(b) DS-CDMA RAKE receiver block diagram

Fig. 5. A DS-CDMA transceiver block diagram

For the reception of the CDMA downlink signal in a receiver, the capability to perform multi-user detection (MUD) in mobile handsets requires significant complexity. The performance of conventional RAKE receivers is dominated by the multiple access interference (MAI) and this can result in a high error rate in a heavily loaded system. Chip level equalization [13] has been proposed as a reasonable approach that achieves a good compromise between receiver complexity and system performance.

As stated previously, there is an increasing desire to integrate OFDM based standards and CDMA systems in a multi-mode receiver [30], and discussions on the coverage and throughput analysis for such integrated system were presented in [15]. The concept of employing a frequency domain equalizer for CDMA systems in the receiver, making use of the powerful FFT/IFFT for both DS-CDMA and OFDM systems in the handset is very attractive from the viewpoint of physical layer implementation.

Recently, single carrier system with frequency domain equalization (SC-FDE) has attracted interest as evidenced by recent publications [16] [17] [18] [19]. The SC-FDE uses the same mechanism as in OFDM, i.e. a cyclic prefix (CP) is inserted to mitigate the multi-path effect and make the channel matrix a circular one in order to simplify the receiver. The CP concept adopted in OFDM was introduced into the conventional DS-CDMA system to enhance current single carrier 3G-system performance [20][21][22]. A CP-CDMA system has the advantage of a simple equalization structure due to the inserted CP. In addition,

[23] reveals that a CP-CDMA system can achieve a comparable system performance to MC-CDMA while having lower peak-to-average power ratio (PAPR).

Unfortunately, a CP-based SC-FDE is not compatible with the current CDMA system because the CP insertion will inevitably destroy the frame structure of the standard. It is desirable to design a receiver without changing the transmitted signal. A number of solutions have been proposed for OFDM systems or SC-FDE without CP [24][25][26][27]. In principle, these proposed schemes can all be extended to single-carrier CDMA systems to enable deployment of an FDE at chip level. In [28][29], the authors proposed a new approach to apply the FDE in the downlink of a broadband CDMA system without redundancy which they call the overlap-cut method. As stated in their papers, applying a conventional FDE on a single carrier system without CP gives errors that are significantly larger at the edges of the block. Therefore samples at the beginning and the end of each equalized blocks are discarded.

In [31], a MMSE-FDE based on self cyclic reconstruction was proposed. The proposed algorithm exploits the relationship between the required cyclic part and the transmitted signal itself. The estimated cyclic part is then added to the received block signal to enable frequency domain equalization. This can be viewed as a cyclic reconstruction process [24]. Simulation results show the effectiveness of the proposed algorithm compared to a MMSE time domain equalizer. In [32], by exploiting the frame and slot structures of the UMTS downlink, the pilots within one slot (for FDD mode) are used for cyclic reconstruction in a FDE. Furthermore, one slot signal is split into multiple segments for the sake of combating channel variance within one slot.

To design a FDE for the current CDMA system is very attractive. OFDM has become a strong candidate for the fourth generation systems and hence a CDMA receiver adopting chip level FDE will be compatible with the current FFT based receiver structures. By adopting the proposed equalization structure for receiving single carrier DS-CDMA signal, a multi-mode receiver can be programmed to switch to a particular system more conveniently. An example of a single-carrier DS-CDMA with FDE will be presented in the next section.

IV. Joint Channel Estimation, Chip-Level Equalization and Parallel Interference Cancellation

The importance of accurate channel estimation for a practical mobile communication system is self evident. To maintain bandwidth and power efficiency, a code-multiplexed pilot channel is transmitted in WCDMA systems [11]. Generally speaking, good estimates can be obtained with a high power pilot channel. Unfortunately, this leads to high interference in the dedicated data channels. Such systems face a dilemma as to whether to adopt a high power pilot channel for better channel estimates. Moreover, practical implementation of the channel estimator should be considered. Consequently, it is of great interest to study an efficient channel estimator for CDMA systems that can work with a low power pilot channel. In this section, as an example of a multi-mode receiver implementation that was presented previously, a joint channel estimation, chip-level frequency domain equalization and parallel interference cancellation scheme for WCDMA systems is discussed [33]. The correlation method (CM) [11][34] widely adopted for channel estimation in WCDMA systems is used for delivering initial channel estimates $\hat{\mathbf{h}}_i$ for the i-th block. Figure 6 shows a conventional CDMA receiver structure with channel estimation.

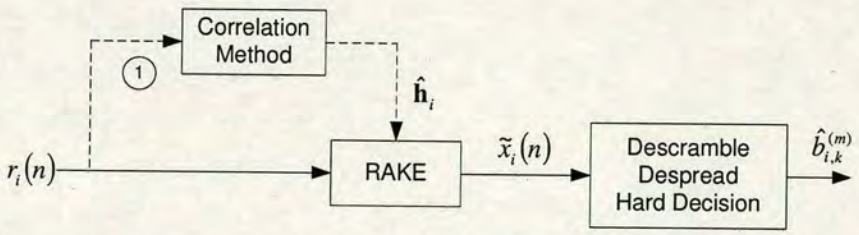

Fig. 6. A conventional CDMA receiver with channel estimation

A RAKE receiver then operates on the received signal and the composite estimated signal $\tilde{x}_i(n)$ is despread and hard detected. K users' transmitted symbols $\hat{b}_{i,k}^{(m)}$ are respread and rescrambled. The scrambled code-multiplexed pilots are added to form an estimated composite signal $\hat{x}_i(n)$. As is well known, time-domain circular convolution is equivalent to frequency-domain multiplication, and vice versa. By the insertion of the CP, linear channel distortion of the signal results in circular convolution of the

transmitted signal and the channel impulse response. With this in mind, it is necessary to reconstruct the resultant effect caused by a virtual CP so that the time and frequency-domain descriptions of the convolution are essentially equivalent. Given the reconstructed transmitted signal $\hat{x}_i(n)$ and the estimated channel $\hat{\mathbf{h}}_i$, the missing effect of a CP can be compensated by cyclic reconstruction [24]. $\hat{x}_i(n)$ is converted to $\hat{X}_i(w)$ in the frequency domain and used for channel estimation together with the modified received frequency domain signal $\tilde{R}_i(w)$ (FFT of $\tilde{r}_i(n)$, received signal generated by cyclic reconstruction). In the estimator, the reconstructed composite signal $\hat{X}_i(w)$ is treated as a virtual pilot signal. A refined channel estimate can be obtained in the frequency domain as: $\hat{H}_i^{IFDCE}(w) = \frac{\tilde{R}_i(w)\cdot\hat{X}_i^*(w)}{|\hat{X}_i(w)|^2+\sigma_n^2}$ where σ_n^2 denotes the variance of the additive Gaussian noise and we assume the channel power is normalized. The estimated channel is converted to the time domain and only the first L values are kept to form the channel estimate $\hat{\mathbf{h}}_i^{IFDCE} = [\hat{h}_{i,0}^{IFDCE}, \cdots, \hat{h}_{i,L-1}^{IFDCE}]$. Subsequently, $\hat{\mathbf{h}}_i^{IFDCE}$ is used for frequency domain equalization. The whole process of the iterative frequency domain channel estimation (IFDCE) is shown in Figure 7.

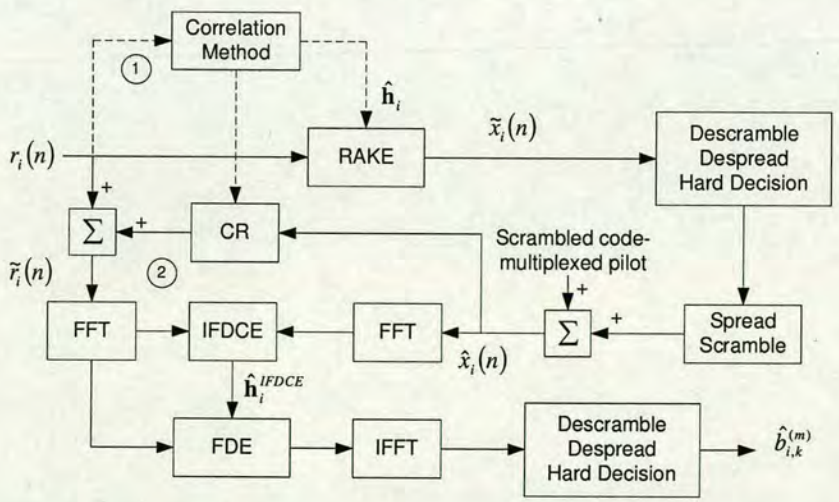

Fig. 7. Iterative frequency domain channel estimation and chip level equalization for WCDMA; CR: cyclic reconstruction

Since the proposed IFDCE and FDE requires user symbol detection and interference reconstruction, a PIC is combined into the iterative structure in order to further enhance the system performance. In other words, the proposed scheme is similar to a conventional PIC scheme, therefore, by combining them

together will improve the system performance. In the iteration cycle, K users' signals are regenerated and summed with the pilot channel for channel estimation purpose. Meanwhile, interference from the interfering K-1 users and the parallel pilot channel are constructed and subtracted from the received composite signal, hence, interference can be reduced through the iteration. Figure 8 shows how we can combine the iterative channel estimation and PIC within one structure.

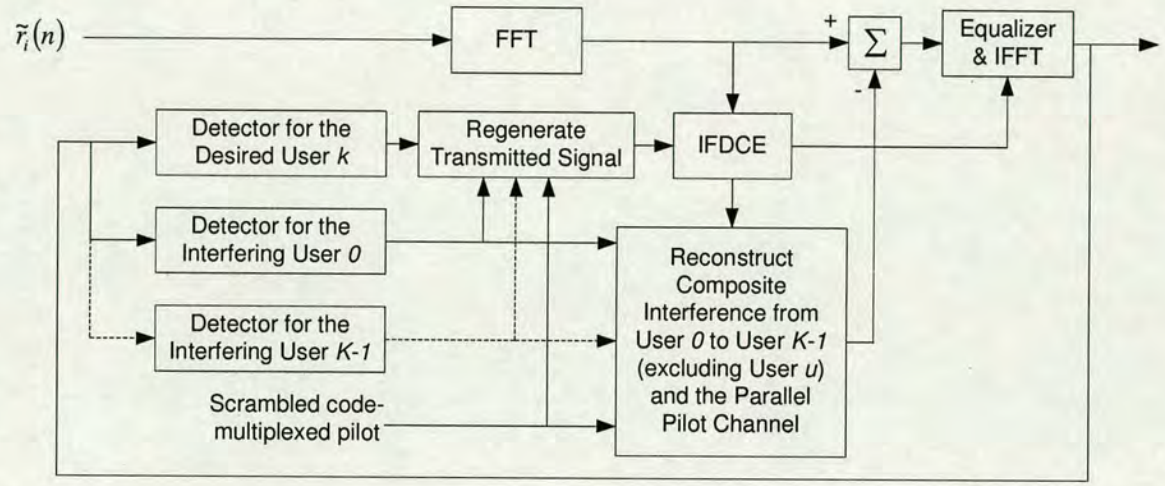

Fig. 8. Combined channel estimation, chip level frequency domain equalization and parallel interference cancellation structure

In order to evaluate the system performance for the proposed structure, computer simulations are carried out at baseband. The chip rate is 3.84 Mchips/s. Walsh codes are used as channelization codes with a fixed spreading factor (SF) of 32 and a 38400 Gold code segment is used as the scrambling code. One pilot channel is code-multiplexed with dedicated data channels. 10% of the whole power is allocated to the pilot channel and the carrier frequency is 2 GHz. The UMTS Vehicular A channel model [35] is used for BER evaluation in our simulation. The mobile terminal is assumed to be moving at a speed of 30 km/h. The BER performances versus SNR per bit are examined. As can be seen in Figure 9, the RAKE performance is dominated by the MAI and this results in saturation at a high error rate. The IFDCE+FDE scheme significantly outperforms the CM+RAKE. The BER performance with a 64 taps chip level mean squared error time domain equalizer (MMSE-TDE) [13] and perfect channel estimation is also simulated as a reference result. It is apparent that the proposed IFDCE+FDE achieves performance close to the

MMSE-TDE with perfect channel estimation. Figure 10 demonstrates the system improvements with PIC.

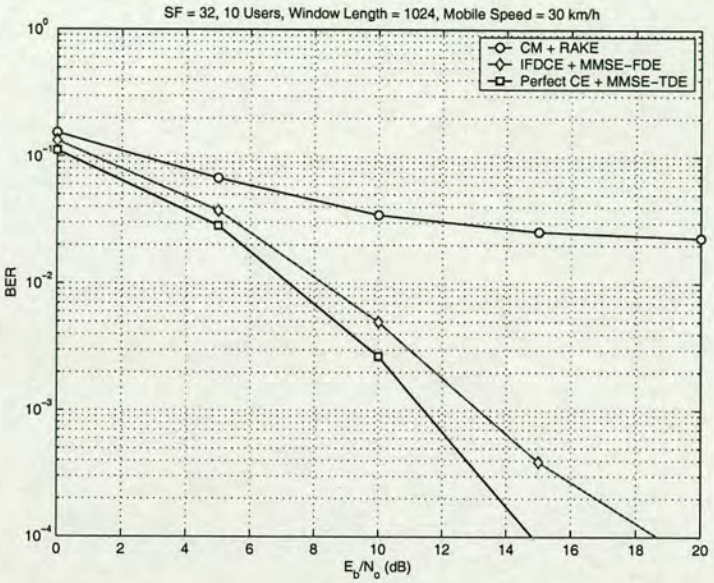

Fig. 9. System BER performance versus E_b/N_0, SF = 32, 10 Active Users, Window Length = 1024, Mobile Speed = 30 km/h

The joint IFDCE+FDE+PIC method achieves only a 1.8dB loss at the BER of 10^{-2} compared to the MMSE-TDE in a single user scenario with perfect channel estimation.

Only 10% transmitted power allocated to the code-multiplexed pilot channel which is compatible with systems like high-speed downlink packet access (HSDPA) [36] where only a small amount of power is transmitted through the pilot channel. In addition, chip level FDE and parallel interference cancellation are introduced into the iterative estimation structure. The iterative cycle can be implemented efficiently in the frequency domain with the overall complexity of $O(NlogN)$ where N is the window length or block size of a FDE. This is much simpler compared to the multiuser detection and the MMSE-TDE which involves matrix inversion. Furthermore, the complexity of the MMSE-FDE does not change significantly with the length of the channel impulse response. The computational complexity of the whole process is comparable to a conventional PIC. On the other hand, since the iterative channel estimator can provide the PIC with better channel estimates, the improvement in system performance that can be achieved is significant.

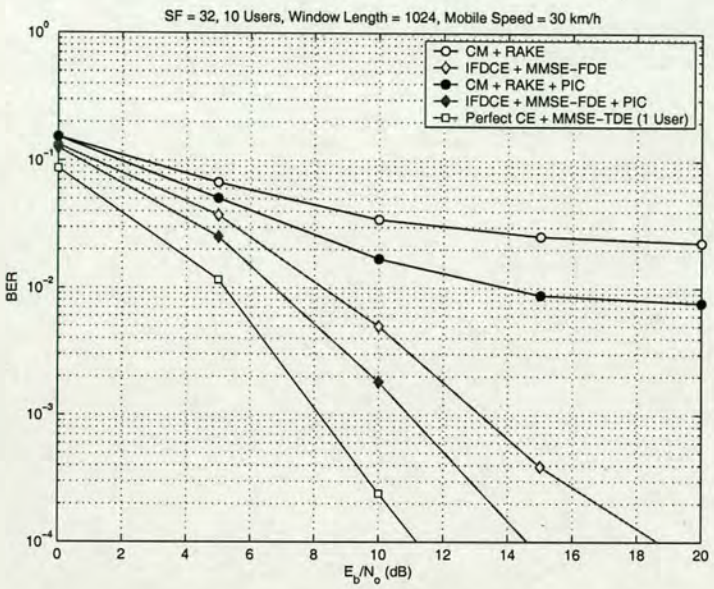

Fig. 10. System BER performance versus E_b/N_0, SF = 32, 10 Active Users, Window Length = 1024, Mobile Speed = 30 km/h

V. Conclusion

In this article the implementation issue of a multi-mode terminal has been discussed. Existing specifications e.g. DAB, DVB-T, HIPERLAN-2 and UMTS have been the main focus of the paper. The problem is separated into two sub-areas. For multi-carrier systems, since they share the same air interface, they are easily to coexist. Common hardware blocks can be reconfigured for different systems as required. For the integration of single-carrier and multi-carrier systems, a number of cyclic reconstruction methods have been proposed to enable frequency domain equalization for single carrier systems without cyclic prefix. In particular, by adopting a frequency domain equalization structure for receiving CDMA signal, the coexistence of OFDM systems and CDMA systems via a simple structure is feasible. A multi-mode receiver can be programmed to switch to a particular transmission more conveniently. So far, research work concentrates on merely a multi-mode receiver handling only one system at one time. As for the further study, simultaneously receiving two or more than two types of signals should be considered. Fast synchronization and identification of signals and information of all available programs and services should be given to users, allowing the users to be made aware of what available on the other services. The multi-mode receiver is desired to switch among different standards, be capable of running a searching or tracking

process at the back of the current working system. A possible solution is to maintain synchronization to each system and decode only the service management data, unless the terminal is requested to switch to a specific network.

ACKNOWLEDGMENT

The work reported in this paper has formed part of the Research Programme of the Virtual Centre of Excellence in Mobile and Personal Communications, Mobile VCE, www.mobilevce.com, whose funding support, including that of EPSRC, is gratefully acknowledged. Fully detailed technical reports on this research are available to Industrial Members of Mobile VCE.

REFERENCES

[1] Research Programme of the Virtual Centre of Excellence in Mobile and Personal Communications, Mobile VCE, http://www.mobilevce.com
[2] ETSI EN 300 744 V1.4.1 (2001-01), "Digital video broadcasting (DVB); Framing structure, channel coding and modulation for digital terrestrial television".
[3] ETSI EN 300 401 V1.3.3 (2001-05), "Radio broadcasting systems; Digital audio broadcasting (DAB) to mobile, portable and fixed receivers".
[4] ETSI TR 101 683 V1.1.1 (2000-02), "Broad radio access networks (BRAN); HIPERLAN Type 2; System Overview".
[5] H. Holma and A. Toskala, *WCDMA for UMTS*, Wiley Publishing House, 2001.
[6] H. Harada, Y. Kamio and M. Fujise, "Multimode software radio system by parameter controlled and telecommunication component block embedded digital signal processing hardware", IEICE Transactions on Communications, E83-B, June 2000, pp. 1217-1228.
[7] H. Harada and M. Fujise, "A new small-size multi-mode and multi-task software radio prototype for future intelligent transport systems", IEICE Transactions on Communications, E85-B, Dec. 2002, pp. 2703-2715.
[8] C. Williams *et al*, "Personal area technologies for internetworked services", IEEE Communications Magazine, Vol. 42, Issue: 12, Dec. 2004, pp. S15-S26.
[9] Y. Li, S. McLaughlin, D.G.M. Cruickshank and C. Williams, "New physical layer architecture for future multi-mode mobile communication systems", the 12th Wireless World Research Forum (WWRF), Toronto, Nov. 2004.
[10] J. Heiskala and J. Terry, *OFDM Wireless LANs: A Theoretical and Practical Guide*, Sams, Dec., 2001.
[11] A. Viterbi, *CDMA Principles of Spread Spectrum Communication*, Addison-Wesley Publishing Company, April 1995.
[12] K. Fazel and S. Kaiser, *Multi-Carrier and Spread Spectrum Systems*, John Wiley and Sons Ltd., 2003
[13] K. Hooli, M. Juntti, M. Heikkila, P. Komulainen, M. Latva-aho and J. Lilleberg, "Chip-level channel equalization in WCDMA downlink", EURASIP Journal on Applied Signal Processing, Vol. 8, 2002, pp. 757-770.
[14] L. Hanzo, L.-L. Yang, E.-L. Kuan and K. Yen, *Single- and Multi-carrier DS-CDMA*, John Wiley & Sons, Ltd, 2003.
[15] A. Doufexi, E. Tameh, A. Nix, S. Armour and A. Molina, "Hotspot wireless LANs to enhance the performance of 3G and beyond cellular networks", IEEE Communications Magazine, Vol. 41, July 2003, pp. 58-65.
[16] D. Falconer, S. Ariyabistakul, A. Benyamin-Seeyar and B. Eidson, "Frequency domain equalization for single-carrier broadband wireless systems", IEEE Communications Magazine, April 2002, pp. 58-66.
[17] N. Benvenuto and S. Tomasin, "On the comparison between OFDM and single carrier modulation with a DFE using a frequency-domain feedforward filter", IEEE Transactions on Communications, Vol. 50, No. 6, June 2002, pp. 947-955.
[18] A. Gusmão, R. Dinis and N. Esteves, "On frequency-domain equalization and diversity combining for broadband wireless communications", IEEE Transactions on Communications, Vol. 51, No. 7, July 2003, pp. 1029-1033.
[19] Z. Liu, "Maximum diversity in single-carrier freqeuncy-domain equalization", IEEE Transactions on Information Theory, Vol. 51, No. 8, Aug. 2005, pp. 2937-2940.
[20] K. Baum, T. Thomas, F. Vook and V. Nangia, "Cyclic-Prefix CDMA: an improved transmission method for broadband DS-CDMA cellular systems", IEEE Wireless and Communications and Networking Conference, Vol. 1, 2002, pp. 183-188.
[21] P. Lin and T. Chiueh, "Low complexity frequency-domain despreading for cyclic-prefix CDMA systems", IEEE Communications Letters, Vol. 8, No. 6, June 2004, pp. 339-341.
[22] A. S. Madhukumar, *et al*, "Single-carrier cyclic prefix-assisted CDMA system with frequency domain equalization for high data rate transmission", EURASIP Journal on Wireless Communications and Networking, Vol. 1, 2004, pp. 149-160.

[23] F. Adachi, D. Garg, S. Takaoka and K. Takeda, "Broadband CDMA techniques", IEEE Wireless Communications, Vol. 12, No. 4, Apr. 2005, pp. 8-18.
[24] D. Kim and G. Stüber, "Residual ISI cancellation for OFDM with applications to HDTV broadcasting", IEEE Journal on Select Areas in Communications, Vol. 16, No. 8, Aug. 1998, pp. 1590-1599.
[25] C. Park and G. Im, "Efficient DMT/OFDM transmission with insufficient cyclic prefix", IEEE Communications Letters, Vol. 8, Issue 9, Sept. 2004, pp. 576-578.
[26] H. Won and G. Im, "Iterative cyclic prefix reconstruction and channel estimation for a STBC OFDM system", IEEE Communications Letters, Vol. 9, Issue 4, Apr. 2005, pp. 307-309.
[27] Y. Li, S. McLaughlin and D.G.M. Cruickshank, "Bandwidth efficient single carrier systems with frequency domain equalization", Electronics Letters, Vol. 41, No. 15, July 2005, pp. 857-858.
[28] M. Vollmer, M. Haardt and J. Gotze, "Comparative study of joint detection techniques for TD-CDMA based mobile radio systems", IEEE Journal on Select Areas in Communications, Vol. 19, No. 8, Aug. 2001, pp. 1461-1475.
[29] I. Martoyo, T. Weiss, F. Capar and F. Jondral, "Low complexity CDMA downlink receiver based on frequency domain equalization", Proceedings of the IEEE Vehicular Technology Conference, Vol. 2, Oct. 2003, pp. 987-991.
[30] P, Rykaczewski, I. Martoyo, Z. Liu and F.K. Jondral, "Multimode detector and I/Q imbalance compensator in a software defined radio", Proceedings of the IEEE 2004 Radio and Wireless Conference, Sept. 2004, pp. 521-524.
[31] Y. Li, S. McLaughlin and D.G.M. Cruickshank, "UMTS FDD frequency domain equalization based on self cyclic reconstruction", IEEE International Conference on Communications, Vol.3, May 2005, pp. 2122-2126.
[32] Y. Li, S. McLaughlin and D.G.M. Cruickshank, "UMTS FDD frequency domain equalization based on slot segmentation", Proceedings of the 61st IEEE Vehicular Technology Conference, May 2005, Stockholm, Sweden.
[33] Y. Li, X. Wei, S. McLaughlin and P. Grant, "Joint Channel Estimation, Frequency Domain Chip-Level Equalization and Parallel Interference Cancellation for WCDMA", Submitted to IEEE Transactions on Vehicular Technology in Nov. 2005.
[34] S. Ko and H. Choi, "Performance analysis of channel estimators for forward link W-CDMA under multipath rayleigh fading channels", IEICE Transactions on Communications, Vol. E86-B, No. 4, 2003, pp. 1212-1223.
[35] ETSI TR 101 112 V3.2.0 (1998-04): Universal Mobile Telecommunications System (UMTS); Selection procedures for the choice of radio transmission technologies of the UMTS.
[36] M. Harteneck and C. Luschi, "Practical implementation aspects of MMSE equalization in a 3GPP HSDPA terminal", Proceedings of the 59th IEEE Vehicular Technology Conference, Vol. 1, May 2004, pp. 445-449.

Joint Channel Estimation, Frequency Domain Chip-Level Equalization and Parallel Interference Cancellation for WCDMA

Yushan Li, Xusheng Wei, Steve McLaughlin, Peter Grant
Institute for Digital Communications, School of Engineering and Electronics,
University of Edinburgh, King's Buildings, Mayfield Road,
Edinburgh EH9 3JL, UK.

Abstract

Code-multiplexed pilots are used for channel estimation to maintain bandwidth efficiency in WCDMA systems. Initially, in this paper, two iterative channel estimation approaches, ICE and IFDCE, are proposed. The ICE method reconstructs received waveforms for each user and removes them from the received signal. Subsequently, the ICE algorithm is modified with the introduction of frequency domain equalization and a new channel estimator (IFDCE) is proposed. The sum of data channels and the pilot channel is reconstructed for frequency domain channel estimation. The received WCDMA signal is then equalized before spreading at chip level in the frequency domain. The chip level equalizer significantly outperforms the RAKE receiver. Compared with time domain chip level equalizers, the computational complexity is reduced by frequency domain processing. Simulation results demonstrate good estimation capability of the ICE and IFDCE schemes with an allocation of only 10% of the whole power to the pilot channel. In addition, an integrated channel estimator, chip level equalizer and parallel interference cancellation detector is presented. As a further enhancement to the scheme, BER performance improvement is achieved.

Index Terms

WCDMA, Iterative channel estimation, RAKE, Frequency domain equalization, Parallel interference cancellation.

I. Introduction

Channel estimation is a major issue for reliable transmission in communication systems. The system performance of WCDMA [1][2] with imperfect channel estimation has been widely studied in recent

years [3][7]. Usually, there are two types of pilots used in the downlink of WCDMA systems: time-multiplexed pilots [4] and code-multiplexed pilots [5]. The time-multiplexed pilots inevitably require extra bandwidth and hence reduce bandwidth efficiency. Inserting code-multiplexed pilots is an effective means to solve this problem by assigning a pilot signal an individual pseudorandom sequence [3]. This only consumes extra power on sending a known pilot sequence while no bandwidth spreading is necessary. The pilot channel is superimposed on the data channel and continuously transmitted through the same mobile propagation channel. In practice, the correlation method (CM) is a simple technique for channel estimation [3][6]. However, the distorted autocorrelation property due to channel impairments degrades its performance hence, a high power code-multiplexed pilot sequence is required for better channel estimates. Unfortunately, this introduces high MAI to the data channels. In this paper, it is demonstrated that with the new approaches, good performance can be achieved while only a small amount of power (10% the whole transmit power) is allocated to the pilot channel.

For the reception of the WCDMA downlink signal in a mobile receiver, the capability to perform multi-user detection in mobile handsets can require high complexity. The performance of conventional RAKE receivers is dominated by the MAI and this can result in a high error rate in a heavily loaded system. Performing equalization at the symbol-level requires the spreading sequences to be short to ensure cyclostationarity of the MAI. Receivers based on TDMA style channel equalization at the chip level have been proposed for WCDMA downlink to ensure adequate performance even with a high number of active users [12]. This has been shown to be a reasonable approach that achieves a good compromise between receiver complexity and system performance. The received chip waveform, distorted by the multi-path channel, is equalized prior to de-spreading. Orthogonality of the signals from the basestation is restored at chip level. In this paper, chip level frequency domain equalization (FDE) is considered. The computational complexity of the equalizer is reduced remarkably by frequency domain processing [9].

Recently, single carrier systems using frequency domain equalization have attracted increasing interest [9] [8]. Most of the systems use the same mechanism adopted in OFDM, i.e. a cyclic prefix (CP) is

inserted to simplify the receiver. The CP of sufficient length can effectively mitigate interference from the preceding block. It is because of the preceding CP that the channel distortion on the transmitted signal becomes a circular convolution process. Only in this case (or with zero-padding) can the distortion of the channel be considered as a multiplication in the frequency domain. Unfortunately, a CP-based FDE is not compatible with the current WCDMA system because the CP insertion will inevitably destroy the frame structure and it is incompatible with the standard. Thus, it is desirable to design a WCDMA receiver without changing the transmitted signal [10]. In this paper, it is demonstrated how cyclic reconstruction [11] can be combined with the iterative channel estimation and thus, frequency domain equalization of the downlink WCDMA signal is possible.

Performance of CDMA based systems is dominated by the amount of interference generated by the simultaneous presence of users. Parallel interference cancellation (PIC) appears as a simple interference suppression scheme, which subtract interference from users other than the desired one simultaneously without too much delay [14]. In this paper, PIC and channel estimation are combined in an iterative process to form a new scheme.

The rest of the paper is organized as follows. The system model of WCDMA systems and a RAKE receiver are introduced in Section II. In Section III, the proposed channel estimation algorithms, ICE and IFDCE are described. Section IV deals with the joint structures. Simulation results are given in Section V. Finally, the paper is concluded in Section VI.

II. WCDMA System with Code-Multiplexed Pilot Channel

In WCDMA systems, a code-multiplexed signal is continuously transmitted from each base station. It is broadcast over the entire cell and used as a phase reference for downlink channels. In this paper only the uncoded downlink scenario is considered: all signals are transmitted symbol and chip synchronously through the same mobile radio channel, perfect synchronization is assumed. Consider K-user's traffic that is QPSK modulated before spreading. The complex envelope of the transmitted signal due to the k-th user

is given as:

$$d_k(t) = \sqrt{E_k} \sum b_k^{(m)} s_k(t - mT), \tag{1}$$

where T denotes the symbol interval; E_k, $b_k^{(m)}$ and $s_k(t)$ denote the average power of the k-th user, the m-th symbol of the k-th user and the spreading chip waveform of the k-th user given by the convolution of spreading sequence and the chip waveform, respectively. The total average data channel power can be represented as $E_d = \sum_{k=1}^{K} E_k$.

After spreading, user data is summed together with the code-multiplexed pilot $p(t)$ which is used to provide phase reference information for data channels. Let E_p be the average power allocated to the pilot channel. The term "g" is used to denote the power ratio of the pilot channel to the whole signal power where $g = E_p/(E_d + E_p)$. The transmitted signal being scrambled by a long code $c(t)$ can be written as:

$$\begin{aligned} x(t) &= c(t)\Big[\sum_{k=1}^{K} d_k(t) + \sqrt{E_p} p(t)\Big] \\ &= c(t)\Big[\sum_{k=1}^{K} \sqrt{E_k} \sum b_k^{(m)} s_k(t - mT) + \sqrt{E_p} p(t)\Big]. \end{aligned} \tag{2}$$

The period of one chip is denoted by T_c. All signals that arrive at the receiver from the same basestation have passed through an identical complex channel. The complex FIR filter $h(\tau; t)$ with order L is a composite successive convolution of the transmitter filter, the mobile radio channel and the receiver filter. $h(\tau; t)$ is normally modeled as a wide-sense stationary uncorrelated scattering (WSSUS) zero-mean white Gaussian process as in [15]:

$$h(\tau; t) = \sum_{l=1}^{L} \alpha_l(t) e^{-j\phi_l(t)} \delta(\tau - \tau_l T_c) \tag{3}$$

where $\alpha_l(t)$, $\phi_l(t)$ and $\tau_l T_c$ are the attenuation factor, phase and the propagation delay of the l-th path, respectively. Each path is faded independently according to the Rayleigh distribution and the phase is uniformly distributed over the interval $[0, 2\pi]$.

In this paper, instead of estimating the exact channel parameters such as attenuation factors and phases,

only the in-phase and quadrature-phase components $Re[h_l(t)]$ and $Im[h_l(t)]$ are estimated as in [7]. These are two conceptually equal viewpoints on channel estimation. The definition of $h(\tau;t)$ can be rewritten as:

$$h(\tau;t) = \sum_{l=0}^{L-1} h_l(t)\delta(\tau - \tau_l T_c) \tag{4}$$

and further assume that $\sum_{l=0}^{L-1} E\left\{|h_l(t)|^2\right\} = 1$.

At the receiver, the received signal can be represented in an equivalent lowpass form as:

$$r(t) = \sum_{l=0}^{L-1} h_l(t)c(t-\tau_l T_c)\Big[\sum_{k=1}^{K}\sqrt{E_k}\sum b_k^{(m)}s_k(t-mT-\tau_l T_c) + \sqrt{E_p}p(t-\tau_l T_c)\Big] + v(t) \tag{5}$$

where $v(t)$ is the complex-valued lowpass equivalent AWGN with variance σ_n^2.

Let N be the spreading factor for both user data channels and the pilot channel, thus, the symbol duration T is N times the chip period or the sample interval T_c. The received signal in (5) can be represented in its discrete form:

$$\begin{aligned} r(mN+n) &= \sum_{l=0}^{L-1} h_l(mN+n)c(mN+n-\tau_l)\Big[\sum_{k=1}^{K}\sqrt{E_k}b_k^{(m)}s_k(n-\tau_l) + \sqrt{E_p}p(mN+n-\tau_l)\Big] \\ &+ v(mN+n) \end{aligned} \tag{6}$$

where $0 \le n \le N-1$. The sampled input signal to the l-th RAKE receiver finger is descrambled as:

$$r_l(mN+n) = h_l(mN+n)\Big[\sum_{k=1}^{K}\sqrt{E_k}b_k^{(m)}s_k(n) + \sqrt{E_p}p(mN+n)\Big] + \eta_l(mN+n) \tag{7}$$

In (7), $\eta_l(mN+n)$ accounts for a mixture of additive Gaussian noise, multipath interference and multiple access interference.

Using $\hat{h}_l(mN+n)$ to denote the channel estimates, the L resolved signals are multiplied by the complex conjugates of $\hat{h}_l(mN+n)$ and maximum ratio combined in the RAKE receiver. Consequently, the output

at the $mN+n$ sample interval can be represented as:

$$\tilde{x}(mN+n) = \sum_{l=0}^{L-1} r_l(mN+n)\hat{h}_l^*(mN+n) \tag{8}$$

Finally, despreading and demapping are performed on $\tilde{x}(mN+n)$ to recover the user data symbol.

III. Iterative Channel Estimation

Channel estimation plays an important role in the receiver especially for a RAKE receiver. The system performance strongly depends on the estimate of the channel impulse response. In this section, a popularly used conventional channel estimator is reviewed and then subsequently two new iterative approaches are proposed.

A. Correlation Method

The correlation method has been widely adopted in the design of RAKE receivers [3][6]. In [7], a symbol level estimator was detailed and is briefly reviewed here. Suppose that $s_p(n)$ is the spreading sequence assigned to the pilot channel, the pilot term $p(mN+n)$ in (7) can be rewritten as:

$$p(mN+n) = S_{pilot}s_p(n) \tag{9}$$

where S_{pilot} denotes the pilot symbol, usually all "1" or "$\frac{1+j}{\sqrt{2}}$". Using the orthogonal property of the spreading codes and assuming the pilot signature sequence is uncorrelated with the noise term $\eta_l(mN+n)$ in (7), if $S_{pilot}=1$, the m-th pilot symbol at the l-th finger $\hat{S}^m_{pilot,l}$ can be recovered as in [7]:

$$\hat{S}^m_{pilot,l} = \frac{1}{N}\sum_{n=0}^{N-1} r_l(mN+n)s_p(n) \tag{10}$$

if $S_{pilot}=\frac{1+j}{\sqrt{2}}$, then $\hat{S}^m_{pilot,l}$ will be detected as:

$$\hat{S}^m_{pilot,l} = \frac{1}{N}\sum_{n=0}^{N-1} r_l(mN+n)s_p(n)(\frac{1-j}{\sqrt{2}}) \tag{11}$$

From (7), the pilot symbol $\hat{S}^m_{pilot,l}$ can be expressed as:

$$\hat{S}^m_{pilot,l} = \sqrt{E_p}|S_{pilot}|^2 \cdot \frac{1}{N}\sum_{n=0}^{N-1}\hat{h}_l(mN+n) = \sqrt{E_p}|S_{pilot}|^2\hat{h}^m_l \tag{12}$$

Usually it is assumed that the channel is invariant within an M symbol observation window, i.e. $N_w = M \times N$ chips. Hence, applying an averaging filter, the channel estimate $\hat{h}_l$ for this observation period is:

$$\hat{h}_l = \sum_{m}^{m+M-1}\hat{h}^m_l = \frac{1}{\sqrt{E_p}|S_{pilot}|^2}\sum_{m}^{m+M-1}\hat{S}^m_{pilot,l} \tag{13}$$

The correlation method is simple, however, its estimation performance degrades due to the non-ideal autocorrelation properties and has significant influence on the BER performance of the system.

B. Iterative Channel Estimation Method

A novel iterative channel estimation for WCDMA systems, the iterative channel estimation (ICE) method, is presented in this section. The estimate $\hat{h}_l$ obtained by the correlation method is used as an initial channel estimate for the system. Consider an uncoded system with only hard detection, consequently, estimates of K users' transmitted symbols $\tilde{b}^{(m)}_k$ can be obtained by despreading as follows:

$$\tilde{b}^{(m)}_k = \frac{1}{N}\sum_{n=0}^{N-1}\tilde{x}(mN+n)s_k(n) \tag{14}$$

Hard detection is performed on $\tilde{b}^{(m)}_k$ and hence $\hat{b}^{(m)}_k$ is obtained. In a similar manner to a PIC scheme, the channel distorted waveforms of the k-th user are regenerated as:

$$\hat{r}_k(mN+n) = \sqrt{E_k}\sum_{l=0}^{L-1}\hat{h}_l(mN+n)c(mN+n-\tau_l) \times \hat{b}^{(m)}_k s_k(n-\tau_l) \tag{15}$$

Then, the reconstructed channel distorted waveforms of all the user channels other than the pilot channel are removed from the composite signal $r(mN+n)$ as follows:

$$\hat{r}(mN+n) = r(mN+n) - \sum_{k=1}^{K}\hat{r}_k(mN+n) \tag{16}$$

Hence, the good autocorrelation property of the pilot channel can be recovered given perfect channel estimates and correctly detected user symbols. Applying the correlation method on the signal $\hat{r}(mN+n)$, channel estimates are refined and system BER performance is enhanced.

In this paper, a different view from the chip level is given on the correlation method. Since user data is treated as an independent signal and the aggregation can be considered to be additive noise on the pilot channel, under the assumption that the pilot sequence is uncorrelated with the data channels and the additive Gaussian white noise, it follows that:

$$E\left\{\begin{bmatrix}\hat{r}(mN+n)\\ \vdots \\ \hat{r}(mN+n+L-1)\end{bmatrix} p^*(mN+n)c^*(mN+n)\right\} = \sqrt{E_p}|S_{pilot}|^2 \begin{bmatrix}\hat{h}_0^{ICE}\\ \vdots \\ \hat{h}_{L-1}^{ICE}\end{bmatrix} \tag{17}$$

where $\hat{h}_l^{ICE}$ is the new channel estimate. Thus, the complex channel coefficients can be determined up to a fixed scaling factor. The expectation operation is a useful means to combat both the AWGN and the MAI, which can be treated as additive noise. The correlation method in [7] and the method presented in (17) are essentially equal. An illustration of the process of ICE is shown in Figure 1.

C. Iterative Frequency Domain Channel Estimation and Chip Level Equalization

In the FDE, the received discrete-time chips are segmented into multiple blocks according to the equalizer length N_c. Assuming that the composite channel response $h_{i,l}$ is stationary within the i-th block and spans over L chips, the received signal in one block can be written as $r_i(n)$, $0 \leq n \leq N_c - 1$, where N_c is the number of chips within one block and $x_i(n)$ denotes the corresponding transmitted signal.

$$r_i(n) = \sum_{l=0}^{L-1} h_{i,l}x_i(n-l)u(n-l) + \left(\sum_{l=0}^{L-1} h_{i-1,l}x_{i-1}(n+N_c-l)(1-u(n-l))\right) + v_i(n) \tag{18}$$

where $u(n)$ represents the unit step function. The second term in (18) represents the inter block interference (IBI) term caused by the *(i-1)*-th block. The IBI is removed from the received signal by subtracting it based on the decision made in the previous block and the estimation of the channel impulse response.

This process is called tail cancellation [13].

$$\bar{r}_i(n) = r_i(n) - \sum_{l=0}^{L-1} \hat{h}_{i-1,l}\hat{x}_{i-1}(n + N_c - l)(1 - u(n - l)) \tag{19}$$

where $\hat{x}_i(n)$ denotes the estimated composite signal. As has been stated previously, time-domain circular convolution is equivalent to frequency-domain multiplication, and vice versa. By the insertion of the CP in OFDM systems, linear channel distortion of the signal results in circular convolution of the transmitted signal and the channel impulse response. With this in mind, it is necessary to reconstruct the resultant effect caused by a virtual CP so that the time and frequency-domain descriptions of the convolution are essentially equivalent. The required circularity is reconstructed as shown in below:

$$\tilde{r}_i(n) = \bar{r}_i(n) + \sum_{l=0}^{L-1} \hat{h}_{i,l}\hat{x}_i(n + N_c - l)(1 - u(n - l)) \tag{20}$$

The process of adding the second term in (20) is called cyclic reconstruction. The linear convolution now becomes a circular convolution in the time domain. Thus, in the frequency domain,

$$\tilde{R}_i(w) \approx H_i(w)\hat{X}_i(w) + V_i(w) \tag{21}$$

where $0 \leq w \leq N_c - 1$, $\tilde{R}_i(w)$, $H_i(w)$, $\hat{X}_i(w)$ and $V_i(w)$ are the FFT of $\tilde{r}_i(n)$, $h_{i,l}$, $\hat{x}_i(n)$ and $v_i(n)$, respectively.

The idea of the IFDCE is that initially a channel estimate $\hat{\mathbf{h}}_i = [\hat{h}_{i,0}, \cdots, \hat{h}_{i,L-1}]$ is made based on the parallel pilot channel and then refined by using both pilots and reconstructed user symbols. Once the RAKE receiver outputs the estimates of users' symbols, they are respread, rescrambled and summed with the code-multiplexed pilots as virtual pilots, which then enhances the estimation performance. The estimated user symbols $\hat{b}_{i,k}^{(m)}$ are used together with code-multiplexed pilots to generate virtual pilots for channel estimation; Let $\mathbf{s}_k = [s_k(0), \cdots, s_k(N-1)]$ be the spreading code vector for user k and $\mathbf{p}_0, ..., \mathbf{p}_{N_c/N-1}$ be the pilot symbols. There are N_c/N data symbols in one block, the regenerated transmitted signal can

be expressed by:

$$\hat{\mathbf{x}}_i = diag\{c_i(0), \cdots, c_i(N_c-1)\} \times \left[\sum_{k=1}^{K} \sqrt{E_k}\hat{b}_{i,k}^{(0)}\mathbf{s}_k + \sqrt{E_p}\mathbf{p}_0, \cdots, \sum_{k=1}^{K} \sqrt{E_k}\hat{b}_{i,k}^{(N_c/N-1)}\mathbf{s}_k + \sqrt{E_p}\mathbf{p}_{N_c/N-1}\right]^T \tag{22}$$

where $\{c_i(0), \cdots, c_i(N_c-1)\}$ represents the scrambling code for the i-th block. Similar to the frequency domain equalization, given (21), the channel estimated by the frequency domain estimator can be expressed as:

$$\hat{h}_{i,l}^{IFDCE} = \frac{1}{N_c} \cdot \sum_{w=0}^{N_c-1} \frac{\hat{X}_i^*(w) \cdot \tilde{R}_i(w)}{|\hat{X}_i(w)|^2 + \sigma_n^2} e^{j2\pi lw/N_c} \tag{23}$$

The modified received signal $\tilde{r}_i(n)$ is then equalized in the frequency domain at chip level. The minimum mean square error (MMSE) equalizer $W_i(w)$ in the frequency domain is given by the following expression [9]:

$$W_i(w) = \frac{\hat{H}_i^{IFDCE*}(w)}{|\hat{H}_i^{IFDCE}(w)|^2 + \sigma_n^2/\sigma_d^2} \tag{24}$$

σ_n^2, σ_d^2 and $\hat{H}_i^{IFDCE}(w)$ are the variance of the additive white Gaussian noise, the variance of the transmitted signal and the FFT of $\hat{h}_{i,l}^{IFDCE}$, respectively. Consequently, the equalized signal is converted back to the time domain as:

$$\hat{x}_i(n) = \frac{1}{N_c} \cdot \sum_{w=0}^{N_c-1} W_i(w)\tilde{R}_i(w)e^{j2\pi nw/N_c} \tag{25}$$

after which, descrambling, despreading and demapping are performed.

The whole process is summarized as follows:

Step 1. Correlation method is used to deliver initial channel estimates $\hat{\boldsymbol{h}}_i$.

Step 2. A RAKE receiver then operates on the received signal and the composite estimated signal $\tilde{x}_i(n)$ *is despread and hard detected.*

Step 3. K users' transmitted symbols $\hat{b}_{i,k}^{(m)}$ are respread and rescrambled. The scrambled code-multiplexed pilots are added to form an estimated composite signal $\hat{x}_i(n)$.

Step 4. $\hat{x}_i(n)$ and the initial channel estimates $\hat{\boldsymbol{h}}_i$ are used for cyclic reconstruction as in (20).

Step 5. $\hat{x}_i(n)$ is converted to $\hat{X}_i(w)$ in the frequency domain and used for channel estimation together with the received frequency domain signal $\tilde{R}_i(w)$. In the estimator, the reconstructed composite signal $\hat{X}_i(w)$ is treated as a virtual pilot signal. A refined channel estimate can be obtained in the frequency domain as: $\hat{H}_i^{IFDCE}(w) = \frac{\tilde{R}_i(w)\cdot\hat{X}_i^*(w)}{|\hat{X}_i(w)|^2+\sigma_n^2}$

Step 6. The result from Step 5 is converted to the time domain and only the first L values are kept to form the channel estimate $\hat{\boldsymbol{h}}_i^{IFDCE} = [\hat{h}_{i,0}^{IFDCE}, \cdots, \hat{h}_{i,L-1}^{IFDCE}]$.

Step 7. $\hat{\boldsymbol{h}}_i^{IFDCE}$ is used for equalization.

An illustration of the steps involved in the process of IFDCE is shown in Figure 2.

IV. Joint Channel Estimation, Chip Level Frequency Domain Equalization and Parallel Interference Cancellation

Multiple access interference cancellation can be achieved by using a PIC stage. The PIC cancels the MAI estimated with the hard decisions made previously. Since the proposed new channel estimator has a similar structure to a parallel interference canceller, the two can easily be integrated together so that the system BER performance can be further improved with only a slight increase in computation complexity.

A. Joint ICE and PIC

After performing the ICE, interference from the interfering $K-1$ users and the parallel pilot channel is regenerated given the new channel estimates $\hat{h}_l^{ICE}$. Let the u-th user be the desired user and the composite signal excluding the u-th user's information can be regenerated as:

$$\check{r}(mN+n) = \sum_{l=0}^{L-1} \hat{h}_l^{ICE}(mN+n)c(mN+n-\tau_l) \times \Big[\sum_{k=1,k\neq u}^{K} \sqrt{E_k}\hat{b}_k^{(m)} s_k(n-\tau_l) + \sqrt{E_p}p(mN+n-\tau_l) \Big] \quad (26)$$

Subsequently, $\check{r}(mN+n)$ is subtracted from the received signal $r(mN+n)$ as:

$$\dot{r}(mN+n) = r(mN+n) - \check{r}(mN+n) \quad (27)$$

A RAKE receiver is then applied to the MAI cleared signal and the output is despread and hard-decision detected. Compared with a conventional PIC scheme, the new joint structure requires extra computations mainly associated with another correlation process and for interference regeneration. It is known that PIC is quite sensitive to channel estimation errors and with a bad initial channel estimate, the PIC would increase the amount of interference rather than cancel it. Adopting the new joint channel estimation and PIC structure, better channel estimates can be obtained. With a slight increase in computational complexity, the improvement in system performance that can be achieved is significant.

B. Joint IFDCE and PIC

In a similar manner to the process for ICE discussed earlier, the IFDCE and the PIC can be jointly combined to enhance system performance. Initially, hard decisions on the user's transmitted symbols $\hat{b}_{i,k}^{(m)}$ are made on the output from the RAKE receiver.

After performing the IFDCE, $\hat{\mathbf{h}}_i^{IFDCE} = [\hat{h}_{i,0}^{IFDCE}, \cdots, \hat{h}_{i,L-1}^{IFDCE}]$ with its frequency domain counterpart $[\hat{H}_i^{IFDCE}(0), \cdots, \hat{H}_i^{IFDCE}(N_c-1)]$ are used for system equalization and interference cancellation. Let the u-th user be the desired user and the estimated composite signal excluding the u-th user's information can be regenerated as:

$$\check{\mathbf{x}}_i = \hat{\mathbf{x}}_i - \hat{\mathbf{x}}_{i,u} = diag\{c_i(0), \cdots, c_i(N_c-1)\} \times \left[\sum_{k=1,k\neq u}^{K} \sqrt{E_k}\hat{b}_{i,k}^{(0)}\mathbf{s}_k + \sqrt{E_p}\mathbf{p}_0, \cdots, \sum_{k=1,k\neq u}^{K} \sqrt{E_k}\hat{b}_{i,k}^{(N_c/N-1)}\mathbf{s}_k + \sqrt{E_p}\mathbf{p}_{N_c/N-1} \right]^T \quad (28)$$

where $\hat{\mathbf{x}}_{i,u}$ denotes the u-th user's transmitted signal within the i-th block. Define the N_c by N_c circular channel matrix as:

$$\mathbf{H}_i^{IFDCE} = \begin{bmatrix} h_{i,0}^{IFDCE} & & & & & & \mathbf{H}_{i,upper}^{IFDCE} \\ \vdots & h_{i,0}^{IFDCE} & & & & & \\ \vdots & \vdots & \ddots & & & & \\ h_{i,L-1}^{IFDCE} & \vdots & \vdots & h_{i,0}^{IFDCE} & & & \\ & h_{i,L-1}^{IFDCE} & \vdots & \vdots & h_{i,0}^{IFDCE} & & \\ & & \ddots & \vdots & \vdots & \ddots & \\ \mathbf{0} & & & h_{i,L-1}^{IFDCE} & h_{i,L-2}^{IFDCE} & \cdots & h_{i,0}^{IFDCE} \end{bmatrix} \quad (29)$$

where $\mathbf{H}_{i,upper}^{IFDCE} = \begin{bmatrix} h_{i,L-1}^{IFDCE} & \cdots & h_{i,1}^{IFDCE} \\ & \ddots & \vdots \\ & & h_{i,L-1}^{IFDCE} \end{bmatrix}$. Hence, parallel interference cancellation can be performed as follows:

$$\dot{\mathbf{r}}_i = \left(\mathbf{r}_i + \mathbf{H}_{i,upper}^{IFDCE}\check{\mathbf{x}}_{i,L-1}\right) - \hat{\mathbf{H}}_i^{IFDCE}\check{\mathbf{x}}_i \quad (30)$$

where $\check{\mathbf{x}}_{i,L-1}$ consists of the last $L-1$ elements of $\check{\mathbf{x}}_i$. Since $\mathbf{H}_i^{IFDCE}$ is a circular matrix, it can be efficiently diagonalized by the use of the FFT and IFFT. Hence, the PIC can be easily performed in the frequency domain, after which FDE is applied.

Figure 3 shows how to combine the iterative channel estimation and PIC within one structure.

In the iteration cycle, K users' signals are regenerated and summed with the pilot channel for the purpose of channel estimation. Meanwhile, interference from the interfering *K-1* users and the parallel

pilot channel are constructed and subtracted from the received composite signal, hence, interference can be reduced through the iteration. For simplicity, only a single stage PIC is considered. The ICE/IFDCE and the PIC can be combined in one iteration, therefore the joint structure, both ICE+PIC and IFDCE+PIC cause comparable computational complexity as a conventional PIC.

V. Simulation Results

Computer simulations are carried out at baseband. The chip rate is 3.84 Mchips/s. Walsh codes are used as channelization codes and a 38400 Gold code segment is used as the scrambling code. One pilot channel is code-multiplexed with dedicated data channels. 10% of the whole power is allocated to the pilot channel and the carrier frequency is 2 GHz. The UMTS Vehicular A channel model [16] is used for BER evaluation in our simulation. Each path is faded independently according to a Rayleigh distribution. The corresponding channel profile is shown in Table I.

TABLE I
Channel profile of the UMTS Vehicular Channel A

Path Delay (nsec)	Avg. Power (dB)
0	0
310	-1.0
710	-9.0
1090	-10.0
1730	-15.0
2510	-20.0

Test Case 1 (Performance of the correlation method and the ICE): Figure 4(a) shows the numerical results of system performances when the mobile terminal is moving at different speed. 10 active users are simulated with a spreading factor of 64 and the SNR per bit is fixed at 10 dB. Imperfect channel estimation is considered (channel is estimated based on the pilot channel). Both the correlation method and the ICE approach are evaluated. It can be seen from Figure 4(a) that $N_w = 1024$ is a suitable window size for both estimators. It achieves a good BER performance compared with a smaller window size and

keeps the performance more stable than choosing a larger window size. It can also be seen from the figure that the ICE approach outperforms the conventional correlation method.

Figure 4(b) demonstrates the performance of the two estimators with different numbers of active users. The mobile terminal is assumed moving at a speed of 30 km/h. At a required target BER of 2×10^{-2}, using the new method can support 5 more users than the conventional one with a fixed window size $N_w = 1024$.

Test Case 2 (Achieved MSE of the correlation method, ICE and the IFDCE): To evaluate the estimator performance, compute the Mean Square Error (MSE) for both the correlation method and the new iterative procedures:

$$MSE(\hat{\mathbf{h}}_i) = E\left\{\sum_{l=0}^{L-1} |h_{i,l} - \hat{h}_{i,l}|^2\right\} \tag{31}$$

In Figure 5(a) and Figure 5(b), it is shown that the MSE curves of channel estimation versus SNR per bit with varying pilot power, i.e. g=10%, 20% and 40%. The mobile terminal is assumed to be traveling at a speed of 30 km/h and 150 km/h. From the simulation results presented, it follows that by using the correlation method, the higher the pilot power is, the better the channel estimates. In other words, if the value of 'g' is large, the channel estimation quality is good. However, this will lead to a large MAI with large error probability. Observe that in both scenarios the new iterative schemes, ICE and IFDCE, can effectively reduce channel estimation errors in comparison with the correlation method. With $g = 10\%$, the IFDCE algorithm outperforms the CM with $g = 40\%$ at E_b/N_0 of 10dB. Notice that with only a small amount of power allocated to the pilots, good performance can still be achieved via this structure. This is important for practical systems since usually only around 10% power can be allocated to the pilot channel, for example, g=10% in HSDPA [17]. Transmitting a small portion of power on the pilot makes the system power efficient and since parallel code-multiplexed pilots are used, bandwidth efficiency can be maintained.

Test Case 3 (Performance comparison of the correlation method, the ICE and the IFDCE): From

Figure 6(a), it is noted that for the IFDCE, $N_w = 1024$ is also a suitable window length in terms of BER performance. IFDCE and chip level FDE contribute to the large BER difference in both Figure 6(a) and Figure 6(b). In addition, Figure 6(b) shows that the BER performance achieved by the ICE+RAKE and the IFDCE+FDE schemes, as shown in Figure 6(a), does not vary significantly with changing mobile speed.

Test Case 4 (Performance comparison among the joint estimation and PIC structures): Now the effect of the PIC in the three schemes is considered. The other user interference as well as interference from pilot channel has considerable impact on multiuser system performance. Not surprisingly, the IFDCE+FDE+PIC scheme performs the best within the three as can be shown in Figure 7(a). Since the PIC is very sensitive to channel estimation errors, the iterative estimation scheme offers good channel estimates and hence improvements in system performance. The proposed joint scheme consistently outperforms the other three and achieves good BER performance. As the number of users increases, the gap between the IFDCE+FDE and the joint IFDCE+FDE+PIC reduces. As depicted in Figure 7(b), when the number of active users is low, we can see the enhancement in performance offered by this joint structure. Nonetheless, with increasing number of users, the performances tend towards the same due to poor channel estimation. This is because the initial channel estimates obtained by the correlation method fail to provide good accuracy and hence the PIC and the imperfect cyclic reconstruction introduce more interference.

Test Case 5 (BER Performance comparison between the estimation approaches and the joint estimation and PIC structures): Finally, the BER performance versus SNR per bit is examined. In Figure 8(a), the BER performance of different detectors with a mobile speed 30 km/h is presented. The RAKE performance is dominated by the MAI and this results in saturation at a high error rate. The gain of IFDCE+FDE and ICE+RAKE over CM+RAKE is about 2dB and 4dB at a BER of 10^{-2}, respectively. The BER performance with a 64 tap chip level MMSE time domain equalizer (MMSE-TDE) [12] and perfect channel estimation is also simulated as a reference. It is apparent that the proposed IFDCE+FDE achieves performance close to the MMSE-TDE with perfect channel estimation.

Figure 8(b) demonstrates the system improvements with PIC. The joint IFDCE+FDE+PIC method achieves only a 1dB lost at the BER of 10^{-2} compared to the MMSE-TDE in a single user scenario with perfect channel estimation.

VI. Conclusion

This paper deals with channel estimation and parallel interference cancellation for WCDMA systems. The new channel estimators, ICE and IFDCE, while different from each other, have the same basic underlying idea. For ICE, the received waveforms for each user are reconstructed and subtracted from the received signal hence the channel estimation accuracy is improved via another correlation process. For IFDCE, the sum of data channels and the pilot channel is reconstructed and is treated as a new compound pilot. With the reconstructed virtual pilot and the received signal, new channel estimates can be computed. Simulation results verify the effectiveness of the new schemes with only 10% transmitted power allocated to the code-multiplexed pilot channel. Therefore it is compatible with systems like HSDPA where only a small amount of power is transmitted through the pilot channel. In addition, chip level FDE and parallel interference cancellation are introduced into the iterative estimation structure; interference is reduced prior to despreading and system performance is significantly improved. The iterative cycle can be implemented efficiently in the frequency domain with the overall complexity of $O(N_c log N_c)$, which is much simpler compared to the multiuser detection and the MMSE-TDE which involves matrix inversion. Furthermore, the complexity of the MMSE-FDE does not change significantly with the length of the channel impulse response.

VII. Acknowledgment

The work reported in this paper has formed part of the Research Programme of the Virtual Centre of Excellence in Mobile and Personal Communications, Mobile VCE, www.mobilevce.com, whose funding support, including that of EPSRC, is gratefully acknowledged. Fully detailed technical reports on this research are available to Industrial Members of Mobile VCE.

REFERENCES

[1] H. Holma and A. Toskala, *WCDMA for UMTS*, Wiley Publishing House, 2001

[2] E. Dahlman, *et al*, "WCDMA-The radio interface for future mobile multimedia communications", IEEE Transactions on Vehicular Technology, Vol. 47, No. 4, 1998, pp.1105-1118.

[3] A. Viterbi, *CDMA Principles of Spred Spectrum Communication*, Addison-Wesley Wireless Communications Series, 1995.

[4] P. Schramm and R. Müller, "Pilot symbol assisted BPSK on Rayleigh fading channels with diversity: performance analysis and parameter optimization", IEEE Transactions on Communications, Vol 46, No. 12, 1998, pp. 1560-1563.

[5] P. Schramm, "Analysis and optimisation of pilot-channel-assisted BPSK for DS-CDMA systems", IEEE Transactions on Communications, Vol 46, No. 9, 1998, pp. 1122-1124.

[6] N. Benvenuto, *et al*, "Performance comparison of chip matched filter and RAKE receiver for WCDMA systems", GLOBECOM 2001, pp. 3060-3064.

[7] S. Ko and H. Choi, "Performance analysis of channel estimators for forward link W-CDMA under multipath rayleigh fading channels", IEICE Transactions on Communications, Vol. E86-B, No. 4, 2003, pp. 1212-1223.

[8] M. Clark, "Adaptive frequency-domain equalization and diversity combining for broadband wireless communications", IEEE Journal on Select Areas in Communications, Vol. 16, No. 8, 1998, pp. 1385-1395.

[9] D. Falconser, S. Ariyabistakul, A. Benyamin-Seeyar and B. Eidson, "Frequency domain equalization for single-carrier broadband wireless systems", IEEE Communications Magazine, No. 4, 2002, pp. 58-66.

[10] Y. Li, S. McLaughlin and D. G. M. Cruickshank, "UMTS FDD Frequency Domain Equalization Based on Self Cyclic Reconstruction", IEEE International Conference on Communications, 16-20 May 2005, Vol.3, pp. 2122-2126.

[11] D. Kim and G. Stüber, "Residual ISI Cancellation for OFDM with Applications to HDTV Broadcasting", IEEE Journal on Select Areas in Communications, Vol. 16, No. 8, 1998, pp. 1590-1599.

[12] K. Hooli, M. Juntti, M. Heikkila, P. Komulainen, M. Latva-aho and J. Lilleberg, "Chip-level channel equalization in WCDMA downlink", EURASIP Journal on Applied Signal Processing, Vol. 8, 2002, pp. 757-770.

[13] J. Cioffi and J. Bingham, "A data-driven multitone echo canceller", IEEE Transactions on Communications, Vol. 42, No. 10, 1994, pp. 2853-2869.

[14] D. Koulakiotis and A. Aghvami, "Data detection techniques for DS/CDMA mobile systems: a review", IEEE Personal Communications, No. 6, 2000, pp. 24-34

[15] J. Proakis, *Digital Communications*, 3rd Edition, New York: McGraw-Hill, 1995

[16] ETSI TR 101 112 V3.2.0 (1998-04): Universal Mobile Telecommunications System (UMTS); Selection procedures for the choice of radio transmission technologies of the UMTS.

[17] M. Harteneck and C. Luschi, "Practical implementation aspects of MMSE equalisation in a 3GPP HSDPA terminal", Proceedings of the 59th IEEE Vehicular Technology Conference, May, 2004, pp. 445-449

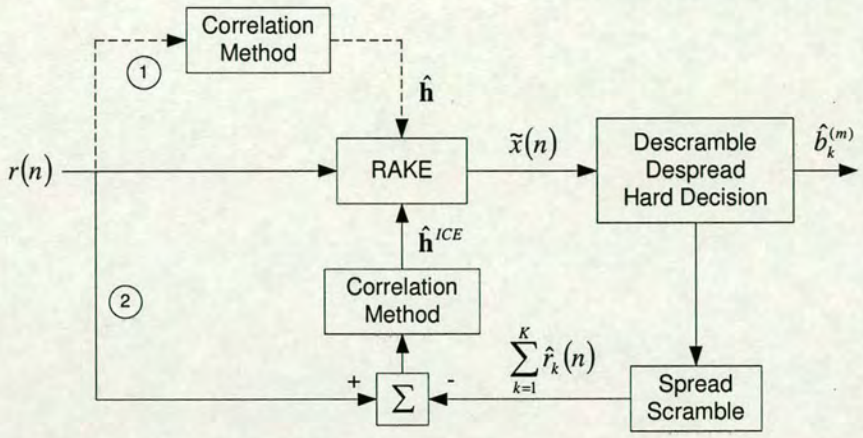

Fig. 1. Iterative channel estimation for WCDMA, RAKE receiver

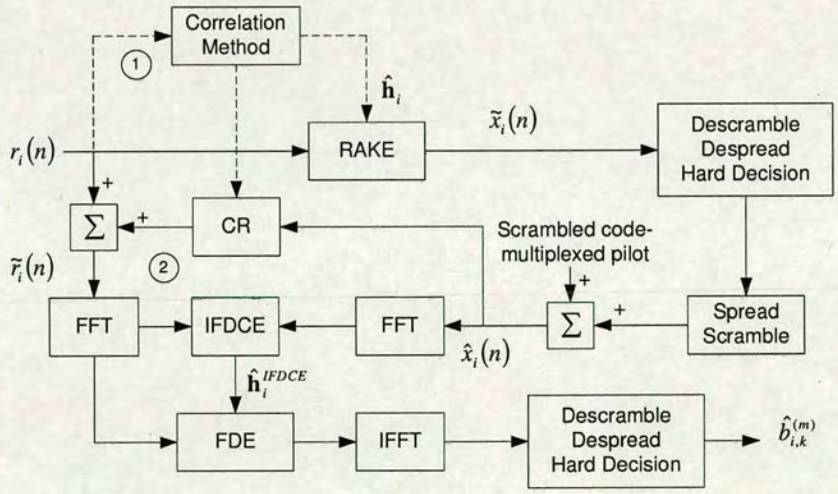

Fig. 2. Iterative frequency domain channel estimation and chip level equalization for WCDMA; CR: cyclic reconstruction

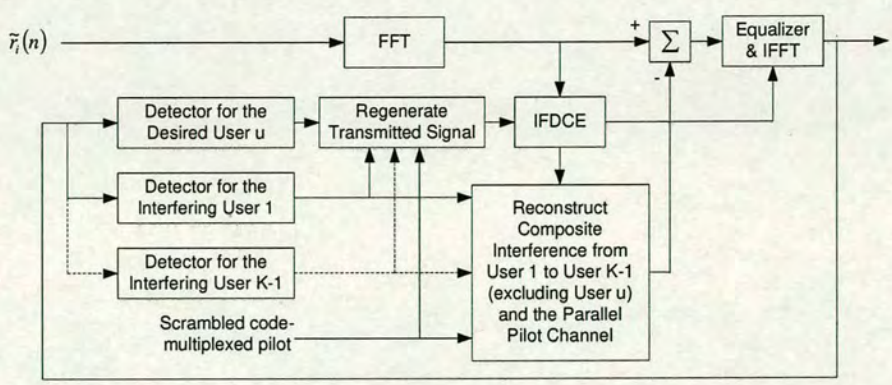

Fig. 3. Combined channel estimation, chip level frequency domain equalization and parallel interference cancellation structure

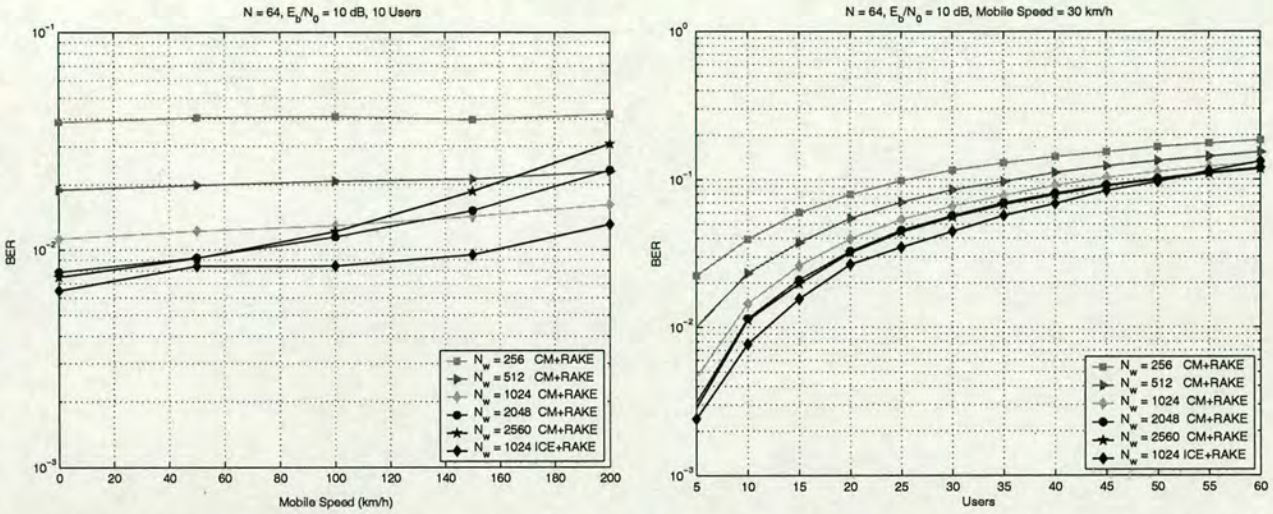

(a) System BER performance versus Varying mobile speed, N = 64, 10 Active users, E_b/N_0 = 10 dB

(b) System BER performance versus Different number of users, N = 64, E_b/N_0 = 10 dB, Mobile Speed = 30 km/h

Fig. 4. Simulation Results for Test Case 1

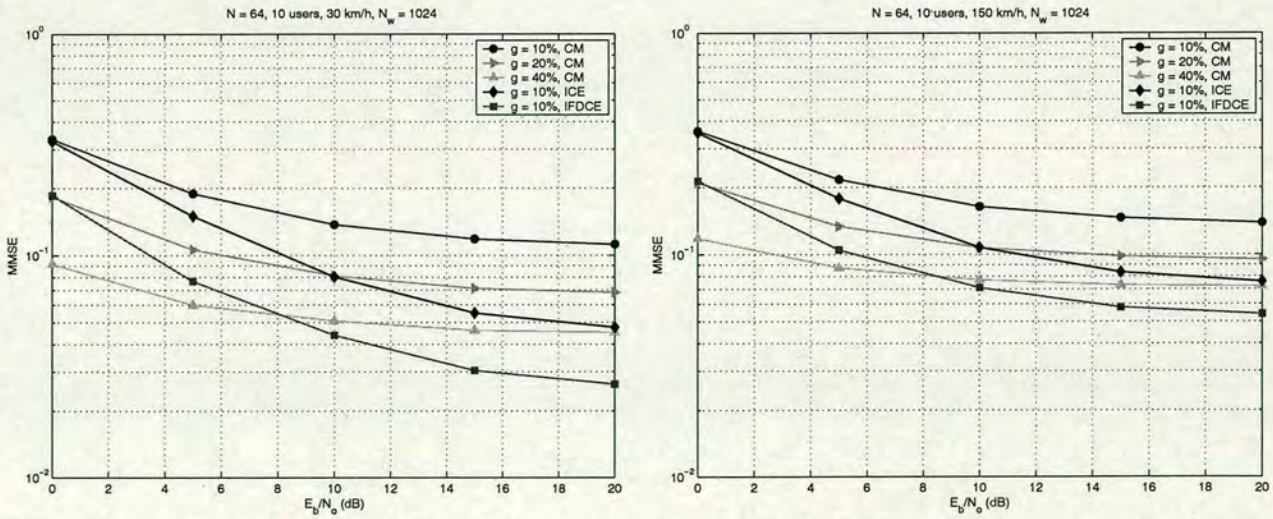

(a) Achieved MSE versus $Eb/N0$, N = 64, 10 Active users, N_w = 1024, Mobile Speed = 30 km/h

(b) Achieved MSE versus $Eb/N0$, N = 64, 10 Active users, N_w = 1024, Mobile Speed = 150 km/h

Fig. 5. Simulation Results for Test Case 2

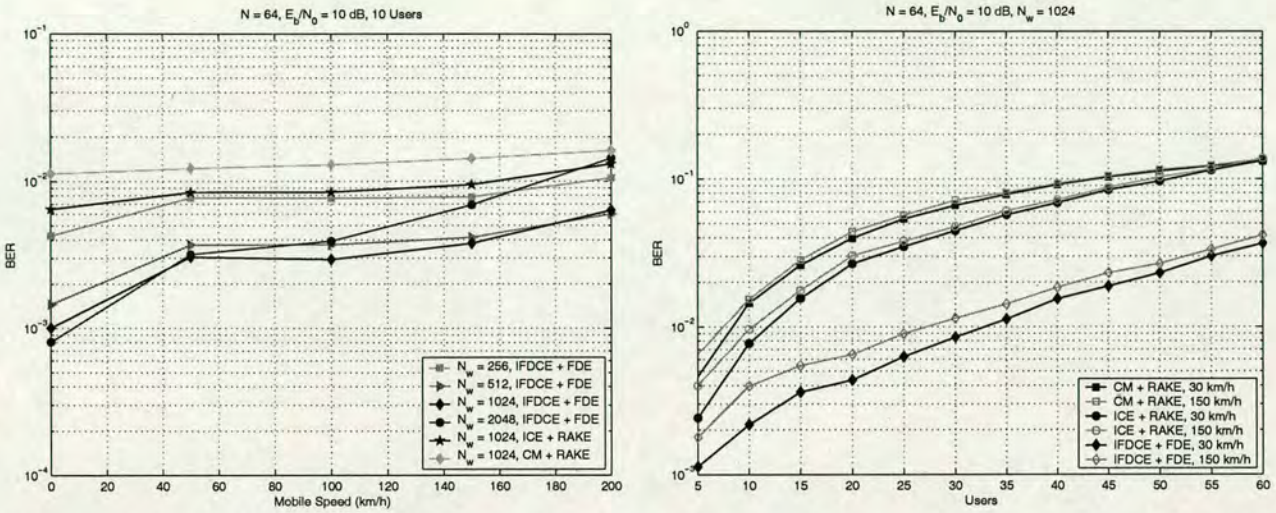

(a) System BER performance versus Varying mobile speed, N = 64, 10 Active users, E_b/N_0 = 10 dB

(b) System BER performance versus Different number of users, N = 64, E_b/N_0 = 10 dB, N_w = 1024

Fig. 6. Simulation Results for Test Case 3

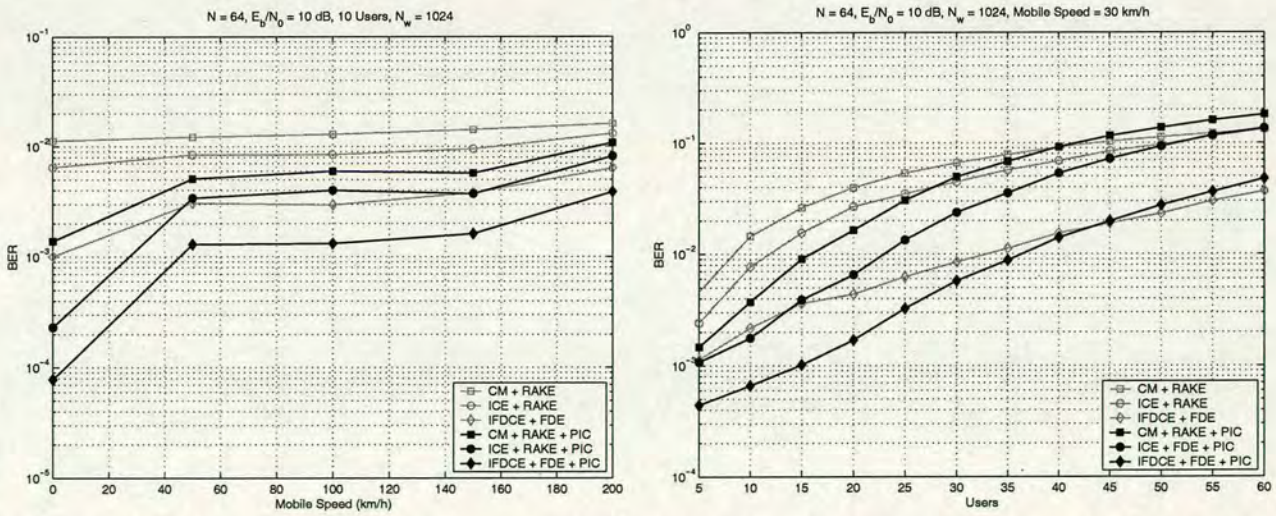

(a) System BER performance versus Varying mobile speed, N = 64, 10 Active users, E_b/N_0 = 10 dB

(b) System BER performance versus Different number of users, N = 64, E_b/N_0 = 10 dB, N_w = 1024, Mobile Speed = 30 km/h

Fig. 7. Simulation Results for Test Case 4

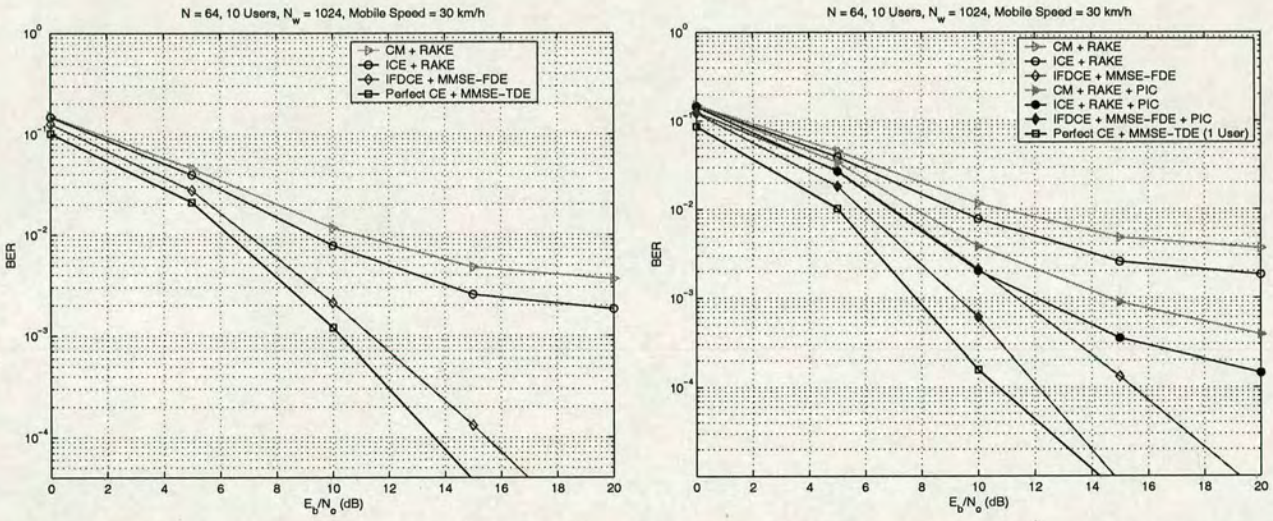

(a) System BER performance versus E_b/N_0, N = 64, 10 Active Users, $N_w = 1024$, Mobile Speed = 30 km/h

(b) System BER performance versus E_b/N_0, N = 64, 10 Active Users, $N_w = 1024$, Mobile Speed = 30 km/h

Fig. 8. Simulation Results for Test Case 5

Channel Estimation and Interference Cancellation in CP-CDMA Systems

Yushan Li, Steve McLaughlin, David G. M. Cruickshank

Institute for Digital Communications, School of Engineering and Electronics

University of Edinburgh, Edinburgh EH9 3JL, UK

Email: Yushan.Li@ee.ed.ac.uk

Abstract

In this paper, a novel iterative channel estimation approach is proposed for Cyclic Prefix – CDMA (CP-CDMA) systems. Code-multiplexed pilots are used for channel estimation while maintaining bandwidth efficiency. The proposed method achieves a significant improvement when compared to the conventional correlation approach by reconstructing data signals for channel estimation. Simulation results demonstrate good estimation capability with an allocation of only 10% of the whole power to the pilot channel. In addition, this paper proposes an integrated channel estimator and parallel interference cancellation (PIC) detector. Data signals are reconstructed for channel estimation while the interference contributed by different data channels as well as the pilot channel are regenerated and subtracted from the received signal at the final stage. The channel estimation error reduces at each iteration and the PIC at the last stage enable further BER performance improvement to be achieved for the system. The performance of the proposed scheme is studied through simulations and results verify its effectiveness.

Keywords: *CP-CDMA, Channel estimation, PIC, BER performance.*

I. Introduction

Orthogonal Frequency Division Multiplexing (OFDM) has emerged as an efficient transmission scheme that is capable of combating inter-symbol-interference (ISI) and providing high data rates as well as high capacity [1]. It is a strong candidate for the next generation of mobile communication systems. There has been significant research activity investigating the use of OFDM in multiuser systems. For example, in [2], multicarrier code-division multiple access (MC-CDMA), multicarrier direct sequence CDMA (MC-DS-CDMA) and multitone CDMA (MT-CDMA) are discussed. However, although the advantages of OFDM are obvious, there are two major inherent difficulties regarding OFDM: OFDM is highly sensitive to frequency offset and phase noise and OFDM exhibits a high instantaneous peak-to-mean power ratio that will decrease the power efficiency of the RF amplifier [1].

Numerous approaches for single-carrier systems with frequency domain equalisation (SC-FDE) have been proposed [3][4]. Most of these use the same mechanism as OFDM, i.e. a cyclic prefix (CP) or a unique word (UW) is inserted to mitigate the multi-path effect and to simplify the receiver. Recently, the cyclic prefix concept from OFDM was introduced into the conventional DS-CDMA system to enhance current single carrier 3G communications system performance in the near future [5][6][7].

The performance of the conventional RAKE receiver is dominated by multiple access interference (MAI) and with a 50% traffic loading this results in saturation at a fairly high error rate. Multiuser detection (MUD) has raised considerable research interest during the past decade; however, the possibility of performing multiuser detection in mobile handsets is limited due to its high complexity. Recently, receivers based on TDMA style channel equalisation at the chip level have been proposed for a wideband CDMA (WCDMA) downlink to ensure adequate performance even with a high number of active users [8]. The received chip waveform, distorted by the multi-path channel, is equalised prior to de-spreading. Orthogonality of the signals from

the basestation is restored at chip-level. A CP-CDMA system has the advantage of a simple equalisation structure due to the inserted CP, hence, chip-level equalisation is even more attractive for such a system. Recent research work reveals that a CP-CDMA system can achieve comparable system performance to MC-CDMA [18].

Channel estimation is a major issue for reliable transmission, usually, there are two types of pilots used in the downlink of DS-CDMA systems: time-multiplexed pilots [9] and code-multiplexed pilots [10]. In this paper, only code-multiplexed pilots for channel estimation are considered in a CP-CDMA system. The pilot channel is superimposed on the data channel and continuously transmitted through the same mobile propagation channel. In [5] and [6], the unique words are used as a CP and pilot symbols for the CP-CDMA systems. In practice, the correlation method (CM) is a simple technique for channel estimation [11]. However, the distortion of the autocorrelation function due to impairments introduced by the multi-path nature of the channel will degrade its performance. In addition, a high power code-multiplexed pilot sequence is required for better channel estimates. Unfortunately, high power pilots introduce high MAI to the data channels. In this paper, inserting a code-multiplexed pilot channel for the system is considered and it is demonstrated that the approach suggested offers good performance which can be achieved while only a small amount of power (10%-20% the whole transmit power) is allocated to the pilot channel. In GSM [19] and UMTS-TDD [20], cyclic patterns (midambles) are inserted for channel estimation purposes. These cyclic patterns can be considered as virtual CPs in the system, however, the block for equalisation is too large so that the channel within the block will change significantly when the terminal is moving at a high speed. In other words, the system performance will drop while using such a frequency domain equaliser and there is no easy way to subdivide one large block into smaller blocks. In this paper, we simply consider a general case, a CP-CDMA system as in [5][6][18].

The performance of CDMA based systems is dominated by the amount of interference generated by the simultaneous presence of users. The PIC is a simple interference suppression scheme, which subtracts interference from users other than the desired one simultaneously without significant delay [12]. Enhanced PIC schemes, such as a multistage PIC [13], a Selective PIC (S-PIC) [14], etc. have been proposed to further improve the system performance. In this paper, PIC and channel estimation are combined in an iterative process to form a new scheme. Data signals are reconstructed for channel estimation at each stage while the interference contributed by different data channel as well as the pilot channel are regenerated and subtracted from the received signal only at the final stage. The channel estimation error diminishes by iterating a sufficient number of times and the use of the PIC at the final stage enables further BER performance improvement to be achieved.

The rest of the paper is organized as follows. The system model of the CP-CDMA system considered here is introduced in Section II. In Section III, the proposed channel estimation algorithm is described, followed by a description of the receiver structure. Section IV deals with the joint channel estimation and PIC structure. Simulation results are presented in Section V and further improvements proposed in Section VI and finally, conclusions are drawn.

II. CP-CDMA System Model and Chip-level Equalisation

In this work only the downlink scenario is considered: all signals are transmitted synchronously through the same mobile radio channel. Consider K-user's traffic that is QPSK modulated before spreading. The complex envelope of the transmitted signal due to the k-th user can be written as:

$$d_k(t) = \sqrt{E_k} \sum b_k^{(j)} s_k(t - jT), \tag{1}$$

where T denotes the symbol interval; E_k, $b_k^{(j)}$ and $s_k(t)$ denote the average power of the k-th user, the j-th symbol of the k-th user and the spreading chip waveform of the k-th user given by the

convolution of spreading sequence and the chip waveform, respectively. The total average data channel power can be represented as $E_d = \sum_{k=1}^{K} E_k$.

After spreading, the user data is summed together with the code-multiplexed pilot *p(t)* which is used to provide phase reference information for data channels. Let E_p be the average power allocated to the pilot channel. The term "g" is used to denote the power ratio of the pilot channel to the whole signal power where $g = E_p/(E_d + E_p)$, and the transmitted signal is scrambled by a long code *c(t)* which can be written as:

$$\begin{aligned} x(t) &= c(t)\left[\sum_{k=1}^{K} d_k(t) + \sqrt{E_p}\, p(t)\right] \\ &= c(t)\left[\sum_{k=1}^{K} \sqrt{E_k} \sum b_k^{(j)} s_k(t - jT) + \sqrt{E_p}\, p(t)\right]. \end{aligned} \tag{2}$$

The scrambled signal is split into successive data blocks with N chips in one block. Unlike MC-CDMA or MC-DS-CDMA, the CP-CDMA system is a single carrier direct sequence CDMA system, with a cyclic prefix. Essentially, a block is cyclically extended to $N+N_{CP}$ chips with the last N_{CP} chips inserted at the beginning of the block. Note that the length of the CP N_{CP} should be no less than the maximum delay of the mobile propagation channel to absorb the ISI. The transmitted block signal is illustrated in Figure 1.

All signals that arrive at the receiver from the same basestation have passed through an identical complex channel. The discrete-time output signal in the receiver can be seen as the response of a complex digital filter to the transmitted signal. The complex FIR filter *h(t;l)* with order L is a composite successive convolution of the transmitter filter, the mobile radio channel and the receiver filter.

At the receiver, perfect synchronisation is assumed and the CP is discarded before equalisation. For such a system, it is convenient to perform block based processing at the receiver. The received signal in one block is $r_i(n)$, $0 \le n \le N-1$, where i is the block index. The term

$x_i(n)$ denotes the corresponding transmitted block signal. Therefore, assuming that the composite channel response $h_i(l)$ is quasi-static within the i-th block and is normalized such that $\sum_{l=0}^{L-1} E\{|h_i(l)|^2\}=1$. The relation between $r_i(n)$ and $x_i(n)$ can be written as

$$r_i(n)=x_i(n)\otimes h_i(n)+v_i(n) \quad , \quad 0\le n\le N-1 \tag{3}$$

where $v_i(n)$ is additive white Gaussian noise and " $\otimes$ " denotes circular convolution. For convenience, the transmitted i-th block signal is rewritten in vector format. Let $\mathbf{s}_k=[s_k(0),\ldots,s_k(SF-1)]$ be the spreading code vector (SF is the spreading factor, single rate is assumed here; i is used to denote the i-th block) for user k and there are N/SF user symbols in one block, the discrete transmitted scrambled signal $\mathbf{x}_i=[x_i(0),\ldots,x_i(N-1)]^T$ can be written as:

$$\mathbf{x}_i = diag\{c(0),\ldots,c(N-1)\}\cdot[\sum_{k=1}^{K}\sqrt{E_k}b_{i,k}^{(0)}\mathbf{s}_k+\sqrt{E_p}\mathbf{p}_0,\ldots,\sum_{k=1}^{K}\sqrt{E_k}b_{i,k}^{(N/SF-1)}\mathbf{s}_k+\sqrt{E_p}\mathbf{p}_{N/SF-1}]^T \tag{4}$$

where $\mathbf{p}_j=[p(j*SF),\ldots,p(j*SF+SF-1)]$, $0\le j\le N/SF-1$.

After removal of the cyclic prefix, the received block signal $\mathbf{r}_i=[r_i(0),\ldots,r_i(N-1)]^T$ can be expressed as:

$$\mathbf{r}_i=\mathbf{H}_i\mathbf{x}_i+\mathbf{v}_i \tag{5}$$

where $\mathbf{v}_i$ is a Gaussian noise vector and $\mathbf{H}_i$ is an N by N circulant matrix defined by:

$$\mathbf{H}_i=\begin{bmatrix} h_i(0) & & & & h_i(L-1) & \cdots & h_i(1) \\ \vdots & h_i(0) & & & & \ddots & \vdots \\ \vdots & \vdots & \ddots & & 0 & & h_i(L-1) \\ h_i(L-1) & \vdots & \vdots & h_i(0) & & & \\ & h_i(L-1) & \vdots & \vdots & h_i(0) & & \\ & & \ddots & \vdots & \vdots & \ddots & \\ 0 & & & h_i(L-1) & h_i(L-2) & \cdots & h_i(0) \end{bmatrix}. \tag{6}$$

The circulant matrix $\mathbf{H}_i$ can be efficiently diagonalized by the use of the Fourier transform and the inverse Fourier transform, hence, (5) can be expressed in the frequency domain as:

$$\mathbf{R}_i=diag\{H_i(0) \quad \cdots \quad H_i(N-1)\}\mathbf{X}_i+\mathbf{V}_i \tag{7}$$

where $\mathbf{R}_i = [R_i(0),...,R_i(N-1)]^T$, $\mathbf{X}_i = [X_i(0),...,X_i(N-1)]^T$ and $\mathbf{V}_i = [V_i(0),...,V_i(N-1)]^T$ are the FFT of $\mathbf{r}_i$, $\mathbf{x}_i$ and $\mathbf{v}_i$, respectively.

In other words, due to the inserted CP, the distortion of the channel is considered as a multiplication in the frequency domain. Thus, in the frequency domain,

$$R_i(w) = H_i(w)X_i(w) + V_i(w), \qquad 0 \le w \le N-1 \tag{8}$$

The minimum mean square error (MMSE) equaliser $W_i(w)$ in the frequency domain is given by the following expression [5]:

$$W_i(w) = \frac{H_i^*(w)}{|H_i(w)|^2 + \sigma_n^2/\sigma_d^2}. \tag{9}$$

where σ_n^2, σ_d^2 and $H_i^*(w)$ are the variance of the additive white Gaussian noise, the variance of the received signal and the conjugate of $H_i(w)$, respectively. Consequently, the equalised signal is converted back to the time domain as $\hat{x}_i(n) = \frac{1}{N}\sum_{w=0}^{N-1} W_i(w)\cdot R_i(w)\cdot e^{j\frac{2\pi wn}{N}}$, after which, descrambling, despreading and demapping are performed.

III. Iterative Channel Estimation

Channel estimation plays an important role in the receiver. The system performance strongly depends on the estimate of the channel impulse response. In this paper, channel estimation based on parallel pilots is considered since it does not require bandwidth spreading.

A. Correlation Method

First, a correlation method for channel estimation is introduced. Code-multiplexed pilots have been used in WCDMA as the parallel primary common pilot channel (P-CPICH) [15]. User data could be treated as an independent signal and the aggregation will be considered to be an additive noise on the high power P-CPICH. For the system described in section II, under the

assumption that the pilot sequence is uncorrelated with the data channels and the additive Gaussian white noise, it is possible to derive the following:

$$E\left\{\begin{bmatrix} r_i(n) \\ \vdots \\ r_i(n+L-1) \end{bmatrix} \times p(n)^* \times c(n)^*\right\} = \sqrt{E_p} E\left\{\begin{bmatrix} h_i(0) \\ \vdots \\ h_i(L-1) \end{bmatrix}\right\} = \sqrt{E_p}\hat{\mathbf{h}}_i^{CORR}, \qquad (10)$$

where $\hat{\mathbf{h}}_i^{CORR}$ is the channel estimate of the *i*-th block. Thus, the complex channel coefficients can be determined up to a fixed scaling factor. Practically, $\hat{\mathbf{h}}_i^{CORR}$ is estimated by:

$$\hat{\mathbf{h}}_i^{CORR} = \frac{1}{(N-L+1)\sqrt{E_p}} \sum_{n=0}^{N-L} \left\{\begin{bmatrix} r_i(n) \\ \vdots \\ r_i(n+L-1) \end{bmatrix} \times p(n)^* \times c(n)^*\right\} \qquad (11)$$

The correlation method had been widely adopted for the design of RAKE receivers. However, its estimation performance degrades due to non-ideal autocorrelation properties and has a significant influence on the BER performance of the system.

B. Iterative Channel Estimation

A novel iterative channel estimator for CP-CDMA systems is developed here, $\hat{\mathbf{h}}_i^{CORR}$ is obtained by the correlation method and is used as an initial channel estimate for the system. The received signal is equalised in the frequency domain and transformed back to the time domain by IFFT. The scrambling code is then removed and the composite signal is despread and detected. In this paper, uncoded systems and only hard detection are considered. Consequently, estimates of *K* users' transmitted symbols $\hat{b}_{i,k}^{(j)}$, $0 \le j \le N/SF-1$ can be obtained. The idea of iterative channel estimation is that initially an estimate is made based on the parallel pilot channel and then refined by using both pilots and reconstructed user symbols. Once the detector outputs the estimates of users' symbols, they are respread, rescrambled and summed with the code-multiplexed pilots as virtual pilots, which then enhances the estimation performance.

The whole process can be summarized as follows:

Step 1. Correlation method is used to deliver initial channel estimates $\hat{\mathbf{h}}_i^{CORR}$.

Step 2. The received signal is equalised in the frequency domain and transformed back to the time domain by IFFT. The scrambling code is then removed and the composite estimated signal $\hat{x}_i(n)$ is despread and hard detected.

Step 3. *K* users' transmitted symbols $\hat{b}_{i,k}^{(j)}$ are respread and rescrambled. The scrambled code-multiplexed pilots are added to form an estimated composite signal $\tilde{x}_i(n)$.

Step 4. $\tilde{x}_i(n)$ is converted to $\tilde{X}_i(w)$ in the frequency domain and used for channel estimation together with the received frequency domain signal $R_i(w)$. In the estimator, the reconstructed composite signal $\tilde{X}_i(w)$ is treated as a pilot signal. A refined channel estimate can be obtained in the frequency domain as: $\tilde{H}_i(w) = \dfrac{R_i(w)\tilde{X}_i^*(w)}{\left|\tilde{X}_i(w)\right|^2 + \sigma_n^2}$.

Step 5. The result from step 4 is converted to the time domain and only the first *L* values are kept to form the channel estimate $\tilde{\mathbf{h}}_i = [\tilde{h}_i(0),...,\tilde{h}_i(L-1)]^T$.

Step 6. $\tilde{\mathbf{h}}_i$ is used for equalisation. Go to step 2 or stop here.

Figure 2 shows the system structure with the proposed iterative channel estimation method.

IV. Joint Channel Estimation and Parallel Interference Cancellation

A multistage PIC can cancel the MAI estimated with the hard decisions made in the previous stage. The received signal $r_i(n)$ is first converted into the frequency domain and passed into a equaliser. The output from the equaliser at the *I*-th stage $\hat{X}_i^I(w)$, $I=1,...,I_{end}$, is then transformed back to the time domain via an IFFT and hard decisions on the user's transmitted symbols $\hat{b}_{i,k}^{I,(j)}$ are made. At each stage, the estimated user symbols $\hat{b}_{i,k}^{I,(j)}$ are used together with code-

multiplexed pilots to generate virtual pilots for channel estimation; the I-th stage regenerated transmitted signal can be expressed by:

$$\tilde{\mathbf{x}}_i^I = diag\{c(0),...,c(N-1)\}\cdot[\sum_{k=1}^{K}\sqrt{E_k}\hat{b}_{i,k}^{I,(0)}\mathbf{s}_k+\sqrt{E_p}\mathbf{p}_0,...,\sum_{k=1}^{K}\sqrt{E_k}\hat{b}_{i,k}^{I,(N/SF-1)}\mathbf{s}_k+\sqrt{E_p}\mathbf{p}_{N/SF-1}]^T \quad (12)$$

After performing iterative channel estimation as in section III, $\tilde{\mathbf{h}}_i^I=[\tilde{h}_i^I(0),...,\tilde{h}_i^I(L-1)]^T$ with its frequency domain counterpart $[\tilde{H}_i^I(0),\cdots,\tilde{H}_i^I(N-1)]^T$ are used for system equalisation and interference cancellation. Let the u-th user be the desired user and the estimated composite signal excluding the u-th user's information can be regenerated as:

$$\dot{\tilde{\mathbf{x}}}_i^I = diag\{c(0),...,c(N-1)\}\cdot[\sum_{k=1,k\neq u}^{K}\sqrt{E_k}\hat{b}_{i,k}^{I,(0)}\mathbf{s}_k+\sqrt{E_p}\mathbf{p}_0,...,\sum_{k=1,k\neq u}^{K}\sqrt{E_k}\hat{b}_{i,k}^{I,(N/SF-1)}\mathbf{s}_k+\sqrt{E_p}\mathbf{p}_{N/SF-1}]^T \quad (13)$$

Parallel interference cancellation can be performed at the I-th stage as follows:

$$\mathbf{r}_i^I=\mathbf{r}_i-\tilde{\mathbf{H}}_i^I\dot{\tilde{\mathbf{x}}}_i^I \quad (14)$$

where $\tilde{\mathbf{H}}_i^I$ is a circulant matrix with elements taken from $\tilde{\mathbf{h}}_i^I=[\tilde{h}_i^I(0),...,\tilde{h}_i^I(L-1)]^T$. This can be done in the frequency domain as:

$$\mathbf{R}_i^I=\mathbf{R}_i-diag\{\tilde{H}_i^I(0),\cdots,\tilde{H}_i^I(N-1)\}\cdot\dot{\tilde{\mathbf{X}}}_i^I \quad (15)$$

where $\mathbf{R}_i^I$ and $\dot{\tilde{\mathbf{X}}}_i^I$ are the Fourier transforms of $\mathbf{r}_i^I$ and $\dot{\tilde{\mathbf{x}}}_i^I$, respectively. Figure 3 shows how we can combine the iterative channel estimation and PIC within one structure.

From Section III, in each iteration cycle, K users' signals are regenerated and summed with the pilot channel for channel estimation purpose. Meanwhile, interference from the interfering K-1 users and the parallel pilot channel are constructed and subtracted from the received composite signal, hence, interference can be reduced through each iteration. It should be noted that the PIC processing is done in a different manner to the conventional approach [13][14]. Since the downlink scenario is simulated in this paper, only a single stage PIC is considered. There may be more than one iteration, but only a single stage PIC for the system.

V. Simulation Results

Computer simulations are carried out at baseband for the investigation. The chip rate is 3.84 Mchips/s. Walsh codes with length 16 are used as channelization codes and a 512 Gold code is used as the scrambling code. One pilot channel is code-multiplexed with dedicated data channels. The block size is 512 excluding the 16 chips CP. In the simulations presented here, the terminal is assumed to be moving at 50 km/h, and the carrier frequency is 2 GHz. The UMTS Vehicular A channel model [16] is used for BER evaluation in our simulation. Each path fades independently according to a Rayleigh distribution. The corresponding channel profile is shown in Table 1. The CP duration 4.16 μs is selected larger enough than the longest channel delay spread 2.51 μs.

Path	Channel	
	Path Delay (nsec)	Avg. Power (dB)
1	0	0
2	310	-1.0
3	710	-9.0
4	1090	-10.0
5	1730	-15.0
6	2510	-20.0

Table 1. Channel profile of the UMTS Vehicular Channel A

To evaluate the estimator performance, the Mean Square Error (MSE) for both the correlation method and the new iterative procedure is computed:

$$MSE(\tilde{\mathbf{h}}_i) = E\left\{\sum_{l=0}^{L-1}\left|h_i(l)-\tilde{h}_i(l)\right|^2\right\} \tag{16}$$

In Figure 4, the MSE curves of channel estimation versus signal to noise ratio per bit with varying pilot power, i.e., g=10%, 20% and 40% are presented. From these, it follows that by using the correlation method, the higher the pilot power is, the better the channel estimates. In

other words, if the value of 'g' is large, the channel estimation quality is good. However, this will lead to a large MAI with large error probability, which is shown in Figure 5. Observe also that the new iterative scheme can effectively reduce channel estimation errors in comparison with the correlation method.

Figure 5 shows the numerical results of system performance simulations. Imperfect channel estimation is considered (The channel is estimated based on the pilot channel). Both the correlation method and the new iterative estimation approach are evaluated. The value of 'g' is chosen to be 10%, 20% and 40%. Ideal channel estimation is also used in the simulation as a reference result to compare BER performance results from the two channel estimation approaches. From Figure 5, it can seen that under the perfect channel knowledge assumption, allocating more power to pilots (larger 'g') introduces more interference to the system and hence a worse BER performance results.

Using the correlation method for channel estimation, the higher the pilot power is, the better the channel estimates can be achieved. However, this will lead to a large MAI with large error probability. Although a pilot channel with only 10%, 20% of the whole signal power induces less interference, the BER performance is worse than that with g=40%. This is because when the power ratio of the pilots over the whole signal power is small, the channel estimation is poor so that the system performance is degraded. The BER performance with the new iterative channel estimation scheme are also shown with g=10%, 20% and 40%. Notice that with only a small amount of power allocated to the pilots, good performance can still be achieved via this structure. As can be seen from Figure 5 when g=10%, at the BER of 10^{-2}, there is only a 2dB performance degradation compared with the system performance with perfect channel estimation. This is important for practical systems since usually only around 10% power can be allocated to the pilot channel, for example, g=10% in HSDPA [17]. Transmitting a small portion of power on the

pilot makes the system power efficient and since parallel code-multiplexed pilots are used, bandwidth efficiency can be maintained.

Figure 6 demonstrates the system improvements with PIC. The single user situation (no MAI) with perfect channel estimation and MMSE-FDE is also simulated as reference results with the name "single user bound".

After interference cancellation, the BER performance is enhanced significantly, especially when the number of active users is large. This shows that the other user interference as well as interference from pilot channel has considerable impact on such multiuser system performance. As mentioned in the previous section, the PIC is performed only at the last stage since it is used only for the desired user. When I=1, decisions $\hat{b}_{i,k}^{1,(j)}$ are made based on the equaliser with the channel estimates obtained by the correlation method and are used for interference regeneration. Since the initial channel impulse response estimates are bad, interference regeneration based on $\hat{b}_{i,k}^{1,(j)}$ is not so accurate. Consequently, with I>1 more reliable estimates $\hat{b}_{i,k}^{I,(j)}$ are available and hence better PIC performance. Starting from the correlation method, the new scheme improves the performance of channel estimation and signal detection iteratively. Results in Figure 6 and Figure 7 demonstrate that the BER performance after PIC is approaching the "single user bound". However, the PIC cannot significantly decrease the BER with more iterations. Figure 7 repeats the experiment for 4 active users; the advantages of the proposed scheme are still evident. From Figure 5, 6, 7, it can be seen that choosing I=1 achieves comparable performance to I>1. Hence, it is suggested that using just one iteration will suffice since more iterations will result in excessive delay and increase in computational complexity to the system.

VI. Further Improvement and Complexity Discussion

The aforementioned channel estimation scheme can be further enhanced based on the fact that the channel will not change significantly across blocks. Using the refined channel estimates in

the i-th block as initial estimates for the $(i+1)$-th block instead of using the correlation method. By doing so, the computation cost will be reduced because the correlation method is applied at the first block only. On the other hand, better initial estimates for successive blocks are available. Figure 8 and Figure 9 demonstrate that the new scheme (IMIE: Iterative Method with Initial Estimates) is able to offer further improvement on system performance. In both situations, whether the PIC is used or not, it is shown that the system performance is enhanced and computations are saved.

From the structures in Figure 2 and Figure 3, it is obvious that the iterative cycle can be implemented efficiently in the frequency domain with complexity of $O(NlogN)$, which is much simpler compared to some optimal detectors such as the maximum-likelihood detector. The complexity will linearly increase with an increasing number of users. Since the proposed iterative channel estimation requires user symbol detection and interference reconstruction, a PIC is combined into the iterative structure in order to further enhance the system performance. The computational complexity of the whole process is comparable to a conventional PIC. On the other hand, since the iterative channel estimator can provide the PIC with better channel estimates, the improvement in system performance that can be achieved is significant.

VII. Conclusion

In this paper a new iterative channel estimation method has been presented and studied for a CP-CDMA system. The new approach was evaluated through simulations and compared with the conventional correlation method in terms of BER performances. The results verify the effectiveness of the new method. Moreover, parallel interference cancellation is introduced into the iterative structure. The proposed joint scheme shows good channel estimation accuracy and significant improvements with respect to equaliser with the conventional correlation CE method.

Acknowledgment

The work reported in this paper has formed part of the Research Programme of the Virtual Centre of Excellence in Mobile and Personal Communications, Mobile VCE, www.mobilevce.com, whose funding support, including that of EPSRC, is gratefully acknowledged. Fully detailed technical reports on this research are available to Industrial Members of Mobile VCE.

References

[1]. R. Prasad, *Universal wireless personal communications*: Artech House, 1998.
[2]. S. Hara, R. Prasad, "Overview of multicarrier CDMA", IEEE Communications Magazine, Vol. 35, Issue. 12, Dec. 1997, pp. 126-133.
[3]. N. Benvenuto and S. Tomasin, "On the comparison between OFDM and single carrier modulation with a DFE using a frequency-domain feedforward filter", IEEE Transactions on Communications, Vol. 50, No. 6, 2002, pp 947-955.
[4]. D. Falconer, *et al*, "Frequency domain equalisation for single-carrier broadband wireless systems", IEEE Communication Magazine, April 2002, pp. 58-66.
[5]. K. Baum, T. Thomas, F. Vook, and V. Nangia, "Cyclic-Prefix CDMA: an improved transmission method for broadband DS-CDMA cellular systems", IEEE Wireless and Communications and Networking Conference 2002. Vol. 1, pp. 183-188
[6]. F. Vook, T. Thomas, and K. Baum, "Cyclic-Prefix CDMA with antenna diversity", Proceedings of the 55th IEEE Vehicular Technology Conference, 2002. Vol. 2, pp.1002-1006.
[7]. P. Lin, T. Chiueh, "Low complexity frequency-domain despreading for cyclic-prefix CDMA systems", IEEE Communications Letters, Vol. 8, No. 6, June 2004, pp. 339-341.
[8]. K. Hooli, et al, "Chip-level Channel equalisation in WCDMA downlink", EURASIP Journal on Applied Signal processing, Vol. 8, 2002, pp. 757-770.
[9]. P. Schramm, R. Müller, "Pilot symbol assisted BPSK on Rayleigh fading channels with diversity: performance analysis and parameter optimization", IEEE Transactions on Communications, Vol. 46, No. 12, 1998, pp. 1560-1563
[10]. P. Schramm, "Analysis and optimisation of pilot-channel-assisted BPSK for DS-CDMA systems", IEEE Transactions on Communications, Vol. 46, No. 9, 1998, pp. 1122-1124
[11]. N. Benvenuto, *et al*, "Performance comparison of chip matched filter and RAKE receiver for WCDMA systems", IEEE Global Telecommunications Conference, 2001, pp. 3060-3064.
[12]. D. Koulakiotis, A. Aghvami, "Data detection techniques for DS/CDMA mobile systems: a review", IEEE Personal Communications, June 2000, pp. 24- 34
[13]. M. Varanasi, B. Aazhang, "Multistage detection in asynchronous code-devision multiple-access communications", IEEE Transactions on Communications, Vol. 38, No. 4, 1990, pp. 509-519.
[14]. R. Fantacci, "Proposal of an interference cancellation receiver with low complexity for DS/CDMA mobile communication systems", IEEE Transactions on Vehicular Technology, Vol. 48, No. 4, 1999, pp. 1039-1046
[15]. H. Holma, A. Toskala, *WCDMA for UMTS*, Wiley Publishing House, 2001
[16]. ETSI TR 101 112 V3.2.0 (1998-04): Universal Mobile Telecommunications System (UMTS); Selection procedures for the choice of radio transmission technologies of the UMTS.

[17]. M. Harteneck, C. Luschi, "Practical implementation aspects of MMSE equalisation in a 3GPP HSDPA terminal", Proceedings of the 59th IEEE Vehicular Technology Conference, Vol. 1, 2004, pp. 445-449

[18]. F. Adachi, D. Garg, S. Takaoka and K. Takeda, "Broadband CDMA techniques", IEEE Wireless Communications, Vol. 12, Apr. 2005, pp. 8-18.

[19]. S. Redl, M. W. Oliphant and M. K. Weber, *An Introduction to GSM*, Artech House, March, 1995.

[20]. M. Morelli, U. Mengali and A. Masciarelli, "Pilot-assisted channel estimation for the downlink of the UMTS-TDD component", IEEE Transactions on Communications, Vol. 52, No. 4, 2004, pp. 595-604.

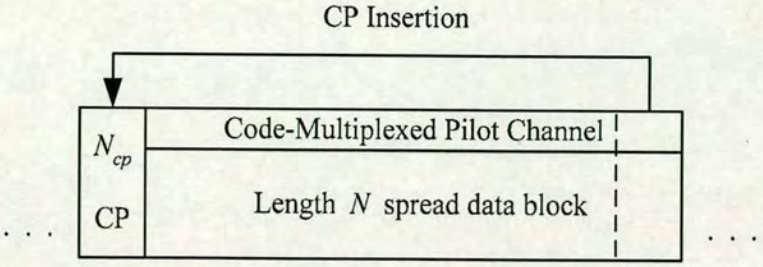

Fig. 1. CP-CDMA block signal

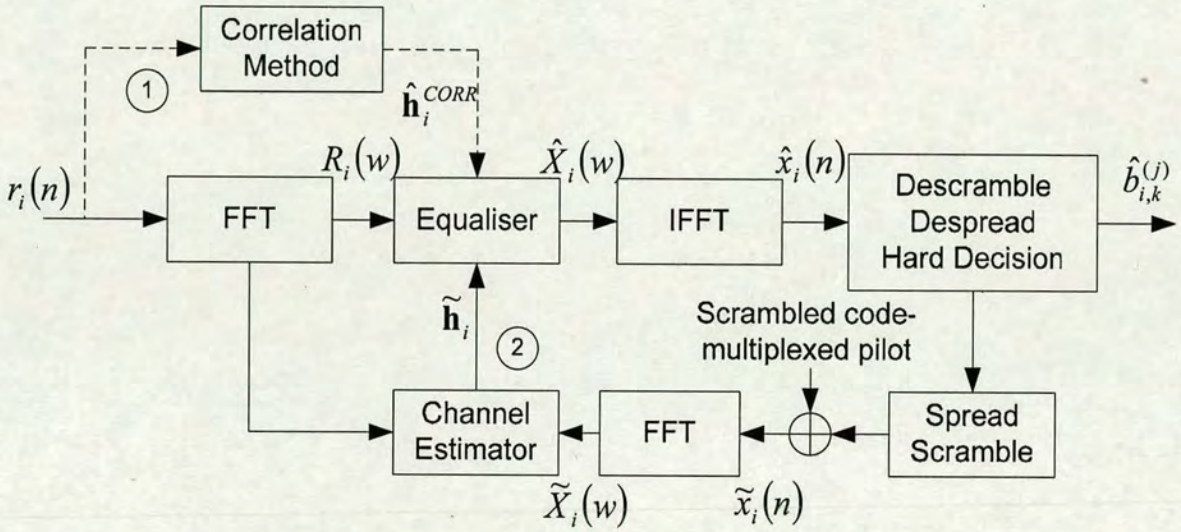

Fig. 2. Iterative channel estimation for CP-CDMA

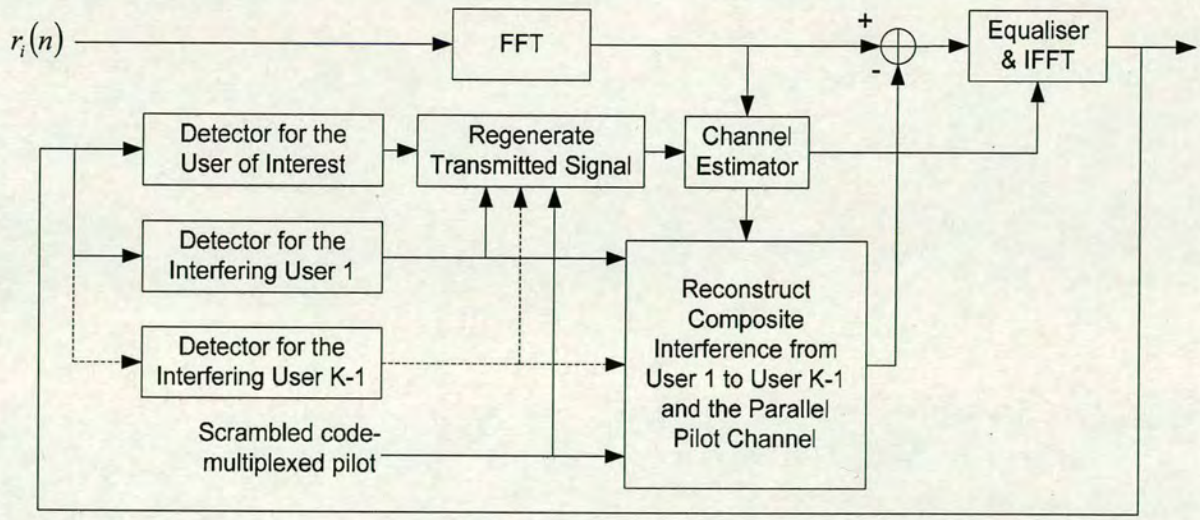

Fig. 3. Combined channel estimation and parallel interference cancellation structure

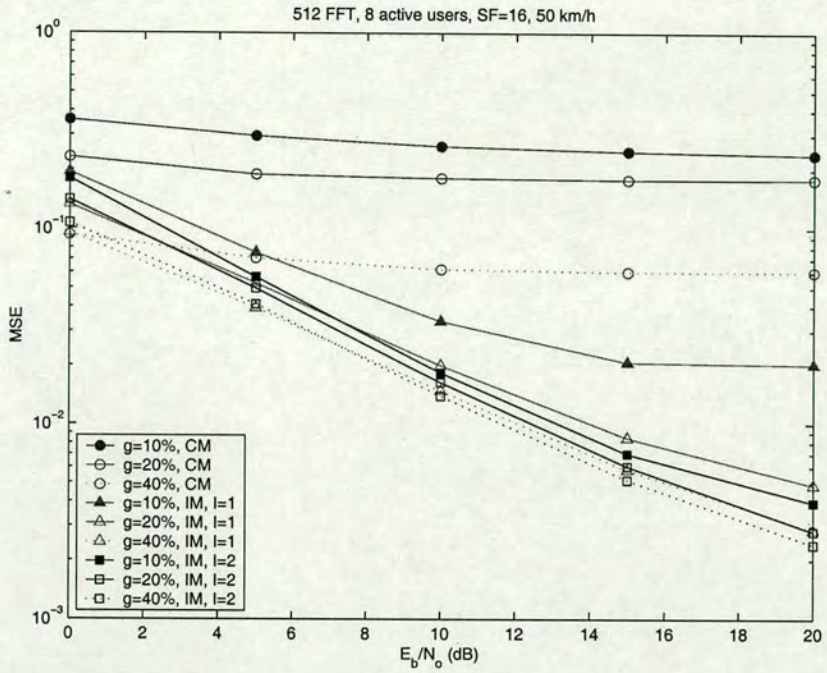

Fig. 4. Channel Estimation MSE versus E_b/N_o, g=10%, 20%, 40%. I: Number of Iterations. CM: Correlation Method, IM: Iterative Method.

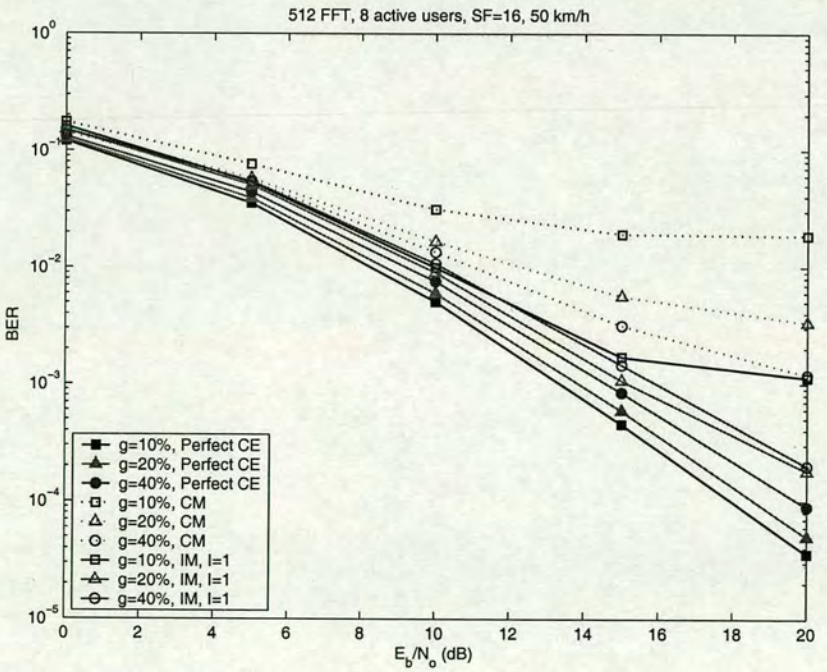

Fig. 5. Simulated BER performances, g=10%, 20%, 40%. CM: Correlation Method, IM: Iterative Method, Perfect CE: Perfect Channel Estimation.

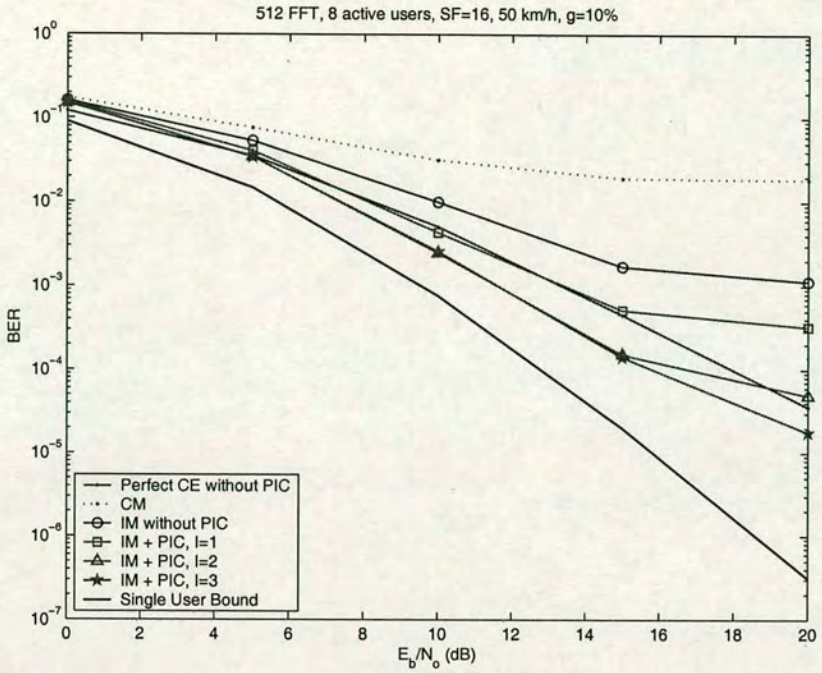

Fig. 6. Simulated BER performances with channel estimations and PIC, 8 active user, CM: Correlation Method, IM: Iterative Method, Perfect CE: Perfect Channel Estimation.

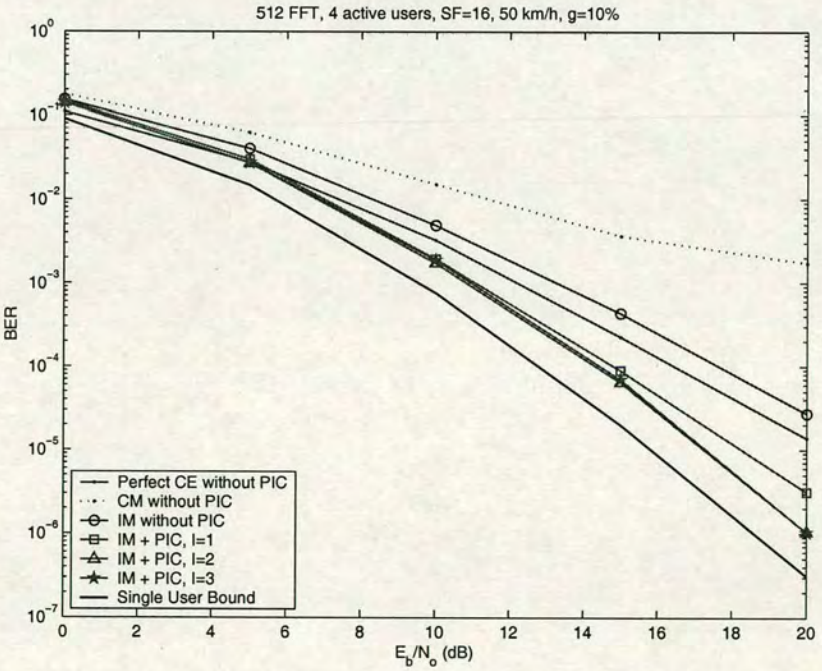

Fig. 7. Simulated BER performances with channel estimations and PIC, 4 active users, CM: Correlation Method, IM: Iterative Method, Perfect CE: Perfect Channel Estimation.

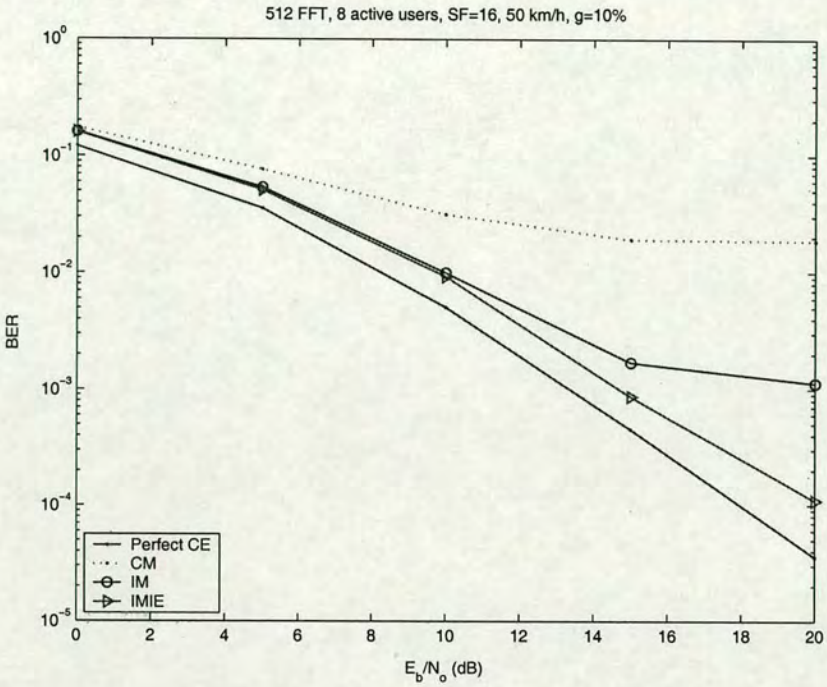

Fig. 8. Simulated BER performances with channel estimations, 8 active users, CM: Correlation Method, IM: Iterative Method, Perfect CE: Perfect Channel Estimation, IMIE: Iterative Method with Initial Estimates.

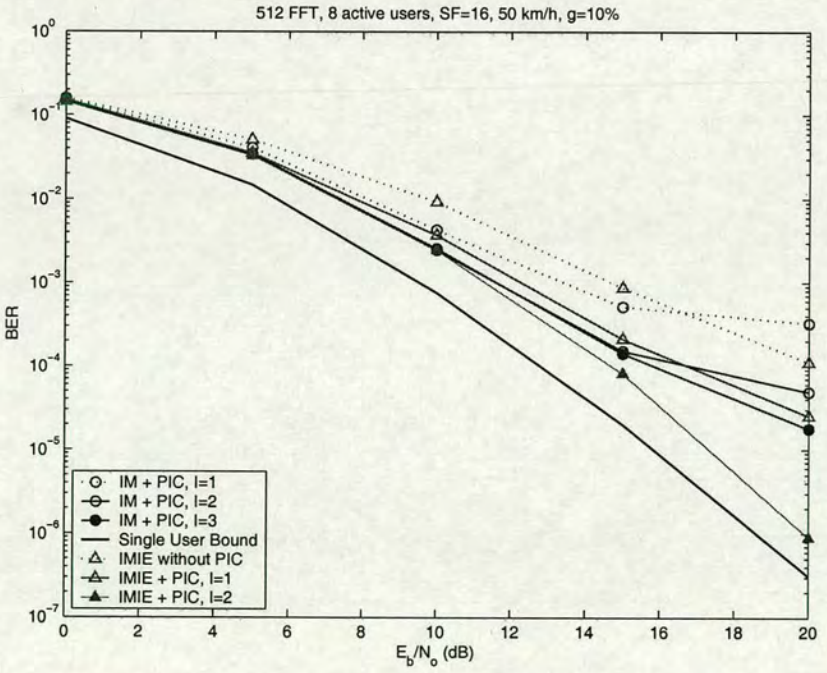

Fig. 9. Simulated BER performances with channel estimations and PIC, 8 active users, CM: Correlation Method, IM: Iterative Method, Perfect CE: Perfect Channel Estimation, IMIE: Iterative Method with Initial Estimates.

Hybrid DFE with Variable Length Feedback Filter

Yushan Li, Xusheng Wei, David G. M. Cruickshank, Steve McLaughlin

Institute for Digital Communications

School of Engineering and Electronics

University of Edinburgh

Edinburgh EH9 3JL, UK

Email: Yushan.Li@ee.ed.ac.uk

*Submitted to **IEE Proceedings – Communications***

No. of words: 3,924

No. of figures: 10

Abstract

In this paper, a hybrid decision feedback equaliser (DFE) with a feedback filter (FBF) whose length can be dynamically adjusted is presented and investigated. The equaliser is an adaptive DFE with a feedforward filter (FFF) implemented in the frequency domain with its length fixed by the FFT/IFFT size and a feedback filter (FBF) in the time domain. The FBF length is adjusted according to the achieved mean squared error (MSE). In addition, the impact of small FBF coefficients on system BER performance is taken into account so that a shorter filter length can be considered. Computer simulations show that the proposed approach is capable of adjusting the feedback filter length to a satisfactory level in terms of MSE and system BER performance and is able to track channel changes successfully.

29 September 2004

I. Introduction

Orthogonal Frequency Division Multiplexed (OFDM) is an air-interface used for both broadcasting and Wireless LAN (WLAN) applications and is a strong candidate for future 4G mobile communications. OFDM can effectively combat multipath distortion of the mobile transmission channel and is able to offer high data rates. However, although the advantages of OFDM are obvious, it should be pointed out that, there are two major inherent difficulties regarding OFDM; 1. OFDM is highly sensitive to frequency offset and phase noise; 2. OFDM exhibits a high instantaneous peak-to-mean power ratio that will decrease the power efficiency of the RF amplifier [1].

An alterative approach, i.e. single carrier transmission with frequency domain equalisation and time domain decision feedback was proposed recently by Falconer in [2],[3] and Benvenuto in [4]. In these papers, they provided a mathematical description of the FFF in the frequency domain and the FBF in the time domain and showed that single carrier transmission with a hybrid decision feedback equalisation yields a capacity close to that of OFDM. For simplicity, Falconer used a one-tap FBF and Benvenuto chose the length of the guard interval between successive blocks as the FBF length.

The length is an important factor for the filter in a variety of aspects: convergence rate, computational complexity, tracking ability and ultimately system performance. But so far, little research work related to this topic has been done. The performance costs for theoretical minimal-length equalisers have been discussed in [5], an algorithm which can adjust the filter length dynamically using a LMS algorithm according to a MSE criterion was proposed in [6]. However, the system BER performance is of most concern in a communication system. A length chosen according to a MSE criterion will not necessarily be reasonable in terms of computational complexity.

In a DFE, a FFF can to some extent eliminate the channel induced inter symbol interference (ISI) and a feedback filter operates on the outputs of the decision device to further reduce the post-cursor ISI. When the FBF is converged, the taps are approximately the negative values of the residual ISI. Small FBF taps coefficients will not contribute very much to the system performance. Therefore, by observing the power of the FBF tap coefficients, we can remove those unnecessary taps. In this paper, we will apply an algorithm based on an MSE criterion to a hybrid DFE and also take into consideration the impact of small FBF coefficients on system BER performance, therefore, a more reasonable length can be found. The purpose of adjusting the FBF length is to avoid using excessively long filters which might induce excessively high computational complexity and achieve a good tradeoff between system performance and computations.

Section II introduces the system model and describes the adaptive hybrid DFE structure. In section III, the dynamic length algorithm is proposed and simulation results are provided. In section IV new criterion which deals more effective with small FBF taps is presented. Finally, conclusions are presented in section V.

II. System Model

The system model used in this paper is given in Fig. 1. As can be seen in Fig. 1, the feedforward part is implemented in the frequency domain while the FBF is operating in the time domain.

The superscript $(*)^{(n)}$ is used to represent the nth block since the hybrid DFE works on a block-by-block basis. Other notations introduced in Fig. 1 are defined as follows:

$\mathbf{W}^{(n)}$: N_f taps FFF vector, $\mathbf{W}^{(n)}=[W_0^{(n)},..., W_{Nf-1}^{(n)}]^T$.

$\mathbf{R}^{(n)}$: Fourier transform of the received signal, $\mathbf{R}^{(n)}=[R_0^{(n)},..., R_{Nf-1}^{(n)}]^T$.

$\mathbf{F}^{(n)}$: N_b taps FBF vector, $\mathbf{F}^{(n)}= [f_0^{(n)},..., f_{Nb-1}^{(n)}]^T$.

$\hat{d}_m^{(n)}$: Detected symbol and inputs to the FBF, $m=1,\ldots, N_f$.

$e_m^{(n)}$: Error signal between equalised and detected symbol. $\mathbf{e}^{(n)}=[e_0^{(n)},\ldots, e_{Nf-1}^{(n)}]^T$.

$\mathbf{E}^{(n)}$: Frequency domain counterpart of the time domain error signal $\mathbf{e}^{(n)}$.

Fig. 2 shows the specific frame structure that is required by such a hybrid DFE. Such a downstream transmission structure is adopted in both [2] and [4] but with slightly different definitions. Each unique word (UW) is generated by a pseudo-noise process and is the counterpart of the cyclic prefix used in an OFDM system. The UW acts as a cyclic prefix for the following block's signal and one block consists of the useful signal and the UW. Such a UW extension is suitable for the hybrid DFE since the first N_b-1 interference symbols on each block signal are generated by the UW signal which is known at the receiver. If the signal data is cyclically extended as in an OFDM system, the DFE is unable to cancel the first N_b-1 interference samples due to lack of the information of the cyclic prefix.

Let us suppose we are using a hybrid DFE with N_f FFT/IFFT FFF taps and N_b feedback taps. The MMSE-DFE solution is given in [2] and [4]. In this paper, we focus on the adaptive DFE based on the LMS algorithm. The output signal from the feedforward frequency domain filter is represented by:

$$s_m^{(n)} = IFFT\left\{\mathbf{R}^{(n)} \otimes \mathbf{W}^{(n)}\right\}, m = 0,1,\cdots, N_f - 1 \tag{1}$$

where $\otimes$ denotes element by element multiplication.

Thus, the nth block time domain output samples can be expressed as:

$$y_m^{(n)} = s_m^{(n)} - \sum_{k=1}^{N_b} f_k \hat{d}_{m-k}^{(n)}, m = 0,1,\cdots, N_f - 1 \tag{2}$$

Detected symbols $\hat{d}_m^{(n)}$ are the decisions being made on the time domain signal $y_m^{(n)}$ and the N_b data symbols of $\hat{d}_m^{(n)}$ when $m=-N_b,..,-1$ should coincide with the N_b UW symbols. The well-

known LMS algorithm can be adopted for both the FFF [7] and the FBF by adjusting tap coefficients in accordance with the error signal $e_m^{(n)}$ defined by:

$$e_m^{(n)} = \hat{d}_m^{(n)} - y_m^{(n)}, \; m = 0,1,\cdots,N_f - 1 \tag{3}$$

The FFF that operates in the frequency domain can be trained as:

$$W_l^{(n+1)} = W_l^{(n)} + \mu E_l^{(n)} R_l^{(n)^*}, \; l = 0,1,\cdots,N_f - 1 \tag{4}$$

while the time domain FBF is updated as:

$$f_k^{(n+1)} = f_k^{(n)} - \mu \sum_{m=0}^{N_f-1} e_m^{(n)} \hat{d}_{m-k}^{(n)^*}, \; k = 1,\cdots,N_b \tag{5}$$

where μ represents the step size and both μ in (4) and (5) are identical.

Equation (5) can be written in a vector form:

$$\mathbf{F}^{(n+1)} = \mathbf{F}^{(n)} - \mu \mathbf{D}^{(n)} \mathbf{e}^{(n)} \tag{6}$$

where the N_b-*by*-N_f decision data matrix $\mathbf{D}^{(n)}$ of the nth block is defined as:

$$\mathbf{D}^{(n)} = \begin{bmatrix} \hat{d}_{-1}^{(n)^*} & \hat{d}_{-2}^{(n)^*} & \cdots & \hat{d}_{N_f-2}^{(n)^*} \\ \vdots & \ddots & \ddots & \vdots \\ \hat{d}_{-N_b}^{(n)^*} & \cdots & \hat{d}_{N_f-N_b-2}^{(n)^*} & \hat{d}_{N_f-N_b-1}^{(n)^*} \end{bmatrix} \tag{7}$$

In (7), the first N_b decision signals are identical to the N_b UW symbols. From equation (6) and (7), we note that, when the FBF length is increased by one tap, N_f complex multiplications are required to update the FBF coefficients.

We therefore illustrate the system performance with different FBF lengths. In Fig. 3, steady state results (via Wiener filtering) are presented. The signal is assumed to be transmitted in an 11 taps fixed additive Gaussian noise channel. The FBF length is increased from 0 (Linear Equaliser case) to 1, 5, 12, 20 and then 32 (The length of the UW is the maximum filter length that is available in the system). It can be seen from Fig. 3 that the DFE offers an improved performance in a multipath channel over a linear equalizer (LE). The system performance improves with an increasing number of FBF taps. Moreover, there is a threshold value for the number of FBF taps;

when the FBF taps reaches the threshold value, as can be seen in Fig. 3, when the FBF tap length reaches approximately 12, further increasing the FBF taps does not gain much improvement in system performance. On the other hand, unnecessarily long length will increase the computational complexity. Hence, it is desirable to search for the length that offers the best trade-off between complexity and system performance. One adaptive length adjusting algorithm for the hybrid DFE is discussed in the following section.

III. Length Adjusting Algorithm Based on MSE Criterion

It has been shown in [5] that varying the length of an equaliser can improve performance by adjusting the length according to the channel conditions. In this paper, we first apply this idea on the feedback section. The total T ($1 \le T \le UW\ Length$) taps of the FBF is split into I concatenated segments of L taps each. Combining with the feedforward frequency domain equaliser, each segment in the FBF produces one equalised symbol $y_{m,i}^{(n)}$ ($1 \le i \le I$) and hence one error signal $e_{m,i}^{(n)}$ ($1 \le i \le I$). From (3), similarly, we can write:

$$e_{m,i}^{(n)} = \hat{d}_m^{(n)} - y_{m,i}^{(n)},\ m = 0,1,\cdots,N_f - 1,\ 1 \le i \le I \tag{8}$$

Since the FFF is operating on a block by block basis, we define the MSE of the nth block by the following expression.

$$J_i(n) = \frac{\sum_{m=0}^{N_f-1} \left\| e_{m,i}^{(n)} \right\|^2}{N_f},\ 1 \le i \le I \tag{9}$$

The output MSE produced by the last two segments are of interest in that they can be used to decide the changing direction of the FBF length as follows. We use $J_{I-1}(n)$ and $J_I(n)$ to denote the MSE corresponding to the (I-1)-th and I-th segment, respectively. Similar to [6], we derive an adaptive algorithm for a hybrid DFE system: If $J_I(n) < \alpha_{up} J_{I-1}(n)$, then add *"L"* extra taps to the FBF, i.e. add one extra segment; If $J_I(n) > \alpha_{down} J_{I-1}(n)$, then remove *"L"* extra taps from the FBF, i.e. remove one segment. α_{up} and α_{down} are two parameters that control the length adjusting

process with $0<\alpha_{up}<1$ and $\alpha_{down}\geq 1$. The closer they are to 1, the more frequently that the length will change. When one extra segment is added to the FBF, the taps in this new segment are initialized to zeros and when one segment is removed, all the remaining taps maintain their value and the $(I-1)$th segment becomes the last segment. Since the FBF coefficients are updated on a block by block basis, the segment changes take effect in the new block. Once an extra segment is added, the tap coefficients are set to zeros and by applying the new FBF on the new block, there will not be any differences between $J_{I-1}(n)$ and $J_I(n)$. Therefore, reapplying the updated filter coefficients on the current processing block signal can accelerate the convergence speed.

The performance of the hybrid DFE with variable length FBF is now examined via computer simulations. The multipath channel is assumed to be quasi-static (static within a block) and is modelled as an 11 taps (with total taps power normalized to 1) channel, Channel 1: $h=\{0.0102+0.2531j,\ 0.0661-0.1224j,\ 0.4763-0.1778j,\ -0.0282-0.0431j,\ 0.0329-0.2228j,\ 0.2588+0.3816j,\ -0.2201-0.1689j,\ 0.0069-0.1322j,\ 0.0873+0.2061j,\ 0.2958-0.3436j,\ 0.1030-0.1770j\}$. There are $L=2$ taps within each segment, $N_f=512$, $N_b=32$, $\alpha_{up}=0.995$, $\alpha_{down}=1$ and $\mu=0.1$ are the selected parameters. In Fig. 4, learning curves for one typical simulation run is given. It can be seen that the adaptive algorithm can effectively adjust the FBF length, the filter length is adjusted from either 2 taps or 32 taps. The filter length converges to around 20-22 taps in both cases under the MSE criterion.

Fig. 5 shows the steady state MSE that is achieved by the hybrid DFE with variable length FBF when the signal to noise ratio per bit is *20 dB*. With a 20 tap FBF, the hybrid DFE reaches its minimum MSE. Using too many taps, besides wasting computations, may increase the MSE owing to algorithm inaccuracies that increase with equaliser length [6]. Therefore, the MSE converge to its minimum when the length is 20 rather than the whole possible value. This fact is well documented in standard adaptive filter textbooks [11].

In Fig. 6, the BER performance of the system is studied. When the FBF length is converged to an optimal value according to the MSE criterion, the simulation curves for FBF with length 22 and 32 are almost identical. However, when compared with using FBF with fixed length 2, there is a significant improvement in the BER performance.

Fig. 7 shows the converged FBF coefficients for $E_b/N_0=20\ dB$. It can be seen in Fig. 7 that the coefficients of taps between 11 and 32 become very small, thus the system performance will not change significantly when we choose only 10 taps. This can be seen from the simulation results given in Fig. 6. Equalisers with longer than 10 taps do not bring any significant advantage to the system performance but will increase the difficulty of convergence and tracking of the LMS algorithm as well as the computational complexity. The reason is that the length of the FBF is adjusted according to the MSE criterion. By applying the MSE criterion in the hybrid DFE may not always bring us to a reasonable length that can achieve good tradeoffs between system BER performance and computational complexity. Merely using the MSE criterion results in the algorithm converging to an equaliser with a larger number of taps than is necessary. For example, choosing only 10 taps for the FBF we see an insignificant degradation in the system performance as measured by the BER compared with using 20 taps, the optimal value in terms of the MSE criterion. The extra taps waste computations and the improvement on the system performance is very limited.

The reason that the FBF length converge to 20 taps is that we choose $\alpha_{up}=0.995$ which is a value very close to but less than 1 and hence we can reach the minimum MSE that can be achieved. In other words, the "resolution" of the MSE is rather high, i.e. even a very small difference between $J_{I-1}(n)$ and $J_I(n)$ will lead to a filter length adjustment. In addition, when an α_{up} value close to 1 is chosen, the filter length will change frequently if it starts learning from a small tap value. Consequently, the convergence speed is greatly accelerated and the filter length will converge to an optimal value according to the MSE criterion. However, this value is not always the best

selection when we consider the BER performances, i.e., extra taps bring us very limited improvement on system performance. When choosing an α_{up} value less than but not so close to 1, for example $\alpha_{up}=0.8$, the filter length will converge to a more reasonable value (as can be seen in Fig. 4, it converges to 10 taps). This is at the expense of slowing down the learning speed. The other problem with the MSE criterion is that with $\alpha_{down}\geq 1$ if we start learning from large taps value, it is hard to converge to the most suitable taps value. Although the hybrid DFE can achieve a minimum steady state MSE with the converged FBF length, there exist some unnecessary taps that do not bring the system much improvement. As an example, in Fig. 5, the filter length will just oscillate around 20 (at 20, the hybrid DFE achieves a minimum steady state MSE) but the more sensible length, based on a trade-off between complexity and performance is 10. From the above statements and simulation results, it is clear that some new restrictions are required complementary to the MSE criterion in order that the FBF length can converge to a more suitable value.

IV. New Criterion

In a DFE, the FBF is being used to eliminate the residual ISI that is not completely removed by the FFF. Unlike a linear equaliser, a DFE has a particular property; in the FBF, when converged, the taps are approximately the negative values of the post-cursor taps of the combined convolution of the channel impulse response and the FFF [8]. Small FBF taps coefficients will not contribute too much to the system performance. Hence, by observing the power of the FBF taps, we can deduce whether we need to add one segment in the FBF or remove one. Usually, the length adjusting algorithms focus on the MSE improvements [9][10] while in this paper we also consider the impact of small FBF coefficients on system BER performance. We consider the impact of small FBF coefficients on BER performance rather than linking the FBF length mathematically to the BER. The purpose of adjusting the FBF length is to avoid using

excessively long filters, which might induce excessively high computational complexity. Thus we achieve a good tradeoff between system performance and computational complexity. Firstly, we sum up the power of all T taps in the FBF and the power of the last two taps, that is

$$P = \sum_{k=1}^{T} \left\| f_k^{(n)} \right\|^2 \qquad P_0 = \left\| f_T^{(n)} \right\|^2 + \left\| f_{T-1}^{(n)} \right\|^2 \tag{10}$$

Subsequently, we adjust both the parameter α_{up} and the length of the FBF according to the ratio $R=P_0/P$. If R is larger than a pre-defined value γ_1, it is clear that we need to increase the FBF length; therefore, we choose a value close to 1 for α_{up} so that the length can be changed frequently and the learning speed is accelerated. Otherwise, we choose a small value for α_{up} to slow down the length changing speed so that it will not converge to an unnecessary long length. If R is below a certain value γ_2 ($\gamma_2<\gamma_1$), we know that there are already extra long taps existing and then the length is reduced by one tap. Since the tap length is updated once a block, we can only use the instantaneous value of P and P_0. If unfortunately, when the algorithm is not converged and the tap length is reduced one tap by mistake, in the next block, the length can still be adjusted in the right direction. The reason is that when one tap is reduced by mistake, $R>\gamma_1>\gamma_2$ will result and a new value which is much closer to 1 (for example, 0.995) will be assigned to α_{up} , therefore, a small difference between $J_{I-1}(n)$ and $J_I(n)$ will require the FBF length to increase. The new criterion is very useful while the learning curve converges from a larger FBF length. Otherwise, by merely applying the MSE criterion, the learning curve will stop at an unnecessary long length value.

By applying the MSE criterion as that in [5] and also taking into account the FBF impact on system performance, we propose a new algorithm as depicted in a flowchart shown in Fig. 8 to control the length of the FBF.

To illustrate the effectiveness of the new algorithm, we consider the same channel: Channel 1 as mentioned in section III and apply the new algorithm. We choose $\alpha_{up}=0.995$, $\alpha_{up}^{1}=0.9$, $\alpha_{up}^{2}=0.995$, $\alpha_{down}=1$, $\gamma_1=0.05$, $\gamma_2=0.02$ and $\mu=0.1$ as the parameters in our algorithm. The FBF

length is initialised to 2 taps in one case and 32 taps in another case. The learning curves of both cases are presented in Fig. 9 based on one simulation run. The BER performance with 8 taps FBF and 10 taps FBF are both shown in Fig. 6. We see that by adopting a 10 tap FBF, the BER performance will not degrade too much compared with that FBF with 20 taps or 32 taps.

Fig. 10 shows the learning curve in scenarios when the channel changes from the previous complex one to a real channel, Channel 2: $h=\{0.7605, 0.5024, 0.3320, 0.2193, 0.0957, 0.0418\}$. It is obtained by averaging the learning curves in 100 simulation runs. During the first 50 blocks, signals are transmitted through Channel 1 (Channel 2) and at the 51st block, the environment changes to Channel 2 (Channel 1). It is clear from Fig. 10 that the new algorithm tracks the channel change successfully in both scenarios.

V. Conclusions

Usually, hybrid DFEs have a fixed feedback length, either 1 or the length of the guard interval between successive blocks. In this paper, a hybrid DFE with variable length FBF was proposed and evaluated. The purpose of adjusting the FBF length is to avoid using excessively long filters, which might induce excessively high computational complexity. The algorithm is based on the length adjustment of the FBF according to MSE criterion, and the impact of small FBF coefficients on system BER performance was also taken into consideration. We show that the proposed algorithm provides a sub-optimal length for the FBF and this filter length is more reasonable than the MMSE optimal one regarding system performance. Although the new FBF length is not the optimal one in terms of the MSE criterion, it achieves a good tradeoff between the MSE and the BER performance. Desired system performance is achieved with a reduced computational complexity. Simulation results show that it is also able to track channel changes successfully.

Acknowledgements

The work reported in this paper has formed part of the Research Programme of the Virtual Centre of Excellence in Mobile and Personal Communications, Mobile VCE, www.mobilevce.com, whose funding support, including that of EPSRC, is gratefully acknowledged. Fully detailed technical reports on this research are available to Industrial Members of Mobile VCE.

Appendix

Pseudo code shown below illustrates the algorithm based on the new criterion.

1). Initialization

Set the value of α_{up}, α_{down}, γ_1, γ_2, *the FBF length T and* $\mathbf{W}^{(n)}=\mathbf{0}$, $\mathbf{F}^{(n)}=\mathbf{0}$

2). LMS algorithm

Use (4) and (5) to update the FFF and FBF coefficients

3). Length update algorithm, MSE criterion

Calculate $J_1(n)$ *and* $J_{I-1}(n)$

If $J_1(n) < \alpha_{up} J_{I-1}(n)$, *then*

add "L" extra taps to the FBF, i.e. add one extra segment

If $J_1(n) > \alpha_{down} J_{I-1}(n)$, *then*

remove "L" extra taps from the FBF, i.e. remove one segment

4). New criterion applied

Calculate P_0 *and* P

If $P_0/P < \gamma_1$

Set α_{up} *a new value* α_{up}^1 *(for example* $\alpha_{up}^1=0.9$*);*

else

Set α_{up} *a new value* α_{up}^2 *closer to 1,* $\alpha_{up}^1 < \alpha_{up}^2 < 1$ *(for example* $\alpha_{up}^2=0.995$*);*

end

If $P_0/P < \gamma_2$ $(\gamma_2 < \gamma_1)$

remove 1 tap from the FBF

end

References

1. R. Prasad, *Universal wireless personal communications*: Artech House Boston/London, 1998.
2. D. Falconer, *et al*, "Frequency domain equalization for single-carrier broadband wireless systems", IEEE Comm. Magazine, April 2002, pp. 58-66.
3. D. Falconer, *et al*, White Paper: Frequency domain equalization for single-carrier broadband wireless systems", Feb. 2002. *http://www.sce.carleton.ca/bbw/papers/whitepaper2.pdf*
4. N. Benvenuto and S. Tomasin, "On the comparison between OFDM and single carrier modulation with a DFE using a frequency-domain feedforward filter", IEEE trans. on Comm., Vol. 50, No. 6, June 2002, pp. 947-955.
5. M. Larimore, S. Wood and J. Treichler, "Performance costs for theoretical minimal-length equalizers", ICASSP 1997, Vol. 3, 21-24, pp. 2477-2480.
6. F. Riera-Palou, J. Noras and D.G.M. Cruickshank, "Linear equalisers with dynamic and automatic length selection", IEE Electronic Letters, Vol. 37, No. 25, Dec 2001, pp. 1553-1554.
7. M. Clark, "Adaptive frequency-domain equalization and diversity combining for broadband wireless communications", IEEE J. Select. Areas Comm., Vol. 16, No. 8, Oct. 1998, pp. 1385-1395.
8. J. Proakis, Digital Communications, 3rd Edition, New York: McGraw-Hill, 1995
9. F. Riera-Palou, J. Noras and D.G.M. Cruickshank, "Variable length equalizers for broadband mobile systems", IEEE Vehicular Technology Conference (VTC), Sept. 2000. Vol. 5, pp. 2478-2485.

10. X. Wei, D. G.M. Cruickshank and B. Mulgrew, "Performance of equalizers with dynamic length," IEEE Vehicular Technology Conference (VTC), May 2004.

11. S. Haykin. *Adaptive Filter Theory*. Prentice Hall, 4th edition, 2001

Figures

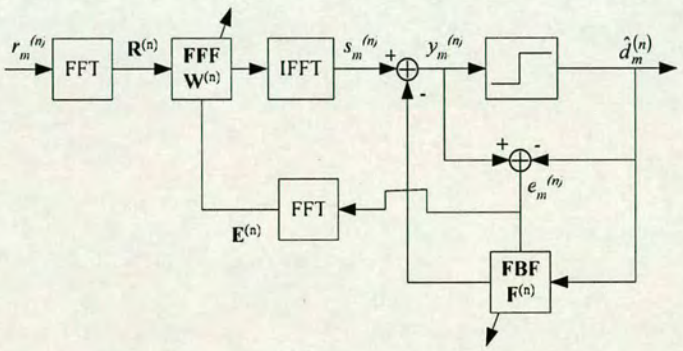

Fig. 1 System Model

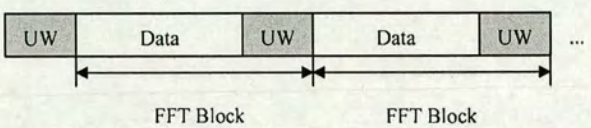

Fig. 2 Frame Structure

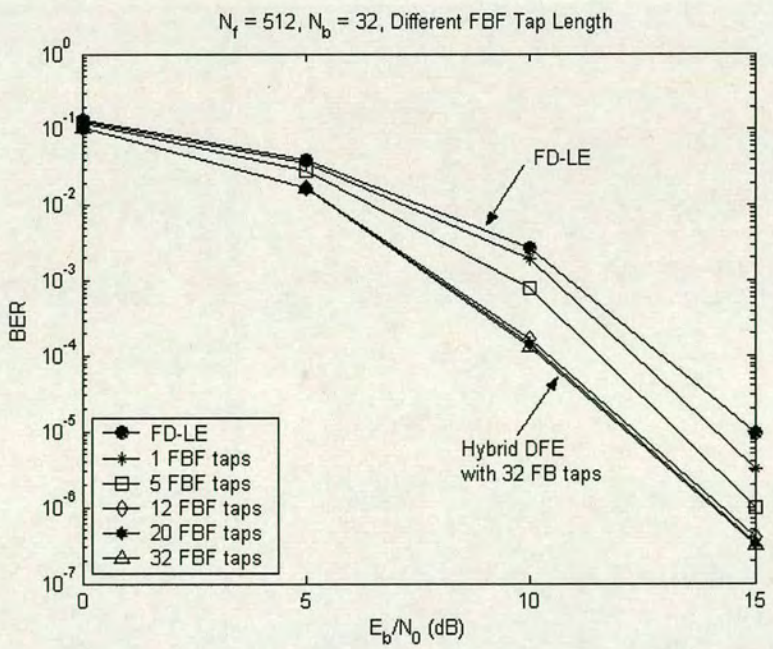

Fig. 3 System performances with different FBF length

(FD-LE: Frequency domain linear equaliser)

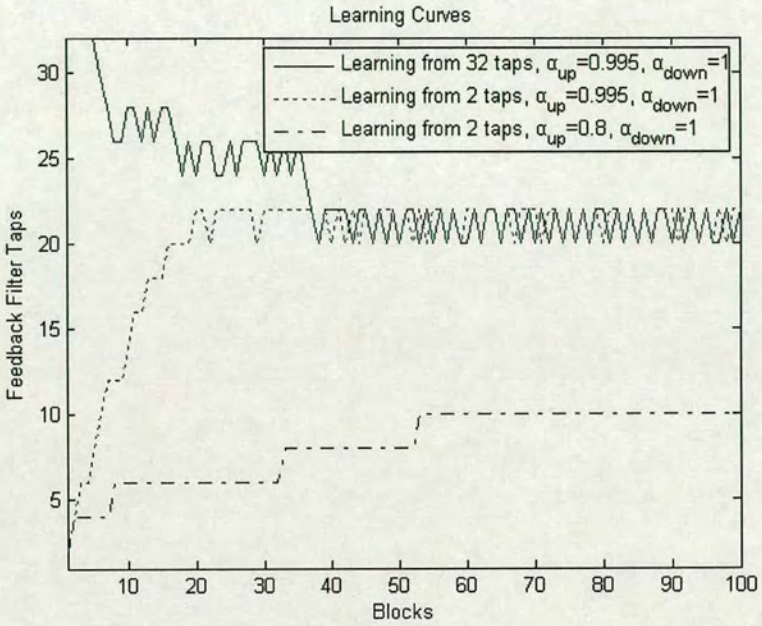

Fig. 4 Learning curves of the adaptive algorithm with different initializations, E_b/N_0=20 dB

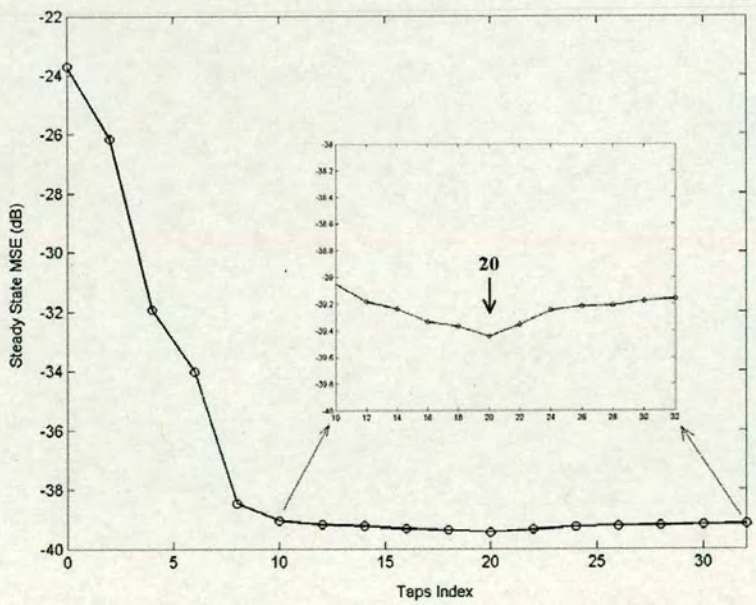

Fig. 5 Steady state MSE achieved vs FBF length

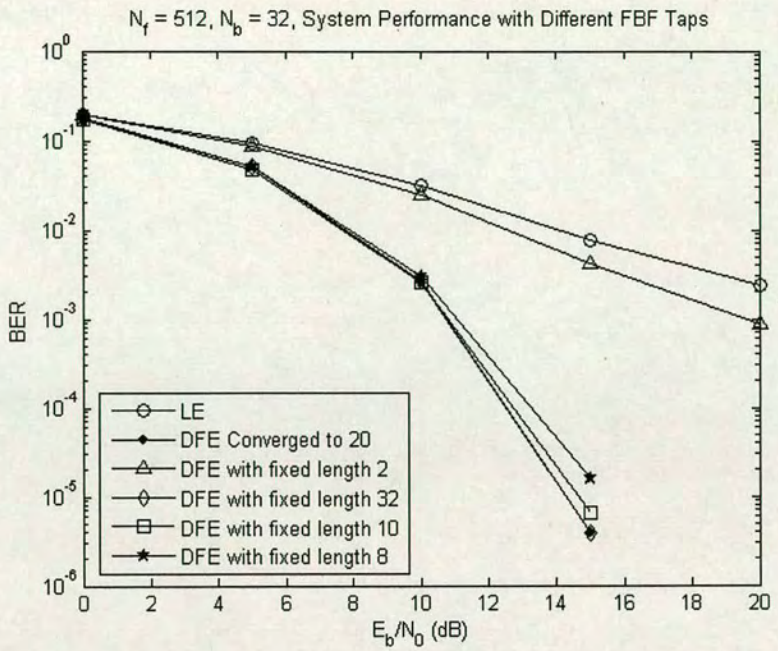

Fig. 6 System performance with variable FBF length

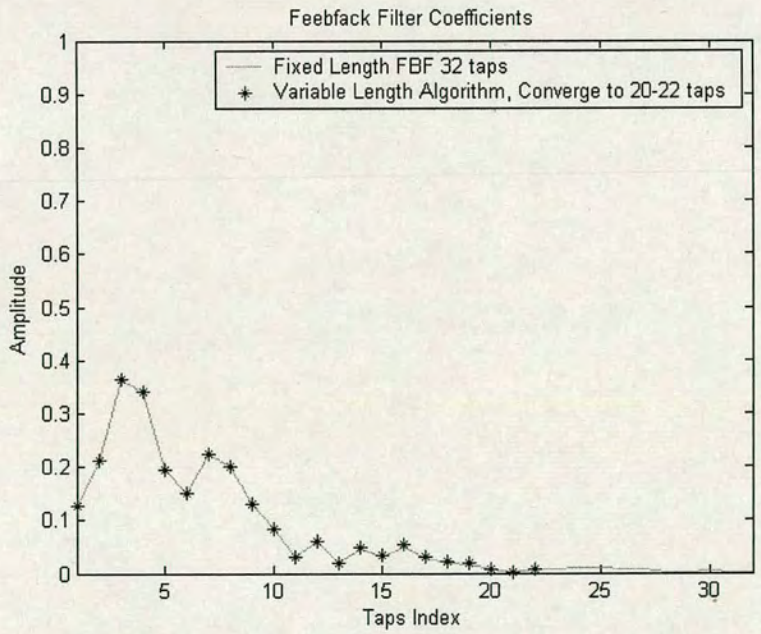

Fig. 7 Converged FBF coefficients, E_b/N_0=20 dB

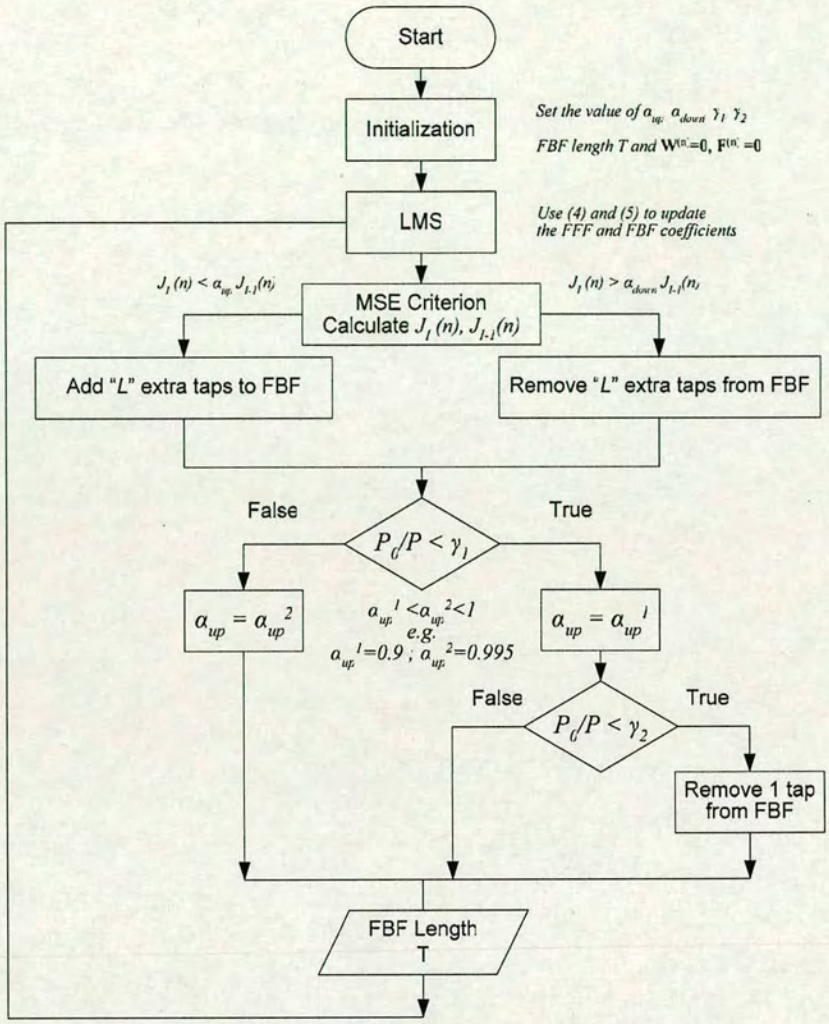

Fig. 8 Flowchart of the new algorithm

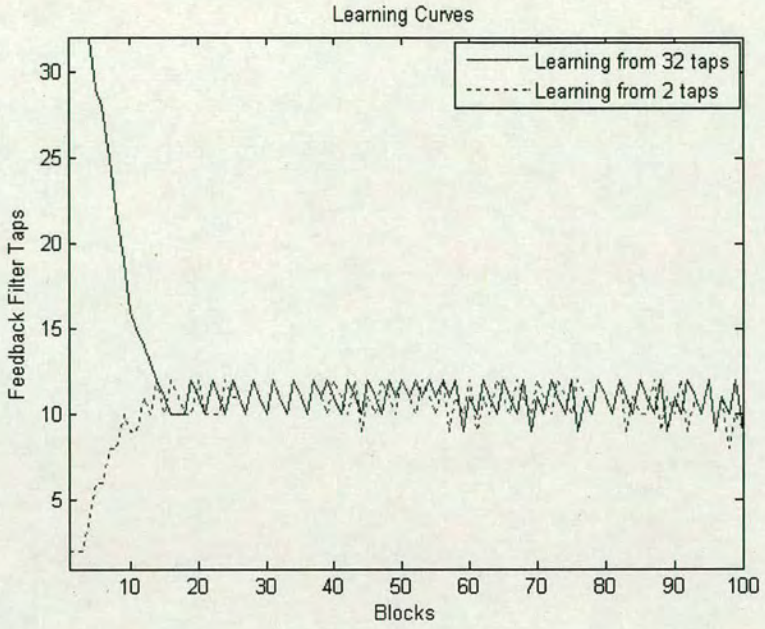

Fig. 9 Learning curves with the new algorithm

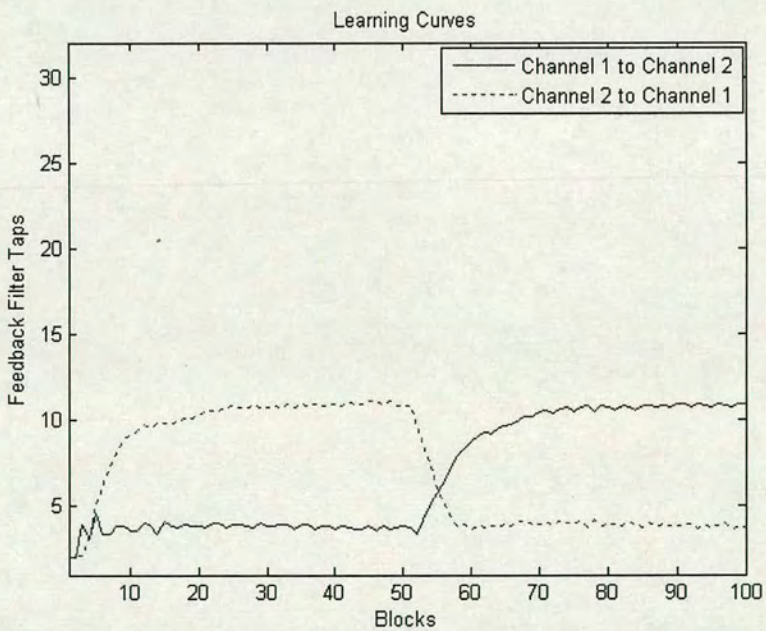

Fig. 10 Learning curves, Channel changes (Y axis feedback filter taps)

Bandwidth Efficient Single Carrier Systems with Frequency Domain Equalization

Y. Li, S. McLaughlin, D. G. M. Cruickshank

A new bandwidth efficient single carrier system with frequency domain equalization (SC-FDE) is proposed. Turbo equalization and cyclic prefix reconstruction are combined together to eliminate the normally required cyclic prefix for such a system. The proposed method achieves much better performance than the residual inter-symbol interference cancellation approach by utilizing soft decoded information and introducing turbo equalization. The performance of the proposed scheme is studied through simulations.

Introduction: Numerous approaches for SC-FDE have been proposed recently [1]. Cyclic prefix (CP) is inserted at the transmitter for such a single carrier system. Like an OFDM system, the CP reduces the bandwidth efficiency. In order to solve this problem, D. Kim proposed a residual inter symbol interference cancellation (RISIC) algorithm in [2]. In [3], soft decoding information has been used for CP reconstruction. This extension of RISIC is of interest in this paper and its performance is compared with our newly proposed algorithm.

Turbo equalization has been a hot topic for the past few years [4]. The turbo concept has been widely studied in equalization, estimation and detection. One drawback of this approach is the exponential increase in complexity with

each iterative process. In order to make it more practical, various sub-optimal methods using minimum mean square error (MMSE) equalizer instead of the maximum a posteriori (MAP) equalizer have been proposed [4][5]. In this paper, a MMSE turbo equalization algorithm and CP reconstruction through an iterative process are combined.

System Model: A convolutionally coded single carrier system is studied. Transmitted signals are BPSK modulated, convolutionally coded, interleaved and divided into successive blocks. Each signal block is then cyclically extended and transmitted through mobile channels. Assuming that the composite channel response $h_i(l)$ is stationary within the i-th block and spans over L symbols, we write the received signal in one block as $r_i(n)$, $0 \le n \le N-1$ where N is the number of symbols within one block. Finally, we use $x_i(n)$ to denote the corresponding transmitted coded signal. At the receiver, the CP is removed and the i-th block signal $r_i(n)$ can be written as:

$$r_i(n) = h_i(l) \otimes x_i(n) + v_i(n) \tag{1}$$

where $\otimes$ and $v_i(n)$ represents circular convolution and a discrete zero mean white Gaussian noise process. When there is no CP, inter block interference (IBI) exists and will affect the current block as:

$$r_i(n) = \sum_{l=0}^{L-1} h_i(l) x_i(n-l) u(n-l) + \sum_{l=0}^{L-1} h_{i-1}(l) x_{i-1}(n+N-l)(1-u(n-l)) + v_i(n) \tag{2}$$

where $u(.)$ represents the unit step function. The IBI caused by the $(i-1)$-th block can be estimated and subtracted from the current block. Then a block signal free of IBI is given by:

$$\tilde{r}_i(n) = r_i(n) - \sum_{l=0}^{L-1} h_{i-1}(l) x_{i-1}(n+N-l)(1-u(n-l)) \tag{3}$$

If the last part of the transmitted signal is known, it can be used for CP reconstruction as shown in (4).

$$\bar{r}_i(n) = \tilde{r}_i(n) + \sum_{l=0}^{L-1} h_i(l) x_i(n+N-l)(1-u(n-l)) \quad (4)$$

Unfortunately, perfect CP reconstruction is not possible since the CP part is not available at the receiver. In the RISIC algorithm [2], the missing CP is regarded as distortion in a time domain block and the amount of distortion is diminished via an iterative CP reconstruction process. However, in channels with deep nulls or long delays, the RISIC fails to achieve a satisfactory performance. The extended version of RISIC [3] exploits the power of feedforward error coding (FEC) for CP reconstruction to obtain more reliable estimates of the missing CP.

Combined turbo equalization and CP reconstruction: Turbo equalization based on MMSE criterion has been widely studied in [4][5]. Since turbo equalization and CP reconstruction are both conducted in an iterative manner, they are jointly combined in one iteration process in a new proposed structure as in Fig. 1. With a slight increase in computational complexity compared to the extended RISIC (For both systems, the complexity is dominated by the MAP decoder), the improvement that can be achieved is significant.

In this paper, we employ the MMSE turbo equalizer for SC-FDE developed by Tüchler in [5]. The extrinsic information $\left[L_E^e(\bar{x}_i(0)),\ldots,L_E^e(\bar{x}_i(N-1))\right]^T$ in Fig. 1 is deinterleaved and delivered to the SISO decoder as $\left[L_E^e(\bar{b}_i(0)),\ldots,L_E^e(\bar{b}_i(N-1))\right]^T$. The SISO decoder delivers the required LLRs for not only the information bits

but also all the coded bits. The hard decision device will decide if the transmitted bit is +1 or -1 based on the sign of the LLRs. The extrinsic LLRs of the coded bits are given by subtracting $\left[L_E^e(\overline{b}_i(0)),...,L_E^e(\overline{b}_i(N-1))\right]^T$ from the output of the SISO decoder $\left[L_D(\overline{b}_i(0)),...,L_D(\overline{b}_i(N-1))\right]^T$, as shown in Fig. 1. $\left[L_D^e(\overline{x}_i(0)),...,L_D^e(\overline{x}_i(N-1))\right]^T$ is then obtained by reinterleaving $\left[L_D^e(\overline{b}_i(0)),...,L_D^e(\overline{b}_i(N-1))\right]^T$. Soft bits generated by $\left[L_D^e(\overline{x}_i(0)),...,L_D^e(\overline{x}_i(N-1))\right]^T$ are used as a-priori information for the MMSE turbo equalizer. They are also utilized in the CP reconstruction block to compensate the effect of the omitting CP. The advantage of using soft bits for CP reconstruction is that it is more reliable since coded bits with small probabilities will not contribute much to the reconstructed part. In comparing the structure of the new scheme and the extended RISIC, we notice that extra computations are for the Fourier transform operations that convert the time domain soft bits $\lambda_i(n)$ into its frequency domain counterpart $\Lambda_i(w)$.

Simulation Results: A coded SC-FDE system with 32 BPSK symbols in each block is first studied. For the FEC code, a 1/2 rate convolutional code with constraint length of 3, the generator polynomials is [1 1 1] and [1 0 1]. Simulations assume perfect knowledge of the channel impulse response. Two kinds of discrete time-invariant channels [6] are used in our simulations: h1 = $[0.227\ 0.460\ 0.688\ 0.460\ 0.227]^T$, h2 = $[0.04\ -0.05\ 0.07\ -0.21\ -0.5\ 0.72\ 0.36\ 0\ 0.21\ 0.03\ 0.07]^T$. There are two deep nulls in the spectrum of channel h1 whilst h2 has moderate nulls but long delay spread. Fig. 2 shows the bit error rate curves of SC-FDE with CP (the CP length is chosen to be 1/4

of the FFT size), extended RISIC for SC-FDE without CP and the new scheme. In Fig. 3, channel h2 is assumed and the coded data symbol per block is changed from 64 to 128. In both cases, the new scheme offers a significant improvement compared to the extended RISIC algorithm.

Conclusion: In this paper, a new combined turbo equalization and CP reconstruction scheme is proposed for a SC-FDE without CP. Two iterative processes are jointly integrated in one structure to compensate for the effect of the missing CP and achieve significant improvements with only a slight increase in computation compared with the extended RISIC method.

References

1 D. Falconer, et al, "Frequency domain equalization for single-carrier broadband wireless systems", IEEE Comm. Mag., April 2002, pp. 58-66.

2 D. Kim, G. Stüber, "Residual ISI Cancellation for OFDM with Applications to HDTV Broadcasting", IEEE J. Select. Areas Comm., Vol. 16, No. 8, Oct. 1998, pp. 1590-1599.

3 T. Hwang; Y. Li, "Iterative cyclic prefix reconstruction for coded single-carrier systems with frequency-domain equalization (SC-FDE)", Vehicular Technology Conference 2003-Spring. Vol. 3 , pp. 1841-1845

4 M. Tüchler, R. Koetter and A. Singer, "Turbo equalization: principles and new results", IEEE Trans. on Comm. Vol. 50, No. 5 , 2002, pp. 754-767

5 M. Tüchler, and J. Hagenauer, "Turbo equalization using frequency domain equalizers", Proc. of the Allerton Conference, Monticello, IL, U.S.A., Oct. 2000.

6 J. Proakis, Digital Communications, 3rd Edition, New York: McGraw-Hill, 1995

Authors' affiliations:

Y. Li, S. McLaughlin, D. G. M. Cruickshank (IDCOM, SEE, University of Edinburgh, Edinburgh EH9 3JL, United Kingdom)
Email: Yushan.Li@ee.ed.ac.uk

Figure captions:

Fig. 1 Combined turbo equalization and CP reconstruction

Fig. 2 Performances for channel h1, FFT size = 64

Fig. 3 Performances for channel h2, FFT size =128

Figure 1

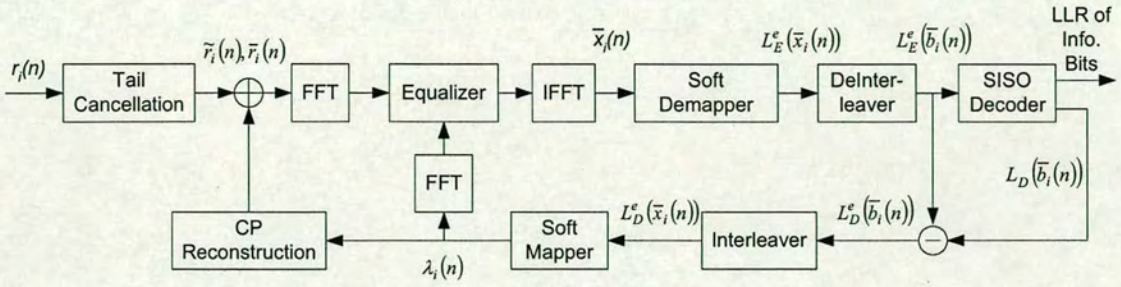
$r_i(n)$
Tail Cancellation
$\tilde{r}_i(n), \bar{r}_i(n)$
FFT
Equalizer
IFFT
$\bar{x}_i(n)$
Soft Demapper
$L_E^e(\bar{x}_i(n))$
DeInter-leaver
$L_E^e(\bar{b}_i(n))$
SISO Decoder
LLR of Info. Bits
$L_D(\bar{b}_i(n))$
FFT
CP Reconstruction
$\lambda_i(n)$
Soft Mapper
$L_D^e(\bar{x}_i(n))$
Interleaver
$L_D^e(\bar{b}_i(n))$

Figure 2

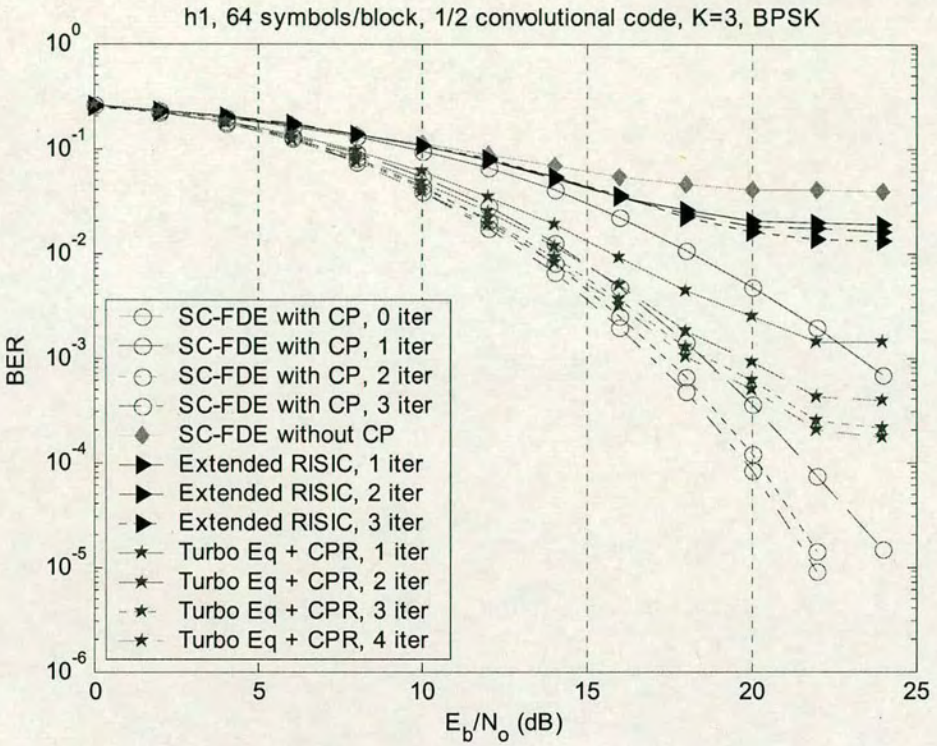
h1, 64 symbols/block, 1/2 convolutional code, K=3, BPSK
BER
E_b/N_o (dB)
SC-FDE with CP, 0 iter
SC-FDE with CP, 1 iter
SC-FDE with CP, 2 iter
SC-FDE with CP, 3 iter
SC-FDE without CP
Extended RISIC, 1 iter
Extended RISIC, 2 iter
Extended RISIC, 3 iter
Turbo Eq + CPR, 1 iter
Turbo Eq + CPR, 2 iter
Turbo Eq + CPR, 3 iter
Turbo Eq + CPR, 4 iter

Figure 3

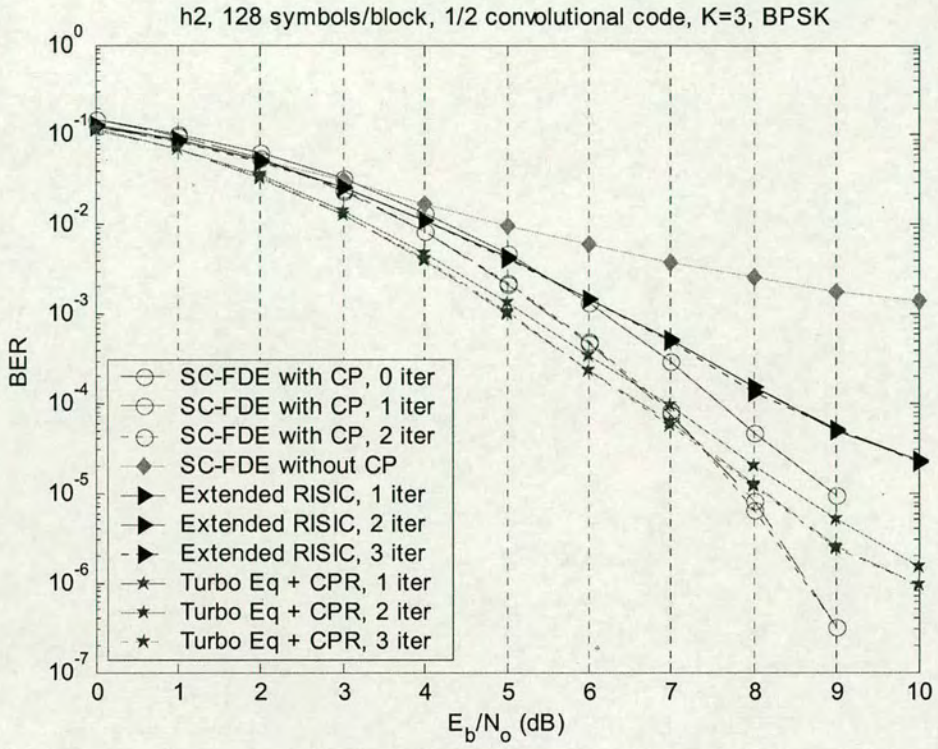
h2, 128 symbols/block, 1/2 convolutional code, K=3, BPSK
BER
E_b/N_o (dB)
SC-FDE with CP, 0 iter
SC-FDE with CP, 1 iter
SC-FDE with CP, 2 iter
SC-FDE without CP
Extended RISIC, 1 iter
Extended RISIC, 2 iter
Extended RISIC, 3 iter
Turbo Eq + CPR, 1 iter
Turbo Eq + CPR, 2 iter
Turbo Eq + CPR, 3 iter

Joint Channel Estimation and Parallel Interference Cancellation for WCDMA

Yushan Li, Steve McLaughlin, David G. M. Cruickshank
Institute for Digital Communications, School of Engineering and Electronics,
University of Edinburgh, King's Buildings, Mayfield Road,
Edinburgh EH9 3JL, UK.
Email: Yushan.Li@ee.ed.ac.uk

Abstract— **In this paper, a novel iterative channel estimation approach is proposed for WCDMA systems. Code-multiplexed pilots are used for channel estimation to maintain bandwidth efficiency. The proposed method reconstructs received waveforms for each user and removes them from the received signal hence the channel estimation accuracy can be improved via another correlation process. Simulation results demonstrate good estimation capability with an allocation of only 10% of the whole power to the pilot channel. In addition, this paper proposes an integrated channel estimator and parallel interference cancellation (PIC) detector. The PIC enables further BER performance improvement to be achieved for the system. The performance of the proposed scheme is studied through simulations and results verify its effectiveness.**

I. Introduction

In 1998, WCDMA was selected as the UMTS terrestrial air interface scheme by the European Telecommunications Standards Institute (ETSI) [1][2]. Channel estimation is a major issue for reliable transmission. The system performance of WCDMA with imperfect channel estimation had been widely studied in recent years [3]-[7]. Usually, there are two types of pilots used in the downlink of WCDMA systems: time-multiplexed pilots [4] and code-multiplexed pilots [5]. The time-multiplexed pilots inevitably require extra bandwidth and hence reduce bandwidth efficiency. Inserting code-multiplexed pilots is an effective means to solve this problem by assigning a pilot signal an individual pseudorandom sequence [3]. This only consumes extra power on sending a known pilot sequence while no bandwidth spreading is necessary. The pilot channel is superimposed on the data channel and continuously transmitted through the same mobile propagation channel. In practice, the correlation method is a simple technique for channel estimation [3][6]. However, the distorted autocorrelation property due to channel impairments degrades its performance, hence a high power code-multiplexed pilot sequence is required for better channel estimates. It introduces high Multiple-Access Interference (MAI) to the data channels. In this paper, we demonstrate that with our new approach, good performance can be achieved while only a small amount of power (10% the whole transmit power) is allocated to the pilot channel.

Performance of CDMA based systems is dominated by the amount of interference generated by simultaneous presence of users. Parallel interference cancellation (PIC) appears as a simple interference suppression scheme, which subtract interferences from users other than the desired one simultaneously without too much delay [8]. In this paper, PIC and channel estimation through one feedback process are combined to form a new scheme.

The rest of the paper is organized as follows. The system model of WCDMA systems and a RAKE receiver are introduced in Section II. In Section III, the proposed channel estimation algorithm is described. Section IV will deal with the joint structure. Simulation results are given in Section V. Finally, conclusions are presented.

II. System Model

In WCDMA systems, a code-multiplexed signal is continuously transmitted from each base station. It is broadcast over the entire cell and used as the phase reference for downlink channels. This channel plays a vital role in the cell searching of mobile station and channel estimation. Two types of chip rate code are used, the scrambling code and the channelization code. The scrambling code is a 38400 chip segment of a Gold code of length $2^{18}-1$ according to the UMTS specifications and it is used for basestation separation. The channelization code is used for separation of different user channels as well as the pilot channel.

In this work only the uncoded downlink scenario is considered: all signals are transmitted symbol and chip synchronously through the same mobile radio channel, perfect synchronization is assumed. Consider K-user's traffic that is QPSK modulated before spreading. The complex envelope of the transmitted signal due to the k-th user can be written as:

$$d_k(t) = \sqrt{E_k} \sum b_k^{(i)} s_k(t - iT), \tag{1}$$

where T denotes the symbol interval; E_k, $b_k^{(i)}$ and $s_k(t)$ denote the average power of the k-th user, the i-th symbol of the k-th user and the spreading chip waveform of the k-th user given by the convolution of spreading sequence and the chip waveform, respectively. The total average data channel power can be represented as $E_d = \sum_{k=1}^{K} E_k$.

After spreading, user data is summed together with the code-multiplexed pilot $p(t)$ which is used to provide phase reference information for data channels. Let E_p be the average power allocated to the pilot channel. We use "g" to denote the

power ratio of the pilot channel to the whole signal power where $g = E_p/(E_d + E_p)$. The transmitted signal being scrambled by a long code $c(t)$ can be written as:

$$x(t) = c(t)\Big[\sum_{k=1}^{K} d_k(t) + \sqrt{E_p}p(t)\Big]$$
$$= c(t)\Big[\sum_{k=1}^{K} \sqrt{E_k}\sum b_k^{(i)} s_k(t - iT) + \sqrt{E_p}p(t)\Big]. \quad (2)$$

The period of one chip is denoted by T_c. All signals that arrive at the receiver from the same basestation have passed through an identical complex channel. The complex FIR filter $h(\tau; t)$ with order L is a composite successive convolution of the transmitter filter, the mobile radio channel and the receiver filter; $h(\tau; t)$ is normally modeled as a wide-sense stationary uncorrelated scattering (WSSUS) zero-mean white Gaussian process as in [9]:

$$h(\tau; t) = \sum_{l=1}^{L} \alpha_l(t) e^{-j\phi_l(t)} \delta(\tau - \tau_l T_c) \quad (3)$$

where $\alpha_l(t)$, $\phi_l(t)$ and $\tau_l T_c$ are the attenuation factor, phase and the propagation delay of the l-th path, respectively. Each path is faded independently according to the Rayleigh distribution and the phase is uniformly distributed over the interval $[0, 2\pi]$.

In this paper, instead of estimating the exact channel parameters like the attenuation factors and phases, we estimate only the in-phase and quadrature-phase components $Re[h_l(t)]$ and $Im[h_l(t)]$ as in [7]. These are two conceptually equal viewpoints on channel estimation. The definition of $h(\tau; t)$ can be rewritten as:

$$h(\tau; t) = \sum_{l=0}^{L-1} h_l(t) \delta(\tau - \tau_l T_c) \quad (4)$$

we further assume that $\sum_{l=0}^{L-1} E\left\{|h_l(t)|^2\right\} = 1$.

At the receiver, the received signal can be represented in an equivalent lowpass form as:

$$r(t) = \sum_{l=0}^{L-1} h_l(t) c(t - \tau_l T_c)\Big[\sum_{k=1}^{K} \sqrt{E_k}\sum b_k^{(i)} s_k(t - iT - \tau_l T_c)$$
$$+ \sqrt{E_p}p(t - \tau_l T_c)\Big] + v(t) \quad (5)$$

where $v(t)$ is the complex-valued lowpass equivalent AWGN.

Let N be the spreading factor for both user data channels and the pilot channel, thus, the symbol duration T is N times the chip period or the sample interval T_c. The received signal in (5) can be represented in its discrete form:

$$r(iN + n) = \sum_{l=0}^{L-1} h_l(iN + n) c(iN + n - \tau_l)$$
$$\times\Big[\sum_{k=1}^{K} \sqrt{E_k} b_k^{(i)} s_k(n - \tau_l)$$
$$+ \sqrt{E_p}p(iN + n - \tau_l)\Big] + v(iN + n) \quad (6)$$

where $0 \le n \le N - 1$ and we use "i" to denote the i-th symbol. The sampled input signal to the l-th RAKE receiver finger is descrambled as:

$$r_l(iN + n) = h_l(iN + n)\Big[\sum_{k=1}^{K} \sqrt{E_k} b_k^{(i)} s_k(n)$$
$$+ \sqrt{E_p}p(iN + n)\Big] + \eta_l(iN + n) \quad (7)$$

In (6), $\eta_l(iN+n)$ accounts for a mixture of additive Gaussian noise, multipath interference and multiple access interference.

We use $\hat{h}_l(iN+n)$ to denote the channel estimates, then the L resolved signals are multiplied by the complex conjugates of $\hat{h}_l(iN + n)$ and maximum ratio combined in the RAKE receiver. Consequently, the output at the $iN+n$ sample interval can be represented as:

$$y(iN + n) = \sum_{l=0}^{L-1} r_l(iN + n)\hat{h}_l^*(iN + n) \quad (8)$$

Finally, despreading and demapping are performed on $y(iN + n)$ to recover the user data symbol.

III. Iterative Channel Estimation

Channel estimation plays an important role in the receiver especially for a RAKE receiver. The system performance strongly depends on the estimate of the channel impulse response. In the section, we review a popularly used conventional channel estimator and subsequently propose a new iterative approach.

A. Correlation Method

The correlation method (CM) had been widely adopted for the design of RAKE receivers [3][6]. In [7], a symbol level estimator is detailed and is briefly reviewed here. Suppose that s_p is the spreading sequence assigned to the pilot channel, the pilot term $p(iN + n)$ in (7) can be rewritten as:

$$p(iN + n) = Ps_p(n) \quad (9)$$

where P denotes the pilot symbol, usually all "1" or "$\frac{1+j}{\sqrt{2}}$". Using the orthogonal property of the spreading codes and assuming the pilot signature sequence is uncorrelated with the noise term $\eta_l(iN + n)$ in (7), if $P = 1$, the i-th pilot symbol at the l-th finger can be recovered as in [7]:

$$\hat{P}_l^i = \frac{1}{N}\sum_{n=0}^{N-1} r_l(iN + n)s_p(n) \quad (10)$$

if $P = \frac{1+j}{\sqrt{2}}$, then $\hat{P}_l^i$ will be detected as:

$$\hat{P}_l^i = \frac{1}{N}\sum_{n=0}^{N-1} r_l(iN + n)s_p(n)(\frac{1-j}{\sqrt{2}}) \quad (11)$$

From (7), we can express the pilot symbol $\hat{P}_l^i$ as:

$$\hat{P}_l^i = \sqrt{E_p}|P|^2 \cdot \frac{1}{N}\sum_{n=0}^{N-1} \hat{h}_l(iN + n) = \sqrt{E_p}|P|^2\hat{h}_l^i \quad (12)$$

Usually we assume that the channel is invariant within an M symbol observation window, i.e. $N_w = M \times N$ chips. Hence, applying a averaging filter, we obtain the channel estimate $\hat{h}_l$ for the this observation period as:

$$\hat{h}_l = \sum_{i}^{i+M-1} \hat{h}_l^i = \frac{1}{\sqrt{E_p}|P|^2} \sum_{i}^{i+M-1} \hat{P}_l^i \tag{13}$$

The correlation method is simple, however, its estimation performance degrades due to the non-ideal autocorrelation properties and has significant influence on the BER performance of the system.

B. Iterative Method

A novel iterative channel estimator for WCDMA systems is introduced in this paper. $\hat{h}_l$ obtained by the correlation method is used as an initial channel estimate for the system. We consider an uncoded system and only hard detection, consequently, estimates of K users' transmitted symbols $\tilde{b}_k^{(i)}$ can be obtained by despreading as:

$$\tilde{b}_k^{(i)} = \frac{1}{N} \sum_{n=0}^{N-1} y(iN+n) s_k(n) \tag{14}$$

Hard detection is performed on $\tilde{b}_k^{(i)}$ and hence $\hat{b}_k^{(i)}$ is obtained. Similar to a PIC scheme, we regenerate the channel distorted waveforms of the k-th user as:

$$\begin{aligned} \hat{r}_k(iN+n) \; = \; & \sqrt{E_k} \sum_{l=0}^{L-1} \hat{h}_l(iN+n) c(iN+n-\tau_l) \\ & \times \hat{b}_k^{(i)} s_k(n-\tau_l) \end{aligned} \tag{15}$$

The reconstructed channel distorted waveforms of all the user channels other than the pilot channel are removed from the composite signal $r(iN+n)$ as:

$$\hat{r}(iN+n) = r(iN+n) - \sum_{k=1}^{K} \hat{r}_k(iN+n) \tag{16}$$

Hence, the good autocorrelation property of the pilot channel can be recovered given perfect channel estimates and correctly detected user symbols. Applying the correlation method on the signal $\hat{r}(iN+n)$, channel estimates are refined and system BER performance is enhaced.

In this paper, a different view from the chip level is given on the correlation method. User data is treated as an independent signal and the aggregation can be considered to be an additive noise on the pilot channel, under the assumption that the pilot sequence is uncorrelated with the data channels and the additive Gaussian white noise, we can derive that:

$$\begin{aligned} & E\left\{ \begin{bmatrix} \hat{r}(iN+n) \\ \vdots \\ \hat{r}(iN+n+L-1) \end{bmatrix} p^*(iN+n) c^*(iN+n) \right\} \\ & = \sqrt{E_p}|P|^2 \begin{bmatrix} \hat{h}_0^{Iter} \\ \vdots \\ \hat{h}_{L-1}^{Iter} \end{bmatrix} \end{aligned} \tag{17}$$

Thus, the complex channel coefficients can be determined up to a fixed scaling factor. The expectation operation is a useful means to combat both the AWGN and the MAI, which can be treated as additive noise. The correlation method in [7] and the one presented in (17) are essentially equal.

IV. Joint Channel Estimation and Parallel Interference Cancellation

Multiple access interference (MAI) cancellation can be achieved in a PIC stage. A multistage PIC cancels the MAI estimated with the hard decisions made in the previous stage. Since the proposed new channel estimator has a similar structure to a parallel interference cancellation, we can easily integrate these two together so that the system BER performance can be further improved with only a slight increase in computation complexity.

After performing the iterative channel estimation in section III, interference from the interfering *K-1* users and the parallel pilot channel are regenerated given the new channel estimates $\hat{h}_l^{Iter}$. Let the u-th user be the desired user and the composite signal excluding the u-th user's information can be regenerated as:

$$\begin{aligned} \tilde{r}(iN+n) = & \sum_{l=0}^{L-1} h_l^{Iter}(iN+n) c(iN+n-\tau_l) \\ & \times \Big[\sum_{k=1, k\neq u}^{K} \sqrt{E_k} \hat{b}_k^{(i)} s_k(n-\tau_l) + \sqrt{E_p} p(iN+n-\tau_l) \Big] \end{aligned} \tag{18}$$

Subsequently, $\tilde{r}(iN+n)$ is subtracted from the received signal $r(iN+n)$ as:

$$\dot{r}(iN+n) = r(iN+n) - \tilde{r}(iN+n) \tag{19}$$

A RAKE receiver is then applied to the MAI cleared signal for a second time and the output is despread and hard-decision detected. Compared with a conventional PIC scheme, the new joint structure requires extra computations mainly on another correlation process and interferences regeneration. It is known that PIC is quite sensitive to channel estimation errors and with a bad initial channel estimate, the PIC would increase the amount of interference rather than cancel it. Adopting the new joint channel estimation and PIC structure, better channel estimates can be obtained for the PIC. With a slight increase in computational complexity, the improvement in system performance that can be achieved is significant.

V. Simulation Results

Computer simulations are carried out at baseband. The chip rate is 3.84 Mchips/s. Walsh codes are used as channelization codes and a 38400 Gold code segment is used as the scrambling code. One pilot channel is code-multiplexed with dedicated data channels. 10% of the whole power is allocated to the pilot channel and the carrier frequency is 2 GHz. The UMTS Vehicular A channel model [10] is used for BER evaluation in our simulation. Each path is faded independently according to a Rayleigh distribution. The corresponding channel profile is shown in Table I.

TABLE I
CHANNEL PROFILE OF THE UMTS VEHICULAR CHANNEL A

Path Delay (nsec)	Avg. Power (dB)
0	0
310	-1.0
710	-9.0
1090	-10.0
1730	-15.0
2510	-20.0

Figure 1 shows the numerical results of system performances when the mobile terminal is moving at different speed. 8 active users are simulated with a spreading factor of 64 and the SNR per bit is fixed at 10 dB. Imperfect channel estimation is considered (channel is estimated based on the pilot channel). Both the correlation method and the new iterative estimation approach are evaluated. It can be seen from Figure 1 that $N_w = 1024$ is a suitable window size for both estimators. It achieves a good BER performance compared with a smaller window size and keeps the performance more stable than choosing a larger window size. We can also see from the figure that the new iterative approach outperforms the conventional correlation method.

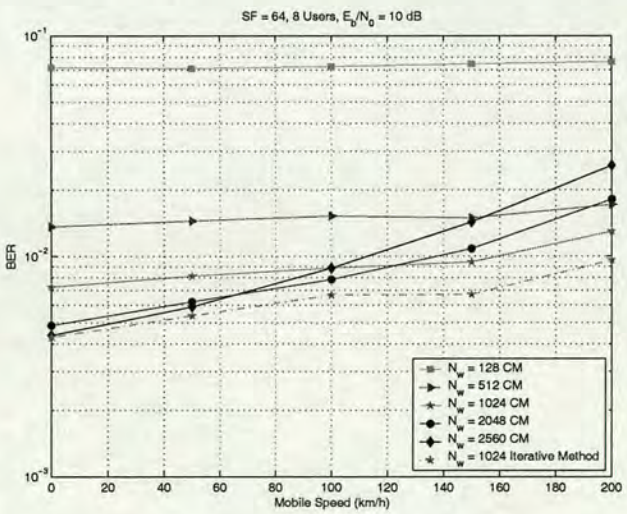

Fig. 1. System BER performance versus Varying mobile speed, SF=64, 8 Active users, $E_b/N_0 = 10$dB

Figure 2 demonstrates the performance of the two estimators with different numbers of active users. The mobile terminal is assumed moving at a speed of 30 km/h. At a required target BER of 2×10^{-2}, using the new method can support 5 more users than the conventional one with a fixed window size $N_w = 1024$.

In Figure 3, we present the BER performance of different detectors with a mobile speed 30 km/h. The spreading factor is 16 and 10 active users are simulated to study their performance

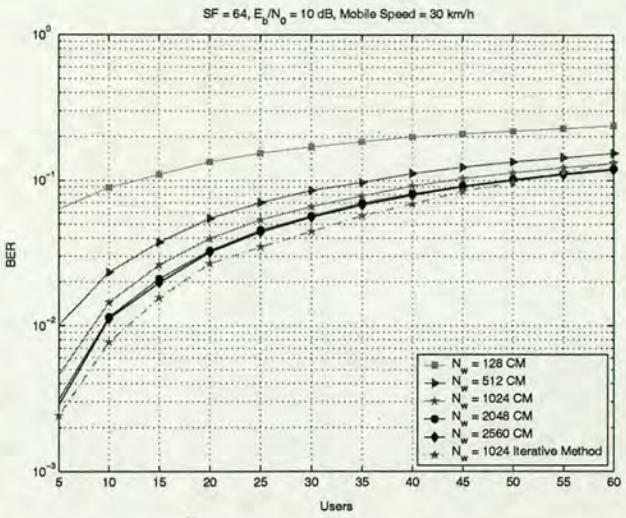

Fig. 2. System BER performance versus Different number of users, SF=64, $E_b/N_0 = 10$dB, Mobile Speed=30 km/h

in a high load scenario. The RAKE performance is dominated by the MAI and with such a high loading this results in saturation at a fairly high error rate. Figure 3 demonstrates the system improvements with PIC. A joint iterative channel estimator and PIC method achieves a 3 dB gain at the BER of 10^{-1} compared with a conventional correlation method with PIC. Since PIC is very sensitive to channel estimation errors, the iterative estimation scheme offers good channel estimates and hence great improvements on system performance. The conventional CM + PIC introduces more interference to the system due to bad channel estimation accuracy and hence worse BER performance. Figure 4 also demonstrates the effectiveness of the joint scheme in a low load scenario when mobile terminal is moving at different speeds. The proposed joint scheme consistently outperforms the other three and achieves good BER performance.

As depicted in Figure 5, in a highly loaded environment, none of the four receiver can achieve good performance. Actually, with the increasing number of users, the performances tend towards the same due to bad channel estimation. Nonetheless, when the number of active users is low, we can still see the enhancement on performance. Interestingly, it can be observed from the results that when there are more than 7 active users in this scenario, even a RAKE receiver with the iterative channel estimator only achieves better performance than the CM + PIC scheme. This is because that the CM fails to provide good estimates and hence the PIC introduces more interference.

VI. CONCLUSION

In this paper a new iterative channel estimation method was studied for WCDMA systems. The new approach is evaluated through simulations and compared with the conventional correlation method in terms of BER performances. Our results

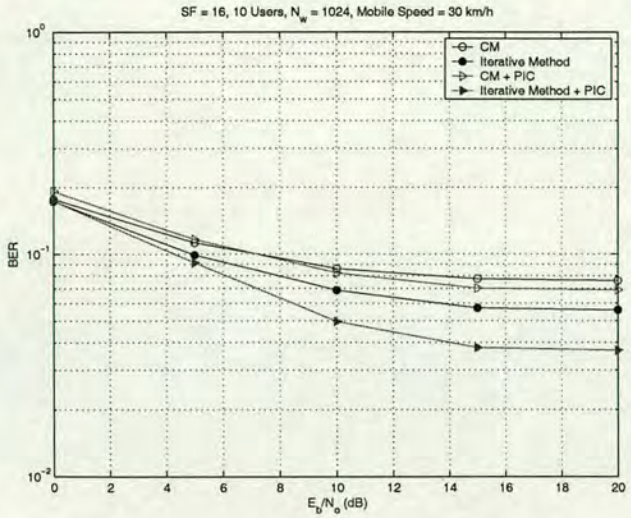

Fig. 3. System BER performance with different detectors, SF=16, 10 Active users, Mobile Speed=30 km/h

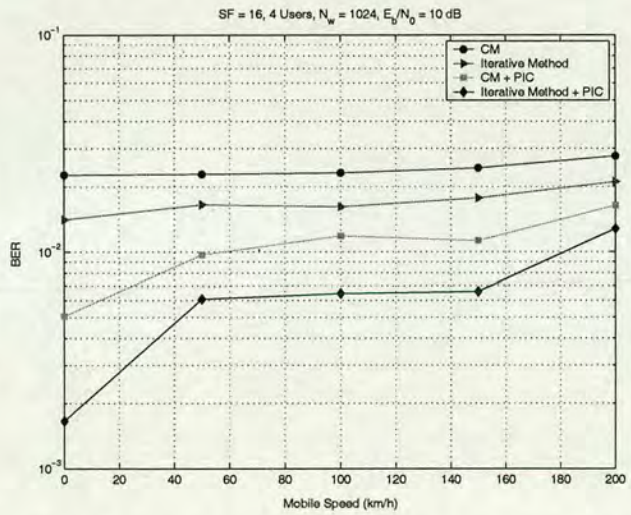

Fig. 4. System BER performance versus Varying mobile speed, SF=16, 4 Active users, $E_b/N_0 = 10$dB

verify the effectiveness of the new method. Moreover, parallel interference cancellation is introduced into the feedback structure. The proposed joint scheme shows good channel estimation accuracy and significant improvements with respect to RAKE receivers with the conventional correlation channel estiamtion.

ACKNOWLEDGMENT

The work reported in this paper has formed part of the Research Programme of the Virtual Centre of Excellence in Mobile and Personal Communications, Mobile VCE, www.mobilevce.com, whose funding support, including that of EPSRC, is gratefully acknowledged. Fully detailed technical reports on this research are available to Industrial Members of Mobile VCE.

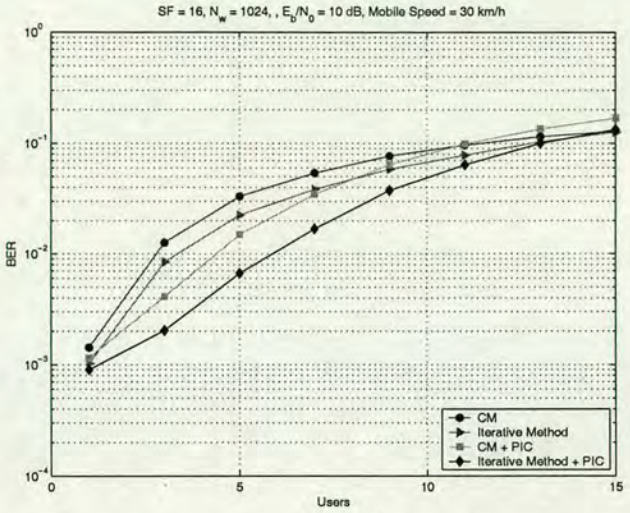

Fig. 5. System BER performance versus Different number of users, SF=16, $E_b/N_0 = 10$dB, Mobile Speed=30 km/h

REFERENCES

[1] H. Holma and A. Toskala, *WCDMA for UMTS*, Wiley Publishing House, 2001

[2] E. Dahlman, *et al*, "WCDMA-The radio interface for future mobile multimedia communications", IEEE Transactions on Vehicular Technology, Vol. 47, No. 4, 1998, pp.1105-1118.

[3] A. Viterbi, *CDMA Principles of Spred Spectrum Communication*, Addison-Wesley Wireless Communications Series, 1995.

[4] P. Schramm and R. Müller, "Pilot symbol assisted BPSK on Rayleigh fading channels with diversity: performance analysis and parameter optimization", IEEE Transactions on Communications, Vol 46, No. 12, 1998, pp. 1560-1563.

[5] P. Schramm, "Analysis and optimisation of pilot-channel-assisted BPSK for DS-CDMA systems", IEEE Transactions on Communications, Vol 46, No. 9, 1998, pp. 1122-1124.

[6] N. Benvenuto, *et al*, "Performance comparison of chip matched filter and RAKE receiver for WCDMA systems", GLOBECOM 2001, pp. 3060-3064.

[7] S. Ko and H. Choi, "Performance analysis of channel estimators for forward link W-CDMA under multipath rayleigh fading channels", IEICE Transactions on Communications, Vol. E86-B, No. 4, 2003, pp. 1212-1223.

[8] D. Koulakiotis and A. Aghvami, "Data detection techniques for DS/CDMA mobile systems: a review", IEEE Personal Communications, No. 6, 2000, pp. 24-34

[9] J. Proakis, *Digital Communications*, 3rd Edition, New York: McGraw-Hill, 1995

[10] ETSI TR 101 112 V3.2.0 (1998-04): Universal Mobile Telecommunications System (UMTS); Selection procedures for the choice of radio transmission technologies of the UMTS.

OFDM System with Cyclic Prefix Reconstruction and MMSE Turbo Equalization

Yushan Li, Steve McLaughlin, David G. M. Cruickshank
Institute for Digital Communications, School of Engineering and Electronics,
University of Edinburgh, King's Buildings, Mayfield Road,
Edinburgh EH9 3JL, UK.
E-Mail: yushan.li@ee.ed.ac.uk

***Abstract*—In this paper, a new OFDM system without a cyclic prefix (CP) is presented. A turbo equalization technique for single carrier systems is extended to OFDM systems. Turbo equalization and cyclic prefix reconstruction are combined together to eliminate the normally required cyclic prefix for such a system. The new method jointly combines turbo equalization and CP reconstruction within the same iterative loop. The performance of the proposed scheme is studied through simulations.**

***Keywords-** OFDM, turbo equalization, CP reconstruction*

I. INTRODUCTION

Orthogonal Frequency Division Multiplexing (OFDM), is capable of providing high rate transmission and has emerged as a strong candidate for the next generation of mobile communications [1]. In OFDM, a cyclic prefix (CP) is inserted at the transmitter to cyclically extend one OFDM symbol. The importance of the CP insertion is twofold; Firstly, the insertion of the CP can effectively mitigate the interference from the preceding block. Secondly, it is because of the preceding CP that the channel distortion on the transmitted signal becomes a circular convolution process. It is worth mentioning that only in this case (or with zero-padding) can the distortion of the channel be considered as a multiplication in the frequency domain.

The CP insertion reduces the bandwidth efficiency of an OFDM system. In order to solve this problem, D. Kim proposed a residual inter symbol interference cancellation (RISIC) algorithm in [2]. In the RISIC algorithm, the missing CP is regarded as bursty distortion in a time domain block and the amount of distortion is diminished in an iterative process with hard decisions being made in the frequency domain. The RISIC approach has been extended by other researchers in [3]. In [3], soft decoding information has been used for CP reconstruction.

The turbo concept has been widely studied in equalization, estimation and detection. In order to make it more practical, various sub-optimal methods using minimum mean square error (MMSE) equalizer instead of the maximum *a posteriori* (MAP) equalizer have been proposed [4][6]. It is shown that the MMSE turbo equalizer is capable of removing the inter symbol interference (ISI) effectively with much less computational complexity.

In this paper, a new algorithm that combines MMSE turbo equalization and CP reconstruction in each iterative loop is presented to form a new OFDM transmission scheme without CP. Hence, the normally required CP is no longer necessary at the transmitter which increases bandwidth efficiency. The extension of RISIC is of interest in this paper and its performance is compared with the new algorithm. Simulation results verify the effectiveness of the proposed scheme.

The rest of the paper is organized as follows. The system model is introduced in Section II. In Section III, the RISIC scheme and its extended version are described. Section IV will deal with a description of the new receiver structure and the algorithm details. Simulation results are given in Section V. Finally, conclusions are presented in Section VI.

II. SYSTEM MODEL

The key point of OFDM is to divide the given channel into several orthogonal sub-channels in the frequency domain. Before the inverse discrete Fast Fourier transform (IFFT)-modulation the original binary input data is encoded by a forward error correction (FEC) code and thereafter interleaved and mapped onto BPSK values $X(w)$, $0 \le w \le N-1$ (N is the IFFT size). Output from the IFFT block is converted into serial data $x(n)$, $0 \le n \le N-1$ in the time domain and a CP is added to form one OFDM symbol for transmission. We assume that the composite channel response $h_i(l)$ is quasi-static within the i-th block and is normalized such that $\sum_{l=0}^{L-1} E\left\{|h_i(l)|^2\right\} = 1$ where L is the channel length.

At the receiver, after discarding the CP, we can write the received signal within the ith OFDM symbol as:

$$\mathbf{r}_i = \mathbf{H}_{c,i}\mathbf{x}_i + \mathbf{v}_i \tag{1}$$

where $\mathbf{r}_i=[r_i(0),\ldots,r_i(N-1)]^T$, $\mathbf{x}_i=[x_i(0),\ldots,x_i(N-1)]^T$, $\mathbf{v}_i=[v_i(0),\ldots,v_i(N-1)]^T$ and $\mathbf{H}_{c,i}$ are one block of the received signal, the transmitted signal with normalized power σ_d^2, discrete zero mean additive white Gaussian noise with variance σ_n^2 and a circular channel matrix with elements $h_i(l)$, respectively. Equation (1) can be rewritten as:

$$r_i(n) = h_i(n) \otimes x_i(n) + v_i(n) \tag{2}$$

where $\otimes$ represents circular convolution.

Using a FFT, the received signal is converted back to the frequency domain and the circular channel matrix is diagonalized, therefore, in the frequency domain,

$$R_i(w) = H_i(w)X_i(w) + V_i(w) \quad , \quad 0 \le w \le N-1 \tag{3}$$

where $0 \le w \le N-1$, $R_i(w), H_i(w), X_i(w)$ and $V_i(w)$ are the DFT of $r_i(n)$, $h_i(l)$, $x_i(n)$ and $v_i(n)$, respectively. A simple one tap per frequency bin MMSE filter can be utilized to deliver equalized signal. If no CP is inserted at the transmitter, a more complex equalizer is necessary at the receiver.

III. RISIC AND ITS EXTENSIONS

In this paper, our purpose is to develop a bandwidth efficient OFDM system, therefore, we first study an OFDM system without CP. When there is no CP inserted, the channel distortion becomes a linear convolution on the transmitted signal and inter symbol interference (ISI) exists, i.e., interference caused by the preceding symbol cannot be eliminated and will affect the current symbol. Thus, we rewrite (2) as:

$$\begin{aligned} r_i(n) &= \sum_{l=0}^{L-1} h_i(l)x_i(n-l)u(n-l) \\ &+ \sum_{l=0}^{L-1} h_{i-1}(l)x_{i-1}(n+N-l)(1-u(n-l)) + v_i(n) \end{aligned} \tag{4}$$

where $u(.)$ represents the unit step function. The second term in (4) represents the ISI caused by the *(i-1)-th* symbol. It can be estimated and subtracted from the current symbol. Then a symbol signal free of ISI is given by:

$$\tilde{r}_i(n) = r_i(n) - \sum_{l=0}^{L-1} h_{i-1}(l)x_{i-1}(n+N-l)(1-u(n-l)) \tag{5}$$

We need to reconstruct the required cyclicity so that the time and frequency-domain descriptions of the convolution are essentially equivalent. If the last part of the transmitted symbol signal is known, then it can be used for CP reconstruction as shown in (6).

$$\bar{r}_i(n) = \tilde{r}_i(n) + \sum_{l=0}^{L-1} h_i(l)x_i(n+N-l)(1-u(n-l)) \tag{6}$$

Correspondingly, in the frequency domain,

$$\bar{R}_i(w) = H_i(w)X_i(w) + V_i(w) \tag{7}$$

Unfortunately, perfect CP reconstruction is not possible since the last part of the signal is not available at the receiver. The RISIC scheme [2] employs an iterative CP reconstruction based on hard detection, and this is discussed together with its extension [3].

In the RISIC algorithm [2], the missing CP is regarded as a distortion in a time domain block and the amount of distortion is diminished via an iterative CP reconstruction process. However, in channels with deep nulls or long delays, RISIC fails to achieve a satisfatory performance. The scheme reported in [3] is an extended version of RISIC that exploits the power of feedforward error coding (FEC) for CP reconstruction to obtain more reliable estimates of the missing CP. Instead of making hard decisions like RISIC, the new approach utilizes soft-input soft-output (SISO) decoder to generate soft information for CP reconstruction. This approach achieves better performance than the RISIC with hard decisions.

IV. COMBINED TURBO EQUALIZATION AND CP RECONSTRUCTION

Motivated by the algorithm proposed in [6], bearing in mind the similarity between a single carrier system with CP and an OFDM system, we derive a MMSE turbo equalizer for OFDM systems and combine it with CP reconstruction through the same iterative process.

Turbo equalization based on MMSE criterion has been widely studied in [4][6]. The channel equalizer can be considered as one component part in a concatenated turbo structure. Extrinsic *posteriori* information from the SISO decoder is utilized to generate "soft bits" as *a priori* information for the MMSE SISO detector. Using the standard BCJR algorithm [5] as the SISO decoder, in turbo equalization, not only the LLRs of information bits are calculated but also the LLR of every coded bit.

Since turbo equalization and CP reconstruction are both conducted in an iterative manner, in a new structure as in Fig. 1, they are jointly combined in one iteration process. With a slight increase in computational complexity compared to the extended RISIC (For both systems, the complexity is dominated by the MAP decoder), the improvement in system performance that can be achieved is significant.

The extrinsic information $\left[L_E^e(\bar{X}_i(0)),\ldots,L_E^e(\bar{X}_i(N-1))\right]^T$ in Fig. 1 is deinterleaved and delivered to the SISO decoder as $\left[L_E^e(\bar{b}_i(0)),\ldots,L_E^e(\bar{b}_i(N-1))\right]^T$. Subscript "*i*" is used to denote the *i*th block. For brevity, the details of the SISO MAP decoding algorithm [5] are omitted. Log-MAP and Max-Log-MAP algorithms can be used to reduce complexity [8][9]. Unlike the decoder in a parallel turbo decoder, the SISO decoder delivers the required LLRs for not only the information bits but also all the coded bits. Only for the last iteration will the SISO decoder generate LLRs for the information bit and feed them to a hard decision device. The hard decision device will decide if the transmitted bit is +1 or -1 based on the sign of the LLRs. The extrinsic LLRs of the coded bits are given by subtracting $\left[L_E^e(\bar{b}_i(0)),\ldots,L_E^e(\bar{b}_i(N-1))\right]^T$ from the output of the SISO decoder $\left[L_D(\bar{b}_i(0)),\ldots,L_D(\bar{b}_i(N-1))\right]^T$, as shown in Fig. 1 and (8):

$$L_D^e(\bar{b}_i(w)) = L_D(\bar{b}_i(w)) - L_E^e(\bar{b}_i(w)) \quad , \quad 0 \le w \le N-1 \tag{8}$$

$\left[L_D^e(\bar{X}_i(0)),\ldots,L_D^e(\bar{X}_i(N-1))\right]^T$ is then obtained by reinterleaving $\left[L_D^e(\bar{b}_i(0)),\ldots,L_D^e(\bar{b}_i(N-1))\right]^T$. Soft bits $\Lambda_i(w)$, $0 \le w \le N-1$, generated by $\Lambda_i(w) = \tanh(\frac{1}{2}L_D^e(\bar{X}_i(w)))$ are used as *a priori* information for the MMSE turbo equalizer. They are also utilized in the CP reconstruction block to compensate

for the effect of omitting the CP. It is more reliable to use soft bits for CP reconstruction since coded bits with small probabilities will not contribute much to the reconstructed part.

The whole process of the new proposed scheme is summarized as follows (I is the iteration index):

Step 1. Tail cancellation (since there is no CP) based on decisions on the previous symbol, for the *i*th symbol, $\tilde{r}_i(n)$ is obtained as in (5).

Step 2. $\tilde{r}_i(n)$ obtained in Step 1 are converted to the frequency domain $\tilde{R}_i(w)$ using FFT,

Step 3. If I=1,

$$\bar{X}_i(w) = W_i^*(w)\tilde{R}_i(w), \quad W_i(w) = \frac{H_i(w)}{|H_i(w)|^2 + \sigma_n^2/\sigma_d^2},$$

and go to Step 5;

Step 4. MMSE equalization. Convert $\bar{r}_i(n)$ into its frequency domain counterpart $\bar{R}_i(w)$.

$$\mu = \frac{1}{N}\cdot\sum_{w=0}^{N-1}\left(\frac{H_i^*(w)H_i(w)}{\sigma_n^2/\sigma_d^2 + H_i^*(w)H_i(w)}\right),$$

$$\bar{X}_i(w) = W_i^*(w)\bar{R}_i(w) + \left(\mu - \frac{H_i^*(w)H_i(w)}{\sigma_n^2/\sigma_d^2 + H_i^*(w)H_i(w)}\right)\Lambda_i(w),$$

Step 5. Soft demapping. $\sigma^2 = \frac{1}{N}\cdot\sum_{n=0}^{N-1}\left|sign\left(\bar{X}_i(w)\right)\cdot\mu - \bar{X}_i(w)\right|$

If I=1, $L_E^e\left(\bar{X}_i(w)\right) = \frac{2}{1-\mu^*}\bar{X}_i(w)$,

else $L_E^e\left(\bar{X}_i(w)\right) = \frac{2\mu}{\sigma^2}\bar{X}_i(w)$, $0 \le w \le N-1$,

Step 6. Deinterleave $L_E^e\left(\bar{X}_i(w)\right)$ for the SISO channel decoder. Compute the *a posteriori* LLRs for the information bits and the coded bits. If I=I_{end}, go to Step 11 (I_{end}: required iterations),

Step 7. Calculate extrinsic information $L_D^e\left(\bar{b}_i(w)\right)$,

Step 8. Interleave $L_D^e\left(\bar{b}_i(w)\right)$ to get $L_D^e\left(\bar{X}_i(w)\right)$. Calculate soft bits, $\Lambda_i(w) = \tanh\left(\frac{1}{2}L_D^e\left(\bar{X}_i(w)\right)\right)$,

Step 9. CP reconstruction ($u(.)$ represents the unit step function, $h_i(.)$ is the time domain channel estimate), Convert $\Lambda_i(w)$ back to the time domain signal $\lambda_i(n)$,

$$\bar{r}_i(n) = \tilde{r}_i(n) + \sum_{l=0}^{L-1} h_i(l)\lambda_i(n+N-l)\left(1-u(n-l)\right),$$

Step 10. I=I+1 and jump to Step 4,

Step 11. Hard decisions are made on the LLRs for the information bits.

V. Simulation Results

A coded OFDM system with 64 BPSK symbols in each block is studied. For the FEC code, a 1/2 rate convolutional code with constraint length of 3, the generator polynomials x^2+x+1 and x^2+1 are used. Coded data are randomly interleaved within one block. No CP is transmitted in our simulations and the missing effect of the CP is reconstructed by both the extended RISIC and our new scheme. Simulations assume perfect knowledge of the channel impulse response. Two kinds of discrete time-invariant channels [6] are used in our simulations:

h1 = $[0.227\ 0.460\ 0.688\ 0.460\ 0.227]^T$,

h2 = $[0.04\ -0.05\ 0.07\ -0.21\ -0.5\ 0.72\ 0.36\ 0\ 0.21\ 0.03\ 0.07]^T$.

There are two deep nulls in the spectrum of channel h1 whilst h2 is a channel with moderate nulls but a long delay spread. The channel power has been normalized to unity and the average transmitted power σ_d^2=1. The frequency selectivity of these channels is given in Fig. 2. In each simulation, turbo equalization performance for OFDM with CP is also given for comparisons.

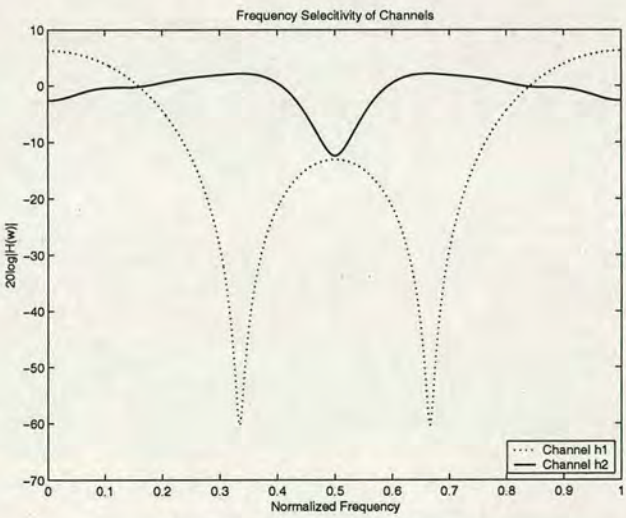

Fig. 2 Frequency selectivity of channels

Fig. 3 and Fig. 4 show the bit error rate curves of an OFDM system with CP (the CP length is chosen to be 1/4 of the FFT size), the extended RISIC and the new scheme when channel h1 and h2 are simulated, respectively. Simulation results with no iterations, after first and second iteration are given in the figure.

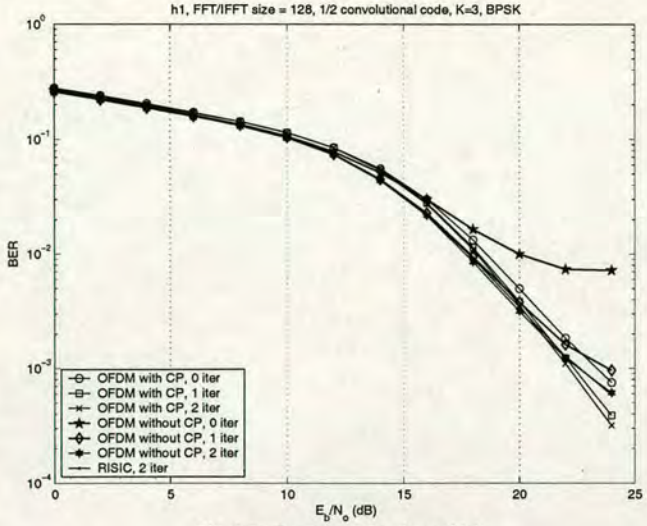

Fig. 3 Performances for channel h1

The new scheme achieves good performance in both cases with only a slight increase in computation compared with the extended RISIC. In Fig.3, it is as good as the extended RISIC while in Fig. 4, it offers about 1dB improvement for the coded system after 2 iterations in terms of BER versus E_b/N_o at the BER of 10^{-3}.

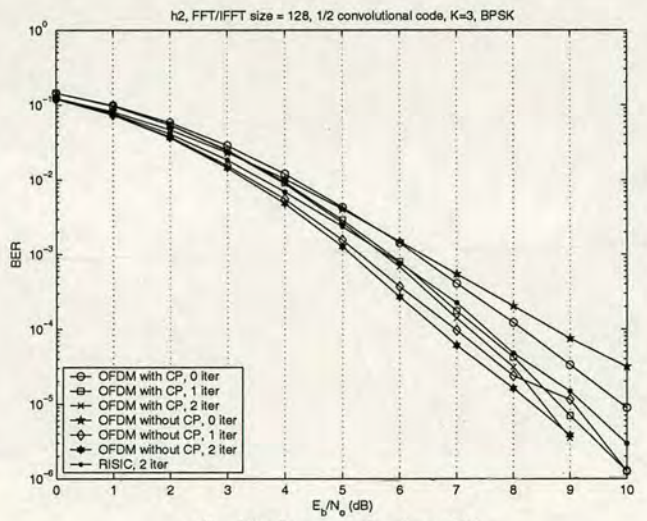

Fig. 4 Performances for channel h2

VI. Conclusion

In this paper, a new combined turbo equalization and CP reconstruction scheme is proposed for an OFDM system without CP. Two iterative processes are jointly integrated in one structure to compensate for the effect of the missing CP and achieve significant improvements with only slightly increasing computations compared with the extended RISIC method. Simulation results verify the effectiveness of the new receiver scheme under two different kinds of channels.

Acknowledgment

The work reported in this paper has formed part of the Research Programme of the Virtual Centre of Excellence in Mobile and Personal Communications, Mobile VCE, www.mobilevce.com, whose funding support, including that of EPSRC, is gratefully acknowledged. Fully detailed technical reports on this research are available to Industrial Members of Mobile VCE.

References

[1] Prasad, R., *Universal wireless personal communications*: Artech House Boston/London, 1998.

[2] D. Kim, G. Stüber, "Residual ISI Cancellation for OFDM with Applications to HDTV Broadcasting", IEEE J. Select. Areas Comm., Vol. 16, No. 8, Oct. 1998, pp. 1590-1599.

[3] T. Hwang; Y. Li, "Iterative cyclic prefix reconstruction for coded single-carrier systems with frequency-domain equalization (SC-FDE)", Vehicular Technology Conference 2003-Spring. Vol. 3 , pp. 1841-1845

[4] R. Koetter, A. Singer, and M. Tüchler, "Turbo equalization", IEEE signal processing magazine, Vol. 21, Issue. 1 , Jan. 2004, pp. 67-80

[5] L. Bahl, J. Cocke, F. Jelinek and J. Raviv, "Optimal decoding of linear codes for minimizing symbol error rate", IEEE Trans. on Info. Theory. Vol. IT-20, Mar. 1974, pp.284-287.

[6] M. Tüchler, and J. Hagenauer, "Turbo equalization using frequency domain equalizers", Proc. of the Allerton Conference, Oct. 2000.

[7] J. Proakis, Digital Communications, 3rd Edition, New York: McGraw-Hill, 1995

[8] P. Robertson, P. Hoeher, "Optimal and sub-optimal maximum a posteriori algorithms suitable for turbo decoding", European Trans. on Telecomm.,Vol. 8, No. 2, March-April 1997, pp. 119-125

[9] J. Hagenauer, E. Offer, and L. Papke, "Iterative decoding of binary block and convolutional codes", IEEE Trans. on Infor. Theory, Vol. 42, No. 2, March 1996, p. 429-445

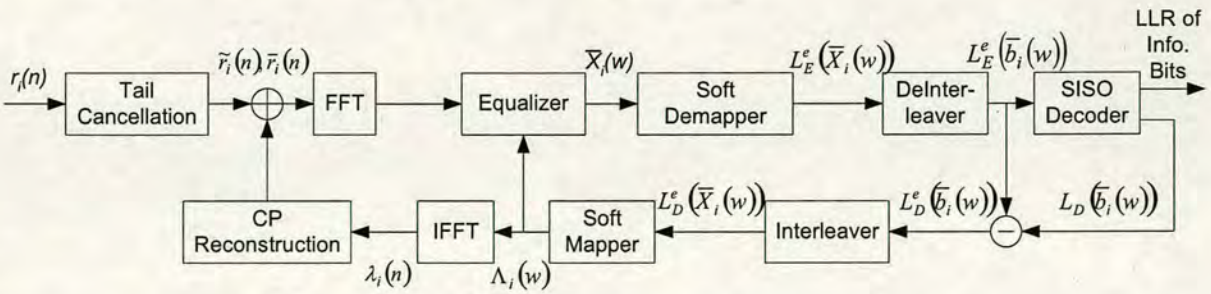

Fig. 1 Combined turbo equalization and CP reconstruction

Cyclic-Prefix CDMA System with Chip Based Equalization and Interference Cancellation

Yushan Li, Steve McLaughlin, David G. M. Cruickshank
Institute for Digital Communications
School of Engineering and Electronics, University of Edinburgh
Edinburgh EH9 3JL, UK Email: Yushan.Li@ee.ed.ac.uk

Abstract—**In this paper, a chip-level MMSE frequency domain equalizer (FDE) is investigated for a Cyclic-Prefix CDMA (CP-CDMA) system. The multiple access interference (MAI) and inter chip interference (ICI) is reduced at the chip level before despreading. One code multiplexed pilot channel carries a higher power than dedicated channels and is utilized for channel estimation. It also brings high MAI to the other users. In this paper, the impact of imperfect channel estimation is studied and a pilot interference cancellation algorithm is proposed. We deploy a high power pilot channel to obtain good channel estimates, subsequently, the high MAI along with the pilot channel is removed by the proposed algorithm. Performance of the proposed algorithm is shown by computer simulations.**

Index Terms—**FDE, chip-level, MAI, interference cancellation**

I. Introduction

ORTHOGONAL Frequency Division Multiplexing (OFDM) has emerged as an efficient transmission scheme that is capable of combating inter-symbol-interference (ISI) and providing high data rates as well as high capacities. It is a strong candidate for the next generation of mobile communication systems. Significant activities have been carried out to employ the OFDM into current systems, especially in multiuser systems. For example, in [1], multicarrier code-division multiple access (MC-CDMA), multicarrier direct sequence CDMA (MC-DS-CDMA) and multitone CDMA (MT-CDMA) had been reviewed. Recently, the cyclic prefix concept from OFDM is introduced into the conventional DS-CDMA system for the sake of enhancing current single carrier 3G-system performance in the near future [2][3][4].

The performance of the conventional RAKE receiver is dominated by the MAI and with 50% traffic loading this will result in saturation at a fairly high error rate. Recently, receivers based on TDMA style channel equalization at the chip level have been proposed for a wideband CDMA (WCDMA) downlink to ensure adequate performance even with a high number of active users [5]. The received chip waveform, distorted by the multi-path channel, is equalized prior to de-spreading. Orthogonality of the signals from the basestation is restored at chip-level.

In this paper, the system performance of a CP-CDMA system with chip-level FDE is studied. The code-multiplexed pilot channel from WCDMA is transmitted for channel estimation and training purposes. It is noteworthy that better channel estimates can be obtained with higher power pilots but this will also result in higher MAI for other users. Therefore, a pilot interference cancellation (IC) scheme is proposed. Unlike the conventional time domain decision feedback equalizer (DFE) [6] and the hybrid DFE structures [7] [8], both the feedforward filter and the feedback filter are designed in the frequency domain, and no decision has to be made since we have the information of pilots at the receiver a-priori. After being used for effective channel estimation and equalization, the interference due to the high power pilot channel is cancelled.

II. CP-CDMA System

A. System Model

In this work only the downlink scenario is considered: all signals are transmitted synchronously through the same mobile radio channel. Let's consider K-user's traffic that is QPSK modulated before spreading. The complex envelope of the transmitted signal due to the k-*th* user can be written as:

$$d_k(t) = A_k \sum b_k^{(i)} s_k(t - iT), \qquad (1)$$

where T denotes the symbol interval; A_k, $b_k^{(i)}$ and $s_k(t)$ denote the average amplitude of the k-*th* user, the i-*th* symbol of the k-*th* user and the spreading chip waveform of the k-*th* user given by the convolution of spreading sequence and the chip waveform, respectively.

Two kinds of different pilot structures are normally used for channel estimation in CDMA systems, i.e., time-multiplexed pilot and code-multiplexed pilot. Time-multiplexed pilot assisted channel estimator performs well for a slow fading and therefore good bit error rate (BER) performance can be achieved. For fast fading channel, code-multiplexed pilot is more attractive since it is continuously transmitted and thus has better tracking capability [10]. In this paper, code-multiplexed pilot structure is employed.

After spreading, user data is summed together with the code-multiplexed pilot $p(t)$ which is used to provide phase

reference information for data channels. We use "α" to denote the power ratio of the pilot channel to the whole signal power. The transmitted signal being scrambled by a long code *c(t)* can be written as:

$$x(t)=c(t)\left[\sum_{k=1}^{K} d_k(t)+p(t)\right]. \quad (2)$$

The scrambled signal is split into successive data blocks with N chips in one block. Unlike MC-CDMA or MC-DS-CDMA, the CP-CDMA system is a single carrier Direct-Sequence CDMA (DS-CDMA) system. With the introduced cyclic prefix concept, a block is cyclic extended to $N+N_{CP}$ chips with the last N_{CP} chips inserted at the beginning of the block. Note that the length of the CP N_{CP} should be no less than the maximum delay of the mobile propagation channel to absorb the ISI. The transmitted block signal is illustrated in Fig. 1.

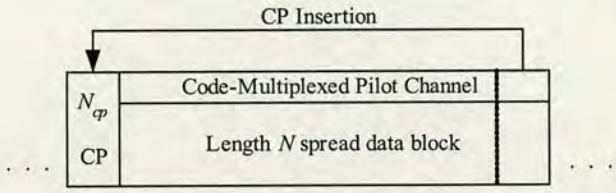

Fig. 1. CP-CDMA block signal

All signals that arrive at the receiver from the same basestation have passed through an identical complex channel. The discrete-time output signal in the receiver can be seen as the response of a complex digital filter to the transmitted signal. The complex FIR filter *h(l)* with order L is a composite successive convolution of the transmitter filter, the mobile radio channel and the receiver filter.

At the receiver, perfect synchronisation is assumed and the CP is discarded before equalization. We write the received signal in one block as $r_i(n)$, $0\le n\le N-1$, where i is the block index. $x_i(n)$ denotes the corresponding transmitted block signal. Therefore, assuming that the composite channel response $h_i(l)$ is quasi-static within the i-th block, the relation between $r_i(n)$ and $x_i(n)$ can be written as:

$$r_i(n)=x_i(n)\otimes h_i(n)+v_i(n), \quad (3)$$

where $v_i(n)$ is additive Gaussian noise and " $\otimes$ " denotes circular convolution. Because of the inserted CP, the distortion of the channel is considered as a multiplication in the frequency domain. Thus, in the frequency domain,

$$R_i(w)=H_i(w)X_i(w)+V_i(w), \quad (4)$$

where $0\le w\le N-1$, $R_i(w)$, $H_i(w)$, $X_i(w)$ and $V_i(w)$ are the DFT of $r_i(n)$, $h_i(l)$, $x_i(n)$ and $v_i(n)$, respectively.

B. Channel Estimation and Equalization

In this paper, the impact of imperfect channel estimation (CE) is taken in consideration. Under the assumption that the pilot sequence is uncorrelated with the data channels and the additive Gaussian white noise, we can derive that:

$$E\left\{\begin{bmatrix} r_i(n-N-L+2) \\ \vdots \\ r_i(n) \end{bmatrix} \times p_i(n-N+1)^* \times c_i(n-N+1)^*\right\}$$
$$=\sigma_P^2 E\left\{\begin{bmatrix} h_i(0) \\ \vdots \\ h_i(L-1) \\ 0 \\ \vdots \\ 0 \end{bmatrix}\right\}=\sigma_P^2\hat{\mathbf{h}}_i, \quad (5)$$

where σ_P^2 is the average power of the pilot sequence and $\hat{\mathbf{h}}_i$ is the channel estimate of the i-th block. The complex channel coefficients can thus be determined with a fixed scaling factor.

The minimum mean square error (MMSE) equalizer $W_i(w)$ in the frequency domain is given by the following expression:

$$W_i(w)=\frac{H_i^*(w)}{|H_i(w)|^2+\sigma_n^2/\sigma_d^2}. \quad (6)$$

σ_n^2, σ_d^2 and $H_i^*(w)$ are the variance of the additive Gaussian noise, the variance of the received signal and the conjugate of $H_i(w)$, respectively. Consequently, the equalized signal is converted back to the time domain. The scrambling code is then removed and the composite signal is despreaded and decoded.

III. Pilot Interference Cancellation

Decision feedback equalization (DFE) is known to outperform linear equalizer especially in cases where deep nulls appear in the channel power spectrum because that it can provide further ISI cancellation with reduced noise enhancement [6]. On the other hand, as a result of its nonlinear feedback nature, the wrong decision will cause error propagation. Some hybrid DFE structures have been proposed recently in [7] and [8]. The feedforward filtering is performed in the frequency domain while the feedback filter still works in the time domain. However, there is no simple solution for the design of the feedback filter in these hybrid structures.

The pilot channel dominates the interference in MAI due to its high power. Obviously, a high power pilot channel can give us a good channel estimates. But, on the other hand, this will lead to two drawbacks, one is the high MAI within the current cell and the other is the resultant high interference for neighbouring cells. It is desirable to remove this part of interference caused by the high power pilot channel as we have enough information at the receiver. Since the pilot channel is known at the receiver, no decision has to be made; we then have a data aided cancellation problem.

We define the cost function in the frequency domain as:

$$J=E\left[\frac{1}{N}\sum_{w=0}^{N-1}\left(\left|W_i(w)R_i(w)-G_i(w)P_i(w)-X_{i,residual}(w)\right|^2\right)\right] \quad (7)$$

where $W_i(w)$, $G_i(w)$, $P_i(w)$ and $X_{i,residual}(w)$ denote frequency response of the feedforward equalizer, frequency response of

the feedback pilot cancellation filter, the DFT of $p_i(n)$ (discrete $p(t)$ in the i-th block) and the time domain signal excluding pilot signal ($x_{i,residual}(n)$), respectively. The first term in the bracket is the output of the feedforward equalizer and the second one represents the feedback for pilot channel interference cancellation. The basic idea of the interference cancellation is to minimize J with respect to both the feedforward equalizer and the interference canceller.

Because $x_{i,residual}(n)$ and $p_i(n)$ are mutually uncorrelated, the cost function in (7) can be converted to:

$$J=\frac{1}{N}\sum_{w=0}^{N-1}\begin{Bmatrix} E\left[\left|X_{i,residual}(w)\right|^2\cdot\left|1-H_i(w)W_i(w)\right|^2\right] \\ +E\left[\left|P_i(w)\right|^2\cdot\left|H_i(w)W_i(w)-G_i(w)\right|^2\right] \\ +E\left[\left|V_i(w)\right|^2\cdot\left|W_i(w)\right|^2\right] \end{Bmatrix}. \quad (8)$$

Given $E\left(\left|X_{i,residual}(w)\right|^2\right)=\sigma^2_{residual}$, $E\left(\left|P_i(w)\right|^2\right)=\sigma_P^2$, (8)

can be written as:

$$J=\frac{1}{N}\sum_{w=0}^{N-1}\begin{bmatrix}\sigma^2_{residual}\left|1-H_i(w)W_i(w)\right|^2+\sigma_n^2\left|W_i(w)\right|^2 \\ +\sigma_P^2\left|G_i(w)-H_i(w)W_i(w)\right|^2\end{bmatrix}. \quad (9)$$

The gradient of J with respect to the equalizer coefficients $W_i(w)$ is given by:

$$\nabla_{W_i(w)}J=\frac{\partial J}{\partial W_i(w)} =\frac{1}{N}\begin{bmatrix}-\left(\sigma^2_{residual}+\sigma_P^2G_i^*(w)\right)H_i(w) \\ +\left(\sigma_n^2+\left(\sigma^2_{residual}+\sigma_P^2\right)H_i(w)\right|^2\Big)W_i^*(w)\end{bmatrix} \quad (10)$$

Let $\nabla_{W_i(w)}J=0$, hence we have:

$$\left(\sigma_n^2+\left(\sigma^2_{residual}+\sigma_P^2\right)H_i(w)\right|^2\Big)W_i(w) =\left(\sigma^2_{residual}+\sigma_P^2G_i(w)\right)H_i^*(w) \quad (11)$$

Therefore, the forward frequency domain equalizer is determined by its coefficients:

$$W_i(w)=\frac{\left(\sigma^2_{residual}+\sigma_P^2G_i(w)\right)H_i^*(w)}{\sigma_n^2+\left(\sigma^2_{residual}+\sigma_P^2\right)H_i(w)\right|^2}, \quad w=0,\ldots,N-1. \quad (12)$$

Now inserting (12) back to (9) and then applying the gradient method to it with respect to the feedback filter $G_i(w)$ this time. Let

$$J_1=\sigma^2_{residual}\left|1-H_i(w)W_i(w)\right|^2,$$

$$J_2=\sigma_n^2\left|W_i(w)\right|^2,$$

$$J_3=\sigma_P^2\left|G_i(w)-H_i(w)W_i(w)\right|^2.$$

Subsequently, we derive the gradients of J_1, J_2, J_3 with respect to $G_i(w)$, respectively. Let $\nabla_{G_i(w)}J=0$, then $\nabla_{G_i(w)}\left(J_1+J_2+J_3\right)=0$, we are able to determine the coefficients of $G_i(w)$. The feedback filter coefficients $G_i(w)$ take the form:

$$G_i(w)=\frac{\sigma^2_{residual}\left|H_i(w)\right|^2}{\sigma^2_{residual}\left|H_i(w)\right|^2+\sigma_n^2}=\frac{\left|H_i(w)\right|^2}{\left|H_i(w)\right|^2+\sigma_n^2/\sigma^2_{residual}} \quad (13)$$

Once $G_i(w)$ is determined, $W_i(w)$ is then given by (12).

It is easily verified that when α=0, i.e. no pilot signal is transmitted, then $\sigma_P^2=0$ and $\sigma^2_{residual}=\sigma_d^2$. Consequently, (12) turns into:

$$W_i(w)=\frac{H_i^*(w)}{\left|H_i(w)\right|^2+\sigma_n^2/\sigma_d^2}, \quad (14)$$

which is identical to (6), a conventional FDE.

First, the received signal will be equalized by the forward filter with coefficients $W_i(w)$, then, in the frequency domain, the feedback interference cancellation filter with coefficients $G_i(w)$ is cancelled because the pilot signal is known at the receiver. The output in the frequency domain, $W_i(w)R_i(w)$-$G_i(w)P_i(w)$, is transformed back to the time domain by IFFT. The procedure is summarised in Fig. 2.

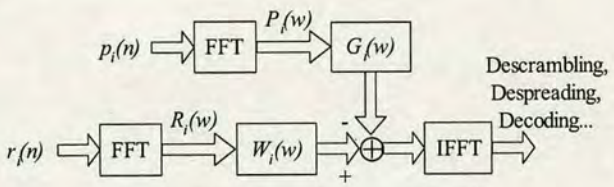

Fig. 2. Interference cancellation system model

IV. Simulation Results

Computer simulations are carried out at base band for the investigation of the proposed algorithm. The system BER performance under the Vehicular A channel [9] is studied. The corresponding channel impulse response is shown in Fig. 3.

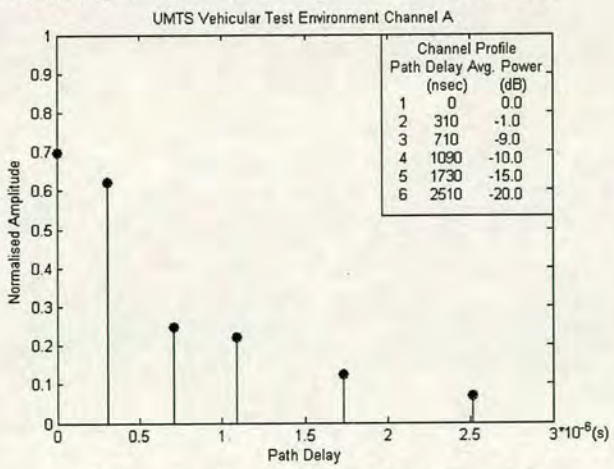

Fig. 3. Channel profile of the UMTS Vehicular Channel A

Each path is faded independently according to the Rayleigh distribution. The chip rate is 3.84 Mchips/s. Walsh codes with length 16 are used as channelization codes and a 512 Gold code is used as the scrambling code. One pilot channel is

code-multiplexed with 8 dedicated data channels. The block size is 512 excluding the 16 chips CP. The CP duration 4.16 μs is selected larger enough than the longest channel delay spread 2.51 μs. In our simulations, the terminal is assumed moving at 50 km/h, and the carrier frequency is 2 GHz.

First, perfect channel knowledge is assumed at the receiver. In Fig. 4, system performances of the FDE with IC and without IC are both shown. Two cases, α=20% and α=40%, are studied. Simulation result with perfect channel estimation and perfect IC is given as a theoretical bound in all figures. It can be seen in Fig. 4 that the pilot channel with α=20% induces less interference than that with α=40%. With the proposed IC algorithm, the interference caused by the pilot channel is removed.

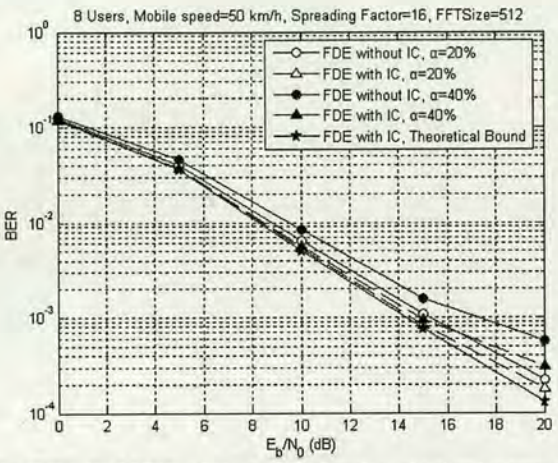

Fig. 4. Simulated BER performances (Perfect channel estimation assumed)

However, such an assumption is not practicable for communication systems since it is impossible to have all the information of the mobile channel. Therefore, imperfect channel estimation is considered (channel is estimated based on the pilot channel). Simulation results in the same scenarios but combined with channel estimation are presented in Fig. 5.

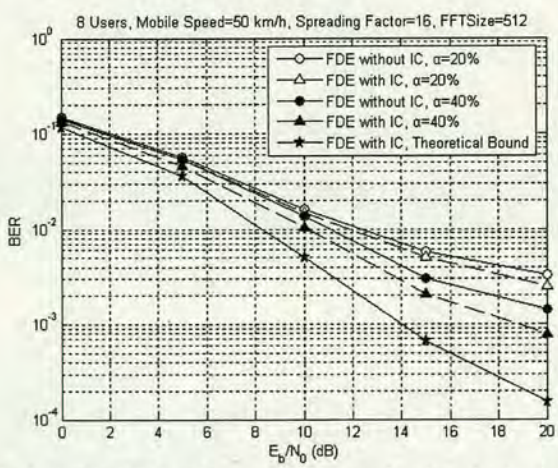

Fig. 5. Simulated BER performances (With imperfect channel estimation)

Now, although a pilot channel with only 20% of the whole signal power induces less interference, the BER performance is worse than that with α=40%. This is because that when the power ratio of the pilots over the whole signal power is small, channel estimation is poor so that the system performance is degraded. The higher the pilot power is, the better the channel estimates can be achieved. However, this will lead to a large MAI with large error probability, as will be shown later in the study of effective throughput. It can be seen in Fig. 5, there is a 2 dB improvement for the FDE with IC (α=40%) over the FDE without IC (α=20%) at the BER of 10^{-2}. With the proposed IC algorithm, we are able to deploy a higher power pilot channel in the CP-CDMA system to obtain a better channel estimates and hence better system performance. The contribution of the pilot channel can be removed from the compound signal to some extent.

V. Conclusions

An interference cancellation algorithm for a CP-CDMA system has been proposed in this paper. A code-multiplexed pilot channel is transmitted for channel estimation purpose. With a higher power code-multiplexed pilot channel, better channel estimate can be obtained. In the meanwhile, this will also cause higher interference than with low power pilots. The contribution of the high power pilots is removed from the compound signal to some extent. The technique of cancelling pilot interference shows much merit. Before the signals are decoded, the interference is made less significant.

Acknowledgment

The work reported in this paper has formed part of the Research Programme of the Virtual Centre of Excellence in Mobile and Personal Communications, Mobile VCE, www.mobilevce.com, whose funding support, including that of EPSRC, is gratefully acknowledged. Fully detailed technical reports on this research are available to Industrial Members of Mobile VCE.

References

[1] S. Hara, R. Prasad, "Overview of multicarrier CDMA", IEEE Communications Magazine, Vol. 35, Issue. 12, Dec. 1997, pp. 126-133.

[2] K. Baum, T. Thomas, F. Vook, and V. Nangia, "Cyclic-Prefix CDMA: an improved transmission method for broadband DS-CDMA cellular systems", WCNC2002. Vol. 1, pp. 183-188.

[3] F. Vook, T. Thomas, and K. Baum, "Cyclic-Prefix CDMA with antenna diversity", VTC Spring 2002. Vol. 2, pp.1002-1006.

[4] P. Lin, T. Chiueh, "Low complexity frequency-domain despreading for cyclic-prefix CDMA systems", IEEE Communications Letters, Vol. 8, No. 6, June 2004, pp. 339-341.

[5] K. Hooli, *et al*, "Chip-level Channel equalization in WCDMA downlink", EURASIP Journal on Applied Signal processing 2002, pp. 757-770.

[6] J. Proakis, *Digital Communications*, 3rd Edition, New York: McGraw-Hill, 1995

[7] N. Benvenuto and S. Tomasin, "On the comparison between OFDM and single carrier modulation with a DFE using a frequency-domain feedforward filter", IEEE Trans. on Comm. Vol. 50, No. 6, 2002, pp 947-955.

[8] D. Falconer, *et al*, "Frequency domain equalization for single-carrier broadband wireless systems", IEEE Comm. Mag., April 2002, pp. 58-66.
[9] ETSI TR 101 112 V3.2.0 (1998-04): Universal Mobile Telecommunications System (UMTS); Selection procedures for the choice of radio transmission technologies of the UMTS.
[10] S. Takaoka and F. Adachi, "Frequency-domain channel estimation using FFT/IFFT for DS-CDMA mobile radio", VTC Fall, 2004.

UMTS FDD Frequency Domain Equalization Based on Self Cyclic Reconstruction

Yushan Li, Steve McLaughlin, David G. M. Cruickshank
Institute for Digital Communications, School of Engineering and Electronics,
University of Edinburgh, King's Buildings, Mayfield Road,
Edinburgh EH9 3JL, UK.
E-Mail: yushan.li@ee.ed.ac.uk

Abstract—**In this paper, a new chip-level MMSE frequency domain equalizer (FDE) is investigated for the downlink frequency division duplex (FDD) mode in UMTS (Universal Mobile Telephone System). The multiple access interference (MAI) and inter chip interference (ICI) can be reduced at the chip level before despreading. For frequency domain equalization, the cyclicity of the received block signal needs to be reconstructed if neither cyclic prefix nor zero-padding are used at the transmitter. We exploit the relationship between the reconstructed part and the equalized signal itself and derive a self cyclic reconstruction scheme. Performance of the proposed MMSE-FDE is shown by computer simulations, compared with performance of FDE with perfect reconstructions. It is shown that the conventional time domain equalization can be implemented in the frequency domain, thus a multimode receiver that can handle both UMTS and OFDM systems in one equalization structure is feasible.**

Keywords- *FDE, UMTS, chip-level, MMSE, multimode receiver*

I. INTRODUCTION

Orthogonal Frequency Division Multiplexed (OFDM) is an air-interface technology that can effectively combat multipath effects in mobile propagation channels. It is a strong candidate for future 4G mobile communications [1]. In many of the discussions regarding 4G communication systems, multimode receivers that are capable of handling different systems are in great demand. Current wireless LAN (WLAN) systems, as well as digital audio broadcasting (DAB) system and digital video broadcasting (DVB) system are all based on OFDM transmission. Thus, there is a demand for the design of a multimode receiver which is capable of handling the OFDM based standards and UMTS. Conventionally, it is easy to design a multimode receiver with two branches, one for OFDM and one for direct sequence CDMA (DS-CDMA) system. However, a wise approach is to employ a frequency domain equalizer for UMTS in the receiver, making use of the powerful FFT/IFFT for both DS-CDMA and OFDM systems in the handset.

Recently, receivers based on TDMA style channel equalization at the chip level have been proposed for a wideband code-division multiple access (WCDMA) downlink to ensure adequate performance even with a high number of active users [2]. The received chip waveform, distorted by the multi-path channel, is equalized prior to de-spreading. Orthogonality of the signal from the basestation is restored at chip-level.

In [3][4], single-carrier systems with frequency domain equalization (SC-FDE) have been proposed recently. They use the same mechanism as in OFDM, i.e. a cyclic prefix (CP) is inserted to absorb the multi-path effect. By inserting the CP at the transmitter and discarding it at the receiver, the linear convolution channel with inter block interference (IBI) is converted to a circular one without IBI. Unfortunately, the CP-based FDE is not compatible with the current WCDMA/UMTS system because the CP insertion will inevitably destroy the frame structure. It is desirable to design a receiver without changing the transmitted signal.

In this paper, a new FDE is proposed and investigated which will not change the format of the transmitted signal. We reconstruct the required cyclicity for the frequency domain equalization. The proposed algorithm fully exploits the relationship between the reconstructed part and the equalized signal itself. Unlike the algorithms proposed in [5][6], the "overlap-cut" processing is not necessary.

The rest of the paper is organized as follows. The system model of UMTS-FDD is introduced in section II. In Section III, the proposed algorithm is described. Section IV will deal with the parameters selection. Simulation results are given in Section V. Finally, conclusions are presented.

II. UMTS DOWNLINK SYSTEM MODEL

A. *UMTS Downlink*

In 1998, WCDMA was selected as the UMTS terrestrial air interface scheme for the FDD mode in European Telecommunications Standards Institute (ETSI) [7][8]. UMTS is capable of providing variable bit rates (144 kbps for vehicle speed, rural environment; 384 kbps for walking speed, urban outdoor; 2048 kbps for fixed, indoor environment) and different quality of service (QoS) for different connections. The frequency division duplex (FDD) mode and the time division duplex TDD mode are both working in the 2 GHz band, with a basic chip rate of 3.84 Mcps and a flexible carrier spacing of 4.4-5.0 MHz. QPSK modulation is adopted and allows use of the same channelization code for both I and Q channels. This paper will only focus on the UMTS FDD downlink transmission. In the FDD downlink, the general frame structure

0-7803-8938-7/05/$20.00 (C) 2005 IEEE

is shown in Fig. 1. It can be seen that one frame with duration of 10 ms can be divided into 15 slots [9].

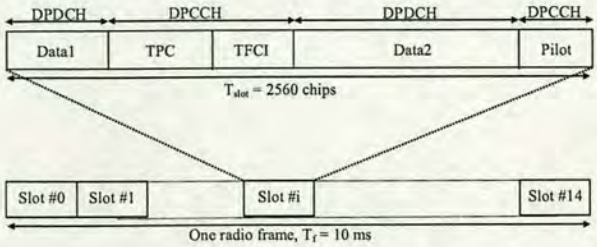

DPDCH: dedicated physical data channel

DPCCH: dedicated physical control channel

TPC: transmit power control TFCI: transport format combination indicator

Figure 1. Frame structure for downlink DPCH

The dedicated physical data channel (DPDCH) with user data is combined by time multiplexing with the dedicated physical control channel (DPCCH) to form the dedicated physical channel (DPCH) and transmitted by the dedicated channel (DCH, a transport channel). Each slot contains the time-multiplexed DPDCH and DPCCH. It can be seen from Fig. 1 that within each slot there is a block of pilot signals transmitted which is known at the receiver. The number of pilot chips differs from 64 to 2048 according to different slot formats [3].

B. System Model

Considering *K*-user's traffic that is QPSK modulated before spreading, we write the complex envelope of the transmitted signal of the k-*th* user as:

$$d_k(t) = A_k \sum b_k^{(i)} s_k(t - iT), \tag{1}$$

where T denotes the symbol interval; A_k, $b_k^{(i)}$ and $s_k(t)$ denote the average amplitude of the k-*th* user, the i-*th* symbol of the k-*th* user and the spreading chip waveform of the k-*th* user given by the convolution of spreading sequence and the chip waveform, respectively.

After spreading, user data is summed together and scrambled by a long code $c(t)$:

$$x(t) = c(t) \sum_{k=1}^{K} d_k(t). \tag{2}$$

All signals from the same basestation then pass through an identical complex channel and arrive simultaneously at the receiver. The discrete-time output signal at the receiver is considered as the response of a complex digital filter to the transmitted signal. The complex FIR filter $h(t,l)$ with order L is a composite successive convolution of the transmitter filter, the mobile radio channel and the receiver filter.

At the receiver, perfect synchronisation is assumed. We write the received signal as $y(t)$, therefore, the relation between $x(t)$ and $y(t)$ can be written as

$$y(t) = x(t) * h(t,l) + v(t), \tag{3}$$

where $v(t)$ is additive Gaussian noise and "*" denotes linear convolution. If the transmitted signal is cyclically extended, the channel distortion becomes a circular convolution process in the time domain and multiplications in the frequency domain. Hence, using a one-tap FDE we can easily compensate the channel distortion. Unfortunately, in UMTS, any attempt to insert CP in the signal will destroy the current frame structure. In order to simplify the equalizer at the receiver, we therefore virtually generate a CP and reconstruct the cyclicity required by the frequency domain equalization.

III. FREQUENCY-DOMAIN CHIP LEVEL EQUALIZATION

In this section, we will exploit the relationship between the required cyclic part and the equalizer output. The frequency domain equalizer will process data on a block by block basis. Applying different size of FFT, we can separate each slot into multiple blocks. Suppose that we extract one block discrete received signals of length N, $\mathbf{y}=[y(0),y(1),\ldots,y(N-1)]^T$ (assuming the inter-block-interference (IBI) from the previous block is cancelled out, which can be done by tail cancellation). A linear convolution output is $L-1$ chips longer than that of a circular convolution. The tail part of a linear convolution process is defined as $\mathbf{y}_{tail}=[y_{tail}(0),y_{tail}(1),\ldots,y_{tail}(L-2)]^T$ which is unknown to the receiver at the moment and L is the length of channel (channel is assumed to be perfectly estimated at the receiver).

By adding elements of $\mathbf{y}_{tail}$ to the first $L-1$ elements of $\mathbf{y}$, we called this process *cyclic reconstruction*. In a DS-CDMA system such as UMTS, this process is of great importance for the frequency domain equalization since there is no cyclic prefix inserted in the transmitted signal. The block signal after cyclic reconstruction can be written as:

$$\mathbf{y}_0 = [y_0(0),\cdots,y_0(L-2),y(L-1),\cdots,y(N-1)]^T,$$
$$y_0(i) = y(i) + y_{tail}(i),\ i = 0,\ldots,L-2. \tag{4}$$

It is worth noting that only the first $L-1$ terms have been modified where L is the channel length and the first $L-1$ elements of $\mathbf{y}_0$ remains unknown. From the above definition, we further define $\mathbf{x}_0 = \left[\underbrace{y_{tail}(0),\cdots,y_{tail}(L-2),0,\cdots 0}_{N}\right]^T$, thus,

$$\mathbf{y}_0 = \mathbf{x}_0 + \mathbf{y}. \tag{5}$$

Firstly, we consider a noise-free environment. We then have the input and output relations:

$$\mathbf{y}_0 = \mathbf{H} \cdot \mathbf{s}, \tag{6}$$

where $\mathbf{H}$ is a circulant channel matrix and $\mathbf{s}$ is a column vector composed of one block transmitted signal. The channel impulse response is denoted by $h(l)$, $l=0,\ldots,L-1$ (The channel is assumed quasi-static within one block) which has an N point Fourier transform $H(k)$, $k=0,\ldots,N-1$. The channel matrix $\mathbf{H}$ is thus defined as:

$$\mathbf{H}=\begin{bmatrix} h(0) & & & & h(L-1) & \cdots & h(1) \\ \vdots & h(0) & & & & \ddots & \vdots \\ \vdots & \vdots & \ddots & & 0 & & h(L-1) \\ h(L-1) & \vdots & \vdots & h(0) & & & \\ & h(L-1) & \vdots & \vdots & h(0) & & \\ & & \ddots & \vdots & \vdots & \ddots & \\ 0 & & & h(L-1) & h(L-2) & \cdots & h(0) \end{bmatrix} \quad (7)$$

According to its special structures, circulant matrix **H** can be efficiently diagonalized by Fourier transform and inverse Fourier transform. Let **F** and $\mathbf{F}^{-1}$ denotes the Fourier transform matrix and the inverse Fourier transform matrix, respectively. Hence,

$$\mathbf{F}\cdot\mathbf{y}_0=\mathbf{F}\cdot\mathbf{H}\cdot\mathbf{s}=\mathbf{F}\cdot\mathbf{H}\cdot\mathbf{F}^{-1}\cdot\mathbf{F}\cdot\mathbf{s}=\mathbf{D}\cdot\mathbf{F}\cdot\mathbf{s}, \quad (8)$$

where **D** is a diagonal matrix with its elements taken from the *N* points Fourier transform of channel impulse response, i.e. $\mathbf{D}=diag\{H(0),...,H(N-1)\}$.

Substituting (5) into (8), we have

$$\mathbf{F}\cdot(\mathbf{x}_0+\mathbf{y})=\mathbf{D}\cdot\mathbf{F}\cdot\mathbf{s}. \quad (9)$$

(9) can be further modified to:

$$\mathbf{F}^{-1}\cdot\mathbf{D}^{-1}\cdot\mathbf{F}\cdot(\mathbf{x}_0+\mathbf{y})=\mathbf{s}. \quad (10)$$

Theoretically, the reconstructed part $\mathbf{y}_{tail}$ is obtained by the multiplication of the upper triangular block matrix in **H** and a vector composed of the last *L-1* elements of **s**. Therefore, given $\mathbf{H}_0=\begin{bmatrix} 0 & \cdots & 0 & h(L-1) & \cdots & h(1) \\ \vdots & \ddots & \vdots & \ddots & \ddots & \vdots \\ 0 & \cdots & \cdots & \cdots & 0 & h(L-1) \end{bmatrix}$ and $\mathbf{H}_1=\mathbf{0}_{N-L+2\_by\_N}$, we can yield:

$$\mathbf{x}_0=[\mathbf{H}_0 \quad \mathbf{H}_1]^T\cdot\mathbf{s}. \quad (11)$$

Substituting (10) into (11), as a result, we have

$$\mathbf{x}_0=[\mathbf{H}_0 \quad \mathbf{H}_1]^T\cdot\mathbf{F}^{-1}\cdot\mathbf{D}^{-1}\cdot\mathbf{F}\cdot(\mathbf{x}_0+\mathbf{y}) \quad (12)$$

In order to simplify the notation, a new *N*×*N* matrix **M** is introduced:

$$\mathbf{M}=[\mathbf{H}_0 \quad \mathbf{H}_1]^T\cdot\mathbf{F}^{-1}\cdot\mathbf{D}^{-1}\cdot\mathbf{F} \quad (13)$$

Matrix **M** has its special structure that it can be further split into blocks, i.e., $\mathbf{M}=\begin{bmatrix}\mathbf{M}_0 & \mathbf{M}_1 \\ \mathbf{0} & \mathbf{0}\end{bmatrix}$, $\mathbf{M}_0$ is a *(L-1)*×*(L-1)* matrix and $\mathbf{M}_1$ is a *(L-1)*×*N* matrix. Matrix **M** can be calculated by the multiplication of matrices from (13) and this will cause a large computational burden for the receiver. However, the computation can be reduced significantly. Since $\mathbf{D}^{-1}$ is a diagonal matrix, it can be decomposed to

$$\mathbf{D}^{-1}=\mathbf{F}\cdot\mathbf{A}\cdot\mathbf{F}^{-1} \quad (14)$$

where **A** is a circulant matrix. Thus,

$$\mathbf{M}=[\mathbf{H}_0 \quad \mathbf{H}_1]^T\cdot\mathbf{F}^{-1}\cdot\mathbf{F}\cdot\mathbf{A}\cdot\mathbf{F}^{-1}\cdot\mathbf{F}=[\mathbf{H}_0 \quad \mathbf{H}_1]^T\cdot\mathbf{A} \quad (15)$$

Since **A** is a circulant matrix, therefore, by knowing only one column or one row elements of **A**, it is possible to generate the whole circulant matrix. We need to point out that there is an interesting property of the Fourier transform matrix **F**, i.e., the first row and the first column elements are all unity elements. It yields that the first column of $\mathbf{D}^{-1}\cdot\mathbf{F}$ can be represented by $\left[\frac{1}{H(0)} \quad \cdots \quad \frac{1}{H(N-1)}\right]^T$ and *H(0),...,H(N-1)* are the *N* point Fourier transform of the channel impulse response. Consequently, the first column of **A** can be calculated by the Fourier transform of vector $\left[\frac{1}{H(0)} \quad \cdots \quad \frac{1}{H(N-1)}\right]^T$ and so that the computational complexity is reduced to *O(NlogN)*.

According to the definition of **M**, $\mathbf{y}_{tail}$ and (13), formula (12) can be rewritten as:

$$\begin{aligned}\mathbf{y}_{tail}&=[\mathbf{M}_0 \quad \mathbf{M}_1]^T\cdot\mathbf{y}+[\mathbf{M}_0 \quad \mathbf{M}_1]^T\cdot\mathbf{x}_0 \\ &=[\mathbf{M}_0 \quad \mathbf{M}_1]^T\cdot\mathbf{y}+\mathbf{M}_0\cdot\mathbf{y}_{tail}\end{aligned} \quad (16)$$

Hence,

$$(\mathbf{I}-\mathbf{M}_0)\cdot\mathbf{y}_{tail}=[\mathbf{M}_0 \quad \mathbf{M}_1]^T\cdot\mathbf{y} \quad (17)$$

From (17), when additive white Gaussian noise exists, the MMSE estimate of $\mathbf{y}_{tail}$ is given by:

$$\mathbf{y}_{tail}=\left((\mathbf{I}-\mathbf{M}_0)\cdot(\mathbf{I}-\mathbf{M}_0)^H+\frac{\sigma_n^2}{\sigma_{tail}^2}\mathbf{I}\right)^{-1}\cdot(\mathbf{I}-\mathbf{M}_0)^H\cdot[\mathbf{M}_0 \quad \mathbf{M}_1]^T\cdot\mathbf{y} \quad (18)$$

where σ_n^2, σ_{tail}^2 and **I** are the noise variance, tail part signal variance and a *(L-1)*×*(L-1)* unitary diagonal matrix, respectively.

However, it is not easy to decide what σ_{tail}^2 should be since a good estimate of the tail part average power is not available. Factors such as user numbers and channel characteristics will affect the tail part signal power. For simplicity, we derive an approximate calculation of σ_{tail}^2. Suppose that the variance of the time domain signal is σ_d^2, channel is normalized and with length equals to *L*. Denote the normalized average power of each channel tap by P_i, *i=0,...,L-1*. The total tail part power can be approximated by:

$$P_{total}=\sigma_d^2\sum_{l=1}^{L-1}\sum_{i=1}^{L-l}P_i \quad (19)$$

Hence, the average tail part signal power per chip is:

$$\sigma_{tail}^2=\frac{P_{total}}{L-1}=\sigma_d^2\sum_{l=1}^{L-1}\sum_{i=1}^{L-l}P_i\Big/L-1 \quad (20)$$

The frequency domain equalization consists of two steps. In the first step, the required tail part is reconstructed. In the second step, the MMSE equalizer in the frequency domain is given by the following expression:

$$W(k)=\frac{H^*(k)}{|H(k)|^2+\sigma_n^2/\sigma_d^2+\alpha}\quad,\quad k=0,...N-1 \qquad (21)$$

In (21), the real factor α is introduced for the purpose of taking into account unpredictable cyclic reconstruction errors. The reason is that if the condition number $cond(\mathbf{I}-\mathbf{M}_0)$ is large, then the exact solution may be changed substantially by even small perturbation in the data due to the additive noise. In the frequency domain, let us define $Y_0(k)$ and $S(k)$, $k=0,...,N-1$ as the Fourier transforms of $\mathbf{y}_0$ and $\mathbf{s}$, respectively. The equalized $S(k)$ can be given by:

$$S(k)=\frac{Y_0(k)\cdot H^*(k)}{|H(k)|^2+\sigma_n^2/\sigma_d^2+\alpha}\quad,\quad k=0,...N-1 \qquad (22)$$

The equalizer output is finally transformed back to the time domain by inverse Fourier transform. The scrambling code is then removed and the composite signal is despreaded and decoded.

Actually, the reconstructed part is exactly the IBI into the next processing block, thus, we can remove this part from the next block to obtain an IBI free block. Inevitably, this will cause error propagation due to imperfect equalization; however, the error propagation can be limited within one slot since pilots transmitted every slot are known to the receiver.

IV. PARAMETERS SELECTION

It gives more freedom if non-radix 2 Fourier transform is adopted. N can be selected freely for different situations. However, if we only consider Radix 2 FFT, then N, the length of one processing block can only be an integer multiple of 2. In both cases, it should be mentioned that L needs to be equal to or larger than the channel length.

Note that, matrix inversion and matrix multiplication are involved in the cyclic reconstruction process. Hence, an equalizer selecting a large N is more efficient than one with a small N in terms of computation complexity. Moreover, larger equalizer length results in smaller processing block numbers, thus, the unpredictable error propagation effect will not be significant. On the other hand, it should be emphasized that because of the channel variation within one block due to high-speed movement, large block length will give raise to the performance degradation (its counterpart in one OFDM system is the induced ICI – inter carrier interference). Usually, we select N to be 512 for mobile speed slower than 90 *km/h* and N equals to 256 for mobile speed higher than 90 *km/h* in order to achieve a good tradeoffs between equalizer performance and error propagations.

In (21), the exact calculation of the real factor α is fairly complicated if not intractable. Taking $0.1<\alpha<0.2$ results in an acceptable system performance given that the transmitted signal power and the propagation channel are both normalized.

V. NUMERICAL RESULTS

In this section, computer simulations show the performance of the proposed frequency domain equalizer. The simulation encompasses most of the features of the UMTS FDD downlink. QPSK data modulation is considered and the chip rate is 3.84 Mchips/s. Walsh codes with length 16 are used as the short spreading codes and Gold codes with length 65536 are used as long scrambling codes. No error correction coding is considered in the simulations. 8 active users are assumed in the simulations. The UMTS Vehicular A channel model [10] is used for BER evaluation in our simulation. The corresponding channel impulse response is shown in Fig. 2.

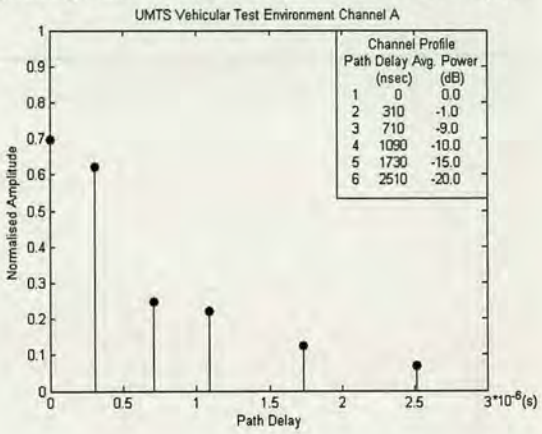

Figure 2. Channel profile of the UMTS Vehicular Channel A

Fig. 3 shows the BER performances of the proposed frequency domain equalizer and the equalizer with perfect cyclic reconstruction (assuming the tail part is known for the equalizer). The terminal is travelling at mobile speed of (a) 50 *km/h* and (b) 150 *km/h*. In Fig. 3 (a), *N=512* is selected for the equalizer. The lower bound performances of equalizer with 64 and 512 FFT size are also given. In Fig. 3 (b), we present the BER performance of the proposed equalizer with *N=256*. Also shown are the lower bounds for frequency domain equalizers with perfect cyclic reconstruction.

We learn from Fig. 3 (a) that for low speed movement, although under high SNR scenarios the performance of the proposed algorithm is not satisfactory compared with the lower bounds. However, with the aid of forward error correction coding, the area in the figure that of interest is $10^{-2}\leq BER\leq 10^{-1}$. In this area, the performance of the proposed equalizer is acceptable. It can be seen from Fig. 3 (b) that for high-speed movement, the performance is close to the lower bounds. A system with perfect cyclic reconstruction is equivalent to a cyclic prefix based single carrier system. In an OFDM system, high-speed movements will cause severe ICI; similarly, for single carrier transmission with cyclic prefix, it will also degrade the BER performance significantly. The channel at the beginning of one block and the channel at the end of one block are no longer the same; therefore, the cyclic prefix and its data part are not transmitted though the same channel. On the other hand, the channel within one block can no longer be assumed to be stationary now.

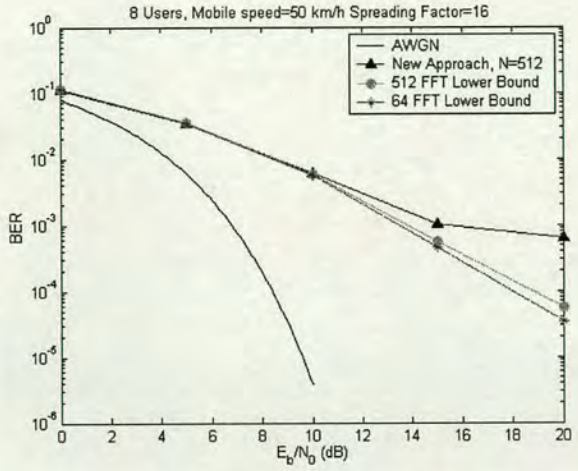

(a) Speed= 50 *km/h*

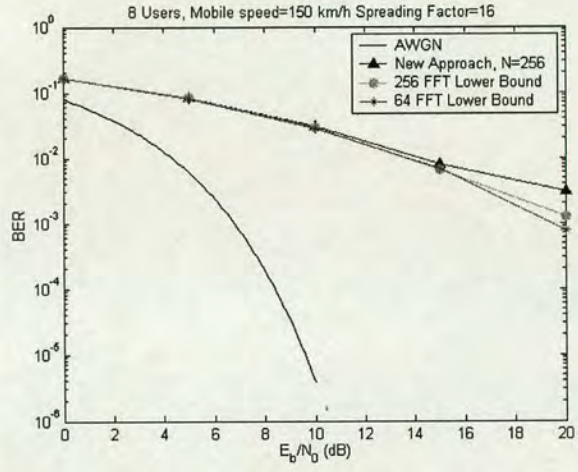

(b) Speed= 150 *km/h*

Figure 3. Performance of the new FDE, UMTS Vehicular A channel, mobile speed=50 km/h and 150 km/h.

VI. CONCLUSION

In this paper, a MMSE frequency domain equalizer based on self cyclic reconstruction is proposed and the BER performance is given. Without the insertion of cyclic prefix at the transmitter, which will change the UMTS signal format, the proposed algorithm exploits the relationship between the required cyclic part and the transmitted signal itself. The estimated cyclic part is then added to the received block signal for doing frequency domain equalization. Simulation results show the effectiveness of the proposed algorithm. To design a frequency domain equalizer for the current WCDMA system is very attractive. OFDM has become a strong candidate for the fourth generation systems and hence a WCDMA receiver adopting chip level frequency domain equalizer will be compatible with the current FFT based receiver structures. By adopting the proposed equalization structure for receiving DS-CDMA signal, a multimode receiver can be programmed to switch to a particular system more conveniently.

ACKNOWLEDGMENT

The work reported in this paper has formed part of the Research Programme of the Virtual Centre of Excellence in Mobile and Personal Communications, Mobile VCE, www.mobilevce.com, whose funding support, including that of EPSRC, is gratefully acknowledged. Fully detailed technical reports on this research are available to Industrial Members of Mobile VCE.

REFERENCES

[1] Prasad, R., *Universal wireless personal communications*: Artech House Boston/London, 1998.

[2] K. Hooli, *et al*, "Chip-level Channel equalization in WCDMA downlink", EURASIP Journal on Applied Signal processing 2002, No.8, pp. 757-770.

[3] D. Falconer, *et al*, "Frequency domain equalization for single-carrier broadband wireless systems", IEEE Comm. Magazine, April 2002, pp 58-66.

[4] M. Clark, 'Adaptive frequency-domain equalization and diversity combining for broadband wireless communications", IEEE J. Select. Areas Comm., Vol.16 , no.8, pp.1385-1395, 1998

[5] M. Vollmer, *et al*, "Comparative study of joint detection techniques for td-cdma based mobile radio systems," IEEE J. Select. Areas Comm., vol. 19, no. 8, pp. 1461-1475 Aug 2001.

[6] I. Martoyo, *et al*, "Low complexity CDMA downlink receiver based on frequency domain equalization", Proc. VTC 2003, Orlando, October 6-9, 2003, Vol. 2, pp. 987 – 991.

[7] E. Dahlman, *et al*, "WCDMA-The radio interface for future mobile multimedia communications", IEEE Trans. on Vehicular Technology, Vol. 47, No. 4, 1998, pp.1105-1118.

[8] H. Holma, A. Toskala, *WCDMA for UMTS*, Wiley Publishing House, 2001

[9] 3GPP TS 25.211: "Physical channels and mapping of transport channels onto physical channels (FDD)".

[10] ETSI TR 101 112 V3.2.0 (1998-04): Universal Mobile Telecommunications System (UMTS); Selection procedures for the choice of radio transmission technologies of the UMTS.

UMTS FDD Frequency Domain Equalization Based on Slot Segmentation

Yushan Li, Steve McLaughlin, David G. M. Cruickshank
Institute for Digital Communications, School of Engineering and Electronics,
University of Edinburgh, King's Buildings, Mayfield Road,
Edinburgh EH9 3JL, UK.
E-Mail: yushan.li@ee.ed.ac.uk

***Abstract*—In this paper, a new chip-level MMSE frequency domain equalizer (FDE) is investigated for a downlink Universal Mobile Telephone System (UMTS) system. The multiple access interferences (MAI) and inter chip interferences (ICI) can be reduced at the chip level before despreading. By exploiting the frame and slot structures of the UMTS downlink, the pilots within one slot (for FDD mode) can be used for the required cyclic reconstruction in a FDE. No cyclic prefix (CP) or zero-padding is required at the transmitter, which would change the signal format of the current UMTS system. Furthermore, one slot signal is split into multiple segments for the sake of combating channel variance within one slot. The performance of the proposed MMSE-FDE is studied through simulation. A multimode receiver that can equalize both UMTS and OFDM systems in one structure is then feasible.**

Keywords- *FDE, UMTS, chip-level, MMSE, multimode receiver*

I. INTRODUCTION

In many of the discussions regarding 4G communication systems, the assumption is that multimode terminals that can handle both Orthogonal Frequency Division Multiplexed (OFDM) and spread spectrum systems will be required. A wise approach to design such a multimode receiver is to employ a frequency domain equalizer (FDE) for UMTS in the receiver, making use of the powerful FFT/IFFT for both UMTS and OFDM systems. Recently, receivers based on TDMA style channel equalization at the chip level have been proposed for a wideband code-division multiple access (WCDMA) downlink [1]. The received chip waveform, distorted by the multi-path channel, is equalized prior to de-spreading. Orthogonality of the signal from the basestation is restored at chip-level.

Numerous approaches for single-carrier frequency domain equalization (SC-FDE) have been proposed during the recent years [2]. However, most of them use the same mechanism as in OFDM, i.e. a cyclic prefix (CP) is inserted in order to simplify the receiver. This is not compatible with the current UMTS system since it will change the format of the frame and the overhead CP will reduce the spectral efficiency. It is desirable to design a receiver without changing the transmitted signal format.

In this paper, a new FDE is proposed and investigated which will not change the format of the transmitted signal. By exploiting the frame and slot structures of the UMTS downlink, the pilots within one slot (for FDD mode) can be used for the required cyclic reconstruction in a FDE.

The rest of the paper is organized as follows. The system model of UMTS-FDD and chip level equalization is introduced in Section II. In Section III, the proposed algorithm is described. Section IV will deal with the computational complexity. Finally, conclusions are presented.

II. SYSTEM MODEL AND CHIP-LEVEL FDE

A. *UMTS-FDD Downlink*

UMTS is capable of providing variable bit rates (144 kbps for vehicle speed, rural environment; 384 kbps for walking speed, urban outdoor; 2048 kbps for fixed, indoor environment) and different quality of service (QoS) for different connections [3]. The frequency division duplex (FDD) mode is working in the 2 GHz band, with a basic chip rate of 3.84 Mcps and a flexible carrier spacing of 4.4-5.0 MHz. QPSK modulation is adopted and allows use of the same channelization code for both I and Q channels. In the FDD downlink, the general frame structure is shown in Fig. 1. It can be seen that one frame with duration of 10 ms can be divided into 15 slots [4].

The dedicated physical data channel (DPDCH) with user data is combined by time multiplexing with the dedicated physical control channel (DPCCH) to form the dedicated physical channel (DPCH) and transmitted by the dedicated channel (DCH, a transport channel). Each slot contains the time-multiplexed DPDCH and DPCCH. It can be seen from Fig. 1 that within each slot there is a block of pilot signals transmitted, which is known at the receiver. The number of pilot chips differs from 64 to 2048 according to different slot formats [4].

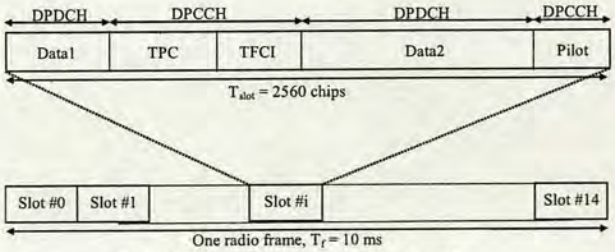

DPDCH: dedicated physical data channel

DPCCH: dedicated physical control channel

TPC: transmit power control TFCI: transport format combination indicator

Figure 1. Frame structure for downlink DPCH

B. Chip-Level FDE

We consider an uncoded *K*-user downlink traffic that is QPSK modulated before spreading. After spreading, user data are summed and then scrambled by a cell-specific long code *s(t)* prior to transmission. The transmitted signal can be represented as:

$$x(t)=s(t)\sum_{k=1}^{K}\left[A_k\sum b_k^{(i)}c_k(t-iT)\right] \quad (1)$$

where T denotes the symbol interval; A_k, $b_k(i)$ and $c_k(t)$ denote the amplitude of the k-th user, the i-th symbol of the k-th user and the spreading chip waveform of the k-th, respectively. At the receiver, the received discrete signal can be represented by:

$$r(n)=\sum_{l=0}^{L-1}h(l)x(n-l)+v(n) \quad (2)$$

where $h(l)$ is the propagation channel and L is the channel length in chips; $x(n)$, $v(n)$ and $r(n)$ denote the discrete transmitted signal, the additive Gaussian white noise with variance σ_n^2 and the sampled received signal, respectively.

By the insertion of the CP in OFDM systems, linear channel distortion of the signal results in circular convolution of the transmitted signal and the channel impulse response. With this in mind, it is necessary to reconstruct the resultant effect caused by a virtual CP so that the time and frequency-domain descriptions of the convolution are essentially equivalent and a simple OFDM type FDE can be derived. In the FDD downlink, pilots are pre-inserted in each slot used for channel estimation purpose. According to the UMTS specification [4], the pilot sequence can be 64-2048 chips corresponding to different slot formats. Since the shortest pilot sequence still consists of 64 chips which is longer than L in most cases, this prior known information can be used to reconstruct the needed cyclicity for the FDE. The insertion of CP as in an OFDM system can be avoided and thus the transmitted signal format will not be changed.

The new FDE is performed on a slot (2560 chips) by slot basis. Assuming that the composite channel response $h_i(l)$ is quasi-stationary within the i-th slot and span over L chips ($L<64$, i.e., channel span is less than 16.64 μs), we may write the received signal in one block as $r_i(n)$, $0\le i\le S-1$, $0\le n\le N-1$, $S=15$ is the number of slots and $N=2560$ is the number of chips within one slot. Finally, we use $x_i(n)$ to denote the corresponding transmitted i-th slot signal. At the receiver, $r_i(n)$ can be written as:

$$\begin{aligned} r_i(n)&=\sum_{l=0}^{L-1}h_i(l)x_i(n-l)u(n-l)\\ &+\sum_{l=0}^{L-1}h_{i-1}(l)x_{i-1}(n+N-l)(1-u(n-l))+v_i(n)\end{aligned} \quad (3)$$

where $u(.)$ represents the unit step function. The second term in (3) represents the inter-slot-interference caused by the $(i-1)$-th slot. It is estimated and subtracted from the current slot. Then the slot signal free of inter-slot-interference is given by:

$$\bar{r}_i(n)=r_i(n)-\sum_{l=0}^{L-1}h_{i-1}(l)x_{i-1}(n+N-l)(1-u(n-l)) \quad (4)$$

Pilot sequences are transmitted at the end of one slot and are known to the receiver. Therefore, pilot signals in the i-th slot can be used to reconstruct the required cyclicity as shown in (5).

$$\tilde{r}_i(n)=\bar{r}_i(n)+\sum_{l=0}^{L-1}h_i(l)x_i(n+N-l)(1-u(n-l)) \quad (5)$$

Correspondingly, in the frequency domain,

$$\tilde{R}_i(w)=H_i(w)X_i(w)+V_i(w) \quad (6)$$

where $0\le w\le N-1$, $\tilde{R}_i(w)$, $H_i(w)$, $X_i(w)$ and $V_i(w)$ are the DFT of $\tilde{r}_i(n)$, $h_i(l)$, $x_i(n)$ and $v_i(n)$, respectively. Further defining $W_i(w)$, $0\le w\le N-1$ as the equalizer coefficients in the frequency domain, the MMSE FDE is given by the following expression:

$$W_i(w)=\frac{H_i^*(w)}{|H_i(w)|^2+\alpha},\ \alpha=\sigma_n^2/\sigma_d^2 \quad (7)$$

where σ_d^2 and $H_i^*(w)$ are the variance of the received signal and the conjugate of $H_i(w)$, respectively. The equalized signal is finally transformed back to the time domain by inverse Fourier transform. The scrambling code is removed and the composite signal is despreaded and detected.

Two sorts of channels are studied in our simulations with their frequency selectivity plotted in Fig. 2. Computer simulations are carried out at base band for the investigation of the proposed algorithm. BER performance is evaluated for the MMSE FDE in both static spectrally-flat channel (Fig. 3) and spectrally-deep-fading channel (Fig. 4). Channel coding is excluded from the study. Perfect knowledge of the channel at the receiver is assumed. In both cases, we use the proposed MMSE FDE, a 32-taps and a 64-taps time domain MMSE equalizer (TDE) [1]. Simulations show that the proposed MMSE chip level FDE can effectively mitigate inter-chip interferences under channels with or without deep nulls.

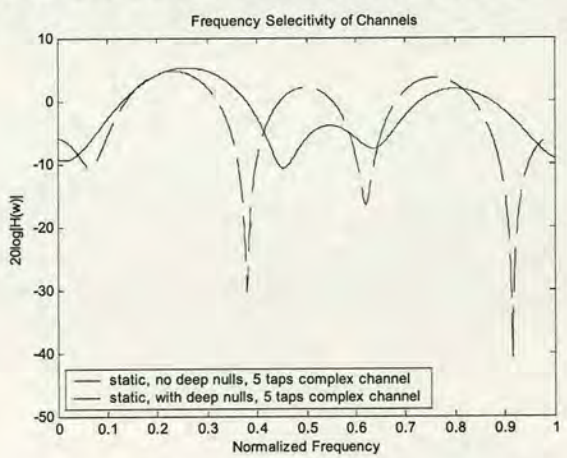

Figure 2. Frequency selectivity of two sorts of channels

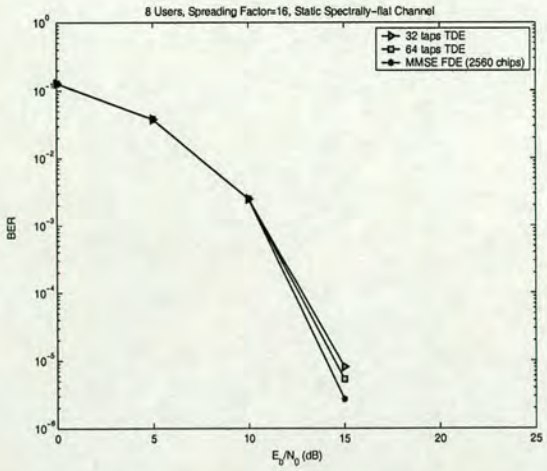

Figure 3. BER versus E_b/N_0 for 8 users, Single cell downlink, Spreading factor=16, Channel without deep nulls

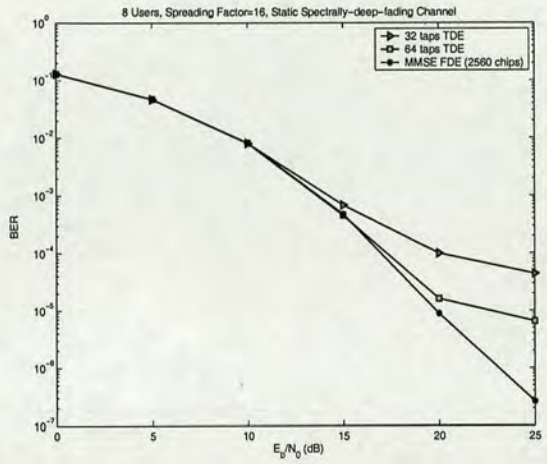

Figure 4. BER versus E_b/N_0 for 8 users, Single cell downlink, Spreading factor=16, Channel with deep nulls

III. SLOT SEGMENTATION

In fact, the assumption that we made in the previous section is not reasonable since the channel's stationary assumption cannot be ensured within one slot. Therefore, the time variation of the mobile radio channel is a main obstacle to the proposed FDE. The study of the MMSE-FDE performance in Rayleigh fading channels (UMTS Vehicular A Channel [5]) is presented in this section. The corresponding channel impulse response is shown in Fig. 5. Each path is faded independently according to the Rayleigh distribution. By breaking the 2560 chips slot into a series of disjoint short segments, the time variations of the mobile channel over one segment are sufficiently small and can be neglected. Hence, we can assume that the channel over one segment is static. The whole time-varying channel over one slot can be partitioned into multiple time-invariant channels approximately. Similar approach had been proposed in [6] for OFDM systems. The system performance can be improved greatly, especially in fast fading channels.

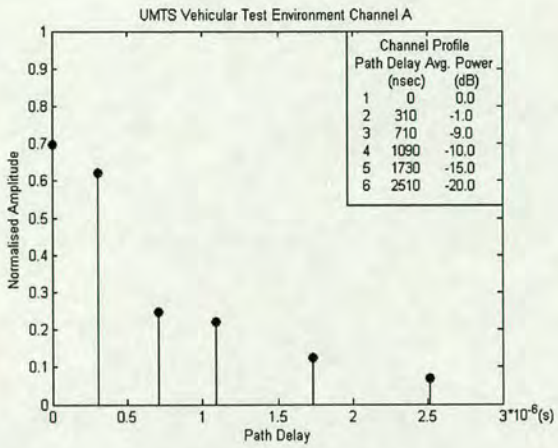

Figure 5. Channel profile of the UMTS Vehicular Channel A

To derive the new equalization scheme, we consider one slot free of interferences from the previous slot. The received signal in the *i-th* slot is expressed as $\overline{\mathbf{r}}_i = [\overline{r}_i(0), \cdots, \overline{r}_i(N-1)]^T$, $0 \le i \le 14$, $N = 2560$. We segment $\overline{\mathbf{r}}_i$ into M blocks $\overline{\mathbf{r}}_{i,k}$, $0 \le k \le M-1$ with fixed length $P=N/M$ and fill zeros to expand them to new N elements vectors as:

$$\overline{\mathbf{r}}_{i,k} = \left[\underbrace{0, \cdots, 0}_{k*P}, \underbrace{\overline{r}_i(k*P), \cdots, \overline{r}_i((k+1)*P-1)}_{P}, \underbrace{0, \cdots, 0}_{N-(k+1)*P} \right]^T, \quad (8)$$

Hence,

$$\overline{\mathbf{r}}_i = \sum_{k=0}^{M-1} \overline{\mathbf{r}}_{i,k}, \quad 0 \le i \le 14, \quad (9)$$

Similarly, the related transmitted signal vector is defined as:

$$\mathbf{x}_{i,k} = \left[\underbrace{0, \cdots, 0}_{k*P}, \underbrace{x_i(k*P), \cdots, x_i((k+1)*P-1)}_{P}, \underbrace{0, \cdots, 0}_{N-(k+1)*P} \right]^T, \quad (10)$$

In the frequency domain, M new signal vectors can be written as $\overline{\mathbf{R}}_{i,k}$. Correspondingly, we estimate the mobile channel in one slot at M sampling instances. The channel estimates are *$h_i(m;l)$, $m=384000*frame\ index+2560*slot\ index+(0,...,M-1)\ *P-1$, $l=0,...,L-1$* where L is the order of the channel, and $\mathbf{H}_{i,m}$ is the 2560 length DFT vector of *$h_i(m;l)$*.The tail part of the convolution process for each block is [*$t_{i,k}(0)$ ... $t_{i,k}(L-2)$*]. Expanded into one slot length with zeros, the tail vector is defined by:

$$\mathbf{t}_{i,k} = \begin{cases} \left[\underbrace{0, \cdots, 0}_{k*P}, \underbrace{t_{i,k}(0), \cdots, t_{i,k}(L-2)}_{L-1}, \underbrace{0, \cdots, 0}_{N-k*P-L+1} \right]^T, & 0 \le k \le M-2 \\ \left[\underbrace{t_{i,M-1}(0), \cdots, t_{i,M-1}(L-2)}_{L-1}, \underbrace{0, \cdots, 0}_{N-L+1} \right]^T, & k = M-1 \end{cases} \quad (11)$$

The frequency domain counterparts of the tail vectors are denoted by $\mathbf{T}_{i,k}$. The desired transmitted signal in the k-th block can then be recovered by the FDE $\mathbf{W}_{i,k}$ as given in (12):

$$\mathbf{x}_{i,k} = IDFT\left(\left(\overline{\mathbf{R}}_{i,k} + \mathbf{T}_{i,k} - \mathbf{T}_{i,k-1}\right) \otimes \mathbf{W}_{i,k}\right) \tag{12}$$

where $\otimes$ represents the element by element multiplication of two vectors.

Hence, the desired signal vector in the i-th slot is the summation of the M virtual FDE output:

$$\mathbf{x}_i = \left[x_i(0), \cdots, x_i(N-1)\right]^T = \sum_{k=0}^{M-1} \mathbf{x}_{i,k} \tag{13}$$

So far we have only the knowledge of $\mathbf{t}_{i,M-1}$ that can be obtained by channel estimate and the pilot information. However, the equation in (13) can be written as:

$$\begin{aligned} \mathbf{x}_i &= \sum_{k=0}^{M-1} \mathbf{x}_{i,k} = \sum_{k=0}^{M-1} IDFT\left(\left(\overline{\mathbf{R}}_{i,k} + \mathbf{T}_{i,k} - \mathbf{T}_{i,k-1}\right) \otimes \mathbf{W}_{i,k}\right) \\ &= IDFT\left(\sum_{k=0}^{M-1} \left(\overline{\mathbf{R}}_{i,k} + \mathbf{T}_{i,k} - \mathbf{T}_{i,k-1}\right) \otimes \mathbf{W}_{i,k}\right) \\ &= IDFT\left(\sum_{k=0}^{M-1} \overline{\mathbf{R}}_{i,k} \otimes \mathbf{W}_{i,k} + \sum_{k=0}^{M-1} \left(\mathbf{T}_{i,k} - \mathbf{T}_{i,k-1}\right) \otimes \mathbf{W}_{i,k}\right) \end{aligned} \tag{14}$$

Since channels in the neighboring segments can be considered almost identical. A reasonable assumption is made here that $\mathbf{W}_{i,0} \approx \mathbf{W}_{i,1}, \ldots, \mathbf{W}_{i,M-2} \approx \mathbf{W}_{i,M-1}$ so long as one slot is segmented into adequate large number of blocks. Therefore,

$$\begin{aligned} \mathbf{x}_i &= IDFT\left(\sum_{k=0}^{M-1} \overline{\mathbf{R}}_{i,k} \otimes \mathbf{W}_{i,k} + \sum_{k=0}^{M-1} \left(\mathbf{T}_{i,k} - \mathbf{T}_{i,k-1}\right) \otimes \mathbf{W}_{i,k}\right) \\ &= IDFT\left(\begin{array}{l} \sum_{k=0}^{M-1} \overline{\mathbf{R}}_{i,k} \otimes \mathbf{W}_{i,k} + \mathbf{T}_{i,0} \otimes \left(\mathbf{W}_{i,0} - \mathbf{W}_{i,1}\right) + \\ \mathbf{T}_{i,1} \otimes \left(\mathbf{W}_{i,1} - \mathbf{W}_{i,2}\right) + \cdots + \mathbf{T}_{i,M-1} \otimes \mathbf{W}_{i,M-1} \end{array}\right) \\ &\approx IDFT\left(\sum_{k=0}^{M-1} \overline{\mathbf{R}}_{i,k} \otimes \mathbf{W}_{i,k} + \mathbf{T}_{i,M-1} \otimes \mathbf{W}_{i,M-1}\right) \end{aligned} \tag{15}$$

From the above equation, the only task then remaining is to reconstruct the cyclicity for the *(M-1)*-th block. We then made Monte Carlo simulations to investigate the achievable BER for different selected M value. The uncoded BER results are averaged over different channels (generated according to the UMTS Vehicular A channel model) for varying E_b/N_0. Obviously, the more segments one slot is broken into, the better performance we may get. However, more segments require more computations. In Fig. 6 and Fig. 7, we observe that for small Doppler frequencies f_d, equalizer with small M value, M=2, offers best tradeoff between complexity and performance. For large Doppler frequencies, larger M value, M=10, is inevitable.

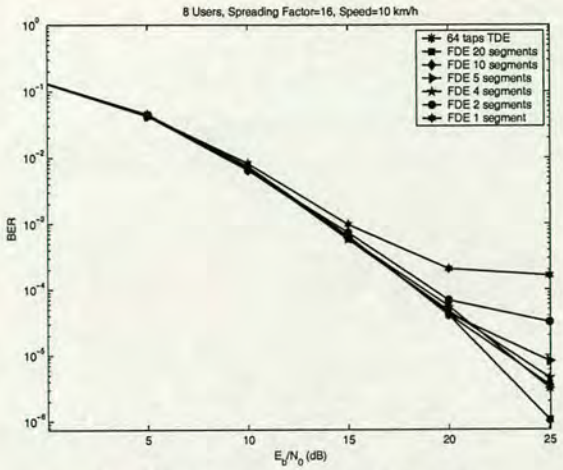

Figure 6. Mobile speed = 10 km/h, f_d=19 Hz

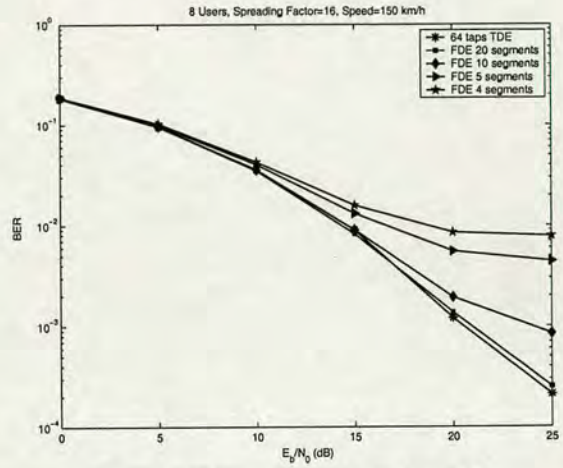

Figure 7. Mobile speed = 150 km/h, f_d=277 Hz

IV. COMPUTATIONAL COMPLEXITY DISCUSSION

Similar to the partial transmit sequence (PTS) approaches [7] in OFDM systems (a solution for the inherited peak-to-average problem, PTS can also be used to reduce the inter-carrier-interference (ICI) in OFDM systems), the input data block is partitioned into disjoint sub-blocks and each sub-block is zero padded to the original block length. The complexity for the proposed algorithm is increased significantly with the increasing segment number M. However, if the transforms can take advantage of the fact that a large fraction of the input values are zero, the complexity can be reduced greatly. We noticed that recently there are already some efficient algorithms in calculating partial DFT (input sequence contains many zeros) such as "FFT pruning" [8] and "Transform decomposition" [9]. These algorithms utilize the redundancy in the input to reduce the number of operations below those of the FFT algorithms and have a computational complexity of $O(N\log_2 P)$ instead of $O(N\log_2 N)$. The algorithm proposed in [10] can further reduce the computational complexity to only $O(N+P\log_2 P)$. It should be mentioned that the frequency domain equalizer is operated on one slot signal; hence, 2560

chips will be equalized at one time. For those segments where non-zero data are not starting from the beginnings, we may use a time-shift means by simply replacing all the Fourier transform twiddle factors of W_N^k with W_N^{k+F}, where F is the time-shift. This operation will not change the algorithm complexity. In addition, the same receiver architecture can be used for the reception of OFDM signals and reduced the ICI due to channel variance.

V. CONCLUSION

This paper has introduced a MMSE FDE for the UMTS in its downlink transmission and has presented a number of results that demonstrate its effectiveness. To design a FDE for the current UMTS receiver is very attractive. OFDM has become a strong candidate for the fourth generation systems and hence a DS-CDMA receiver adopting chip level frequency domain equalizer will be compatible with the current FFT based receiver structures. The coexistence of OFDM systems and UMTS via a simple structure is feasible. By adopting the proposed frequency domain equalization structure for receiving UMTS signal, a multimode receiver can be programmed to switch to a particular transmission more conveniently.

ACKNOWLEDGMENT

The work reported in this paper has formed part of the Research Programme of the Virtual Centre of Excellence in Mobile and Personal Communications, Mobile VCE, www.mobilevce.com, whose funding support, including that of EPSRC, is gratefully acknowledged. Fully detailed technical reports on this research are available to Industrial Members of Mobile VCE.

REFERENCES

[1] K. Hooli, *et al*, "Chip-level Channel equalization in WCDMA downlink", EURASIP Journal on Applied Signal processing 2002, No.8, pp. 757-770.

[2] D. Falconer, *et al*, "Frequency domain equalization for single-carrier broadband wireless systems" , IEEE Comm. Magazine, April 2002, pp 58-66

[3] H. Holma, A. Toskala, WCDMA for UMTS, Wiley Publishing House, 2001

[4] 3GPP TS 25.211, "Physical channels and mapping of transport channels onto physical channels (FDD)"

[5] ETSI TR 101 112 V3.2.0 (1998-04): Universal Mobile Telecommunications System (UMTS); Selection procedures for the choice of radio transmission technologies of the UMTS.

[6] X. Dai, X. Xie, "Adaptive blind equalization of the time-and frequency-selective ofdm system based on the local approximation", Neural Networks and Signal Processing, International Conference, 2003, Vol. 2, pp.1402-1405

[7] S. G. Kang, J. G. Kim and E. Y. Joo, "A Novel subblock partition scheme for partial transmit sequence OFDM", IEEE Trans. on Broadcasting, Vol. 45, No. 3, Sept. 1999, pp 333-338

[8] J. Markel, " FFT pruning " , IEEE Trans. on Audio and Electroacoustics, Vol. 19 , Issue: 4 , Dec 1971, pp.305 – 311

[9] H. Sorensen and C. Burrus, "Efficient computation of the DFT with only a subset of input or output points" , IEEE Trans. on Signal Processing, Vol. 41 , Issue: 3 , March 1993 pp.1184 – 1200

[10] S. He and M. Torkelson, "Computing partial DFT for comb spectrum evaluation", IEEE Signal Processing Letters, Vol. 3, No. 6, 1996, pp.173-175

Wireless World Research Forum
(WWRF)

New Physical Layer Architecture for Future Multi-Mode Mobile Communication Systems

Yushan Li[1], Steve McLaughlin[1], David G. M. Cruickshank[1], Chris Williams[2]
1. University of Edinburgh 2. Bristol University

***Abstract*—This paper provides a study on the convergence issue of several complementary wireless access networks, namely DAB, DVB-T and HIPERLAN-2 and suggests possible physical layer architecture for a suitable multimode terminal. Sampling rate adaptation is the major concern in this paper. By using a fixed system clock, a sampling rate conversion (SRC) scheme based on Sigma-Delta modulation and linear interpolation is proposed for the multimode receiver. Moreover, a new receiver architecture combining SRC and symbol synchronization is suggested. Simulation result shows that the three OFDM systems can use a single system clock effectively.**

***Index Terms*—Multimode terminal, SRC, Sigma-Delta modulation.**

I. Introduction

Recent advances in wireless and multimedia data communications have urged the development of low-cost and low power multimode receivers that are capable of accessing different networks while providing mobility and reliability over the mobile radio channels. Digital Video Broadcasting – Terrestrial (DVB-T), Digital Audio Broadcasting (DAB) and High Performance Radio Local Area Network-type 2 (HIPERLAN-2) are the three standards to be investigated in this paper. The three networks to be converged use a number of key "common" technologies among them, such as same coding and air-interface techniques (Orthogonal Frequency Division Multiplexing (OFDM)), which provides a good platform to merge such systems into a single structure. Cosmas [1] have recently proposed a portable multimode multimedia mobile terminal that incorporates DVB-T reception equipment with a UMTS/GPRS transceiver device. The concept of software-defined radio (SDR) has also been suggested as a means of expanding the flexibility of handsets to operate as multimode terminals by employing a programmable software core that allows common hardware blocks of different standards to be reused for different services and applications [2]. The aim of this paper is to expand more on the issues concerning multimode terminals, which are largely uncovered, and suggest possible physical layer architecture for a future multi-mode terminal. A new Sigma-Delta modulation combined sampling rate conversion structure for the multi-mode receiver is proposed which can integrate the three OFDM systems with a single system clock effectively. Moreover, the symbol synchronization of the OFDM systems can benefit from this particular structure.

II. Sampling rate of DVB-T/DAB/HIPERLAN-2

In a multi-mode digital communication receiver, it is required that the terminal must be able to handle various communications standards. When comparing the architectures of the aforementioned three standards, it is quite obvious that a strong resemblance among their receiver architectures exists. This implies that a multimode receiver could be implemented if those commonalities are fully exploited. Generally, different chip/sample/symbol rates are specified in different standards. The obvious simple solution is to adopt different dedicated clock for different standards. However, it seems to be costly and cumbersome, and the receiver size will be greatly enlarged with the increasing of standard numbers.

The three systems deploy three different sampling rates, 64/7 = 9.1428571 MHz for DVB-T, 2.048 MHz for DAB and 20 MHz for HIPERLAN-2, respectively. Sampling rate adaptation is the first key issue to be considered for a multi-mode receiver even

before synchronization. Because the sampling rate of HIPERLAN-2 is the highest one among the sampling rates of the three investigated standards, a possible solution for this sampling rate conversion problem might be based on the over-sampling of HIPERLAN-2 and then approximating sampling data or sampling instants for DAB and DVB-T. The reason for doing so is twofold,

1. 20 MHz is the highest signalling rate among the targeted systems; the multi-mode receiver should be able to handle the highest signalling rate system;
2. No fractional SRC is required for the HIPERLAN-2 system except a simple decimation process;

In this section, we illustrate the sampling rate relationship of the three standards. First, the DVB-T 2k mode is considered. There are 2048 sub-carriers in the DVB-T 2k mode, with Tu (useful symbol duration) = 224 μs and cyclic prefix (CP) Δ=1/4 Tu = 56 μs. The OFDM symbol duration equals to 224 + 56 =280 μs which exactly consists of 280 μs / 0.05 μs = 5600 samples while sampled at the frequency of 20 MHz (Sampling rate of the HIPERLAN-2). To make it more meaningful, we now give an example. When the starting position of an OFDM symbol is given, assuming that it is the 0th sample, and then by sampling at 20 MHz, the 5599th sample will be the last sample of one DVB-T symbol. Not caring about the exact alignment of every sample at this first stage, we know that these 5600 samples contain the full information of a DVB-T symbol. In addition, the starting/ending position of the CP and the useful OFDM symbol can also be determined. Using the new sampling rate, although not every sample within the OFDM symbol is exactly aligned, due to the special characteristic discussed earlier, the coarse timing synchronization can still be realized.

The ratio of the sampling rate of HIPERLAN-2 and the sampling rate of DVB-T is 20/(64/7)=2.1875. While sampling the received DVB-T signal at 20 MHz we notice that 0.1875 multiplied by 16 results in an integer; the 16th DVB-T sample will coincide with the 35th new sample (sampled at 20 MHz). The boundary of one useful DVB-T OFDM symbol can now be expressed by means of the new samples (sampled at 20 MHz). When sampled at 16*20 = 320 MHz, which is 35 times (320/(64/7) = 35) the sampling rate of the DVB-T system, exact samples of the DVB-T system can be collected from the new samples after 35 times decimation. Now let us consider the DAB system case. Mode I in DAB uses 2048 sub-carriers with a sampling rate of 2.048 MHz. When 320 MHz is deployed as the sampling rate of the new system, a DVB-T system will be sampled at a sufficient rate. Consequently, for a DAB system, since 320 MHz is 156.25 times the sampling rate of the DAB system, every 4th DAB sample will happen to coincide with the 625th new sample. The boundary of the useful DAB OFDM symbol can also be expressed by means of the new samples (sampled at 320 MHz). Coming to this, a simple SRC via interpolation and decimation can produce the required DAB symbols from the new samples.

III. New sampling rate adaptation structure for a multi-mode OFDM receiver

A. Timing Adjustment by Interpolation

From the previous discussion, we can conclude that using 320 MHz as a new sampling rate for this particular multi-mode OFDM receiver is a pretty good decision. However, 320 MHz is a very high frequency for a mobile terminal when power consumption is considered.

Interpolation technique, a timing-adjustment operation on the received signal, had been already deployed in digital modems successfully [3] [4]. The fixed free running sampling clock remains independent on the symbol timing. The sample times never coincide perfectly on desired instants. Assume that the received signal $x(t)$ is band limited and being sampled at a rate $1/T_s$. After 'virtually' (we name it virtually because that actually no analogue signal has been produced) reconstructing the received signal, we resample the time-continuous output of the interpolating filter $y(t)$ at time instants $t=T$ where $1/T$ is the sampling rate specified in the standard. There is no attempt to recover the continuous analogue signal, what we are interested in is the sample value at the very time instants $t=kT$. The new time instant $t=kT$ can be represented by T_s in the form

$$t = kT = (m_k + \mu_k)T_s \qquad (1)$$

where $m_k=\mathbf{int}[kT/T_s]$, the integer part of kT/T_s means the largest integer less than or equal to kT/T_s and $\mu_k= kT/T_s-m_k$ is a fractional difference. Only the samples at time instants $t=kT$ are required for further processing. The

interpolants (new samples) can be calculated as in [3] by:

$$y(kT) = y[(m_k + \mu_k)T_s] = \sum_{i=I_1}^{I_2} x[(m_k - i)T_s]h_I[(i + \mu_k)T_s] \quad (2)$$

where $\{x(m)\}$ is a sequence of signal samples taken at intervals T_s, and $h_I(t)$ is the finite-duration impulse response of a fictitious, time-continuous, analogue interpolating filter. $\{I_1T \ldots I_2T\}$ is the area that the interpolating filter operates on. An ideal interpolation filter is $h_I(t) = \frac{\sin \pi t/T_s}{\pi t/T_s}$ with a transfer function $H_I(f) = \begin{cases} T_s, |f| < 1/2T_s \\ 0, |f| > 1/2T_s \end{cases}$. Practically, a linear interpolator is adequate and efficient if the samples are closely spaced. Hence, in a discrete form,

$$y(k) = (1 - \mu_k)x(m_k) + \mu_k x(m_k + 1) = x(m_k) + \mu_k[x(m_k + 1) - x(m_k)] \quad (3)$$

B. Proposed Receiver Architecture with Sigma-Delta Modulation

Sigma-Delta modulation is the most popular form of the noise-shaping quantization that uses oversampling and 1-bit quantization. Mathematical explanation of the Sigma-Delta data converters can be found in [5]. In principle, a Sigma-Delta A/D converter consists of two functional blocks: a Sigma-Delta modulator and a decimator. The Sigma-Delta data converter has the advantage of requiring less restrictive anti-aliasing filters by benefiting from the high sampling rate in the modulation process; the anti-alias filter requirements are relaxed.

For a multi-mode DVB-T/DAB/HIPERLAN-2 receiver, when sampled at the integer multiple of 20 MHz (sampling rate of HIPERLAN-2), the new sampling rate (40 MHz, 60 MHz, 80 MHz...), the fractional interval μ_k will cyclically repeat a finite set of values. These fractional intervals μ_k and the integer value m_k in (3) can be computed in advance, stored in ROMs and loaded when necessary. We assume perfect synchronization here; otherwise, fractional intervals need to be corrected on-line due to the synchronization offsets.

Generally, an OFDM system achieves symbol synchronization by adjusting the FFT position, including coarse synchronization and fine synchronization. The coarse synchronization can be done by some cyclic prefix (CP) based approaches. After coarse symbol synchronization, the residual timing offset will be estimated though pilots and then be compensated.

The fractional timing offset is required to be quantized into L uniform intervals where L is the integer part of the oversampling ratio. Consequently, it is now easy to adjust the starting instant of an OFDM symbol by fractional offset for the fine symbol synchronization purpose, which is not a simple task for conventional OFDM receivers. A new multimode OFDM receiver architecture is proposed in Fig. 1. In an ideal case there is no sampling frequency offset. Based on our knowledge on the sampling rate of the three different systems, the known coefficients μ_k and m_k in (3) can be stored in memory and loaded into the SRC process while needed (shown by ① in Fig.1).

Unfortunately, using a free running clock, the sampling frequency error (the clock used in the transmitter may not be exactly identical to that used in the receiver) is inevitable. Conventional OFDM receivers adopt feedback using a voltage-controlled oscillator (VCO) to adjust the sampling frequency, the disadvantage of which is that a feedback loop is unavoidable. In case of the sampling frequency error impairment, all computations need to be performed on line and no extra memory for storing coefficients is required. Instead, a numerically controlled oscillator (NCO) controlled interpolator was investigated in [3] by Gardner. In practice, after the fine time synchronization process, the output ε ($\varepsilon=\varepsilon_i+\varepsilon_f$, ε_i: integer offset and ε_f: fractional offset) is feed back to the NCO controller, which is responsible for determining μ_k and m_k, and making that information available to the interpolator. Since the fine symbol synchronization can be done symbol by symbol only, thus, the coefficients μ_k and m_k will be only updated once per OFDM symbol. The above discussion are based on the assumption that the sample frequency offset is small; otherwise, the drift between ideal and true sample points will be significant for 8k mode. In that case, the clock rate needs to be adjusted for sample rate offset, or timing offset, μ_k and m_k, will need to be changed linearly.

For the sake of convenience, attention is paid to the timing recovery process, which is closely related to the SRC while the

frequency synchronization blocks are left out in the architecture. In the first stage, the received signal is down converted to baseband and the complex baseband signals are generated. By passing the analogue pre-filter, the useful signals are band limited. The analogue input signals are then sampled at the sampling frequency, which is much higher than its signalling rate. According to the receiver structure, signals sampled at high frequency were pushed to a Sigma-Delta modulator and then, a low pass filter (LPF) preceding the interpolation and decimation block is used for anti-aliasing purpose and quantization noise attenuation. Before the interpolation and decimation block is working, the receiver works under the coarse symbol-acquiring mode. As has been stated, the symbol starting instant θ could be coarsely determined by the CP based pre-FFT approaches, thus the starting position of an OFDM symbol hence the FFT window position can be determined and set. In this stage, the feedback loop from the post-FFT fine symbol synchronization is switched off. The window controller uses the information provided by the coarse symbol synchronization to adjust the starting position for the interpolation and decimation block, which strictly speaking, is an interpolation, based decimation process.

The sampling clock frequency error Δf might cause inter-carrier interference (ICI) and furthermore, a drift in the symbol timing [6]. Nevertheless, in most cases, the sampling frequency offset is very small compared with the high sampling frequency, the ICI caused can be considered as additional noise and the feedback loop in the receiver may be used to periodically compensated for the drift, either integer or fractional. Via ① in Fig.1, the pre-stored μ_k and m_k will be loaded to the interpolation based decimator for linear interpolation or polynomial interpolation processing, etc. The sampling rate of the output is approximate to the targeted system signalling rate $1/T$ and post-FFT fine symbol synchronization is now carried out. Since each different system has its own offset estimation mechanism, we will not focus on every detail (the DVB-T system, for example, examines the phase rotation on pilots to estimate the averaged timing offset). The averaged residual timing offset ε consists of the integer part ε_i and the fractional part ε_f, both of them will be fed back to the window controller to adjust the symbol position. Since the fractional timing offset can also be compensated via the interpolation based decimation block by shifting quantized fractional samples, which are integer samples with respect to the high sampling rate, the residual timing error will remain comparatively small. In addition, the accumulating timing error due to sampling frequency error can be compensated by the feedback from the error estimation every OFDM symbol.

Alternatively, Gardner's NCO controlling method could be an efficient approach in providing the information of $\{\mu_k, m_k\}$ figured out from the output of the fine symbol synchronization process (see ② in Fig.1). Fig.2 shows the performance of a multimode receiver with different sampling rates deployed in the Sigma-Delta modulation block. The mean square error (MSE) of the uncoded data in the frequency domain against E_b/N_o is plotted, a DVB-T receiver is being considered in the simulation.

In this paper, we have only studied the impact of linear interpolation based on the Sigma-Delta modulation output at different sampling rate (20 MHz, 40 MHz, 60 MHz and 80 MHz) and the perfect timing case in a DVB-T system while the DAB system is not considered. The reason is that the sampling rate of DVB-T is up to 4 times higher than the sampling rate of DAB, so that if a sampling rate selected is suitable for DVB-T, then it should with no doubt be suitable for DAB as well in terms of using linear interpolation. As can be seen in Fig. 2, for a DVB-T system, 40 MHz can be chosen as the best compromise between the system performance and hardware expenses. If is possible to have higher sampling frequency with not too much power consumption, this will definitely improve the system performance and also enable a fractional spaced equalization (FSE) which is not sensitive to sample timing.

IV. Conclusions

This paper presents a study on the issues concerning the convergence of DAB, DVB-T and HIPERLAN-2 and suggests a possible architecture for a suitable multimode terminal. Sigma-Delta modulation and linear interpolation are deployed in the receiver for sampling rate adaptation purpose. A new sampling rate is adopted in the multimode receiver, which is a multiple integer times of

20 MHz (the sampling rate of HIPERLAN-2). A new proposed structure can integrate the three OFDM based systems by a single system clock effectively and in addition, bring advantages to symbol synchronization of the OFDM systems. Since the other standards (DAB & WCDMA) have lower sample rate requirements than DVB-T, 40 MHz is a good initial choice.

ACKNOWLEDGMENT

The work reported in this paper has formed part of the Research Programme of the Virtual Centre of Excellence in Mobile and Personal Communications, Mobile VCE, www.mobilevce.com, whose funding support, including that of EPSRC, is gratefully acknowledged. Fully detailed technical reports on this research are available to Industrial Members of Mobile VCE.

REFERENCES

[1] J. Cosmas, T. Itagaki, L. Cruickshank, L. Zheng, K. Krishnapillai, A. Lucas, L. Elgohari , "System Concept of a Novel Converging DVB-T and UMTS Mobile System", *London Communications Symposium 2002*, London, 2002.

[2] Xiaojun Wu, Bofeng Jiang, Qinye Yin, "Software-defined radio based baseband discrete model for orthogonal frequency division multiplexing CDMA systems", *Vehicular Technology Conference*, 2001. VTC 53rd, Vol. 2, pp: 771 -775, 2001.

[3] F. Gardner, "Interpolation in digital modems-Part I: fundamentals", IEEE Trans. on Comm., Vol. 41, No.3, 1993, pp 501-507.

[4] L. Erup, F. Gardner and R. Harris, "Interpolation in digital modems-Part II: Implementation and Performance", IEEE Trans. on Comm., Vol. 41, No. 6, 1993, pp 998-1008.

[5] J. Candy, G. Temes, *Oversampling delta-sigma data converters – theory, design and simulation*, The institute of electrical and electronics engineering, New York, 1992

[6] T. Pollet, P. Spruyt, and M. Moeneclaey, "The BER performance of OFDM system using non-synchronized sampling", Proc. Globecomm'94, pp. 253-257, Nov. 1994

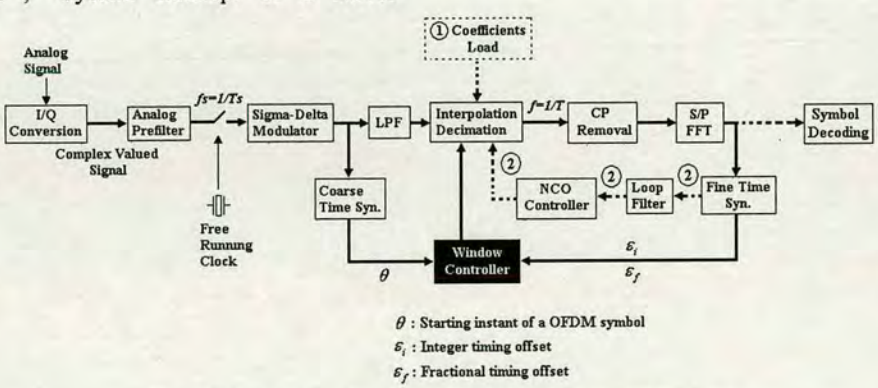

Fig. 1 Proposed multi-mode OFDM receiver architecture

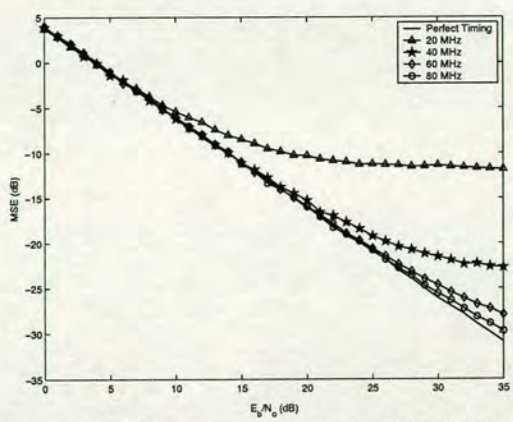

Fig. 2 Performance of different sampling rate in DVB-T with interpolation